

PRINCIPLES OF APPLIED RESERVOIR SIMULATION

Second Edition

*Clear, concise
computer-based
introduction to
practical reservoir
modeling complete
with fully-functioning
reservoir simulator*

John R. Fanchi



TEAM LinG - Live, Informative, Non-cost and Genuine!

Principles of Applied Reservoir Simulation

This page intentionally left blank

Principles of Applied Reservoir Simulation

Second Edition

John R. Fanchi



Gulf Professional Publishing
an imprint of Butterworth-Heinemann

Amsterdam Boston Heidelberg London New York Oxford Paris San Diego
San Francisco Singapore Sydney Tokyo

TEAM LinG - Live, Informative, Non-cost and Genuine!

Gulf Professional Publishing is an imprint of Elsevier.
Copyright © 2001 by Elsevier (USA).

All rights reserved.

Originally published by Gulf Publishing Company, Houston, TX.

No part of this publication may be reproduced, stored in a retrieval system, or transmitted in any form or by any means, electronic, mechanical, photocopying, recording, or otherwise, without the prior written permission of the publisher.

Permissions may be sought directly from Elsevier's Science & Technology Rights Department in Oxford, UK: phone: (+44) 1865 843830, fax: (+44) 1865 853333, e-mail: permissions@elsevier.co.uk. You may also complete your request on-line via the Elsevier Science homepage (<http://www.elsevier.com>), by selecting 'Customer Support' and then 'Obtaining Permissions'.



This book is printed on acid-free paper.

Library of Congress Cataloging-in-Publication Date

Fanchi, John R.

Principles of applied reservoir simulation/John Fanchi. – 2nd edition

p. cm.

Includes bibliographical references and index.

ISBN 0-88415-372-X (alk. paper)

1. Oil fields-Computer simulation. 2. Petroleum-Geology-Mathematical models.

I. Title

TN870.53.F36 2000

622'.3382'0113-dc21

00-064650

British Library Cataloguing-in-Publication Data

A catalogue record for this book is available from the British Library.

The publisher offers special discounts on bulk orders of this book.

For information, please contact:

Manager of Special Sales

Elsevier Science

200 Wheeler Road

Burlington, MA 01803

Tel: 781-313-4700

Fax: 781-313-4802

For information on all Gulf publications available, contact our World Wide Web homepage at <http://www.bh.com/gulf>

10 9 8 7 6 5 4 3 2

Printed in the United States of America.

Disclaimer:

Some images in the original version of this book are not available for inclusion in the eBook.

To my parents,
John A. and Shirley M. Fanchi

This page intentionally left blank

CONTENTS

About the Author	xiv
Preface to Second Edition	xv
Preface to First Edition	xvi
1 Introduction to Reservoir Management	1
1.1 Consensus Modeling	2
1.2 Management of Simulation Studies	4
1.3 Outline of the Text	6
Exercises	7
Part I - Reservoir Engineering Primer	
2 Basic Reservoir Analysis	11
2.1 Volumetrics	11
2.2 Material Balance	12
2.3 Decline Curve Analysis	16
Exercises	17
3 Multiphase Flow Concepts	19
3.1 Basic Concepts	19
3.2 Capillary Pressure	22
3.3 Mobility	24
3.4 Fractional Flow	26
Exercises	30

4	Derivation of the Flow Equations	31
4.1	Conservation of Mass	31
4.2	Flow Equations for Three-Phase Flow	33
4.3	Flow Equations in Vector Notation	36
	Exercises	37
5	Fluid Displacement	39
5.1	Buckley-Leverett Theory	39
5.2	Welge's Method	42
5.3	Miscible Displacement	44
	Exercises	46
6	Frontal Stability	48
6.1	Frontal Advance Neglecting Gravity	48
6.2	Frontal Advance Including Gravity	51
6.3	Linear Stability Analysis	53
	Exercises	55
7	Pattern Floods	56
7.1	Recovery Efficiency	56
7.2	Patterns and Spacing	58
7.3	Pattern Recovery	61
	Exercises	63
8	Recovery of Subsurface Resources	64
8.1	Production Stages	64
8.2	Enhanced Oil Recovery	69
8.3	Nonconventional Fossil Fuels	71
	Exercises	73
9	Economics and the Environment	75
9.1	SPE/WPC Reserves	75
9.2	Basic Economic Concepts	77
9.3	Investment Decision Analysis	81
9.4	Environmental Impact	82
	Exercises	85

Part II - Reservoir Simulation

10 Overview of the Modeling Process	89
10.1 Basics Reservoir Analysis	89
10.2 Prerequisites	90
10.3 Computer Modeling	90
10.4 Major Elements of a Reservoir Simulation	
Study	92
Exercises	94
11 Conceptual Reservoir Scales	95
11.1 Reservoir Sampling and Scales	95
11.2 Integrating Scales - the Flow Unit	97
11.3 Geostatistical Case Study	101
Exercises	104
12 Reservoir Structure	106
12.1 Giga Scale	106
12.2 Mega Scale	111
12.3 Reservoir Description Using Seismic Data	115
Exercises	119
13 Fluid Properties	120
13.1 Fluid Types	120
13.2 Fluid Modeling	124
13.3 Fluid Sampling	128
Exercises	128
14 Rock-Fluid Interaction	131
14.1 Porosity, Permeability, Saturation and	
Darcy's Law	131
14.2 Relative Permeability and Capillary	
Pressure	135
14.3 Viscous Fingering	139
Exercises	141

15	Fundamentals of Reservoir Simulation	142
15.1	Conservation Laws	142
15.2	Flow Equations	143
15.3	Well and Facilities Modeling	145
15.4	Simulator Solution Procedures	146
15.5	Simulator Selection	153
	Exercises	154
16	Modeling Reservoir Architecture	156
16.1	Mapping	156
16.2	Grid Preparation	158
16.3	Model Types	164
16.4	Basic Simulator Volumetrics	166
	Exercises	166
17	Data Preparation for a Typical Study	168
17.1	Data Preparation	168
17.2	Pressure Correction	170
17.3	Simulator Selection and Ockham's Razor	172
	Exercises	175
18	History Matching	176
18.1	Illustrative History Matching Strategies	177
18.2	Key History Matching Parameters	180
18.3	Evaluating the History Match	182
18.4	Deciding on a Match	183
18.5	History Match Limitations	184
	Exercises	185
19	Predictions	186
19.1	Prediction Capabilities	186
19.2	Prediction Process	187
19.3	Sensitivity Analyses	188
19.4	Economic Analysis	190
19.5	Validity of Model Predictions	191
	Exercises	192

Part III - Case Study

20 Study Objectives and Data Gathering	197
20.1 Study Objectives	197
20.2 Reservoir Structure	197
20.3 Production History	199
20.4 Drill Stem Test	201
20.5 Fluid Properties	203
20.6 Reservoir Management Constraints	207
Exercises	207
21 Model Initialization	208
21.1 Volumetrics	208
21.2 Material Balance	209
21.3 Relative Permeability	212
21.4 Fluid Contacts	214
21.5 Grid Preparation	215
Exercises	216
22 History Matching and Predictions	218
22.1 Well Model Preparation	218
22.2 Full Field (3D) Model History Match	222
22.3 Predictions	223
Exercises	224

Part IV - WINB4D User's Manual

23 Introduction to WINB4D	229
23.1 Program Configuration	231
23.2 Input Data File - WTEMP.DAT	232
23.2 Data Input Requirements	233
23.4 Example Input Data Sets	234
24 Initialization Data	239
24.1 Grid Dimensions and Geometry	239
24.2 Seismic Velocity Parameters	245
24.3 Porosity, Permeability, and Transmissibility Distributions	249

24.4	Rock and PVT Regions	255
24.5	Relative Permeability and Capillary Pressure Tables	257
24.6	Fluid PVT Tables	258
24.7	Pressure and Saturation Initialization	262
24.8	Run Control Parameters	264
24.9	Solution Method Specification	265
24.10	Analytic Aquifer Models	267
25	Recurrent Data	270
25.1	Timestep and Output Control	270
25.2	Well Information	272
26	Program Output Evaluation	278
26.1	Initialization Data	278
26.2	Recurrent Data	279
Part V: Technical Supplements		
27	Simulator Formulation	285
27.1	Equations	285
27.2	Coordinate Orientation	287
27.3	Petrophysical Model	288
27.4	Material Balance	291
28	Rock and Fluid Models	292
28.1	Three-Phase Relative Permeability	292
28.2	Transmissibility	294
28.3	Terminology and General Comments	295
28.4	Extrapolating Saturated Curves	300
28.5	Gas PVT Correlation Option	301
29	Initialization	304
29.1	Pressure Initialization	304
29.2	Gravity Segregated Saturation Initialization	305
29.3	Aquifer Models	307
30	Well Models	310
30.1	Rate Constraint Representation	310

30.2	Explicit Pressure Constraint Representation	314
30.3	GOR/WOR Constraints	315
30.4	Fluid Withdrawal Constraints	316
30.5	Fluid Injection Constraints	316
31	Well Flow Index (PID)	318
31.1	Productivity Index	318
31.2	Vertical Wells	319
31.3	Horizontal Wells	320
32	The IMPES Formulation	322
32.1	Flow Equations and Phase Potentials	322
32.2	Introduction of the Capillary Pressure Concept	323
32.3	The Pressure Equation	325
	REFERENCES	333
	INDEX	347

About the Author

John R. Fanchi is a Professor of Petroleum Engineering at the Colorado School of Mines. He has worked in the technology centers of three major oil companies (Marathon, Cities Service, and Getty), and served as an international consultant. His oil and gas industry responsibilities have revolved around reservoir modeling, both in the areas of simulator development and practical reservoir management applications. Dr. Fanchi's publications include software systems for the United States Department of Energy and numerous articles. He is the author of four books, including *Math Refresher for Scientists and Engineers, Second Edition* and *Integrated Flow Modeling*. He has a Ph.D. in physics from the University of Houston.

Preface to the Second Edition

The second edition of *Principles of Applied Reservoir Simulation* has been expanded to include background material on reservoir engineering. The chapters in **Part I – Reservoir Engineering Primer** are intended to make the book more accessible to people from such disciplines as geology, geophysics, and hydrology. The material should serve as a review for petroleum engineers. Chapters in **Part II – Modeling Principles** have been substantially revised and updated where appropriate. Exercises have been added or modified to improve their usefulness. Much of the material in the program technical supplement has been integrated into the main body of the text because it is relevant for flow simulators in general, and not just for the accompanying software.

The simulator WINB4D accompanying the text is a version of the original BOAST4D flow simulator modified for use in a Windows operating environment with a dynamic memory management system. The dynamic memory management system expands the range of applicability of the program. A visualization program (3DVIEW) is included on the accompanying CD. It lets the reader obtain a 3D perspective of the reservoir using WINB4D output.

I would like to thank my students in the undergraduate senior reservoir engineering course at the Colorado School of Mines for their comments and suggestions. I would also like to thank Kathy Fanchi for helping complete the revisions to the second edition, and David Abbott for providing the original version of 3DVIEW. Any written comments or suggestions for improving the material are welcome.

John R. Fanchi, Ph.D.
Golden, Colorado
June 2000

Preface

Principles of Applied Reservoir Simulation is a vehicle for widely disseminating reservoir simulation technology. It is not a mathematical treatise about reservoir simulation, nor is it a compendium of case histories. Both of these topics are covered in several other readily available sources. Instead, *Principles of Applied Reservoir Simulation* is a practical guide to reservoir simulation that introduces the novice to the process of reservoir modeling and includes a fully functioning reservoir simulator for the reader's personal use.

Part I explains the concepts and terminology of reservoir simulation. The selection of topics and references is based on what I have found to be most useful over the past two decades as both a developer and user of reservoir simulators. I have provided advice gleaned from model studies of a variety of oil, gas, and condensate fields.

Participation is one of the best ways to learn a subject. The exercises in Part I give you an opportunity to apply the principles that are discussed in each chapter. As a means of integrating the material, the principles of reservoir simulation are applied to the study of a particular case in Part II. By the time you have completed the case study, you will have participated in each technical phase of a typical model study.

Parts III and IV are the User's Manual and Technical Supplement, respectively, for the three-dimensional, three-phase black oil simulator BOAST4D that accompanies the text. BOAST4D is a streamlined and upgraded version of BOAST II, a public domain black oil simulator developed for the U.S. Department of Energy in the 1980's. As principal author of BOAST II, I have added several features and made corrections to create BOAST4D. For example, you can now use BOAST4D to model horizontal wells and perform reservoir geophysical calculations. The latter calculations are applicable to an emerging technology: 4D seismic monitoring of fluid flow. The inclusion of reservoir

geophysical calculations is the motivation for appending “4D” to the program name. In addition, BOAST4D includes code changes to improve computational performance, to allow the solution of material balance problems, and to reduce material balance error.

BOAST4D was designed to run on DOS-based personal computers with 486 or better math co-processors. The simulator included with this book is well-suited for learning how to use a reservoir simulator, for developing an understanding of reservoir management concepts, and for solving many types of reservoir engineering problems. It is an inexpensive tool for performing studies that require more sophistication than is provided by analytical solutions, yet do not require the use of full-featured commercial simulators. Several example data sets are provided on disk to help you apply the simulator to a wide range of practical problems.

The text and software are suitable for use in a variety of settings, e.g. in an undergraduate course for petroleum engineers, earth scientists such as geologists and geophysicists, or hydrologists; in a graduate course for modelers; and in continuing education courses. An Instructor’s Guide is available from the publisher.

I developed much of the material in this book as course notes for a continuing education course I taught in Houston. I would like to thank Bob Hubbell and the University of Houston for sponsoring this course and Tim Calk of Gulf Publishing for shepherding the manuscript through the publication process. I am grateful to my industrial and academic employers, both past and present, for the opportunity to work on a wide variety of problems. I would also like to acknowledge the contributions of Ken Harpole, Stan Bujnowski, Jane Kennedy, Dwight Dauben and Herb Carroll for their work on earlier versions of BOAST. I would especially like to thank my wife, Kathy Fanchi, for her moral support and for the many hours at the computer creating the graphics and refining the presentation of this material.

Any written comments or suggestions for improving the material are welcome.

*John R. Fanchi, Ph.D.
Houston, Texas
August 1997*

This page intentionally left blank

Chapter 1

Introduction to Reservoir Management

Reservoir modeling exists within the context of the reservoir management function. Although not universally adopted, reservoir management is often defined as the allocation of resources to optimize hydrocarbon recovery from a reservoir while minimizing capital investments and operating expenses [Wiggins and Startzman, 1990; Satter and Thakur, 1994; Al-Hussainy and Humphreys, 1996; Thakur, 1996]. These two outcomes – optimizing recovery and minimizing cost – often conflict with each other. Hydrocarbon recovery could be maximized if cost was not an issue, while costs could be minimized if the field operator had no interest in or obligation to prudently manage a finite resource. *The primary objective in a reservoir management study is to determine the optimum conditions needed to maximize the economic recovery of hydrocarbons from a prudently operated field.* Reservoir modeling is the most sophisticated methodology available for achieving the primary reservoir management objective.

There are many reasons to perform a model study. Perhaps the most important, from a commercial perspective, is the ability to generate cash flow predictions. Simulation provides a production profile for preparing economic forecasts. The combination of production profile and price forecast gives an estimate of future cash flow. Other reasons for performing a simulation study from a reservoir management perspective are listed in Table 1-1. Several of the items are discussed in greater detail in later chapters.

Table 1-1
Why Simulate?

Corporate Impact <ul style="list-style-type: none">◆ Cash Flow Prediction<ul style="list-style-type: none">◇ Need Economic Forecast of Hydrocarbon Price
Reservoir Management <ul style="list-style-type: none">◆ Coordinate Reservoir Management Activities◆ Evaluate Project Performance<ul style="list-style-type: none">◇ Interpret/Understand Reservoir Behavior◆ Model Sensitivity to Estimated Data<ul style="list-style-type: none">◇ Determine Need for Additional Data◆ Estimate Project Life◆ Predict Recovery vs Time◆ Compare Different Recovery Processes◆ Plan Development or Operational Changes◆ Select and Optimize Project Design<ul style="list-style-type: none">◇ Maximize Economic Recovery

1.1 Consensus Modeling

Reservoir modeling is the application of a computer simulation system to the description of fluid flow in a reservoir [for example, see Peaceman, 1977; Aziz and Settari, 1979; Mattax and Dalton, 1990]. The computer simulation system is usually just one or more computer programs. To minimize confusion in this text, the computer simulation system is called the reservoir simulator, and the input data set is called the reservoir model.

Many different disciplines contribute to the preparation of the input data set. The information is integrated during the reservoir modeling process, and the concept of the reservoir is quantified in the reservoir simulator. Figure 1-1 illustrates the contributions different disciplines make to reservoir modeling.

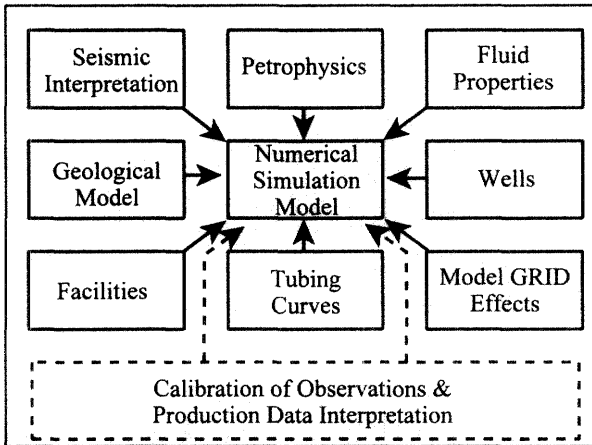


Figure 1-1. Disciplinary contributions to reservoir modeling (after H.H. Haldorsen and E. Damsleth, ©1993; reprinted by permission of the American Association of Petroleum Geologists).

The simulator is the point of contact between disciplines. It serves as a filter that selects from among all of the proposed descriptions of the reservoir. The simulator is not influenced by hand-waving arguments or presentation style. It provides an objective appraisal of each hypothesis, and constrains the power of personal influence described by Millheim [1997]. As a filter of hypotheses, the reservoir modeler is often the first to know when a proposed hypothesis about the reservoir is inadequate.

One of the most important tasks of the modeler is to achieve consensus in support of a reservoir representation. This task is made more complex when available field performance data can be matched by more than one reservoir model. The non-uniqueness of the model is discussed in greater detail throughout the text. It means that there is more than one way to perceive and represent available data. The modeler must sort through the various reservoir representations and seek consensus among all stakeholders. This is often done by rejecting one or more proposed representations. As a consequence, the human element is a factor in the process, particularly when the data do not clearly support the selection of a single reservoir representation from a set of competing representations. The dual criteria of reasonableness and Ockham's Razor

4 Principles of Applied Reservoir Simulation

[Chapter 9.3; Jefferys and Berger, 1992] are essential to this process, as is an understanding of how individuals can most effectively contribute to the modeling effort.

1.2 Management of Simulation Studies

Ideally, specialists from different disciplines will work together as a team to develop a meaningful reservoir model. Team development proceeds in well known stages [Sears, 1994]:

- ◆ Introductions: Getting to know each other
- ◆ “Storming”: Team members disagree over how to proceed
 - ◇ Members can lose sight of goals
- ◆ “Norming”: Members set standards for team productivity
- ◆ “Performing”: Team members understand
 - ◇ what each member can contribute
 - ◇ how the team works best

Proper management recognizes these stages and allows time for the team building process to mature.

Modern simulation studies of major fields are performed by teams that function as project teams in a matrix management organization. Matrix management is synonymous here with Project Management and has two distinct characteristics:

- ◆ “Cross-functional organization with members from different work areas who take on a project.” [Staff-JPT, 1994]
- ◆ “One employee is accountable to two or more superiors, which can cause difficulties for managers and employees.” [Staff-JPT, 1994]

To alleviate potential problems, the project team should be constituted such that:

- ◆ Each member of the team is assigned a different task.
- ◆ All members work toward the same goal.

Team members should have unique roles to avoid redundant functions. If the responsibilities of two or more members of the team overlap considerably, confusion may ensue with regard to areas of responsibility and, by implication, of accountability. Each team member must be the key decision maker in a particular discipline, otherwise disputes may not get resolved in the time avail-

able for completing a study. Teams should not be allowed to flounder in an egalitarian utopia that does not work.

Effective teams may strive for consensus, but the pressure of meeting deadlines will require one team member to serve as team leader. Deadlines cannot be met if a team cannot agree, and there are many areas where decisions may have to be made that will not be by consensus. For this reason, teams should have a team leader with the following characteristics:

- ◆ Significant technical skills
- ◆ Broad experience

Team leaders should have technical and monetary authority over the project. If they are perceived as being without authority, they will be unable to fulfill their function. On the other hand, team leaders must avoid authoritarian control or they will weaken the team and wind up with a group.

According to Maddox [1988], teams and groups differ in the way they behave. Group behavior exhibits the following characteristics:

- ◆ “Members think they are grouped together for administrative purposes only. Individuals work independently, sometimes at cross purposes.”
- ◆ “Members tend to focus on themselves because they are not sufficiently involved in planning the unit's objectives. They approach their job simply as hired hands.”

By contrast, the characteristics of team behavior are the following:

- ◆ “Members recognize their interdependence and understand both personal and team goals are best accomplished with mutual support. Time is not wasted struggling over territory or seeking personal gain at the expense of others.”
- ◆ “Members feel a sense of ownership for their jobs and unit because they are committed to goals they helped to establish.”

Similar observations were made by Haldorsen and Damsleth [1993]:

- ◆ “Members of a team should necessarily understand each other, respect each other, act as a devil's advocate to each other, and keep each other informed.”

Haldorsen and Damsleth [1993] argue that each team member should have the following focus:

- ◆ Innovation and creation of value through the team approach

◆ Customer orientation with focus on “my output is your input”

McIntosh, et al. [1991] support the notion that each team member should fulfill a functional role, for example, geoscientist, engineer, etc. A corollary is that team members can understand their roles because the roles have been clearly defined.

Proper management can improve the likelihood that a team will function as it should. A sense of ownership or “buy-in” can be fostered if team members participate in planning and decision making. Team member views should influence the work scope and schedule of activity. Many problems can be avoided if realistic expectations are built into project schedules at the beginning, and then adhered to throughout the project. Expanding work scope without altering resource allocation or deadlines can be demoralizing and undermine the team concept.

Finally, one important caution should be borne in mind when performing studies using teams: “Fewer ideas are generated by groups than by individuals working alone – a conclusion supported by empirical evidence from psychology [Norton, 1994].” In describing changes in the work flow of exploration and development studies, Tobias [1998, pg. 38] observed that “asset teams have their drawbacks. The enhanced teamwork achieved through a team approach often comes at the expense of individual creativity, as group dynamics can and often does inhibit individual initiative [Kanter, 1988].” Tobias recommended that organizations allow “the coexistence of both asset teams and individual work environments.” His solution is a work flow that allows the “simultaneous coexistence of decoupled individual efforts and recoupled asset team coordination.”

1.3 Outline of the Text

The remainder of the text is organized as follows. Part I presents a primer on reservoir engineering. The primer is designed to provide background concepts and terminology in the reservoir engineering aspects of fluid flow in porous media. Material in Part II explains the concepts and terminology of reservoir simulation. A typical exercise in Part II asks you to find and change data records in a specified example data file. These records of data must be modified based

on an understanding of the reservoir problem and a familiarity with the accompanying computer program WINB4D. WINB4D is a three-dimensional, three-phase reservoir simulator. These terms are discussed in detail in subsequent chapters.

The exercises in Part II use different sections of the user's manual presented in Part IV. If you work all the exercises, you will be familiar with the user's manual and WINB4D by the time the exercises are completed. Much of the experience gained by running WINB4D is applicable in principle to other simulators.

Successful completion of the exercises in Part II will prepare you for the case study presented in Part III. The case study is designed to integrate the material discussed in Parts I and II. By the time Part III is completed, you will have participated in each technical phase of a typical model study.

Parts IV and V are the User's Manual and Technical Supplement, respectively, for WINB4D. Supplemental information in Part V provides more detailed descriptions of the algorithms coded in WINB4D.

Exercises

Exercise 1.1 WINB4D Folder: A three-dimensional, three-phase reservoir simulator (WINB4D) is included on a disk with this book. The WINB4D user's manual is presented in Part IV, and a technical supplement is provided in Part V. Prepare a folder on your hard drive for running WINB4D using the procedure outlined in Chapter 23. What is the size of the file WINB4D.EXE in kilobytes (KB)?

Exercise 1.2 WINB4D Example Data Sets: Several example data sets are provided on the WINB4D disk. Copy all files from your disk to the \WINB4D folder on your hard drive. Make a list of the data files (files with extension "dat"). Unless stated otherwise, all exercises assume WINB4D and its data sets reside in the \WINB4D directory.

Exercise 1.3 The program 3DVIEW may be used to view the reservoir structure associated with WINB4D data sets. 3DVIEW is a visualization program that

8 Principles of Applied Reservoir Simulation

reads WINB4D output files with the extension “arr”. To view a reservoir structure, proceed as follows:

Use your file manager to open your folder containing the WINB4D files.

Unless stated otherwise, all mouse clicks use the left mouse button.

Start 3DVIEW (double click on the application 3DVIEW.EXE)

Click on the button “File”.

Click on “Open Array File”.

Click on “CS_Rim.arr” in the File List.

Click on “OK”.

At this point you should see a structure in the middle of the screen. The structure is an anticlinal reservoir with a gas cap and oil rim. To view different perspectives of the structure, hold the left mouse button down and move the mouse. With practice, you can learn to control the orientation of the structure on the screen.

The gridblock display may be smoothed by clicking on the “Project” button and selecting “Smooth Model Display”. The attribute shown on the screen is pressure “P”. To view other attributes, click on the “Model” button, set the cursor on “Select Active Attribute” and then click on oil saturation “SO”. The oil rim should be visible on the screen.

To exit 3DVIEW, click on the “File” button and then click on “Exit”.

Part I

Reservoir Engineering Primer

This page intentionally left blank

Chapter 2

Basic Reservoir Analysis

The tasks associated with basic reservoir analyses provide information that is needed to prepare input data for a simulation study. These tasks include volumetric analysis, material balance analysis, and decline curve analysis. In addition to providing estimates of fluids in place and forecasts of fieldwide production, they also provide an initial concept of the reservoir which can be used to design a model study. Each of these tasks is outlined below.

2.1 Volumetrics

Fluid volumes in a reservoir are values that can be obtained from a variety of sources, and therefore serve as a quality control point at the interface between disciplines. Geoscientists use static information to determine volume in a process that is often referred to as volumetric analysis [see, for example, Mian, 1992; Tearpock and Bischke, 1991]. Material balance and reservoir simulation techniques use dynamic data to obtain the same information. Consequently, an accurate characterization of the reservoir should yield consistent estimates of fluid volumes originally in place in the reservoir regardless of the method chosen to determine the fluid volumes. In this section, we present the equations for volumetric estimates of original oil and gas in place.

Original oil in place (OOIP) in an oil reservoir is given by

$$N = \frac{7758 \phi A h_o S_{oi}}{B_{oi}} \quad (2.1)$$

12 Principles of Applied Reservoir Simulation

where

- N original oil in place [STB]
- ϕ reservoir porosity [fraction]
- A reservoir area [acres]
- h_o net thickness of oil zone [feet]
- S_{oi} initial reservoir oil saturation [fraction]
- B_{oi} initial oil formation volume factor [RB/STB]

Associated gas, or gas in solution, is the product of solution gas-oil ratio R_{so} and original oil in place N .

Original free gas in place for a gas reservoir is given by

$$G = \frac{7758\phi Ah_g S_{gi}}{B_{gi}} \quad (2.2)$$

where

- G original free gas in place [SCF]
- h_g net thickness of gas zone [feet]
- S_{gi} initial reservoir gas saturation [fraction]
- B_{gi} initial gas formation volume factor [RB/SCF]

Equation (2.2) is often expressed in terms of initial water saturation S_{wi} by writing $S_{gi} = 1 - S_{wi}$. Initial water saturation is usually determined by well log or core analysis.

2.2 Material Balance

The law of conservation of mass is the basis of material balance calculations. Material balance is an accounting of material entering or leaving a system. The calculation treats the reservoir as a large tank of material and uses quantities that can be measured to determine the amount of a material that cannot be directly measured. Measurable quantities include cumulative fluid production volumes for oil, water, and gas phases; accurate reservoir pressures; and fluid property data from samples of produced fluids.

Material balance calculations may be used for several purposes. They

provide an independent method of estimating the volume of oil, water and gas in a reservoir for comparison with volumetric estimates. The magnitude of various factors in the material balance equation indicates the relative contribution of different drive mechanisms at work in the reservoir. Material balance can be used to predict future reservoir performance and aid in estimating cumulative recovery efficiency. More discussion of these topics can be found in references such as Dake [1978] and Craft, et al. [1991].

The form of the material balance equation depends on whether the reservoir is predominately an oil reservoir or a gas reservoir. Each of these cases is considered separately.

Oil Reservoir Material Balance

The general material balance equation for an oil reservoir is the Schilthuis equation [1961] expressed in a form given by Guerrero [1966]:

$$\begin{aligned}
 & N(B_t - B_{ti}) + NmB_{ti} \left(\frac{B_{gc} - B_{gi}}{B_{gi}} \right) + N \frac{B_{ti} S_{wio}}{1 - S_{wio}} \left(\frac{B_{tw} - B_{twi}}{B_{twi}} \right) \\
 & + N \frac{mB_{ti} S_{wig}}{1 - S_{wig}} \left(\frac{B_{tw} - B_{twi}}{B_{twi}} \right) + N \left(\frac{1}{1 - S_{wio}} + \frac{m}{1 - S_{wig}} \right) B_{ti} c_f \Delta P \\
 & = N_p B_o + [G_{ps} B_g + G_{pc} B_{gc} - G_i B_g] - N_p R_{so} B_g - (W_e + W_i - W_p) B_w
 \end{aligned} \tag{2.3}$$

All of these terms are defined in the Nomenclature at the end of this chapter. The unit of each quantity is presented in square brackets in the Nomenclature. The physical significance of the terms in Eq. (2.3) can be displayed by first defining the terms

$$\begin{aligned}
 D_o &= B_t - B_{ti}, \quad D_{go} = mB_{ti} \left(\frac{B_{gc} - B_{gi}}{B_{gi}} \right), \\
 D_w &= \frac{B_{ti} S_{wio}}{1 - S_{wio}} \left(\frac{B_{tw} - B_{twi}}{B_{twi}} \right), \quad D_{gw} = \frac{mB_{ti} S_{wig}}{1 - S_{wig}} \left(\frac{B_{tw} - B_{twi}}{B_{twi}} \right), \\
 D_r &= \left(\frac{1}{1 - S_{wio}} + \frac{m}{1 - S_{wig}} \right) B_{ti} c_f \Delta P.
 \end{aligned} \tag{2.4}$$

Substituting Eq. (2.4) in Eq. (2.3) gives the general material balance equation in the form

$$N[D_o + D_{go} + D_w + D_{gw} + D_r] = N_p B_o + [G_{ps} B_g + G_{pc} B_{gc} - G_i B_g'] - N_p R_{so} B_g - (W_e + W_i - W_p) B_w \quad (2.5)$$

The terms in Eq. (2.5) have a physical significance. The terms on the right hand side of Eq. (2.3) represent fluid production and injection, while the terms on the left hand side represent volume changes. The significance of the terms is summarized in Table 2-1.

Table 2-1
Physical Significance of Material Balance Terms

Term	Physical Significance
ND_o	Change in volume of initial oil and associated gas
ND_{go}	Change in volume of free gas
$N(D_w + D_{gw})$	Change in volume of initial connate water
ND_r	Change in formation pore volume
$N_p B_o$	Cumulative oil production
$N_p R_{so} B_g$	Cumulative gas produced in solution with oil
$G_{ps} B_g$	Cumulative solution gas produced as evolved gas
$G_{pc} B_{gc}$	Cumulative gas cap gas production
$G_i B_g'$	Cumulative gas injection
$W_e B_w$	Cumulative water influx
$W_i B_w$	Cumulative water injection
$W_p B_w$	Cumulative water production

Equation (2.3) is considered a general material balance equation because it can be applied to an oil reservoir with a gas cap and an aquifer. The derivation of the material balance equation is based on several assumptions: the system is in pressure equilibrium; the system is isothermal; available fluid property data are representative of reservoir fluids; the reservoir has a constant volume;

production data is reliable; and gravity segregation of phases can be neglected. A discussion of the relative importance of drive mechanisms obtained from Eq. (2.3) is presented in Chapter 8.

Gas Reservoir Material Balance

The general material balance equation for a gas reservoir can be derived from Eq. (2.3) by first recognizing the relationship

$$GB_{gi} = NmB_{ti} \quad (2.6)$$

defines original gas in place G . Substituting Eq. (2.6) into Eq. (2.3) gives the general material balance equation

$$\begin{aligned} & N(B_t - B_{ti}) + GB_{gi} \left(\frac{B_{gc} - B_{gi}}{B_{gi}} \right) + N \frac{B_{ti} S_{wio}}{1 - S_{wio}} \left(\frac{B_{rw} - B_{twi}}{B_{twi}} \right) \\ & + G \frac{B_{gi} S_{wig}}{1 - S_{wig}} \left(\frac{B_{rw} - B_{twi}}{B_{twi}} \right) + \left(\frac{NB_{ti}}{1 - S_{wio}} + \frac{GB_{gi}}{1 - S_{wig}} \right) c_f \Delta P \\ & = N_p B_o + [G_{ps} B_g + G_{pc} B_{gc} - G_i B_g'] - N_p R_{so} B_g - (W_e + W_i - W_p) B_w \end{aligned} \quad (2.7)$$

Equation (2.7) is further simplified by recognizing that the material balance for a gas reservoir does not include oil in place so that $N = 0$ and $N_p = 0$. The resulting material balance equation is

$$\begin{aligned} & GB_{gi} \left(\frac{B_{gc} - B_{gi}}{B_{gi}} \right) + G \frac{B_{gi} S_{wig}}{1 - S_{wig}} \left(\frac{B_{rw} - B_{twi}}{B_{twi}} \right) + \left(\frac{GB_{gi}}{1 - S_{wig}} \right) c_f \Delta P \\ & = [G_{pc} B_{gc} - G_i B_g'] - (W_e + W_i - W_p) B_w \end{aligned} \quad (2.8)$$

Water compressibility and formation compressibility are relatively small compared to gas compressibility. Consequently, Eq. (2.8) is often written in the simplified form

$$GB_{gi} \left(\frac{B_{gc} - B_{gi}}{B_{gi}} \right) = [G_{pc} B_{gc} - G_i B_g'] - (W_e + W_i - W_p) B_w \quad (2.9)$$

2.3 Decline Curve Analysis

Arps [1945] studied the relationship between flow rate and time for producing wells. Assuming constant flowing pressure, he found the relationship:

$$\frac{dq}{dt} = -aq^{n+1} \quad (2.10)$$

where a and n are empirically determined constants. The empirical constant n ranges from 0 to 1.

Solutions to Eq. (2.10) show the expected decline in flow rate as the production time increases. A fit of an equation of the form of Eq. (2.10) to flow rate data is referred to as decline curve analysis. Three decline curves have been identified based on the value of n .

The Exponential Decline curve corresponds to $n = 0$. It has the solution

$$q = q_i e^{-at} \quad (2.11)$$

where q_i is initial rate and a is a factor that is determined by fitting Eq. (2.11) to well or field data.

The Hyperbolic Decline curve corresponds to a value of n in the range $0 < n < 1$. The rate solution has the form

$$q^{-n} = nat + q_i^{-n} \quad (2.12)$$

where q_i is initial rate and a is a factor that is determined by fitting Eq. (2.12) to well or field data.

The Harmonic Decline curve corresponds to $n = 1$. The rate solution is equivalent to Eq. (2.12) with $n = 1$, thus

$$q^{-1} = nat + q_i^{-1} \quad (2.13)$$

where q_i is initial rate and a is a factor that is determined by fitting Eq. (2.13) to well or field data.

Decline curves are fit to actual data by plotting the logarithm of observed rates versus time t . The semi-log plot yields the following equation for exponential decline:

$$\ln q = \ln q_i - at \quad (2.14)$$

Equation (2.14) has the form $y = mx + b$ for a straight line with slope m and intercept b . In the case of exponential decline, time t corresponds to the

independent variable x , $\ln q$ corresponds to the dependent variable y , $\ln q_i$ is the intercept b , and $-a$ is the slope m of the straight line. Cumulative production for decline curve analysis is the integral of the rate from the initial rate q_i at $t = 0$ to the rate q at time t . For example, the cumulative production for the exponential decline case is

$$N_p = \int_0^t q dt = \frac{q_i - q}{a} \quad (2.15)$$

The decline factor a is for the exponential decline case and is found by rearranging Eq. (2.11), thus

$$a = -\frac{1}{t} \ln \frac{q}{q_i} \quad (2.16)$$

Exercises

Exercise 2.1 Copy file EXAM1.DAT to file WTEMP.DAT and run WINB4D. What are the volumes of initial fluids in place in the model? Hint: Open the run output file WTEMP.ROF to find initial fluids in place.

Exercise 2.2 Derive the material balance equation for a system with no gas cap beginning with Eqs. (2.3) and (2.4).

Exercise 2.3 Use Eq. (2.9) to show that the material balance equation for a depletion drive gas reservoir is

$$G_{pc} = \frac{[(P/Z)_i - (P/Z)_t] \times G}{(P/Z)_i}$$

where G is original free gas in place, G_{pc} is cumulative free gas produced, P is reservoir pressure, and Z is the real gas compressibility factor. Subscript t indicates that the ratio P/Z should be calculated at the time t that corresponds to G_{pc} , and subscript i indicates that the ratio P/Z should be calculated at the initial time. The units of G_p and G must agree for the equation to be consistent.

Exercise 2.4 Derive Eq. (2.15) for the exponential decline case by using Eq. (2.11) as the integrand and performing the integration.

**Nomenclature
for Equation (2.3)**

B_g	gas formation volume factor (FVF) [RB/SCF]
B_{gc}	gas cap FVF [RB/SCF]
B_g^i	injected gas FVF [RB/SCF]
B_o	oil FVF [RB/STB]
B_t	$B_o + (R_{si} - R_{so})B_g =$ composite oil FVF [RB/STB]
B_{tw}	$B_w + (R_{swi} - R_{sw})B_g =$ composite water FVF [RB/STB]
c_f	formation (rock) compressibility [1/psia]
G	initial gas in place [SCF]
G_i	cumulative gas injected [SCF]
G_{pc}	cumulative gas cap gas produced [SCF]
G_{ps}	cumulative solution gas produced as evolved gas [SCF]
m	ratio of gas reservoir volume to oil reservoir volume
N	initial oil in place [STB]
N_p	cumulative oil produced [STB]
R_{so}	solution gas-oil ratio [SCF/STB]
R_{si}	initial solution gas-oil ratio [SCF/STB]
R_{sw}	solution gas-water ratio [SCF/STB]
R_{swi}	initial solution gas-water ratio [SCF/STB]
S_g	gas saturation [frac.]
S_o	oil saturation [frac.]
S_w	water saturation [frac.]
S_{wi}	initial water saturation [frac.]
S_{wig}	initial water saturation in gas cap [frac.]
S_{wio}	initial water saturation in oil zone [frac.]
W_e	cumulative water influx [STB]
W_i	cumulative water injected [STB]
W_p	cumulative water produced [STB]
ΔP	$P_i - P =$ reservoir pressure change [psia]
P_i	initial reservoir pressure [psia]
P	reservoir pressure corresponding to cumulative fluid times [psia]

Chapter 3

Multiphase Flow Concepts

This chapter summarizes the basic concepts of multiphase flow including interfacial tension, wettability, and contact angle. These concepts lead naturally to a discussion of capillary pressure, mobility, and fractional flow.

3.1 Basic Concepts

Some basic concepts must be introduced as prerequisites for understanding capillary pressure. The concepts are interfacial tension, wettability, and contact angle. They are defined here.

Interfacial Tension

On all interfaces between solids and fluids, and between immiscible fluids, there is a surface free energy resulting from electrical forces. These forces cause the surface of a liquid to occupy the smallest possible area and act like a membrane. Interfacial tension (IFT) refers to the tension between liquids at a liquid/liquid interface. Surface tension refers to the tension between fluids at a gas/liquid interface.

Interfacial tension is energy per unit of surface area, or force per unit length. Interfacial tension is often abbreviated as IFT. The units of IFT are typically expressed in milli-Newtons/meter or the equivalent dynes/cm. The value of IFT depends on the composition of the two fluids at the interface between phases. Table 3-1 lists a few examples:

Table 3-1
Examples of Interfacial Tension

Fluid Pair	IFT Range (mN/m or dyne/cm)
Air-Brine	72-100
Oil-Brine	15-40
Gas-Oil	35-65

Interfacial tension (IFT) can be estimated using the Macleod-Sugden correlation. The Weinaug-Katz variation of the Macleod-Sugden correlation is

$$\sigma^{1/4} = \sum_{i=1}^{N_c} P_{chi} \left(x_i \frac{\rho_L}{M_L} - y_i \frac{\rho_V}{M_V} \right) \quad (3.1)$$

where

- σ interfacial tension [dyne/cm]
- P_{chi} parachor of component i [(dynes/cm)^{1/4}/(g/cm³)]
- M_L molecular weight of liquid phase
- M_V molecular weight of vapor phase
- ρ_L liquid phase density [g/cm³]
- ρ_V vapor phase density [g/cm³]
- x_i mole fraction of component i in liquid phase
- y_i mole fraction of component i in vapor phase

Parachors are empirical parameters. The parachor of component i can be estimated using the molecular weight M_i of component i and the empirical regression equation

$$P_{chi} = 10.0 + 2.92 M_i \quad (3.2)$$

This procedure works reasonably well for molecular weights ranging from 100 to 500. A more accurate procedure for a wider range of molecular weights is given by Fanchi [1990].

Wettability

Wettability is the ability of a fluid phase to preferentially wet a solid surface in the presence of a second immiscible phase. The wetting, or wettability,

condition in a rock/fluid system depends on IFT. Changing the type of rock or fluid can change IFT and, hence, wettability of the system. Adding a chemical such as surfactant, polymer, corrosion inhibitor, or scale inhibitor can alter wettability.

Contact Angle

Wettability is measured by contact angle. Contact angle is always measured through the more dense phase. Contact angle is related to interfacial energies by

$$\sigma_{OS} - \sigma_{WS} = \sigma_{OW} \cos\theta \tag{3.3}$$

where

- σ_{os} interfacial energy between oil and solid [dyne/cm]
- σ_{ws} interfacial energy between water and solid [dyne/cm]
- σ_{ow} interfacial energy, or IFT, between oil and water [dyne/cm]
- θ contact angle at oil-water-solid interface measured through the water phase [degrees]

Examples of contact angle are presented in Table 3-2 for different wetting conditions.

**Table 3-2
Examples of Contact Angle**

Wetting Condition	Contact Angle, degrees
Strongly Water-wet	0-30
Moderately Water-wet	30-75
Neutrally Wet	75-105
Moderately Oil-wet	105-150
Strongly Oil-wet	150-180

Wettability is usually measured in the laboratory. Several factors can affect laboratory measurements of wettability. Wettability can be changed by contact of the core during coring with drilling fluids or fluids on the rig floor, and contact of the core during core handling with oxygen and/or water from the

atmosphere. Laboratory fluids should also be at reservoir conditions to obtain the most reliable measurements of wettability. Based on laboratory tests, most known reservoirs have intermediate wettability and are preferentially water wet.

3.2 Capillary Pressure

Capillary pressure is the pressure difference across the curved interface formed by two immiscible fluids in a small capillary tube:

$$P_c = P_{nw} - P_w \tag{3.4}$$

where

- P_c capillary pressure [psi]
- P_{nw} pressure in nonwetting phase [psi]
- P_w pressure in wetting phase [psi]

Capillary Pressure Theory

Equilibrium between fluid phases in a capillary tube is satisfied by the relationship *force up = force down*. These forces are expressed in terms of the radius r of the capillary tube, the contact angle θ , and the interfacial tension σ . The forces are given by

$$\begin{aligned} \text{force up} &= \text{IFT acting around perimeter of capillary tube} \\ &= \sigma \cos \theta \times 2\pi r \end{aligned}$$

and

$$\text{force down} = \text{density gradient difference} \times \text{cross-sectional area} \times \text{height } h \text{ of capillary rise in tube}$$

The density gradient Γ is the weight of the fluid per unit length per unit cross-sectional area. For example, the density gradient of water Γ_w is approximately 0.433 psia/ft at standard conditions. If we assume an air-water system, the force down is

$$\text{force down} = (\Gamma_w - \Gamma_{air})\pi r^2 h$$

where the cross-sectional area of the capillary tube is πr^2 . Capillary pressure P_c is defined as the force/unit area, thus

$$P_c = \text{force up} / \pi r^2 = \text{force down} / \pi r^2.$$

Capillary Pressure and Pore Radius

Expressing capillary pressure in terms of force up per unit area gives:

$$P_c = \frac{2\pi r\sigma \cos\theta}{\pi r^2} = \frac{2\sigma \cos\theta}{r} \quad (3.5)$$

where

r pore radius [cm]

σ interfacial (or surface) tension [mN/m or dynes/cm]

θ contact angle [degrees]

Equation (3.5) shows that an increase in pore radius will cause a reduction in capillary pressure while a decrease in IFT will cause a decrease in capillary pressure.

Equivalent Height

Expressing P_c in terms of force down leads to the expression

$$P_c = \frac{\pi r^2 h (\Gamma_w - \Gamma_{air})}{\pi r^2} = h (\Gamma_w - \Gamma_{air}) \quad (3.6)$$

where

h height of capillary rise [ft]

P_c capillary pressure [psi]

Γ_w water, or wetting phase, density gradient [psi/ft]

Γ_{air} air, or nonwetting phase, density gradient [psi/ft]

Solving for h yields the defining relationship between capillary pressure and equivalent height, namely

$$h = \frac{P_c}{(\Gamma_w - \Gamma_{air})} \quad (3.7)$$

The equivalent height provides an estimate of the height of the transition zone between immiscible phases. A more precise definition of transition zone is given

in the following section. Equivalent height is inversely proportional to the difference in densities between two immiscible phases. The relatively large density difference between gas and liquid results in a smaller transition zone height than the relatively small difference between two liquid phase densities.

Oil-Water Capillary Pressure

Oil is the nonwetting phase in a water-wet reservoir. Capillary pressure for an oil-water system is

$$P_{cow} = P_o - P_w \quad (3.8)$$

where

P_o pressure in the oil phase [psi]

P_w pressure in the water phase [psi]

Capillary pressure increases with height above the oil-water contact (OWC) as water saturation decreases.

Gas-Oil Capillary Pressure

In gas-oil systems, gas usually behaves as the nonwetting phase and oil is the wetting phase. Capillary pressure between oil and gas in such a system is

$$P_{cgo} = P_g - P_o \quad (3.9)$$

where

P_g pressure in the gas phase [psi]

P_o pressure in the oil phase [psi]

Capillary pressure increases with height above the gas-oil contact (GOC) as gas saturation decreases.

3.3 Mobility

A measure of the ability of a fluid to move through interconnected pore space is the concept of mobility. It is defined here for single phase and multiphase flow. The multiphase flow definition is based on the concept of relative permeability, which is presented next.

Relative Permeability

The general definition of relative permeability is

$$k_r = \frac{k_{eff}}{k_{abs}} \quad (3.10)$$

where

- k_r relative permeability between 0 and 1,
- k_{eff} effective permeability [md]
- k_{abs} absolute permeability [md]

Fluid phase relative permeabilities for oil, water and gas phases, respectively, are

$$k_{r_o} = k_o/k, \quad k_{r_w} = k_w/k, \quad k_{r_g} = k_g/k \quad (3.11)$$

where k_ℓ is the effective permeability of phase ℓ , k_{r_ℓ} is the relative permeability of phase ℓ , and k is absolute permeability.

Mobility

Fluid phase mobility is defined as the ratio of effective phase permeability to phase viscosity. Mobility for oil, water and gas phases respectively are

$$\lambda_o = \frac{k_o}{\mu_o}, \quad \lambda_w = \frac{k_w}{\mu_w}, \quad \lambda_g = \frac{k_g}{\mu_g} \quad (3.12)$$

where μ_ℓ is the viscosity of phase ℓ . Relative mobility is defined as relative permeability divided by viscosity [Dake, 1978]. Absolute permeability is not a factor in the definition of relative mobility.

Mobility Ratio

Mobility ratio is defined as the mobility of the displacing fluid λ_D behind the front divided by the mobility of the displaced fluid λ_d ahead of the front, thus

$$M = \frac{\lambda_D}{\lambda_d} \quad (3.13)$$

An example of mobility ratio is the mobility ratio of water to oil for a waterflood:

$$M_{w,o} = \frac{(\lambda_w)_{S_{or}}}{(\lambda_o)_{S_{wc}}} = \frac{k_{rw}(S_{or})/\mu_w}{k_{ro}(S_{wc})/\mu_o} \quad (3.14)$$

In this case, relative permeability to water is evaluated at residual oil saturation S_{or} , and relative permeability to oil is evaluated at connate water saturation S_{wc} . Notice that absolute permeability factors out of the expression for mobility ratio. Consequently, mobility ratio can be calculated using either mobilities or relative mobilities.

3.4 Fractional Flow

The fractional flow of water is the ratio of water production rate to total production rate. In the case of an oil-water system, the fractional flow of water is given by

$$f_w = \frac{q_w}{q_t} = \frac{q_w}{q_w + q_o} \quad (3.15)$$

where

- f_w fractional flow of water
- q_w water volumetric flow rate [RB]
- q_o oil volumetric flow rate [RB]
- q_t total volumetric flow rate [RB]

Notice that the flow rates are expressed in terms of reservoir volumes. The fractional flow of oil f_o and the fractional flow of water are related by $f_w = 1 - f_o$ for an oil-water system. Based on the definition of fractional flow, we see that fractional flow should be a value between 0 and 1.

Simplified Fractional Flow Equation

A simplified fractional flow equation is obtained by replacing flow rates with Darcy's Law in the definition of fractional flow. If we neglect capillary pressure and gravity for simplicity, we obtain

$$f_w = \frac{\frac{kk_{r_w}A}{\mu_w} \frac{\partial P_w}{\partial x}}{\frac{kk_{r_w}A}{\mu_w} \frac{\partial P_w}{\partial x} + \frac{kk_{r_o}A}{\mu_o} \frac{\partial P_o}{\partial x}} \quad (3.16)$$

where A is cross-sectional area and P_ℓ is the pressure of phase ℓ . Since capillary pressure is neglected, we have the equality of phase pressures $P_w = P_o$ so that

$$f_w = \frac{\frac{k_{r_w}}{\mu_w}}{\frac{k_{r_w}}{\mu_w} + \frac{k_{r_o}}{\mu_o}} \quad (3.17)$$

Equation (3.17) can be expressed in terms of mobilities as

$$f_w = \frac{1}{1 + \frac{k_{r_o}}{k_{r_w}} \frac{\mu_w}{\mu_o}} = \frac{1}{1 + \frac{\lambda_o}{\lambda_w}} \quad (3.18)$$

The construction of Eq. (3.18) is based on the following simplifying assumptions: Darcy's Law adequately describes flow rate, and capillary pressure and gravity are negligible. Given these assumptions, we can calculate f_w at reservoir conditions.

Fractional Flow Equation with Gravity

Gravity can be included in the fractional flow equation as follows. First, let us consider the two-phase flow of oil and water in a tilted linear system. Darcy's Law including capillary pressure and gravity effects for linear flow is

$$\begin{aligned} q_w &= - \frac{k k_{r_w} A}{\mu_w} \left(\frac{\partial P_w}{\partial x} + \rho_w g \sin \alpha \right), \\ q_o &= - \frac{k k_{r_o} A}{\mu_o} \left(\frac{\partial P_o}{\partial x} + \rho_o g \sin \alpha' \right) \end{aligned} \quad (3.19)$$

where

- α dip angle of formation
- g gravitational constant

If we differentiate capillary pressure for a water-wet system with respect to position x along the dipping bed, we find

$$\frac{\partial P_{cow}}{\partial x} = \frac{\partial P_o}{\partial x} - \frac{\partial P_w}{\partial x} \tag{3.20}$$

Combining Eqs. (3.19) and (3.20) gives

$$\frac{\partial P_{cow}}{\partial x} = - \frac{(q_t - q_w)\mu_o}{Akk_{ro}} - \rho_o g \sin \alpha + \frac{q_w \mu_w}{Akk_w} + \rho_w g \sin \alpha \tag{3.21}$$

where we have used $q_t = q_o + q_w$. If we write the density difference as

$$\Delta \rho = \rho_w - \rho_o, \tag{3.22}$$

collect terms, and simplify we obtain

$$\frac{q_w}{Ak} \left(\frac{\mu_o}{k_{ro}} + \frac{\mu_w}{k_{rw}} \right) = \frac{q_t \mu_o}{Akk_{ro}} + \frac{\partial P_{cow}}{\partial x} - g \Delta \rho \sin \alpha \tag{3.23}$$

Rearranging and collecting terms gives the fractional flow to water f_w in conventional oilfield units:

$$f_w = \frac{q_w}{q_t} = \frac{1 + 0.001127 \frac{Akk_{ro}}{\mu_o q_t} \left(\frac{\partial P_{cow}}{\partial x} - 0.433(\gamma_w - \gamma_o) \sin \alpha \right)}{1 + \frac{k_{ro}}{k_{rw}} \frac{\mu_w}{\mu_o}} \tag{3.24}$$

where

- A cross-sectional area of flow system [ft²]
- k absolute permeability [md]
- k_{ro} relative permeability to oil
- k_{rw} relative permeability to water
- μ_o oil viscosity [cp]
- μ_w water viscosity [cp]
- P_{cow} oil-water capillary pressure [psi] = $P_o - P_w$

- x direction of linear flow [ft]
- α dip angle of formation [degrees]
- γ_o oil specific gravity (water = 1)
- γ_w water specific gravity (water = 1)

The general expression for f_w includes all three terms governing immiscible displacement, namely the viscous term $(k_{ro}/k_{rw})(\mu_w/\mu_o)$, the capillary pressure term $\partial P_{cow}/\partial x$, and the gravity term $(\gamma_w - \gamma_o) \sin \alpha$.

It is interesting to note that the capillary pressure and gravity terms are multiplied by $1/q_t$ in Eq. (3.24). Most waterfloods have sufficiently high flow rates that capillary pressure and gravity effects can be neglected, leaving the simplified expression:

$$f_w \approx \frac{1}{1 + \frac{k_{ro}}{k_{rw}} \frac{\mu_w}{\mu_o}} \tag{3.25}$$

Equation (3.25) is in agreement with Eq. (3.18), as it should be.

Gas Fractional Flow

A similar analysis can be performed to determine the fractional flow of gas f_g . The result for a gas-oil system is

$$f_g = \frac{1 + 0.001127 \frac{Akk_{ro}}{\mu_o q_t'} \left(\frac{\partial P_{cgo}}{\partial x} - 0.433(\gamma_g - \gamma_o) \sin \alpha \right)}{1 + \frac{k_{ro}}{k_{rg}} \frac{\mu_g}{\mu_o}} \tag{3.26}$$

where

- k_{rg} relative permeability to gas
- μ_g gas viscosity [cp]
- P_{cgo} gas-oil capillary pressure = $P_g - P_o$ [psi]
- γ_g gas specific gravity [water = 1]
- q_g gas volumetric flow rate [RB/D]
- q_t' total volumetric flow rate = $q_o + q_g$ [RB/D]

Immiscible displacement of oil by gas is analogous to water displacing oil with

the water terms replaced by gas terms. In general, the gravity term in f_g should not be neglected unless q_t' is very high because of the specific gravity difference between gas and oil.

Exercises

Exercise 3.1 Estimate the parachors for butane and decane.

Exercise 3.2 Derive the relationship between the equivalent height of a transition zone and pore radius by using Eq. (3.5) to eliminate capillary pressure from Eq. (3.7).

Exercise 3.3 Suppose $k_{rw}(S_{or}) \approx k_{ro}(S_{wc})$ in Eq. (3.14) and water viscosity is 1 cp. Plot $M_{w,o}$ versus oil viscosity for oil viscosity ranging from 0.1 cp to 100 cp.

Exercise 3.4 Derive Eq. (3.21) from Eqs. (3.19) and (3.20).

Chapter 4

Derivation of the Flow Equations

Many derivations of the oil, water, and gas fluid flow equations exist in the literature [for example, see Crichlow, 1977; Peaceman, 1977]. Consequently, only a brief discussion will be presented here. It closely follows the presentation originally published in Fanchi, et al. [1982].

4.1 Conservation of Mass

We begin by considering the flow of fluid into and out of a single reservoir block (Figure 4-1). Let the symbol J denote fluid flux. Flux is defined as the rate

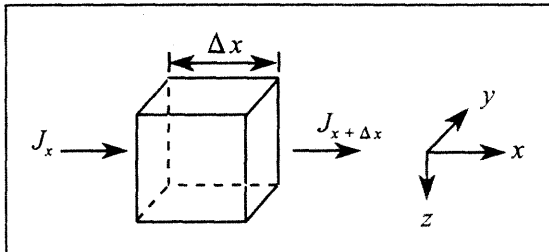


Figure 4-1. Reservoir block: the coordinate convention follows Sawyer and Mercer [1978].

of flow of mass per unit cross-sectional area normal to the direction of flow, which is the x direction in the present case. Assume fluid flows into the block at x (J_x) and out of the block at $x + \Delta x$ ($J_{x+\Delta x}$). By conservation of mass, we have the equality:

mass entering the block - mass leaving the block
 = accumulation of mass in the block.

If the block has length Δx , width Δy , and depth Δz , then we can write the mass entering the block in a time interval Δt as

$$\left[(J_x)_x \Delta y \Delta z + (J_y)_y \Delta x \Delta z + (J_z)_z \Delta x \Delta y \right] \Delta t = \text{Mass in} \quad (4.1)$$

where we have generalized to allow flux in the y and z directions as well. The notation $(J_x)_x$ denotes the x direction flux at location x , with analogous meanings for the remaining terms.

Corresponding to mass entering is a term for mass exiting which has the form

$$\begin{aligned} & [(J_x)_{x+\Delta x} \Delta y \Delta z + (J_y)_{y+\Delta y} \Delta x \Delta z + (J_z)_{z+\Delta z} \Delta x \Delta y] \Delta t \\ & + q \Delta x \Delta y \Delta z \Delta t = \text{Mass out} \end{aligned} \quad (4.2)$$

We have added a source/sink term q which represents mass flow into (source) or out of (sink) a well. A producer is represented by $q > 0$, and an injector by $q < 0$.

Accumulation of mass in the block is the change in concentration of phase ℓ (C_ℓ) in the block over the time interval Δt . If the concentration C_ℓ is defined as the total mass of phase ℓ (oil, water, or gas) in the entire reservoir block divided by the block volume, then the accumulation term becomes

$$[(C_\ell)_{t+\Delta t} - (C_\ell)_t] \Delta x \Delta y \Delta z = \text{Mass accumulation} \quad (4.3)$$

Using Eqs. (4.1) through (4.2) in the mass conservation equality

$$\text{Mass in} - \text{Mass out} = \text{Mass accumulation}$$

gives

$$\begin{aligned} & [(J_x)_x \Delta y \Delta z + (J_y)_y \Delta x \Delta z + (J_z)_z \Delta x \Delta y] \Delta t \\ - & [(J_x)_{x+\Delta x} \Delta y \Delta z + (J_y)_{y+\Delta y} \Delta x \Delta z + (J_z)_{z+\Delta z} \Delta x \Delta y] \Delta t \\ & - q \Delta x \Delta y \Delta z \Delta t = [(C_\ell)_{t+\Delta t} - (C_\ell)_t] \Delta x \Delta y \Delta z \end{aligned} \quad (4.4)$$

Dividing Eq. (4.4) by $\Delta x \Delta y \Delta z \Delta t$ and rearranging gives

$$\begin{aligned}
 - \frac{(J_x)_{x+\Delta x} - (J_x)_x}{\Delta x} - \frac{(J_y)_{y+\Delta y} - (J_y)_y}{\Delta y} \\
 - \frac{(J_z)_{z+\Delta z} - (J_z)_z}{\Delta z} - q = \frac{(C_t)_{t+\Delta t} - (C_t)_t}{\Delta t}
 \end{aligned}
 \tag{4.5}$$

In the limit as Δx , Δy , Δz , and Δt go to zero, Eq. (4.5) becomes the continuity equation

$$- \frac{\partial J_x}{\partial x} - \frac{\partial J_y}{\partial y} - \frac{\partial J_z}{\partial z} - q = \frac{\partial C_t}{\partial t}
 \tag{4.6}$$

The oil, water, and gas phases each satisfy a mass conservation equation having the form of Eq. (4.6).

4.2 Flow Equations for Three-Phase Flow

The flow equations for an oil, water, and gas system are determined by specifying the fluxes and concentrations of the conservation equations for each of the three phases. A flux in a given direction can be written as the density of the fluid times its velocity in the given direction. Letting the subscripts o , w , and g denote oil, water, and gas, respectively, the fluxes become:

$$(\vec{J})_o = \frac{\rho_{osc}}{B_o} \vec{v}_o
 \tag{4.7}$$

$$(\vec{J})_w = \frac{\rho_{wsc}}{B_w} \vec{v}_w
 \tag{4.8}$$

$$(\vec{J})_g = \frac{\rho_{gsc}}{B_g} \vec{v}_g + \frac{R_{so}\rho_{gsc}}{B_o} \vec{v}_o + \frac{R_{sw}\rho_{gsc}}{B_w} \vec{v}_w
 \tag{4.9}$$

where R_{so} and R_{sw} are gas solubilities; B_o , B_w , and B_g are formation volume factors; the subscript sc denotes standard conditions (usually 60°F and 14.7 psia in oilfield units); and ρ denotes fluid densities. The velocities \vec{v} are assumed to be Darcy velocities and their x components are

$$v_{xo} = -K_x \lambda_o \frac{\partial}{\partial x} \left[P_o - \frac{\rho_o g z}{144 g_c} \right] \quad (4.10)$$

$$v_{xw} = -K_x \lambda_w \frac{\partial}{\partial x} \left[P_w - \frac{\rho_w g z}{144 g_c} \right] \quad (4.11)$$

$$v_{xg} = -K_x \lambda_g \frac{\partial}{\partial x} \left[P_g - \frac{\rho_g g z}{144 g_c} \right] \quad (4.12)$$

where g is the acceleration of gravity in ft/sec^2 , and g_c is $32.174 \text{ ft}/\text{sec}^2$ (WINB4D assumes $g = g_c$). These equations should be valid for describing fluid flow in porous media even if g and g_c change, such as on the Moon, Mars, or the space shuttle. Similar expressions can be written for the y and z components.

The phase mobility λ_i is defined as the ratio of the relative permeability to flow of the phase divided by its viscosity, thus

$$\lambda_i = k_{ri} / \mu_i \quad (4.13)$$

The phase densities are related to formation volume factors and gas solubilities by

$$\rho_o = \frac{1}{B_o} [\rho_{osc} + R_{so} \rho_{gsc}], \quad (4.14)$$

$$\rho_w = \frac{1}{B_w} [\rho_{wsc} + R_{sw} \rho_{gsc}], \quad (4.15)$$

$$\rho_g = \frac{\rho_{gsc}}{B_g}. \quad (4.16)$$

Besides fluxes, we also need concentrations. These are given by

$$C_o = \phi \rho_{osc} S_o / B_o, \quad (4.17)$$

$$C_w = \phi \rho_{wsc} S_w / B_w, \quad (4.18)$$

$$C_g = \phi \rho_{gsc} \left[\frac{S_g}{B_g} + R_{so} \frac{S_o}{B_o} + R_{sw} \frac{S_w}{B_w} \right] \quad (4.19)$$

where ϕ is the porosity and S_ℓ is the saturation of phase ℓ . The saturations satisfy the constraint

$$S_o + S_w + S_g = 1 \quad (4.20)$$

Combining Eqs. (4.6), (4.7) through (4.9), and (4.17) through (4.19) gives a mass conservation equation for each phase:

Oil

$$\begin{aligned} & - \left[\frac{\partial}{\partial x} \left(\frac{\rho_{osc}}{B_o} v_{xo} \right) + \frac{\partial}{\partial y} \left(\frac{\rho_{osc}}{B_o} v_{yo} \right) + \frac{\partial}{\partial z} \left(\frac{\rho_{osc}}{B_o} v_{zo} \right) \right] \\ & - q_o = \frac{\partial}{\partial t} \left(\phi \rho_{osc} \frac{S_o}{B_o} \right) \end{aligned} \quad (4.21)$$

Water

$$\begin{aligned} & - \left[\frac{\partial}{\partial x} \left(\frac{\rho_{wsc}}{B_w} v_{xw} \right) + \frac{\partial}{\partial y} \left(\frac{\rho_{wsc}}{B_w} v_{yw} \right) + \frac{\partial}{\partial z} \left(\frac{\rho_{wsc}}{B_w} v_{zw} \right) \right] \\ & - q_w = \frac{\partial}{\partial t} \left(\phi \rho_{wsc} \frac{S_w}{B_o} \right) \end{aligned} \quad (4.22)$$

Gas

$$\begin{aligned} & - \frac{\partial}{\partial x} \left(\frac{\rho_{gsc}}{B_g} v_{xg} + \frac{R_{so} \rho_{gsc}}{B_o} v_{xo} + \frac{R_{sw} \rho_{gsc}}{B_w} v_{xw} \right) \\ & - \frac{\partial}{\partial y} \left(\frac{\rho_{gsc}}{B_g} v_{yg} + \frac{R_{so} \rho_{gsc}}{B_o} v_{yo} + \frac{R_{sw} \rho_{gsc}}{B_w} v_{yw} \right) \\ & - \frac{\partial}{\partial z} \left(\frac{\rho_{gsc}}{B_g} v_{zg} + \frac{R_{so} \rho_{gsc}}{B_o} v_{zo} + \frac{R_{sw} \rho_{gsc}}{B_w} v_{zw} \right) - q_g \\ & = \frac{\partial}{\partial t} \left[\phi \rho_{gsc} \left(\frac{S_g}{B_g} + \frac{R_{so} S_o}{B_o} + \frac{R_{sw} S_w}{B_w} \right) \right] \end{aligned} \quad (4.23)$$

The densities at standard conditions are constants and can be divided out of the above equations. This reduces the equations to the following form:

Oil

$$\begin{aligned}
 & - \left[\frac{\partial}{\partial x} \left(\frac{v_{xo}}{B_o} \right) + \frac{\partial}{\partial y} \left(\frac{v_{yo}}{B_o} \right) + \frac{\partial}{\partial z} \left(\frac{v_{zo}}{B_o} \right) \right] \\
 & - \frac{q_o}{\rho_{osc}} = \frac{\partial}{\partial t} \left(\phi \frac{S_o}{B_o} \right)
 \end{aligned} \tag{4.24}$$

Water

$$\begin{aligned}
 & - \left[\frac{\partial}{\partial x} \left(\frac{v_{xw}}{B_w} \right) + \frac{\partial}{\partial y} \left(\frac{v_{yw}}{B_w} \right) + \frac{\partial}{\partial z} \left(\frac{v_{zw}}{B_w} \right) \right] \\
 & - \frac{q_w}{\rho_{wsc}} = \frac{\partial}{\partial t} \left(\phi \frac{S_w}{B_w} \right)
 \end{aligned} \tag{4.25}$$

Gas

$$\begin{aligned}
 & - \frac{\partial}{\partial x} \left(\frac{v_{xg}}{B_g} + \frac{R_{so}}{B_o} v_{xo} + \frac{R_{sw}}{B_w} v_{xw} \right) \\
 & - \frac{\partial}{\partial y} \left(\frac{v_{yg}}{B_g} + \frac{R_{so}}{B_o} v_{yo} + \frac{R_{sw}}{B_w} v_{yw} \right) \\
 & - \frac{\partial}{\partial z} \left(\frac{v_{zg}}{B_g} + \frac{R_{so}}{B_o} v_{zo} + \frac{R_{sw}}{B_w} v_{zw} \right) \\
 & - \frac{q_g}{\rho_{gsc}} = \frac{\partial}{\partial t} \left[\phi \left(\frac{S_g}{B_g} + R_{so} \frac{S_o}{B_o} + R_{sw} \frac{S_w}{B_w} \right) \right]
 \end{aligned} \tag{4.26}$$

4.3 Flow Equations in Vector Notation

Equations (4.10) through (4.16), (4.20), and (4.24) through (4.26) are the basic fluid flow equations which are numerically solved in a black oil simulator. A glance at Eqs. (4.24) through (4.26) illustrates the computational complexity

of the basic three-dimensional, three-phase black oil simulator equations. Equivalent but much simpler appearing forms of the flow equations are presented in terms of vector operators as

$$-\nabla \cdot \frac{\vec{v}_o}{B_o} - \frac{q_o}{\rho_{osc}} = \frac{\partial}{\partial t} \left(\phi \frac{S_o}{B_o} \right), \quad (4.27)$$

$$-\nabla \cdot \frac{\vec{v}_w}{B_w} - \frac{q_w}{\rho_{wsc}} = \frac{\partial}{\partial t} \left(\phi \frac{S_w}{B_w} \right), \quad (4.28)$$

and

$$\begin{aligned} -\nabla \cdot \left(\frac{\vec{v}_g}{B_g} + \frac{R_{so}}{B_o} \vec{v}_o + \frac{R_{sw}}{B_w} \vec{v}_w \right) - \frac{q_g}{\rho_{gsc}} \\ = \frac{\partial}{\partial t} \left[\phi \left(\frac{S_g}{B_g} + R_{so} \frac{S_o}{B_o} + R_{sw} \frac{S_w}{B_w} \right) \right] \end{aligned} \quad (4.29)$$

where the symbol $\nabla \cdot \vec{v}$ for the divergence of the velocity vector is shorthand for the expression

$$\nabla \cdot \vec{v} = \frac{\partial}{\partial x} v_x + \frac{\partial}{\partial y} v_y + \frac{\partial}{\partial z} v_z. \quad (4.30)$$

A review of vector analysis can be found in many references, such as Kreyszig [1999] and Fanchi [2000].

Exercises

Exercise 4.1 Suppose the unit of density ρ_{osc} is mass per volume at standard conditions, and the unit of Darcy velocity is length per time. Use dimensional analysis to determine the unit of flux in Eq. (4.7).

Exercise 4.2 The densities in Eqs. (4.14) and (4.15) include gas dissolution. Rewrite Eqs. (4.19), (4.23), and (4.29) for a system with no gas dissolved in either the oil or water phases.

38 *Principles of Applied Reservoir Simulation*

Exercise 4.3 Run EXAM3.DAT and record the time, pressure, oil rate, water rate, gas rate, and GOR at the end of the run. These values are obtained from the one line timestep summary file WTEMP.TSS (also see Chapter 26.2). Is gas significant in this model?

Chapter 5

Fluid Displacement

Fluid displacement processes require contact between the displacing fluid and the displaced fluid. The movement of the interface between displacing and displaced fluids and the breakthrough time associated with the production of injected fluids at producing wells are indicators of sweep efficiency. This chapter shows how to calculate such indicators using two analytical techniques: Buckley-Leverett theory with Welge's method for immiscible fluid displacement, and solution of the convection-dispersion equation for miscible fluid displacement.

5.1 Buckley-Leverett Theory

One of the simplest and most widely used methods of estimating the advance of a fluid displacement front in an immiscible displacement process is the Buckley-Leverett method. Buckley-Leverett Theory [1942] estimates the rate at which an injected water bank moves through a porous medium. The approach uses fractional flow theory and is based on the following assumptions:

- Flow is linear and horizontal
- Water is injected into an oil reservoir
- Oil and water are both incompressible
- Oil and water are immiscible
- Gravity and capillary pressure effects are negligible

The following analysis can be found in a variety of sources, such as Collins [1961], Dake [1978], Wilhite [1986], and Craft, et al. [1991].

Frontal advance theory is an application of the law of conservation of mass. Flow through a small volume element (Figure 5-1) with length Δx and

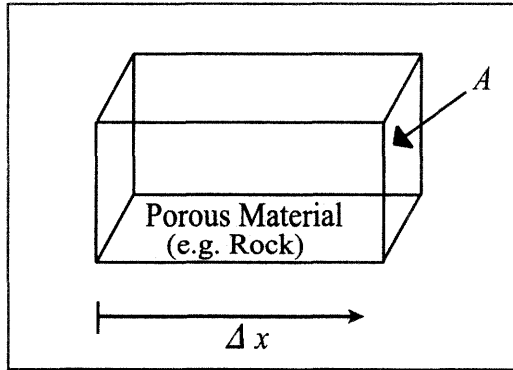


Figure 5-1. Flow Geometry

cross-sectional area A can be expressed in terms of total flow rate q_t , as

$$q_t = q_o + q_w \tag{5.1}$$

where q denotes volumetric flow rate at reservoir conditions and the subscripts $\{o, w, t\}$ refer to oil, water, and total rate, respectively. The rate of water entering the element on the left hand side (LHS) is

$$q_t f_w = \text{entering LHS} \tag{5.2}$$

for a fractional flow to water f_w . The rate of water leaving the element on the right hand side (RHS) is

$$q_t (f_w + \Delta f_w) = \text{leaving RHS} \tag{5.3}$$

The change in water flow rate across the element is found by balancing mass for an immiscible, incompressible system, thus

$$\begin{aligned} \text{rate change} &= \text{water entering} - \text{water leaving} \\ &= q_t f_w - q_t (f_w + \Delta f_w) \\ &= -q_t \Delta f_w \end{aligned} \tag{5.4}$$

The change in water saturation per unit time is the rate change in Eq. (5.4) divided by the pore volume of the element, thus

$$\frac{\Delta S_w}{\Delta t} = \frac{-q_t}{A\phi} \frac{\Delta f_w}{\Delta x} \tag{5.5}$$

In the limit as $\Delta t \rightarrow 0$ and $\Delta x \rightarrow 0$, we pass to the differential form of Eq. (5.5) for the water phase:

$$\frac{\partial S_w}{\partial t} = \frac{-q_t}{A\phi} \frac{\partial f_w}{\partial x} \quad (5.6)$$

A similar equation applies to the oil phase:

$$\frac{\partial S_o}{\partial t} = \frac{-q_t}{A\phi} \frac{\partial f_o}{\partial x} \quad (5.7)$$

Since f_w depends only on S_w , we can write the derivative of fractional flow as

$$\frac{\partial f_w}{\partial x} = \frac{df_w}{dS_w} \frac{\partial S_w}{\partial x} \quad (5.8)$$

Substituting $\partial f_w/\partial x$ into $\partial S_w/\partial x$ yields

$$\frac{\partial S_w}{\partial t} = \frac{-q_t}{A\phi} \frac{df_w}{dS_w} \frac{\partial S_w}{\partial x} \quad (5.9)$$

It is not possible to solve for the general distribution of water saturation $S_w(x, t)$ in most realistic cases because of the nonlinearity of the problem. For example, water fractional flow is usually a nonlinear function of water saturation. It is therefore necessary to consider a simplified approach to solving Eq. (5.9).

We begin by considering the total differential of $S_w(x, t)$:

$$\frac{dS_w}{dt} = \frac{\partial S_w}{\partial x} \frac{dx}{dt} + \frac{\partial S_w}{\partial t} \quad (5.10)$$

Equation (5.10) can be simplified by choosing x to coincide with a surface of fixed S_w so that $dS_w/dt = 0$ and

$$\left(\frac{dx}{dt} \right)_{S_w} = - \frac{\left(\frac{\partial S_w}{\partial t} \right)}{\left(\frac{\partial S_w}{\partial x} \right)} \quad (5.11)$$

Substituting Eqs. (5.8) and (5.9) into Eq. (5.11) gives the Buckley-Leverett frontal advance equation:

$$\left(\frac{dx}{dt} \right)_{S_w} = \frac{-q_t}{A\phi} \left(\frac{df_w}{dS_w} \right)_{S_w} \quad (5.12)$$

The derivative $(dx/dt)_{S_w}$ is the velocity of the moving plane S_w , and $(df_w/dS_w)_{S_w}$ is the slope of the fractional flow curve. The integral of the frontal advance equation gives

$$x_{S_w} = \frac{W_i}{A\phi} \left(\frac{df_w}{dS_w} \right)_{S_w} \quad (5.13)$$

where

x_{S_w}	distance traveled by a particular S_w contour [ft]
W_i	cumulative water injected [cu ft]
$(df_w/dS_w)_{S_w}$	slope of fractional flow curve

Water Saturation Profile

A plot of S_w versus distance using Eq. (5.13) and typical fractional flow curves leads to the physically impossible situation of multiple values of S_w at a given location. A discontinuity in S_w at a cutoff location x_c is needed to make the water saturation distribution single valued and to provide a material balance for wetting fluids. The procedure is described by Collins [1961] and summarized below.

5.2 Welge's Method

In 1952, Welge published an approach that is widely used to perform the Buckley-Leverett frontal advance calculation. Welge's approach is best demonstrated using a plot of f_w vs S_w (Figure 5-2).

A line is drawn from the water saturation S_w before the waterflood – irreducible water saturation S_{wirr} – and tangent to a point on the f_w curve. The resulting tangent line is called the breakthrough tangent, or slope. It is illustrated in Figure 5-2. Water saturation at the flood front S_{wf} is the point of tangency on the f_w curve. Fractional flow of water at the flood front is f_{wf} and occurs at the point of tangency S_{wf} on the f_w curve. In Figure 5-2, S_{wf} is 65% and f_{wf} is 95%

Average water saturation behind the flood front S_{wbt} is the intercept of the main tangent line with the upper limiting line where $f_w = 1.0$. In Figure 5-2, average S_{wbt} is 67%.

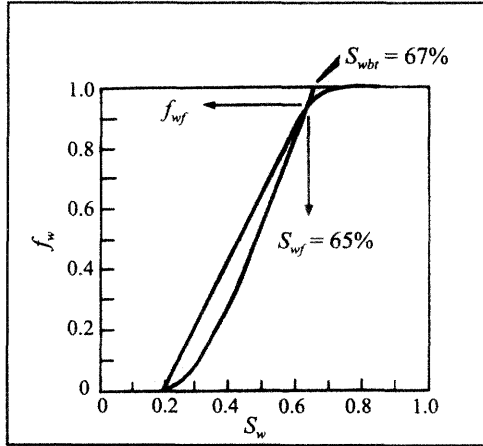


Figure 5-2. Welge's Method

In summary, when water reaches the producer, Welge's approach gives the following results:

- Water saturation at the producing well is S_{wf}
- Average water saturation behind the front is S_{wbt}
- Producing water cut at reservoir conditions is f_{wf}

Other useful information about the waterflood can be obtained from Welge's approach.

The time to water breakthrough at the producer is

$$t_{bt} = \frac{LA\phi}{q_i \left(\frac{df_w}{dS_w} \right)_{S_{wf}}}, \quad (5.14)$$

where

- q_i injection rate
- $\left(\frac{df_w}{dS_w} \right)_{S_{wf}}$ slope of main tangent line

L linear distance from injection well to production well

Cumulative water injected is given by

$$Q_i = \frac{1}{\left(\frac{df_w}{dS_w}\right)_{S_{wf}}} \tag{5.15}$$

where Q_i is the cumulative pore volume of injected water. The slope of the water fractional flow curve with respect to water saturation evaluated at the water saturation at breakthrough gives Q_i at breakthrough.

Effects of Capillary Pressure and Gravity

In the absence of capillary pressure and gravity effects, the flood front propagates as a "sharp" step function, or piston-like displacement. The presence of capillary pressure leads to the imbibition of water ahead of the front. This causes a change in the behavior of produced fluid ratios. Rather than an abrupt increase in WOR associated with piston-like displacement, the WOR will increase gradually as the leading edge of the mobile water reaches the well and is produced. In addition, the WOR will begin to increase sooner than it would have in the absence of capillary pressure. By contrast, gravity causes high S_w values to lag behind the front. The result is a smeared or "dispersed" flood front.

5.3 Miscible Displacement

Buckley-Leverett theory treats the displacement of one fluid by another under immiscible, piston-like conditions. An immiscible displacement occurs when the displaced and displacing fluids do not mix. The result is a readily discernible interface between the two fluids. In a miscible displacement, the fluids mix and the interfacial tension approaches zero at the interface. A miscible displacement system is described by a convection-dispersion (C-D) equation. As an illustration, consider the one-dimensional C-D equation for the concentration C of the displacing fluid:

$$D \frac{\partial^2 C}{\partial x^2} - v \frac{\partial C}{\partial x} = \frac{\partial C}{\partial t} \tag{5.16}$$

We assume here that dispersion D and velocity v are real, scalar constants. The diffusion term has the Fickian form $D \cdot \partial^2 C / \partial x^2$ and the convection term is $v \partial C / \partial x$. When the diffusion term is much larger than the convection term, the

$v \partial C / \partial x$. When the diffusion term is much larger than the convection term, the C - D equation behaves like the heat conduction equation, which is a parabolic partial differential equation (PDE). If the diffusion term is much smaller than the convection term, the C - D equation behaves like a first-order hyperbolic PDE.

The C - D equation is especially valuable for studying numerical solutions of fluid flow equations because the C - D equation can be solved analytically and the C - D equation may be used to examine two important classes of PDEs (parabolic and hyperbolic). To solve the C - D equation, we must specify two boundary conditions and an initial condition. The two boundary conditions are needed because the C - D equation is second-order in the space derivative. The initial condition satisfies the need for a boundary condition in time associated with the first-order derivative in time. The boundary conditions for the miscible displacement process are that the initial concentration of displacing fluid is equal to one at the inlet ($x = 0$), and zero for all other values of x . The mathematical expressions for these boundary conditions are concentration $C(0, t) = 1$ at the inlet, concentration $C(\infty, t) = 0$ at the edge of the linear system for all times t greater than the initial time $t = 0$, and the initial condition $C(x, 0) = 0$ for all values of x greater than 0.

The propagation of the miscible displacement front is calculated by solving the C - D equation. The analytical solution of the one-dimensional C - D equation is [Peaceman, 1977]

$$C(x, t) = \frac{1}{2} \left\{ \operatorname{erfc} \left[\frac{x - vt}{2\sqrt{Dt}} \right] + e^{(vx/D)} \operatorname{erfc} \left[\frac{x + vt}{2\sqrt{Dt}} \right] \right\} \quad (5.17)$$

where the complementary error function $\operatorname{erfc}(y)$ is defined as

$$\operatorname{erfc}(y) = 1 - \frac{2}{\sqrt{\pi}} \int_0^y e^{-z^2} dz \quad (5.18)$$

Abramowitz and Stegun [1972] have presented an accurate numerical algorithm for calculating the complementary error function $\operatorname{erfc}(y)$. A comparison of the analytical solution of the C - D equation with numerical solutions is given in Fanchi [2000].

Exercises

Exercise 5.1 Consider an oil-water system in which oil viscosity is 0.64 cp and water viscosity is 0.5 cp. Oil relative permeability (k_{row}) and water relative permeability (k_{rw}) are given in the following table as a function of water saturation (S_w). Complete the table by using the viscosity and relative permeability information to calculate oil mobility (λ_o), water mobility (λ_w), total mobility (λ_t), water fractional flow (f_w), and oil fractional flow (f_o). Total mobility is the sum of oil mobility and water mobility. Assume absolute permeability is 100 md.

S_w	k_{rw}	k_{row}	λ_w	λ_o	λ_t	f_w	f_o
0.30	0.000	1.000					
0.35	0.005	0.590					
0.40	0.010	0.320					
0.45	0.017	0.180					
0.50	0.023	0.080					
0.55	0.034	0.030					
0.60	0.045	0.010					
0.65	0.064	0.001					
0.70	0.083	0.000					
0.80	0.120	0.000					

Exercise 5.2 Plot λ_o , λ_w , and λ_t in Exercise 5.1 as a function of S_w . What is the mobility ratio of the oil-water system? Hint: See Eq. (3.14).

Exercise 5.3 Plot f_o and f_w in Exercise 5.1 as a function of S_w . Use the plot of f_w versus S_w and Welge's method to determine water saturation at the producing well, average water saturation behind the front, and producing water cut at reservoir conditions.

Exercise 5.4 Run EXAM3.DAT and plot water saturation as a function of distance between wells at the midpoint of the run and at the end of the run. Hint: water saturation is reported in the run output file WTEMP.ROF.

Chapter 6

Frontal Stability

The stability of a flood front can influence the efficiency of fluid displacement. A front is stable if it retains the shape of the interface between displaced and displacing fluids as the front moves through the medium. An analysis of frontal stability is presented in this chapter in terms of a specific example – the advance of a water-oil displacement front in the absence of gravity and in the presence of gravity. The stability of the front is then studied using linear stability analysis.

6.1 Frontal Advance Neglecting Gravity

The displacement of one phase by another may be analytically studied if a linear, homogenous porous medium is assumed. Let us first consider the displacement of oil by water in a horizontal porous medium of length L . We assume piston-like displacement of a front located at x_f . Application of Darcy's law and the continuity equation leads to a pressure distribution described by Poisson's equation. The absence of sources or sinks in the medium reduces Poisson's equation to the Laplace equation for the water phase pressure:

$$\frac{\partial^2 P_w}{\partial x^2} = 0, 0 < x < x_f \quad (6.1)$$

The corresponding equation for oil phase pressure is

$$\frac{\partial^2 P_o}{\partial x^2} = 0, x_f < x < L \quad (6.2)$$

Equations (6.1) and (6.2) apply to those parts of the medium containing water and oil respectively. They assume that the fluids are incompressible, and that the oil-water interface is a piston-like displacement in the x -direction. The piston-like displacement assumption implies a discontinuous change from mobile oil to mobile water at the displacement front. This concept differs from the Buckley-Leverett analysis presented in Chapter 5. Buckley-Leverett theory with Welge's method shows the existence of a transition zone as saturations grade from mobile oil to mobile water. The saturation profile at the interface between the immiscible phases depends on the fractional flow characteristics of the system. The present method has less structure in the saturation profile, but is more readily suited for analyzing the stability of the displacement front.

Boundary conditions at the displacement front are given by continuity of phase pressure

$$P_o = P_w \text{ at } x = x_f(t) \quad (6.3)$$

and continuity of phase velocity

$$v_w = v_o \text{ or } \lambda_w \frac{\partial P_w}{\partial x} = \lambda_o \frac{\partial P_o}{\partial x} \quad (6.4)$$

where λ_ℓ is the mobility of phase ℓ . Equation (6.3) is valid when we neglect capillary pressure, and the effect of gravity has been excluded from Eq. (6.4). The exclusion of gravity corresponds physically to flow in a horizontal medium. Boundary conditions at the edges of the porous medium are

$$P_w = P_1 \text{ at } x = 0 \quad (6.5)$$

and

$$P_o = P_2 \text{ at } x = L \quad (6.6)$$

Equations (6.1) through (6.6) may be solved analytically. We begin by integrating Eqs. (6.1) and (6.2) to find the general solutions

$$P_w = A_w x + B_w \quad (6.7)$$

and

$$P_o = A_o x + B_o \quad (6.8)$$

where the constant coefficients $\{A_i, B_i\}$ are determined by applying the boundary conditions. Substituting Eq. (6.5) in Eq. (6.7) gives

$$B_w = P_1 \quad (6.9)$$

The remaining coefficients are found by simultaneously solving Eqs. (6.4), (6.7), and (6.8) subject to Eqs. (6.3), (6.5), and (6.6). The resulting coefficients are

$$A_w = -\frac{\Delta P}{ML + (1 - M)x_f} \quad (6.10)$$

$$A_o = M A_w \quad (6.11)$$

$$B_o = P_1 = (A_w - A_o)x_f = P_1 + (1 - M)A_w x_f \quad (6.12)$$

where M is the mobility ratio

$$M = \frac{\lambda_w}{\lambda_o} \quad (6.13)$$

and the pressure difference is

$$\Delta P = P_1 - P_2 \quad (6.14)$$

The frontal velocity v_f is given by

$$v_f \equiv \frac{dx_f}{dt} = \frac{v_w}{\phi(1 - S_{or} - S_{wc})} \quad (6.15)$$

where S_{or} is residual oil saturation, S_{wc} is connate water saturation, and v_w is the Darcy velocity:

$$v_w = -\lambda_w \frac{\partial P_w}{\partial x} = -\lambda_w A_w \quad (6.16)$$

Substituting Eq. (6.16) into (6.15) gives

$$\frac{dx_f}{dt} = \frac{\lambda_w \Delta P}{\phi(1 - S_{or} - S_{wc})} \frac{1}{[ML + (1 - M)x_f]} \quad (6.17)$$

The integral of Eq. (6.17) with respect to time gives the frontal advance.

6.2 Frontal Advance Including Gravity

Gravity is included in the analysis of frontal advance in a dipping reservoir (Figure 6-1) by replacing phase pressure in Eqs. (6.1) through (6.6) with phase

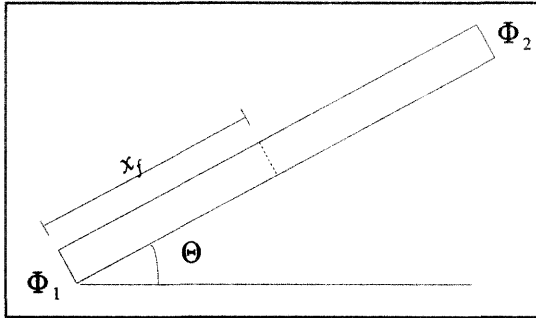


Figure 6-1. Geometry of Frontal Advance

potential

$$\Phi_\ell = P_\ell - \rho_\ell g x \sin\theta$$

The resulting equations for phase potentials are

$$\frac{\partial^2 \Phi_w}{\partial x^2} = 0, 0 < x < x_f \tag{6.18}$$

$$\frac{\partial^2 \Phi_o}{\partial x^2} = 0, x_f < x < L \tag{6.19}$$

The phase potentials at the flood front are related by

$$\Phi_o = \Phi_w + (\rho_o - \rho_w) g x_f \sin\theta \tag{6.20}$$

with continuity of phase velocities

$$\lambda_w \frac{\partial \Phi_w}{\partial x} = \lambda_o \frac{\partial \Phi_o}{\partial x} \tag{6.21}$$

The boundary conditions for the phase potentials are

$$\Phi_w = \Phi_1 \text{ at } x = 0 \quad (6.22)$$

and

$$\Phi_o = \Phi_2 \text{ at } x = L \quad (6.23)$$

Capillary pressure is still neglected in this formulation. Equation (6.20) is the analog of Eq. (6.3).

The solutions of the second-order ordinary differential equations Eqs. (6.18) and (6.19) are the linear relationships

$$\Phi_w = A'_w x + B'_w \quad (6.24)$$

$$\Phi_o = A'_o x + B'_o \quad (6.25)$$

The coefficients are evaluated by substituting Eqs. (6.24) and (6.25) into Eqs. (6.18) and (6.19) and applying the boundary conditions. The coefficients are

$$A'_w = - \left[\frac{(\Phi_1 - \Phi_2) + x_f(\rho_o - \rho_w)g \sin \Theta}{ML + (1 - M)x_f} \right] \quad (6.26)$$

$$A'_o = M A'_w \quad (6.27)$$

$$B'_w = \Phi_1 \quad (6.28)$$

$$B'_o = \Phi_2 - A'_o L = \Phi_2 - M A'_w L \quad (6.29)$$

The Darcy velocity of the water phase is

$$v_w = -\lambda_w \frac{\partial \Phi_w}{\partial x} = -\lambda_w A'_w \quad (6.30)$$

The velocity of frontal advance in a dipping reservoir is found by substituting Eq. (6.30) into Eq. (6.15) to find

$$\frac{dx_f}{dt} = \frac{\lambda_w}{\phi(1 - S_{or} - S_{wc})} \left\{ \frac{(\Phi_1 - \Phi_2) + [(\rho_o - \rho_w)g \sin \Theta] x_f}{ML + (1 - M)x_f} \right\} \quad (6.31)$$

6.3 Linear Stability Analysis

The stability of frontal advance is determined by considering the rate of growth of a perturbation at the front. We first express the frontal advance velocity Eqs. (6.17) and (6.31) in the general form

$$\frac{dx_f}{dt} = \frac{\alpha + \beta x_f}{\gamma + \delta x_f} \quad (6.32)$$

where the coefficients are independent of time and frontal location. Equation (6.32) is a nonlinear, first-order differential equation. Imposing a slight perturbation on the front location gives

$$\frac{d(x_f + \varepsilon)}{dt} = \frac{\alpha + \beta(x_f + \varepsilon)}{\gamma + \delta(x_f + \varepsilon)} \quad (6.33)$$

The velocity of propagation of the perturbation is given by the difference between Eqs. (6.33) and (6.32):

$$\frac{d\varepsilon}{dt} = \frac{\alpha + \beta x_f + \beta\varepsilon}{\gamma + \delta x_f + \delta\varepsilon} - \frac{\alpha + \beta x_f}{\gamma + \delta x_f} \quad (6.34)$$

Combining fractions and simplifying yields

$$\frac{d\varepsilon}{dt} = \left\{ \frac{\beta(\gamma + \delta x_f) - \delta(\alpha + \beta x_f)}{(\gamma + \delta x_f)^2 \left[1 + \frac{\delta\varepsilon}{\gamma + \delta x_f} \right]} \right\} \varepsilon \quad (6.35)$$

Further simplification is achieved by recognizing that the perturbation is slight so that we have the approximation

$$\frac{1}{1 + \frac{\delta\varepsilon}{\gamma + \delta x_f}} \approx 1 - \frac{\delta\varepsilon}{\gamma + \delta x_f} \quad \text{for } \delta\varepsilon \ll \gamma + \delta x_f \quad (6.36)$$

Substituting Eq. (6.36) into Eq. (6.35) gives

$$\frac{d\varepsilon}{dt} = \left\{ \frac{\beta(\gamma + \delta x_f) - \delta(\alpha + \beta x_f)}{(\gamma + \delta x_f)^2} \right\} \left[1 - \frac{\delta\varepsilon}{\gamma + \delta x_f} \right] \varepsilon \quad (6.37)$$

Keeping only terms to first order in ϵ and simplifying gives

$$\frac{d\epsilon}{dt} = \frac{(\beta\gamma - \delta\alpha)\epsilon}{(\gamma + \delta x_f)^2} \quad (6.38)$$

Equation (6.38) has the solution

$$\epsilon = \epsilon_0 e^{t/\tau} \quad (6.39)$$

where ϵ_0 is an integration constant, and

$$\tau = \frac{\beta\gamma - \delta\alpha}{(\gamma + \delta x_f)^2} \quad (6.40)$$

If τ is negative, the perturbation decays exponentially. If τ is greater than zero, the perturbation grows exponentially. Finally, if τ equals zero, the perturbation does not propagate because $d\epsilon/dt = 0$ in Eq. (6.38).

We can now examine the stability of a displacement front. Comparing Eq. (6.32) with (6.31) lets us make the identifications

$$\alpha = \frac{\lambda_w(\Phi_1 - \Phi_2)}{\phi(1 - S_{or} - S_{wc})} \quad (6.41)$$

$$\beta = \frac{\lambda_w(\rho_o - \rho_w)g \sin \Theta}{\phi(1 - S_{or} - S_{wc})} \quad (6.42)$$

$$\gamma = ML \quad (6.43)$$

$$\delta = (1 - M) \quad (6.44)$$

The resulting expression for the growth of a perturbation is

$$\frac{d\epsilon}{dt} = - \frac{\lambda_w \epsilon}{\phi(1 - S_{or} - S_{wc})} \frac{(1 - M)(\Phi_1 - \Phi_2) + ML(\rho_o - \rho_w)g \sin \Theta}{[ML + (1 - M)x_f]^2} \quad (6.45)$$

Equation (6.45) agrees with Eq. (7-104) in Collins [1961].

Zero growth rate of a perturbation is determined by setting the derivative $d\epsilon/dt = 0$ in Eq. (6.45). The resulting condition for zero growth rate is

$$(1 - M)(\Phi_1 - \Phi_2) + ML(\rho_o - \rho_w)g \sin \Theta = 0 \quad (6.46)$$

If the medium is horizontal, the condition for a system without gravity is

$$(1 - M)\Delta P = 0 \quad (6.47)$$

To see the effect of mobility ratio M on finger growth for the gravity-free case, we set $g = 0$ in Eq. (6.45) to get

$$\frac{d\varepsilon}{dt} = - \frac{\lambda_w \varepsilon}{\phi(1 - S_{or} - S_{wc})} \frac{(1 - M)\Delta P}{[ML + (1 - M)x_f]^2} \quad (6.48)$$

The finger grows exponentially if $M > 1$, decays exponentially if $M < 1$, and does not propagate if $M = 1$.

Exercises

Exercise 6.1 Show that Eq. (6.7) is a solution of Eq. (6.1).

Exercise 6.2 Use Eq. (6.45) to determine the rate of finger growth of a unit mobility flood in a horizontal medium. Hint: Set $M = 1$ in Eq. (6.45) and simplify.

Exercise 6.3 Use Eq. (6.48) to explain why the mobility ratio condition $M < 1$ is considered “favorable” for a displacement flood.

Chapter 7

Pattern Floods

The effectiveness of a displacement process depends on many factors. These factors include reservoir and fluid characteristics that are beyond our control, such as depth, structure, and fluid type. Other factors that influence displacement efficiency can be controlled, however. They include the number and type of wells, well rates, and well locations. The distribution of wells is known as the well pattern. The impact of well pattern on displacement effectiveness is discussed after definitions of recovery efficiency are presented.

7.1 Recovery Efficiency

Recovery efficiency is quantified by comparing initial and final volumes of fluid in place. It takes into account volumetric and displacement efficiencies. The different aspects of recovery efficiency are defined and then combined to form overall recovery efficiency.

Displacement efficiency accounts for the efficiency of recovering mobile hydrocarbon. To be specific, we define displacement efficiency for oil as the ratio of mobile oil to original oil in place at reservoir conditions:

$$E_D = \frac{V_p S_{oi} - V_p S_{or}}{V_p S_{oi}} = \frac{S_{oi} - S_{or}}{S_{oi}} \quad (7.1)$$

where

V_p initial pore volume
 S_{oi} initial oil saturation

S_{or} residual oil saturation

Displacement efficiency can approach 100% if residual oil saturation can be driven to zero. One of the goals of enhanced oil recovery processes such as micellar-polymer flooding or miscible flooding is to reduce residual oil saturation and increase displacement efficiency.

The definition of displacement efficiency can be modified to include the effects of swelling. Swelling is represented by using surface volume rather than reservoir volume in the definition of displacement efficiency. The volume conversion is achieved by dividing reservoir volume by formation volume factor. For example, the displacement efficiency of a waterflood is

$$E_D = \frac{\frac{V_p S_{oi}}{B_{oi}} - \frac{V_p S_{or}}{B_{oa}}}{\frac{V_p S_{oi}}{B_{oi}}} = \frac{\frac{S_{oi}}{B_{oi}} - \frac{S_{or}}{B_{oa}}}{\frac{S_{oi}}{B_{oi}}} \quad (7.2)$$

where

B_{oi} oil FVF at the beginning of waterflood

B_{oa} oil FVF at the waterflood pressure

Notice that oil formation volume factor is a maximum at the bubble point pressure of the oil. If the waterflood is conducted at or just above bubble point pressure, the value of B_{oa} will be maximized and the residual oil term will be minimized. The resulting displacement efficiency for a waterflood is then maximized.

Displacement efficiency is a measure of how effectively mobile hydrocarbons can be recovered. Although the above definitions of displacement efficiency have been given for oil, similar definitions can be provided for gas.

In addition to displacement efficiency, volumetric factors are needed to determine overall recovery efficiency. Areal and vertical sweep efficiencies are defined by

$$E_A = \frac{\text{swept area}}{\text{total area}} \quad (7.3)$$

and

$$E_V = \frac{\text{swept thickness}}{\text{total thickness}} \quad (7.4)$$

Reservoir flow models are useful tools for quantifying both swept area and swept thickness. The product of areal and vertical sweep efficiency is the volumetric sweep efficiency E_{vol} :

$$E_{vol} = E_A \times E_V \quad (7.5)$$

where

E_A areal sweep efficiency

E_V vertical sweep efficiency

Overall recovery efficiency must account for both volumetric and displacement effects. It is therefore defined as the product of volumetric sweep efficiency and displacement efficiency:

$$RE = E_D \times E_{vol} = E_D \times E_A \times E_V \quad (7.6)$$

where

RE recovery efficiency

Notice that each of the efficiency factors in recovery efficiency can be relatively large, and yet recovery efficiency will be relatively small. For example, suppose the areal and vertical efficiencies are each 70% and displacement efficiency is 80%, the product of these efficiencies is approximately 39%. This means that even the reservoirs with the best recovery efficiency often have a substantial volume of unrecovered hydrocarbon remaining in the ground. The most important goal of improved recovery techniques is to recover this remaining resource.

7.2 Patterns and Spacing

The displacement processes discussed in Chapters 5 and 6 study fluid displacement between one injection well and one production well. The alignment of the injector-producer pair represents a linear displacement process. It is the simplest pattern involving injection and production wells. A variety of other

patterns may be defined. Several examples are shown in Figure 7-1. A representative pattern element for the five-spot pattern is shown using lines between wells to denote boundary wells.

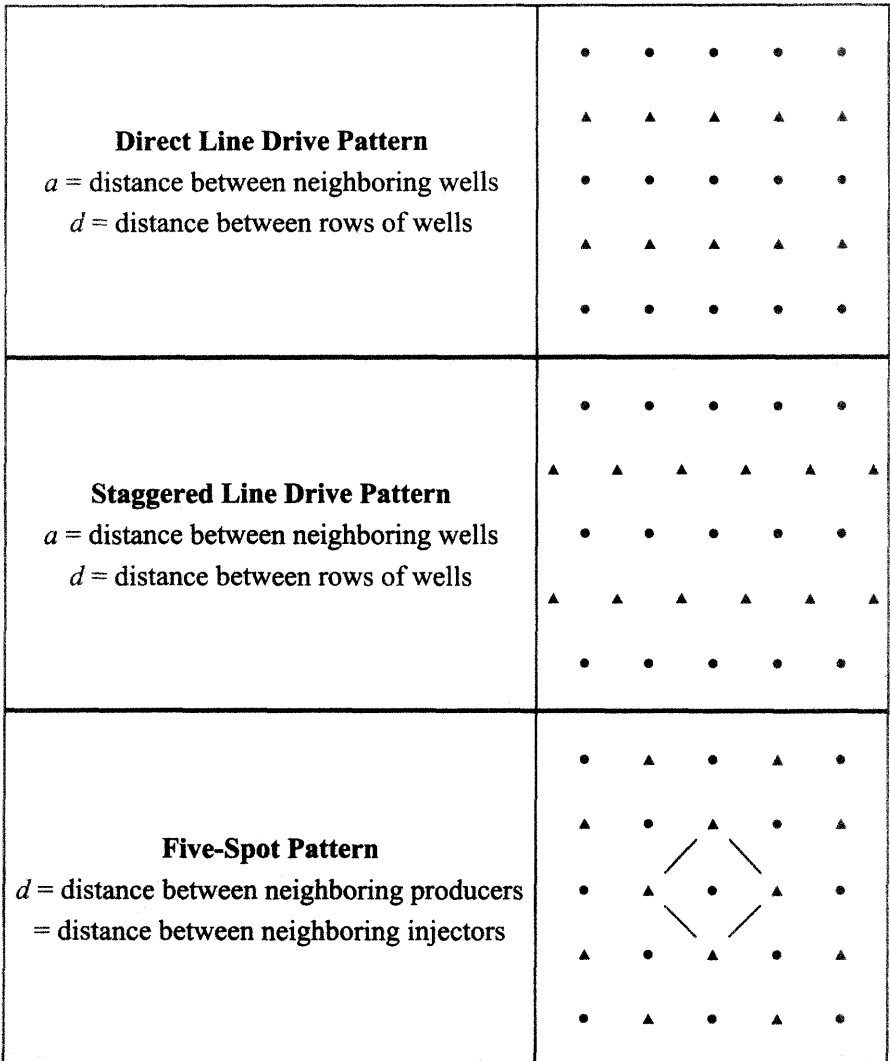


Figure 7-1. Well Locations in Selected Well Patterns. Production Well •; Injection Well ▲.

The ratio of the number of producing wells to the number of injection wells is shown in Table 7-1. The patterns depicted in Table 7-1 and Figure 7-1 are symmetric patterns that are especially effective for reservoirs with relatively small dip and large areal extent. The injectors and producers are generally interspersed. Other patterns in which injectors and producers are grouped together may be needed for reservoirs with significant dip. For example, a peripheral or flank injection pattern may be needed to effectively flood an anticlinal or monoclinical reservoir.

Table 7-1
Producer-to-Injector Ratios for Common Well Patterns

Well Pattern	Producer : Injector Ratio
Four-Spot	2
Five-Spot	1
Direct Line-drive	1
Staggered Line-drive	1
Seven-Spot	1 / 2
Nine-Spot	1 / 3

The location of injection wells depends on factors such as reservoir structure, injected fluid type, and displacement mechanism. For example, upstructure gas injection can be an effective displacement process for producing a monoclinical reservoir containing oil. It relies on the movement of a gas-oil contact and the displacement of oil to downstructure production wells. On the other hand, downstructure peripheral injection of water can be used to displace oil to upstructure producers in an anticlinal reservoir. In this case, downstructure water injection is used to move the oil-water contact upstructure and displace oil to upstructure production wells. The same displacement concept applies to production of an anticlinal oil reservoir with strong aquifer support.

In addition to reservoir geometry and displacement process, the well pattern depends on the distribution of existing production wells and the desired spacing of wells. Well spacing is an estimate of the area being drained by a

production well. A reduction in well spacing requires an increase in the density of production wells. The density of production wells is the number of production wells in a specified area. Well density can be increased by drilling additional wells in the space between wells in a process called infill drilling. Infill drilling is an effective means of altering flow patterns and improving recovery efficiency, but can be more expensive than a fluid displacement process. The selection of a development plan depends on a comparison of the economics of alternative development concepts. Reservoir models are especially useful tools for performing these studies.

7.3 Pattern Recovery

Optimum performance may be achieved with the patterns defined in the previous section by controlling the rates of injectors and producers. These calculations can be performed analytically if we assume the displacing and displaced fluids are incompressible, the mobility ratio is one, and the reservoir has uniform properties. Values of injection rates for the three patterns shown in Figure 7-1 are presented in Table 7-2 [Wilhite, 1986]. Units and nomenclature for the rate equations in Table 7-2 are barrels per day for rate q ; darcies for permeability k ; feet for thickness h ; well separations a and d , and wellbore radius r_w ; pounds per square inch for pressure change ΔP ; and centipoise for viscosity μ . The well separations are defined in Figure 7-1.

Table 7-2
Analytical Injection Rates for Selected Well Patterns

Pattern	Rate
Direct Line Drive	$q_D = \frac{3.541 kh \Delta P}{\mu \left[\ln \left(\frac{a}{r_w} \right) + 1.571 \frac{d}{a} - 1.838 \right]}, \frac{d}{a} \geq 1$
Staggered Line Drive	$q_S = \frac{3.541 kh \Delta P}{\mu \left[\ln \left(\frac{a}{r_w} \right) + 1.571 \frac{d}{a} - 1.838 \right]}$

Table 7-2
Analytical Injection Rates for Selected Well Patterns

Pattern	Rate
Five-Spot	$q_F = \frac{3.541 kh \Delta P}{\mu \left[\ln \left(\frac{a}{r_w} \right) - 0.619 \right]}$

The calculation of analytical injection rates, even under a set of restrictive assumptions, provides a methodology for designing well patterns without using a reservoir simulator. More accurate estimates of injection rates under a less restrictive set of assumptions are obtained using reservoir simulators. For example, simulators have been used to correlate volumetric sweep efficiency with mobility ratio and permeability variation in a reservoir that is being subjected to a pattern flood [Wilhite, 1986]. One measure of permeability variation is the Dykstra-Parsons coefficient of permeability variation.

The Dykstra-Parsons coefficient can be estimated for a log-normal permeability distribution as

$$V_{DP} = 1 - \exp \left[- \sqrt{\ln \left(k_A / k_H \right)} \right]$$

where k_A is the arithmetic average permeability for n samples

$$k_A = \frac{1}{n} \sum_{i=1}^n k_i$$

and k_H is the harmonic average permeability

$$\frac{1}{k_H} = \frac{1}{n} \sum_{i=1}^n \frac{1}{k_i}$$

The Dykstra-Parsons coefficient should be in the range $0 \leq V_{DP} \leq 1$. For a perfectly homogeneous reservoir, $V_{DP} = 0$ because $k_A = k_H$. An increase in reservoir heterogeneity increases V_{DP} . Typical values of the Dykstra-Parsons coefficient are in the range $0.4 \leq V_{DP} \leq 0.9$.

Correlations of volumetric sweep efficiency with mobility ratio and permeability variation show that volumetric sweep efficiency declines as

reservoir heterogeneity increases or mobility ratio increases, particularly for mobility ratios greater than one. This makes sense physically if we recall the definition of mobility ratio.

Mobility ratio is the mobility of the displacing fluid behind the front divided by the mobility of the displaced fluid ahead of the front. If the mobility of the displacing fluid is greater than the mobility of the displaced fluid, then the mobility ratio is greater than one. On the other hand, if the mobility of the displacing fluid is less than the mobility of the displaced fluid, then the mobility ratio is less than one. Mobility ratios less than or equal to one are considered favorable, while mobility ratios greater than one are considered unfavorable. Unfavorable mobility ratios often occur when gas is displacing oil or water is displacing high viscosity oil. An example of a flood with a favorable mobility ratio is the displacement of a low-viscosity oil by water.

Exercises

Exercise 7.1 Core floods show that the waterflood of a core with 80% initial oil saturation leaves a residual oil saturation of 30%. If the same core is resaturated with oil and then flooded with carbon dioxide, the residual oil saturation is 10%. What are the displacement efficiencies for the waterflood and the carbon dioxide flood?

Exercise 7.2 Assuming a log-normal distribution, estimate the Dykstra-Parsons coefficient for three sample permeabilities: $k_1 = 35$ md; $k_2 = 48$ md; $k_3 = 126$ md.

Exercise 7.3 (A) Run EXAM6.DAT and record the time, pressure, oil rate, water rate, gas rate, cumulative oil produced, and cumulative gas produced at the end of the run. (B) What is the oil recovery efficiency at the end of the run? Hint: original oil in place is output in the run output file WTEMP.ROF.

Chapter 8

Recovery of Subsurface Resources

Fluid recovery concepts during the life of a reservoir are summarized in this chapter. A review of the various production stages during the life of a conventional reservoir is followed by a discussion of recovery mechanisms for enhanced oil recovery and non-conventional fossil fuels.

8.1 Production Stages

The production life of a reservoir begins when reservoir fluid is withdrawn from the reservoir. Production can begin immediately after the discovery well is drilled, or several years later after several delineation wells have been drilled. Delineation wells are used to define the reservoir boundaries, while development wells are used to optimize resource recovery. Optimization criteria are defined by management and should take into account relevant governmental regulations. The optimization criteria may change during the life of the reservoir for a variety of reasons, including changes in technology, economic factors, and new information obtained during various stages of reservoir production. The stages of reservoir production are described below.

Primary Production

Primary production is ordinarily the first stage of production. It relies entirely on natural energy sources. To remove petroleum from the pore space it occupies, the petroleum must be replaced by another fluid, such as water, natural gas, or air. Oil displacement is caused by the expansion of *in situ* fluids

as pressure declines during primary reservoir depletion. The natural forces involved in the displacement of oil during primary production are called reservoir drives. The most common reservoir drives for oil reservoirs are water drive, solution or dissolved gas drive, and gas cap drive.

The most efficient drive mechanism is water drive. In this case, water displaces oil as oil flows to production wells. An effective reservoir management strategy for a water drive reservoir is to balance oil withdrawal with the rate of water influx. Water drive recovery typically ranges from 35% to 75% of the original oil in place (OOIP).

In a solution gas drive, gas dissolved in the oil phase at reservoir temperature and pressure is liberated as pressure declines. Some oil moves with the gas to the production wells as the gas expands and moves to the lower pressure zones in the reservoir. Recovery by solution gas drive ranges from 5% to 30% OOIP.

A gas cap is a large volume of gas at the top of a reservoir. When production wells are completed in the oil zone below the gas cap, the drop in pressure associated with pressure decline causes gas to move from the higher pressure gas cap down toward the producing wells. The gas movement drives oil to the wells, and eventually large volumes of gas will be produced with the oil. Gas cap drive recovery ranges from 20% to 40% OOIP, although recoveries as high as 60% can occur in steeply dipping reservoirs with enough permeability to allow oil to drain to downstructure production wells.

Gravity drainage is the least common of the primary production mechanisms. In this case oil flows downstructure to a producing well. This is the result of a pressure gradient that favors downstructure oil flow to oil movement upstructure due to gravity segregation. Gravity drainage can be effective when it works. It is most likely to happen in shallow, highly permeable, steeply dipping reservoirs.

A schematic comparison of primary production mechanisms on reservoir pressure and recovery efficiency is sketched in Figure 8-1. In many cases, one or more drive mechanisms are functioning simultaneously. The behavior of the field depends on which mechanism is most important at various times during the life of the field. The best way to predict the behavior of such fields is with

sophisticated reservoir flow models.

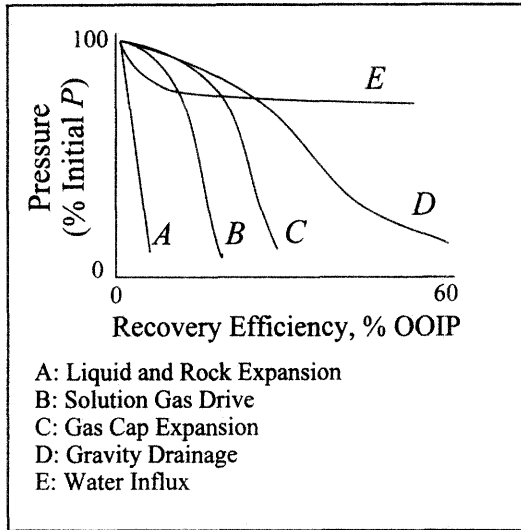


Figure 8-1. Comparison of primary production mechanisms

If we rearrange the terms in the general material balance equation for an oil reservoir, Eq. (2.3), we can estimate the relative importance of different drive mechanisms. The indices representing different drives are given in Table 8-1 relative to the hydrocarbon production given by

$$D_{HC} = N_p B_o + [G_{ps} - N_p R_{so}] B_g + G_{pc} B_{gs} \tag{8.1}$$

Table 8-1

Drive Indices from the Schilthuis Material Balance Equation

Drive	Index
Solution Gas	$I_{sg} = ND_o / D_{HC}$
Gas Cap	$I_{gc} = ND_{go} / D_{HC}$
Water	$I_w = [(W_e - W_p)B_w] / D_{HC}$
Injected Fluids	$I_i = [W_i B_w + G_i B'_g] / D_{HC}$
Connate Water and Rock Expansion	$I_e = [N(D_w + D_{gw}) + ND_r] / D_{HC}$

The sum of the drive indices equals one, thus

$$I_{sg} + I_{gc} + I_w + I_i + I_e = 1 \quad (8.2)$$

Equation (8.2) can be derived by rearranging Eq. (2.3). A comparison of the magnitudes of the drive indices indicates which drive is dominating the performance of the reservoir.

Although the above discussion referred to oil reservoirs, similar comments apply to gas reservoirs. Water drive and gas expansion with reservoir pressure depletion are the most common drives for gas reservoirs. Gas reservoir recovery can be as high as 70% to 90% of original gas in place (OGIP) because of the relatively high mobility of gas.

Gas storage reservoirs have a different life cycle than gas reservoirs that are being depleted. Gas storage reservoirs are used as a warehouse for gas. If the gas is used as a fuel for power plants, it will also need to be periodically produced and replenished. The performance attributes of a gas storage reservoir are [Tek, 1996, pg. 4]:

- Verification of inventory
- Assurance of deliverability
- Containment against migration

The gas inventory consists of working gas and cushion gas. Gas deliverability must be sufficient to account for swings in demand. Demand swings arise from such factors as seasonal variations. Gas containment is needed to conserve the amount of stored gas. For more discussion of natural gas storage in reservoirs, see references such as Tek [1996], Smith [1990], and Katz and Lee [1990].

Secondary Production

Primary depletion is usually not sufficient to optimize recovery from an oil reservoir. Oil recovery can be doubled or tripled by supplemental natural reservoir energy. The supplemental energy is provided using an external energy source, such as water injection or gas injection. The injection of water or natural gas may be referred to as pressure maintenance or secondary production. The latter term arose because injection usually followed a period of primary pressure depletion, and was therefore the second production method used in a field. Many

modern reservoirs incorporate pressure maintenance early in the production life of the field, sometimes from the beginning of production. In this case the reservoir is not subjected to a conventional primary production phase. The term “pressure maintenance” is a more accurate description of the reservoir management strategy for these fields than the term “secondary production.”

Alternative Classifications

Both primary and secondary recovery processes are designed to produce oil using immiscible methods. Additional methods may be used to improve oil recovery efficiency by reducing residual oil saturation. The reduction of residual oil saturation requires a change in such factors as interfacial tension or wettability. Methods designed to reduce residual oil saturation have been referred to in the literature as:

- Tertiary Production
- Enhanced Oil Recovery
- Improved Oil Recovery

The term tertiary production was originally used to identify the third stage of the production life of the field. Typically the third stage occurred after waterflooding. The third stage of oil production would involve a process that was designed to mobilize waterflood residual oil. An example of a tertiary production process is a chemical flood process such as surfactant flooding. Tertiary production processes were designed to improve displacement efficiency by injecting fluids or heat. They were referred to as enhanced recovery processes. It was soon learned, however, that some fields would perform better if the enhanced recovery process was implemented before the third stage in the life of the field. In addition, it was found that enhanced recovery processes were often more expensive than just drilling more wells in a denser pattern.

The drilling of wells to reduce well spacing and increase well density is called infill drilling. The birth of the term “infill drilling” was coincident with the birth of another term, “improved recovery.” Improved recovery includes enhanced oil recovery and infill drilling. Some major improved recovery processes are waterflooding, gasflooding, chemical flooding, and thermal recovery, [Dyke, 1997]. They are discussed in more detail below.

8.2 Enhanced Oil Recovery

Improved recovery technology includes traditional secondary recovery processes such as waterflooding and immiscible gas injection, as well as enhanced oil recovery (EOR) processes. EOR processes are usually classified as one of the following processes: chemical, miscible, thermal, and microbial. A brief description of each of these processes is presented here. The literature on EOR processes is extensive. For more detailed discussions of EOR processes, including screening criteria and analyses of displacement mechanisms, see such references as Taber and Martin [1983], Lake [1989], Martin [1992], Taber, et al. [1996], and Green and Willhite [1998].

Chemical

Chemical flooding methods include polymer flooding, micellar-polymer or surfactant-polymer flooding, and alkaline or caustic flooding. Polymer flooding is designed to improve the mobility ratio and fluid flow patterns of a displacement process by increasing the viscosity of injected water containing polymer. Micellar-polymer flooding uses a detergent-like solution to lower residual oil saturation to waterflooding. The polymer slug injected after the micellar slug is designed to improve displacement efficiency. Alkaline flooding uses alkaline chemicals that can react with certain types of *in situ* crude. The resulting chemical product is miscible with the oil and can reduce residual oil saturation to waterflooding.

Miscible

Miscible flooding methods include carbon dioxide injection, natural gas injection, and nitrogen injection. Miscible gas injection must be performed at a high enough pressure to ensure miscibility between the injected gas and *in situ* oil. Miscibility is achieved when interfacial tension (IFT) between the aqueous and oleic phases is significantly reduced. The desired IFT reduction is typically from around 1 dyne/cm to 0.001 dyne/cm or less. Any reduction in IFT can improve displacement efficiency, and a near miscible process can yield much of the incremental oil that might be obtained from a miscible process. If reservoir

pressure is not maintained above the minimum miscibility pressure (MMP) of the system, the gasflood will be an immiscible gas injection process.

Immiscible gas can be used as the principal injection fluid in a secondary displacement process, or it can be used as the injection fluid for a tertiary process. Two improved recovery processes based on immiscible gas injection are the double displacement process (DDP) and the second contact water displacement (SCWD) process [Novakovic, 1999]. Both processes require the injection of immiscible gas into reservoirs that have been previously waterflooded. Oil remaining after waterflood can coalesce into a film when exposed to an immiscible gas. The processes require favorable gas-oil and oil-water interfacial tensions. The oil film can be mobilized and produced by down-dip gravity drainage (the DDP) process or by water influx from either an aquifer or water injection (SCWD) following the immiscible gas injection period.

Thermal

Thermal flooding methods include hot water injection, steam drive, steam soak, and *in situ* combustion. The injection or generation of heat in a reservoir is designed to reduce the viscosity of *in situ* oil and improve the mobility ratio of the displacement process. Electrical methods can also be used to heat fluids in relatively shallow reservoirs containing high-viscosity oil, but electrical methods are not as common as hot-fluid injection methods. Steam injection methods work by injecting steam into the reservoir, while *in situ* combustion requires compressed air injection after *in situ* oil has been ignited. Steam and hot water injection processes are the most common thermal methods because of the relative ease of generating hot water and steam. The *in situ* combustion process is more difficult to control than steam injection processes and it requires an *in situ* oil that can be set on fire. Hot gases and heat advance through the formation and displace the heated oil to production wells.

Microbial

Microbial EOR uses the injection of microorganisms and nutrients in a carrier medium to increase oil recovery and/or reduce water production in petroleum reservoirs. Dietrich, et al.[1996] summarized the results of five

successful commercial microbial EOR projects. The projects reflected a diversity of locations, lithologies, depths, porosities, permeabilities, and temperatures. Two of the projects were in the U.S., two in China, and one in Argentina, and included sandstone, fractured dolomite, siltstone/sandstone, and fractured sandstone reservoirs. Reservoir depths ranged from 4450 to 6900 feet, temperatures from 110° to 180° F, porosity from 0.079 to 0.232, and effective permeability from 1.7 to 300 md. Evidence from laboratory research and case/field studies shows that microbial EOR processes can result in the incremental recovery of oil and also reduce water production from high permeability zones. However, more research needs to be done to maximize the potential for microbial EOR. Some effort in this direction has been conducted. A microbial transport simulator was developed under the auspices of the U.S. Department of Energy as a modification to the black oil simulator BOAST.

8.3 Nonconventional Fossil Fuels

Clean energy refers to energy that is generated with little environmental pollution. Natural gas is a source of clean energy. Oil and gas fields are considered conventional sources of natural gas. In the following, we discuss two nonconventional sources of natural gas: coalbed methane, and gas hydrates.

Coalbed Methane

Coalbeds are an abundant source of methane [Selley, 1998; Rogers, 1994]. The presence of methane gas in coal has been well known to coal miners as a safety hazard, but is now being viewed as a source of natural gas. The gas is bound in the micropore structure of the coalbed. It is able to diffuse into the natural fracture network when a pressure gradient exists between the matrix and the fracture network. The fracture network in coalbeds consists of microfractures. The microfractures allow Darcy flow and are called “cleats.”

Gas recovery from coalbeds depends on three processes [Kuuskraa and Brandenburg, 1989]. Coalbed methane exists as a monomolecular layer on the internal surface of the coal matrix. Its composition is predominately methane, but can also include other constituents, such as ethane, carbon dioxide, nitrogen

and hydrogen [Mavor, et al., 1999]. Gas content can range from approximately 20 SCF gas per ton of coal in the Powder River Basin of Wyoming [Mavor, et al., 1999] to 600 SCF/ton in the Appalachian Basin [Gaddy, 1999]. Gas recovery begins with the desorption of gas from the internal surface to the coal matrix and micropores. The gas then diffuses through the coal matrix and micropores into the cleats. Finally, gas flows through the cleats to the production well. The flow rate depends, in part, on the pressure gradient in the cleats and the density and distribution of cleats. The controlling mechanisms for gas production from coalbeds are the rate of desorption from the coal surface to the coal matrix, the rate of diffusion from the coal matrix to the cleats, and the rate of flow of gas through the cleats.

The production performance of a coalbed methane well typically exhibits three stages. The reservoir dewateres and methane production increases during the first stage of pressure depletion. Methane production peaks during the second stage. The amount of water produced is relatively small compared to gas production during the second stage because of gas-water relative permeability effects, and desorption of natural gas provides a counterbalance to permeability loss as a result of formation compaction. The third stage of production is similar to conventional gas field production in which gas rate declines as reservoir pressure declines.

Gas Hydrates

The entrapment of natural gas molecules in ice at very low temperatures forms an ice-like solid. The ice-like solid substance is a metastable complex called a gas hydrate. Gas hydrates are clathrates. A clathrate is a chemical complex that is formed when one type of molecule completely encloses another type of molecule in a lattice. In the case of gas hydrates, hydrogen-bonded water molecules form a cage-like structure in which mobile molecules of gas are absorbed or bound.

The presence of gas hydrates can complicate field operations. For example, the existence of hydrates on the ocean floor can affect drilling operations in deep water. The simultaneous flow of natural gas and water in tubing and pipelines can result in the formation of gas hydrates that can impede

or completely block the flow of fluids through pipeline networks. Heating the gas or treating the gas-water system with chemical inhibitors can prevent the formation of hydrates, but increases operating costs.

Gas hydrates are generally considered a problem for oil and gas field operations, but their potential commercial value as a clean energy resource is changing the industry perception. The potential as a gas resource is due to the relatively large volume of gas contained in the gas hydrate complex. In particular, Makogon, et al. [1997] have reported that one cubic meter of gas hydrate contains 164.6 m³ of methane. This is equivalent to one barrel of gas hydrate containing 924 ft³ of methane, and is approximately six times as much gas as the gas contained in an unimpeded gas-filled pore system [Selley, 1998, pg. 25]. The gas in gas hydrates occupies approximately 20% of the volume of the gas hydrate complex. The remaining 80% of gas hydrate complex volume is occupied by water.

Gas hydrates can be found throughout the world [Selley, 1998; Makogon, et al., 1997]. They exist on land in sub-Arctic sediments and on seabeds where the water is near freezing at depths of at least 600 to 1500 feet. For instance, favorable conditions for gas hydrate formation exist at sea floor temperatures as low as 39°F in the Gulf of Mexico and as low as 30°F in some sections of the North Sea. According to Makogon, et al. [1997], over 700 trillion m³ in explored reserves of methane in the hydrate state exist. Difficulties in cost-effective production have hampered development of the resource.

Exercises

Exercise 8.1 Use the definitions in Table 8-1 and Eq. (8-1) to derive Eq. (8-2) from Eq. (2.3).

Exercise 8.2 (A) Which drive index in Table 8-1 will be largest in a field containing a dead oil that is subjected to pressure depletion? (B) Suppose a dead oil reservoir is subjected to a peripheral waterflood. Identify the two drive indices in Table 8-1 that will have the greatest influence on oil recovery.

Exercise 8.3 EOR simulators can be found on the internet. Access the internet and search for a website containing public domain EOR simulators. Hint: The United States Department of Energy is one governmental agency that has distributed EOR software using a website.

Chapter 9

Economics and the Environment

Economic analyses are an essential aspect of a reservoir management study. The economic performance of a prospective project is often the deciding factor in determining whether or not a project is undertaken. Consequently, it is important to be aware of basic economic concepts and factors that may effect the economic performance of a project. These topics are introduced here. Further details can be found in references such as Thompson and Wright [1985] and Satter and Thakur [1994].

9.1 SPE/WPC Reserves

The analysis of a petroleum project depends on the amount of commercially valuable resource that is available. According to the Society of Petroleum Engineers and the World Petroleum Congress [Staff-JPT, 1997], reserves are those quantities of petroleum which are anticipated to be commercially recoverable from known accumulations from a given date forward. Table 9-1 summarizes the SPE/WPC definitions of reserves. The definitions of reserves include both qualitative and quantitative criteria. Although the SPE/WPC definitions have been adopted in many parts of the world, they are not universal. For example, a different, yet analogous, set of definitions exists in the Russian Federation [Nemchenko, et al., 1995; Grace, et al., 1993].

Table 9-1
SPE/WPC Reserves Definitions

<p>Proved reserves</p>	<ul style="list-style-type: none"> ◆ Those quantities of petroleum which, by analysis of geological and engineering data, can be estimated with reasonable certainty to be commercially recoverable, from a given date forward, from known reservoirs and under current economic conditions, operating methods, and government regulation. ◆ In general, reserves are considered proved if the commercial producibility of the reservoir is supported by actual production or formation tests. ◆ There should be at least a 90% probability (P_{90}) that the quantities actually recovered will equal or exceed the estimate.
<p>Unproved reserves</p>	<p>Those quantities of petroleum which are based on geologic and/or engineering data similar to that used in estimates of proved reserves; but technical, contractual, economic, or regulatory uncertainties preclude such reserves being classified as proved.</p>
<p>Probable reserves</p>	<ul style="list-style-type: none"> ◆ Those unproved reserves which analysis of geological and engineering data suggests are more likely than not to be recoverable. ◆ There should be at least a 50% probability (P_{50}) that the quantities actually recovered will equal or exceed the estimate.
<p>Possible reserves</p>	<ul style="list-style-type: none"> ◆ Those unproved reserves which analysis of geological and engineering data suggests are less likely to be recoverable than probable reserves. ◆ There should be at least a 10% probability (P_{10}) that the quantities actually recovered will equal or exceed the estimate.

The probability distribution associated with the SPE/WPC reserves definitions can be estimated with relative ease if the modeling team has performed a sensitivity analysis that generates a set of cases that yield low, medium, and high reserves estimates. In the absence of data to the contrary, a reasonable first approximation is that each case is equally likely to occur. Given this assumption, an average μ and standard derivation σ may be calculated from the sensitivity analysis results to prepare a normal distribution of reserves. For a normal distribution with mean μ and standard deviation σ , the SPE/WPC

reserves definitions are quantified as follows:

$$\text{Proved reserves} = P_{90} = \mu - 1.28\sigma$$

$$\text{Probable reserves} = P_{50} = \mu$$

$$\text{Possible reserves} = P_{10} = \mu + 1.28\sigma$$

The normal distribution can be used to associate an estimate of the likelihood of occurrence of any particular prediction case with its corresponding economic forecast.

9.2 Basic Economic Concepts

The cash flow of a project is the net cash generated or expended on the project as a function of time. The time value of money is included in economic analyses by applying a discount rate to adjust the value of money to the value during a base year. The discount rate is the adjustment factor, and the resulting cash flow is called the discounted cash flow. The net present value (NPV) of the cash flow is the value of the cash flow at a specified discount rate. The discount rate at which NPV is zero is called the discounted cash flow return on investment (DCFROI) or Internal Rate of Return (IRR).

A typical plot of NPV as a function of time is shown in Figure 9-1. The early time part of the figure shows a negative NPV and indicates that the project

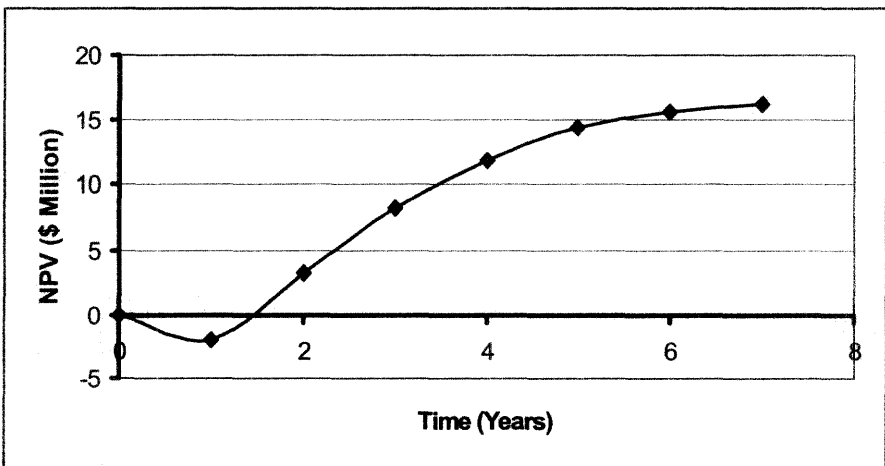


Figure 9-1. Typical cash flow

is operating at a loss. The loss is usually associated with initial capital investments and operating expenses that are incurred before the project begins to generate revenue. The reduction in loss and eventual growth in positive NPV is due to the generation of revenue in excess of expenses. The point in time on the graph when the NPV is zero after the project has begun is the payout time. The concept of payout time applies to either discounted or undiscounted cash flow. Payout time on Figure 9-1 is approximately 1.5 years.

The discounted cash flow return on investment (DCFROI) and payout time are measures of the economic viability of a project. Another measure is the profit-to-investment ratio. The profit-to-investment (PI) ratio is a measure of profitability. It is defined as the total undiscounted cash flow without capital investment divided by total investment. Unlike DCFROI, the PI ratio does not take into account the time value of money. The definitions of several commonly used economic measures are presented in Table 9-2. Useful plots include a plot of NPV versus time and a plot of NPV versus discount rate.

Table 9-2
Definitions of Selected Economic Measures

Discount Rate	Factor to adjust the value of money to a base year.
Net Present Value (NPV)	Value of cash flow at a specified discount rate.
DCFROI or IRR	Discount rate at which NPV = 0.
Payout Time	Time when NPV = 0.
Profit-to-Investment (PI) Ratio	Undiscounted cash flow without capital investment divided by total investment.

The ideas discussed above are quantified as follows. Net present value is the difference between the present value of revenue R and the present value of expenses E , thus

$$NPV = R - E \tag{9.1}$$

If we define $\Delta E(k)$ as the expenses incurred during a time period k , then E may be written as

$$E = \sum_{k=0}^{N*Q} \frac{\Delta E(k)}{\left(1 + \frac{i'}{Q}\right)^k} \tag{9.2}$$

where i' is the annual inflation rate, N is the number of years of the expenditure schedule, and Q is the number of times interest is compounded each year. A similar expression is written for revenue R :

$$R = \sum_{k=0}^{N*Q} \frac{\Delta R(k)}{\left(1 + \frac{i}{Q}\right)^k} \tag{9.3}$$

where $\Delta R(k)$ is revenue obtained during time period k , and i is the annual interest or discount rate. Equations (9.2) and (9.3) include the assumptions that i and i' are constants over the life of the project, but i and i' are not necessarily equal. These assumptions let us compute the present value of money expended relative to a given inflation rate i' and compare the result to the present value of revenue associated with a specified interest or discount rate i .

Illustration: Application to an Oil Production Project

The net present value and break-even oil price for an oil production project can be obtained from the above analysis as an illustration of the concepts. We specify the base year for present value calculations as the year when the project begins. In this case, we have no initial revenue and the initial expense is just initial investment II , thus

$$\Delta R(0) = 0 \text{ and } \Delta E(0) = II \tag{9.4}$$

Substituting Eqs. (9.2) through (9.4) into Eq. (9.1) gives

$$NPV = \sum_{k=1}^{N*Q} \frac{\Delta R(k)}{\left(1 + \frac{i}{Q}\right)^k} - II - \sum_{k=1}^{N*Q} \frac{\Delta E(k)}{\left(1 + \frac{i'}{Q}\right)^k} \tag{9.5}$$

Revenue from the sale of oil during period k has the form

$$\Delta R(k) = P_o \left(1 + \frac{i'}{Q}\right)^k \Delta N_p(k) \tag{9.6}$$

where P_o is the present price of oil, and $\Delta N_p(k)$ is the incremental oil production during period k . Notice that we are assuming the value of produced gas is negligible in this example. An inflation factor on the price of oil is included in Eq. (9.6). Combining Eqs. (9.4), (9.5), and (9.6) yields net present value for this project:

$$NPV = \sum_{k=1}^{N*Q} \frac{P_o \left(1 + \frac{i'}{Q}\right)^k \Delta N_p(k)}{\left(1 + \frac{i}{Q}\right)^k} - II - \sum_{k=1}^{N*Q} \frac{\Delta E(k)}{\left(1 + \frac{i'}{Q}\right)^k} \tag{9.7}$$

The incremental oil production in Eq. (9.7) is typically obtained as a forecast using reservoir engineering methods. Some of the most frequently used methods include decline curve analysis, material balance analysis, or reservoir simulation. The oil production profile used in the economic analysis may represent both historical and predicted oil recovery. The predicted oil recovery is used to determine project reserves. Several different production profiles may be required to determine the probabilistic distribution of reserves and associated economic sensitivity.

A break-even oil price P_{oe} for a specified rate of return $i = ROR$ and production profile is calculated by setting $NPV = 0$ as the break-even condition in Eq. (9.7). Rearranging the resulting equation gives the following estimate of break-even oil price:

$$P_{oe} = \left[II + \sum_{k=1}^{N*Q} \frac{DE(k)}{\left(1 + \frac{i'}{Q}\right)^k} \right] / \left[\sum_{k=1}^{N*Q} \frac{\left(1 + \frac{i'}{Q}\right)^k}{\left(1 + \frac{ROR}{Q}\right)^k} DN_p(k) \right] \tag{9.8}$$

A plot of P_{oe} versus ROR shows the sensitivity of break-even oil price to different rates of return.

9.3 Investment Decision Analysis

Economic analyses are performed to provide information about the economic performance that can be expected from a project relative to alternative investment options. The decision to invest in a project depends on many factors. Thompson and Wright [1985, pg. 3-2] list the following set of characteristics for measures of investment worth that can be used to compare and rank competing projects:

- Consistent with corporate goals.
- Easy to understand and apply.
- Permits cost-effective decision making.
- Provides a quantitative measure for acceptance or rejection.
- Permits alternatives to be compared and ranked.
- Incorporates the time value of money.

The economic measures that are used in investment decision analysis depend on the experience of the decision makers who will use the economic measures. Some of the most commonly used economic measures are payout, present worth, net present value, discount rate, profit-to-investment ratio, and internal rate of return. The relative importance of each economic measure is determined by the decision makers. For example, a proposed project with an early payout but relatively low discount rate may be more attractive to a company that needs to maintain a positive cash flow than another project with a higher discount rate but which does not payout as soon. The criteria for acceptance or rejection of a project may change, even within a company, as the economic environment changes.

Combinations of economic measures are often used as economic criteria for making decisions about projects. For example, a project may be considered economically viable if the internal rate of return (IRR) is greater than 30% and the profit-to-investment ratio (PI) is greater than 0.5. Economic viability is influenced by both tangible and intangible factors. Intangible factors such as environmental and socio-political concerns are relatively difficult to quantify, yet may have a greater influence on the final decision than tangible factors. Tangible factors, such as well costs and reserves, are relatively easy to quantify.

9.4 Environmental Impact

Environmental issues must always be considered when developing a reservoir management strategy. For example, the Louisiana Offshore Oil Production (LOOP) facility is designed to keep hydrocarbon transfer operations from pipelines to tankers away from sensitive coastal areas. Periodic water sampling of surface and produced waters can assure the fresh water sources are not contaminated. In addition, periodic testing for the excavation or production of naturally occurring radioactive materials helps assure environmental compliance.

A well-managed field should be compatible with both the surface and subsurface environment. The advantages of operating a field with prudent consideration of environmental issues can pay economic dividends. In addition to improved public relations, a sensitivity to environmental issues can minimize adverse environmental effects that may require costly remediation and financial penalties. Remediation is often in the form of clean-up, such as the clean-up required after the oil spill from the Exxon-Valdez oil tanker in Alaska. New technologies are being developed to improve our ability to clean-up environmental pollutants. For example, bioremediation uses living microorganisms or their enzymes to accelerate the rate of degradation of environmental pollutants [Westlake, 1999].

Subsidence

An issue of special importance to reservoir characterization is subsidence. Subsidence is a compressibility effect that depends on the geomechanics of the produced interval and its overburden. Subsidence, or the change in thickness Δh of the reservoir, can be estimated from the compressibility and pressure depletion of the system using the equation

$$\Delta h = c_B h \Delta P = \phi c_f h \Delta P$$

where

- c_B bulk compressibility [psia⁻¹]
- c_f formation compressibility [psia⁻¹]

- h net thickness of reservoir [ft]
 ϕ porosity [frac]
 ΔP pressure depletion [psia]

If properties like compressibility are measured hydrostatically, they should be corrected to uniaxial compressibilities [Teeuw, 1971] so that the subsidence estimate becomes

$$\Delta h_u = \frac{1}{3} \left(\frac{1 + \nu}{1 - \nu} \right) \phi c_f h \Delta P$$

where ν is Poisson's ratio and the subscript u denotes uniaxial compressibility. The correction for uniaxial compaction recognizes that reservoirs with large lateral dimensions relative to their vertical thickness deform mainly in the vertical direction.

In many cases, subsidence has little or no adverse environmental effects. In some cases, however, subsidence can be a significant concern. For example, a pressure maintenance program in a field where surface subsidence is a likely consequence of pressure depletion can improve resource recovery and help avoid economic liabilities resulting from damage caused by surface subsidence. Subsidence in the Long Beach, California, area due to production of the Wilmington field had to be mitigated with a pressure maintenance program.

Subsidence has been responsible for production induced seismicity in areas such as the Rocky Mountain Arsenal near Denver, Colorado, where production induced seismicity was identified as the cause of earthquakes. Earthquakes due to natural causes have led to fatalities in tectonically active areas like the Sea of Okhotsk, offshore Sakhalin Island, Russia. Development activities in tectonically active areas, such as offshore Sakhalin Island, need to anticipate the impact of subsidence and production induced seismicity as part of their reservoir management plans. Examples of compaction studies are presented by Fredrich, et al. [1998] and Settari and Walters [1999].

Sustainable Development

Failure to adequately consider environmental issues can lead to both tangible and intangible losses. Intangible losses are difficult to quantify, but can include loss of public support for an otherwise economically viable project.

Tangible losses have more readily quantifiable economic consequences. For example, near- and long-term economic liabilities associated with potable water contamination can adversely effect project economics. It becomes a question of business ethics whether a practice that is legal but can lead to an adverse environmental consequence should nonetheless be pursued because a cost-benefit analysis showed that economic liabilities were less than economic benefits.

Typically, arguments to pursue an environmentally undesirable practice based on cost-benefit analyses do not adequately account for intangible costs. For example, the decision by Shell to dispose of the Brent Spar platform by sinking it in the Atlantic Ocean led to public outrage in Europe in 1995. Reversing the decision and disassembling the platform for use as a quay in Norway resolved the resulting public relations problem, but the damage had been done. The failure to anticipate the public reaction reinforced a lack of public confidence in the oil and gas industry, and helped motivate government action to regulate the decommissioning of offshore platforms in northwest Europe [Offshore Staff, 1998].

The problem facing the industry is to learn how to achieve sustainable development. One industry response to environmental and social concerns in the context of sustainable development is the “triple bottom line” [Whittaker, 1999]. According to this view, sustainable development must integrate social and environmental concerns into a development plan that optimizes economic profitability and value creation. The three components of sustainable development, and the three goals of the triple bottom line (TBL), are economic prosperity, social equity, and environmental protection. The focus of TBL is the creation of long-term shareholder value by recognizing that corporations are dependent on licenses provided by society to do business. Whittaker [1999, pg. 25] reports that “After a period of serious introspection following the Brent Spar debacle, Royal Dutch/Shell is perhaps the most enthusiastic supporter of TBL.” Although TBL is in its infancy, key elements of TBL policy are beginning to emerge. They include [Whittaker, 1999, pg. 25]:

- Performance measurements that include qualitative social indicators and ecoefficiency measures (such as energy consumption and recycling) in addition to compliance and pollutant emissions.

- Development and implementation of strategies that will enable the industry to meet both future global energy needs and environmental objectives.
- Investment in natural gas, low or zero-emissions fuels, and renewable forms of energy.
- Improved communications with communities affected by operations.

Global Climate Change

One of the most pressing environmental concerns is global climate change. A purported cause of adverse global climate change is due to the “greenhouse effect.” Increasing levels of carbon dioxide in the atmosphere absorb infrared radiation rather than letting it escape into space. The resulting atmospheric heating is attributed to excessive emissions of carbon dioxide into the atmosphere. Government and industry are undertaking programs to address this issue. For example, one possible solution is to collect and store carbon dioxide in reservoirs in a process known as CO₂ sequestration. The goal of CO₂ sequestration and similar programs is to provide economically competitive and environmentally safe options to offset all projected growth in baseline emissions of greenhouse gases.

Exercises

Exercise 9.1 Five independent studies determined the following reserves for Reservoir A:

Study	1	2	3	4	5
Oil Recovery (MSTBO)	320	150	480	260	370

Assuming a normal distribution of reserves, estimate proved, probable and possible reserves. Hint: Calculate the average and standard deviation for the oil recoveries reported above.

Exercise 9.2 Suppose a reservoir has an average porosity of 20%, a formation compressibility of 20×10^{-6} psia⁻¹, and a net thickness of 500 feet; and the reservoir is subjected to a pressure depletion of 3000 psia. (A) Plot subsidence

as a function of Poisson's ratio for a Poisson's ratio ranging from 0.1 to 0.35.

(B) If you are operating the field from a platform that is built with a deck that is 10 feet above maximum wave height, discuss the possible impact of subsidence on operations? (C) Discuss the possible impact of subsidence on wellbore stability for deviated wells drilled from the platform.

Part II

Reservoir Simulation

This page intentionally left blank

Chapter 10

Overview of the Modeling Process

The process of applying a reservoir flow simulator to the study of a physical system is outlined here. The best technology for making reservoir performance predictions today is to model fluid flow in porous media using computer programs known as simulators.

10.1 Basic Reservoir Analysis

Reservoir characterization and reservoir engineering evaluations are usually performed as a part of standard business practice independent of a reservoir simulation study. The tasks associated with basic reservoir analysis are described in Chapter 2 and in such references as Craft, et al. [1991], Mian [1992], and Tearpock and Bischke [1991]. They provide information that is needed to prepare input data for a simulation study. For example, material balance studies require the acquisition of fluid property data, field pressures, and production volumes. This information is also needed to conduct a model study using a reservoir simulator. Volumetric analyses provide independent appraisals of reservoir volume that can be used to check the original fluid volumes calculated by a reservoir model. In addition, basic reservoir analysis can provide an initial concept of the reservoir and associated drive mechanisms. These concepts can be used to design the model study. The modeling team needs to be aware of existing studies and should relate model performance to previous studies whenever possible.

10.2 Prerequisites

Several prerequisites should be satisfied before a model study is undertaken [Coats, 1969]. The most important, from a business perspective, is the existence of a problem of economic importance. At the very least, the objectives of a model study should yield a solution to the economically important problem.

Once the objectives of a study are specified, the modeler should gather all available data and reports relating to the field. The term “modeler” is used in the remainder of the text as a synonym for “modeling team” unless an explicit distinction must be made. If necessary data is not available, the modeler should determine if the data can be obtained, either by analogy with other reservoirs or by correlation. Values for all model input data must be obtained because the simulator will not run without a complete set of data. In some cases, simplifying assumptions about the reservoir may have to be made because there is not enough data available to quantitatively represent the system in greater detail.

In addition to clearly defined objectives, another prerequisite that must be satisfied before committing to a simulation study is to determine that the objectives of the study cannot be achieved using simpler techniques. If less expensive techniques, such as decline curve analysis or the Buckley-Leverett waterflood displacement algorithm [Collins, 1961; Craig, 1971; and Dake, 1978], do not provide adequate results, then more sophisticated and costly methods are justified.

10.3 Computer Modeling

A comprehensive reservoir management model can be thought of as four interacting models: the reservoir model, the well model, the wellbore model, and the surface model. The spatial relationship between these models is illustrated in Figure 10-1. The reservoir model represents fluid flow within the reservoir. The reservoir is modeled by subdividing the reservoir volume into an array, or grid, of smaller volume elements (Figure 10-2). Many names are used to denote the individual volume elements: for example, gridblock, cell, or node. The set of all volume elements is known by such names as grid or mesh.

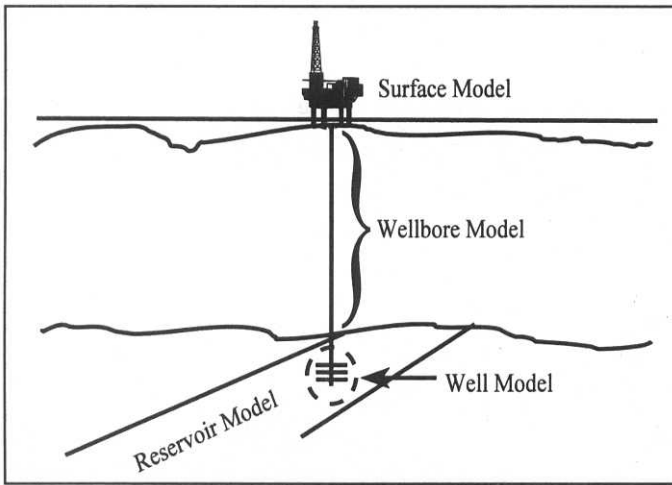


Figure 10-1. Reservoir management system.

Every practical reservoir simulator includes both a reservoir model and a well model. The well model is a term in the fluid flow equations that represents the extraction of fluids from the reservoir or the injection of fluids into the reservoir. Full-featured commercial simulators also include a wellbore model and a surface facility model. The wellbore model represents flow from the sandface to the surface. The surface model represents constraints associated with surface facilities, such as platform and separator limitations.

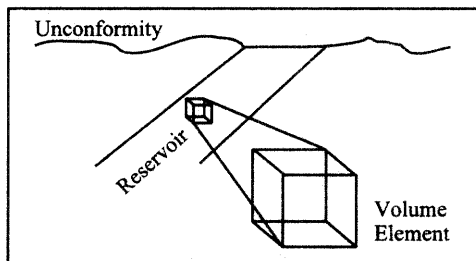


Figure 10-2. Subdivide reservoir.

The mathematical algorithms associated with each model depend on physical conservation laws and empirical relationships. Computer simulators are based on conservation of mass, momentum, and energy. The most widely used simulators assume the reservoir is isothermal, that is, constant temperature. If we are modeling a reservoir where thermal effects matter, such as a secondary

recovery process where heat has been injected in some form, then we need to use a simulator that accounts for temperature variation and associated thermodynamic effects. The set of algorithms is sufficiently complex that high-speed computers are the only practical means of solving the mathematics associated with a reservoir simulation study. These topics are discussed in more detail in later chapters.

10.4 Major Elements of a Reservoir Simulation Study

The essential elements of a simulation study include matching field history; making predictions, including a forecast based on the existing operating strategy; and evaluating alternative operating scenarios [Mattax and Dalton, 1990; Thomas, 1982]. During the history match, the modeler will verify and refine the reservoir description. Starting with an initial reservoir description, the model is used to match and predict reservoir performance. If necessary, the modeler will modify the reservoir description until an acceptable match is obtained. The history matching phase of the study is an iterative process that makes it possible to integrate reservoir geoscience and engineering data.

The history matching process may be considered an inverse problem because an answer already exists. We know how the reservoir performed; we want to understand why. Our task is to find the set of reservoir parameters that minimizes the difference between the model performance and the historical performance of the field. This is a non-unique problem since there is usually more than one way to match the available data.

Once a match of historical data is available, the next step is to make a base case prediction, which is essentially just a continuation of existing operating practice. The base case prediction gives a baseline for comparison with other reservoir management strategies.

Model users should be aware of the validity of model predictions. One way to get an idea of the accuracy of predictions is to measure the success of forecasts made in the past. Lynch [1996] looked at the evolution of the United States Department of Energy price forecast over a period of several years for both oil and gas. The quality of price forecasts is illustrated in Figure 10-3.

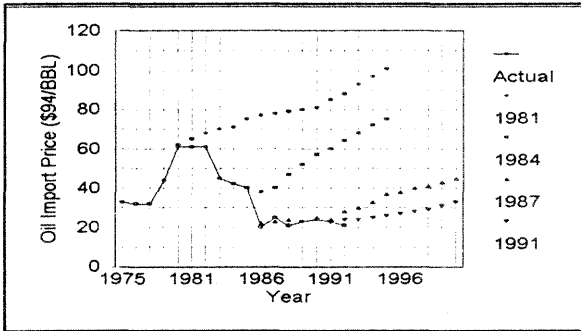


Figure 10-3. Price forecasting.

Forecasts that were made in years 1981, 1984, 1987, and 1991 are compared to the actual prices. Even though price forecast is essential to a commercial enterprise, it is clear from Lynch's study that there is considerable uncertainty associated with the price forecast. The wide swing in oil price in the late 1990's where oil price varied by a factor of two indicates the volatility of economic factors that are needed in forecasts.

In addition to uncertainty in economic parameters, there is uncertainty in the forecasted production performance of a field. Forecasts do not account for discontinuities in historical patterns that arise from unexpected effects. This is as true in the physical world as it is in the social [Oreskes, et al., 1994]. Simulators do not eliminate uncertainty; they give us the ability to assess and better manage the risk associated with the prediction of production performance.

A valuable but intangible benefit of the process associated with reservoir simulation is the help it provides in managing the reservoir. One of the critical tasks of reservoir management is the acquisition and maintenance of an up-to-date data base. A simulation study can help coordinate activities as a modeling team gathers the resources it needs to determine the optimum plan for operating a field. Collecting input data for a model is a good way to ensure that every important technical variable is considered as data is collected from the many disciplines that contribute to reservoir management. If model performance is especially sensitive to a particular parameter, then a plan should be made to determine that parameter more accurately, for example, from either laboratory or appropriate field tests.

Exercises

Exercise 10.1 Original Volume In Place: Data file EXAM1.DAT is a material balance model of an undersaturated oil reservoir undergoing pressure depletion. Run EXAM1.DAT and find the volume of oil and gas originally in place.

Exercise 10.2 Gas Reservoir Material Balance: Suppose a gas reservoir has the following production history:

G_p (Bscf)	P (psia)	Z	P/Z (psia)
0.015	1946	0.813	2393
0.123	1934	0.813	2378
0.312	1913	0.814	2350
0.652	1873	0.815	2297
1.382	1793	0.819	2190
2.210	1702	0.823	2068
2.973	1617	0.828	1953
3.355	1576	0.830	1899
4.092	1490	0.835	1783
4.447	1453	0.838	1734
4.822	1413	0.841	1680

where G_p is cumulative gas production, P is pressure, and Z is gas compressibility factor. Draw a straight line through a plot of G_p vs P/Z to find original gas in place (OGIP). OGIP corresponds to $P/Z = 0$. These results were obtained from data file EXAM8.DAT. Verify that the OGIP for the model is about 15.9 Bscf by running EXAM8.DAT and finding the OGIP in WTEMP.ROF. How much oil and water are originally in place?

Chapter 11

Conceptual Reservoir Scales

One of the most important goals of modeling is to reduce the risk associated with making decisions in an environment where knowledge is limited. The range of applicability of acquired data and the integration of scale-dependent data into a cohesive reservoir concept are discussed below.

11.1 Reservoir Sampling and Scales

A sense of just how well we understand the reservoir can be obtained by considering the fraction of reservoir area sampled by different techniques. As an example, suppose we want to find the size of the area sampled by a wellbore that has a six-inch radius. If we assume the area is circular, we can calculate the area as πr^2 where r is the sampled radius. The resulting sampled area is less than a square foot. To determine the fraction of area sampled, we normalize the sampled area with respect to the drainage area of a well, say a very modest five acres. What fraction of the area is directly sampled by the wellbore? The drainage area is 218,000 square feet. The fraction of the area sampled by the well is three to four parts in a million. This is a tiny fraction of the area of interest.

A well log signal will expand the area that is being sampled. Suppose a well log can penetrate the formation up to five feet from the wellbore, which is a reasonably generous assumption. The fraction of area that has been sampled is now approximately four parts in ten thousand. The sample size in a drainage area of five acres, which is a small drainage area, is still a fraction of a percent.

Core and well log information gives us a very limited view of the reservoir. A seismic section expands the fraction of area sampled, but the interpretation of seismic data is less precise. Seismic data is often viewed as “soft data” because of its dependence on interpretation. The reliability of seismic interpretation can be improved when correlated with “hard data” such as core and well log measurements.

The range of applicability of measured data depends on the sampling technique. Did we take some core out of the ground, measure an electrical response from a well log, or detect acoustical energy? The ranges are illustrated in Figure 11-1. Fayers and Hewett [1992] point out that scale definitions are not universally accepted, but do illustrate the relative scale associated with reservoir property measurements. Scale sizes range from the very big to the microscopic. To recognize variations in the range of data applicability, four conceptual scales have been defined (Figure 11-2) and will be adopted for use in the following discussion.

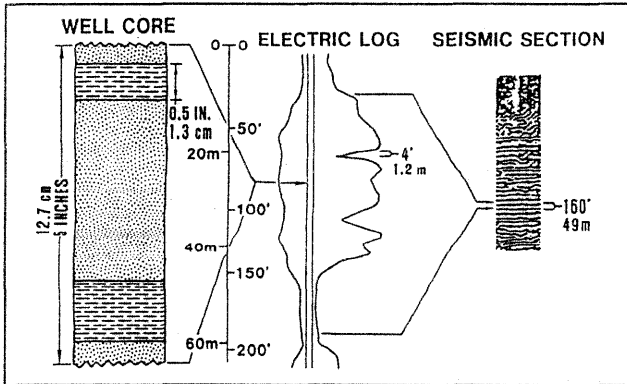


Figure 11-1. Range of data sampling techniques (after Richardson, et al., 1987a; reprinted by permission of the Society of Petroleum Engineers).

The Giga Scale includes information associated with geophysical techniques, such as reservoir architecture. Theories of regional characterization, such as plate tectonics, provide an intellectual framework within which Giga Scale measurement techniques, like seismic and satellite data, can be interpreted. The Mega Scale is the scale of reservoir characterization and includes well

logging, well testing, and 3D seismic analysis. The Macro Scale focuses on data sampling at the level of core analysis and fluid property analysis. The Micro Scale includes pore scale data obtained from techniques such as thin section analysis and measurements of grain-size distribution. Each of these scales contributes to the final reservoir model.

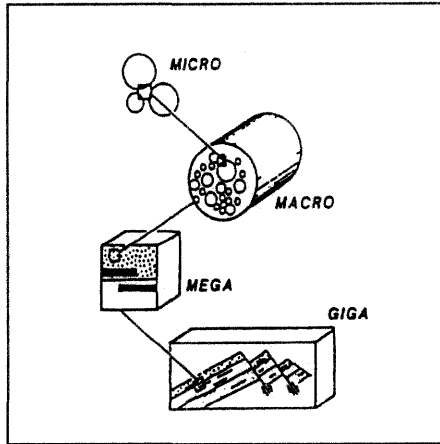


Figure 11-2. Reservoir scales (after Haldorsen and Lake, 1989; reprinted by permission of the Society of Petroleum Engineers).

11.2 Integrating Scales – the Flow Unit

All of the information collected at various scales must be integrated into a single, comprehensive, and consistent representation of the reservoir. The integration of data obtained at different scales is a difficult issue that is often referred to as the “scale-up” problem [for example, see Oreskes, et al., 1994]. Attempts to relate data from two different scales can be difficult. For example, permeability is often obtained from both pressure transient testing and routine core analysis. The respective permeabilities, however, may appear to be uncorrelated because they represent two different measurement scales. An important task of the scale-up problem is to develop a detailed understanding of how measured parameters vary with scale. The focus on detail in one or more

aspects of the reservoir modeling process can obscure the fundamental reservoir concept in a model study. One way to integrate available data within the context of a “big picture” is to apply the flow unit concept.

A flow unit is defined as “a volume of rock subdivided according to geological and petrophysical properties that influence the flow of fluids through it” [Ebanks, 1987]. Typical geologic and petrophysical properties are shown in Table 11-1. A classic application of the flow unit concept is presented in a paper by Slatt and Hopkins [1990].

Table 11-1
Properties Typically Needed to Define a Flow Unit

Geologic	Petrophysical
Texture Mineralogy Sedimentary Structure Bedding Contacts Permeability Barriers	Porosity Permeability Compressibility Fluid Saturations

A reservoir is modeled by subdividing its volume into an array of representative elementary volumes (REV). The REV concept is not the same as the flow unit concept. A flow unit is a contiguous part of the reservoir that has similar flow properties as characterized by geological and petrophysical data. Several flow unit identification techniques are proposed in the literature, such as the modified Lorenz plot used by Gunter, et al. [1997].

A simplified variation of the modified Lorenz plot technique is to identify a flow unit by plotting cumulative flow capacity as a function of depth. Cumulative flow capacity F_m is calculated as

$$F_m = \text{cum flow capacity} = \sum_{i=1}^m k_i h_i / \sum_{i=1}^n k_i h_i ; m = 1, \dots, n$$

where n is the total number of reservoir layers. The layers are numbered in order from the shallowest layer $i = 1$ to the deepest layer $i = m$ for a cumulative flow capacity F_m at depth

$$Z_m = Z_0 + \sum_{i=1}^m h_i$$

where Z_0 is the depth to the top of layer 1 from a specified datum. A flow unit will appear on the plot as a line with constant slope. A change in slope is interpreted as a change from one flow unit to another, as illustrated in Figure 11-3. Slope changes in Figure 11-3 occur at depths of 36 feet, 76 feet, 92 feet, 108 feet, 116 feet, 124 feet, 140 feet, 152 feet, and 172 feet. The largest slope is between 108 feet and 116 feet, and corresponds to a high permeability zone. It is followed immediately by a low permeability zone at a depth of approximately 120 feet.

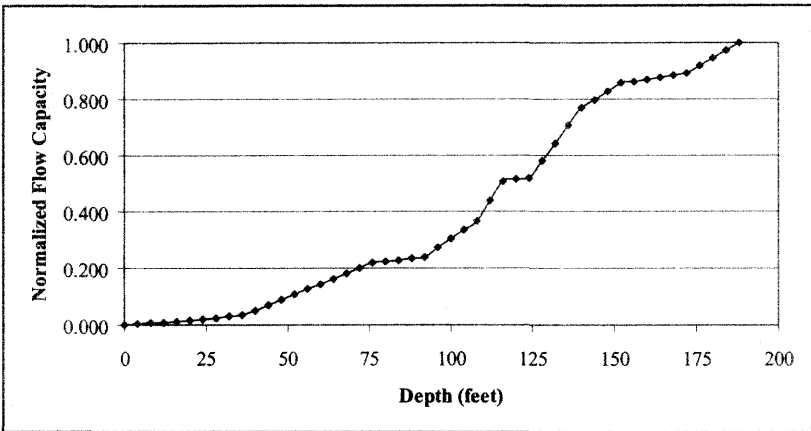


Figure 11-3. Identifying flow units.

Flow units usually contain one or more REV's. By contrast, the REV is the volume element that is large enough to provide statistically significant average values of parameters describing flow in the contained volume, but small enough to provide a meaningful numerical approximation of the fundamental flow equations [for example, see Bear, 1972]. As noted by Fayers and Hewett [1992], "It is somewhat an act of faith that reservoirs can be described by relatively few REV types at each scale with stationary average properties."

The flow unit concept is an effective means of managing the growing base of data being provided by geoscientists. Increasing refinement in geoscientific

analysis gives modelers more detail than they can use. Even today, with 100,000 to one million gridblock flow models, modelers cannot use all of the information that is provided by computer-based geologic models. Computer-based geologic models often have in excess of one million grid points. It is still necessary to coarsen detailed geologic models into representative flow units.

An understanding of the big picture, even as a simple sketch, is a valuable resource for validating the ideas being quantified in a model. Richardson, et al. [1987b] sketched several common types of reservoir models: a deep-water fan; a sand-rich delta; a deltaic channel contrasted with a deltaic bar, etc. Their sketches illustrate what the reservoir might look like for a specified set of assumptions. A sketch such as Figure 11-4 is a good tool for confirming that people from different disciplines share the same concept of a reservoir; it is a simple visual aid that enhances communication. In many cases, especially the case of relatively small fields, the best picture of the reservoir may only be a qualitative picture. When a more detailed study begins, the qualitative picture can be upgraded by quantifying parameters such as gross thickness in the context of the conceptual sketch of the reservoir.



Figure 11-4. Mississippi Delta.

Confidence in model performance is acquired by using the model to match historical field performance. History matching and model validation will be discussed in greater detail later. From a technical perspective, flow models should be updated and refined as additional information is obtained from the

field. In practice, the frequency of model updates depends on the importance of the resource being modeled to the enterprise.

11.3 Geostatistical Case Study

The process of characterizing a reservoir in a format that is suitable for use in a reservoir simulator begins with the gathering of data at control points such as wells. Once this occurs, the data can be contoured and digitized. The resulting set of digitized maps becomes part of the input data set for a reservoir simulator.

The contouring step in the process outlined above is changing. Contouring is the step in which reservoir parameters such as thickness and porosity are spatially distributed. The spatial distribution of reservoir parameters is a fundamental aspect of the reservoir characterization process. Two methods for spatially distributing reservoir parameters are emerging: geostatistics and reservoir geophysics.

Many modelers view geostatistics as the method of choice for sophisticated reservoir flow modeling [for example, see Lieber, 1996; Haldorsen and Damsleth, 1993; and Rossini, et al., 1994], even though the resulting reservoir characterization is statistical. By contrast, information obtained from reservoir geophysics is improving our ability to “see” between wells in a deterministic sense. Are these methods competing or complementary? This section presents a case study that demonstrates several points about geostatistics. A reservoir geophysical case study is presented in the next chapter. A review of these studies can help you decide whether either method is appropriate for a particular application.

An example of a full field model study using a geostatistical reservoir realization is the reservoir management study of the N.E. Nash Unit in Oklahoma [Fanchi, et al., 1996]. The goal of the study was to prepare a full field reservoir model that could be used to identify unswept parts of the field. We knew, based on the history of the field, that water was breaking through at several wells. The study was designed to look for places where an additional production well could be economically drilled.

The N.E. Nash Unit has a gradual dip from north to south. The Misener sandstone reservoir is bounded above by the Woodford shale, on the flanks by the Sylvan shale, and below by the Viola limestone. The Viola limestone does allow some aquifer support for the Misener sandstone.

One of the primary tasks of the study was to map the N.E. Nash Unit. Two sets of maps were prepared: conventional hand-drawn maps, and a set of maps based on a geostatistical analysis of the field. The hand-drawn maps correspond to the deterministic approach in which a single realization is used, while the geostatistical maps correspond to a stochastic image of the reservoir.

A geostatistical analysis was performed using 42 well control points to calculate structural tops, gross thickness, net-to-gross ratio, and porosity. A cross-plot between porosity and core permeability yielded a relationship for calculating permeability from porosity. From this data, directional semi-variograms (Table 11-2) were prepared to describe the spatial continuity of each parameter. The semi-variograms represent parameter changes as functions of distance and direction. For a detailed technical discussion of geostatistics, see a text such as Isaaks and Srivastava [1989]. Hebert, et al. [1993] have published some geostatistical software that is compatible with BOAST II.

Table 11-2
Semi-Variogram Model

Goal: Model spatial correlation of data with semi-variance $\gamma(h)$	
Semi-Variance	
$\gamma(h) = \frac{1}{2N(h)} \sum_{i=1}^{N(h)} [Z(x_i) - Z(x_i + h)]^2$	
$Z(x_i)$	Value of spatially distributed property at point x_i , for example, ϕ , K .
h	Spatial vector or “lag” distance between data point at $x_i + h$ and data point at x_i . “Lag” h is a vector with length and direction.
$N(h)$	Number of data pairs approximately separated by vector h .

When two sets of maps were compared, the hand-drawn maps were found to be more homogenous than the geostatistical maps. The geostatistical maps

exhibited the large-scale trends shown in the hand-drawn maps, but contained more local variability. This was not surprising, since additional heterogeneity is expected to arise as a result of geostatistical mapping.

The choice of final maps was based on management priorities: minimize the risk of drilling a dry hole on the flanks of the field, and complete the study before water breakthrough occurred in the remaining oil producers. The geostatistical model satisfied both of these criteria. The main flow path in the reservoir was narrower in the geostatistically generated maps than in the hand-drawn maps, and the geostatistical realization could be modified in a day or two.

Once a set of maps was chosen, the history match process could begin. Tracer information in the form of salinity changes was useful in helping identify sources of injection water as the water was produced. This was valuable in defining flow channels that could not otherwise be inferred. In some areas, transmissibility and porosity changes were needed to match water cut and reservoir pressure.

The geostatistical realization used in the N.E. Nash study was just a single realization. It was selected because it satisfied constraints imposed by previous volumetric and material balance studies. If these constraints were not available or were less reliable, which would be the case early in the life of a field, a geostatistical study would require the use of multiple realizations to characterize the reservoir. This raises the question of how many realizations are necessary.

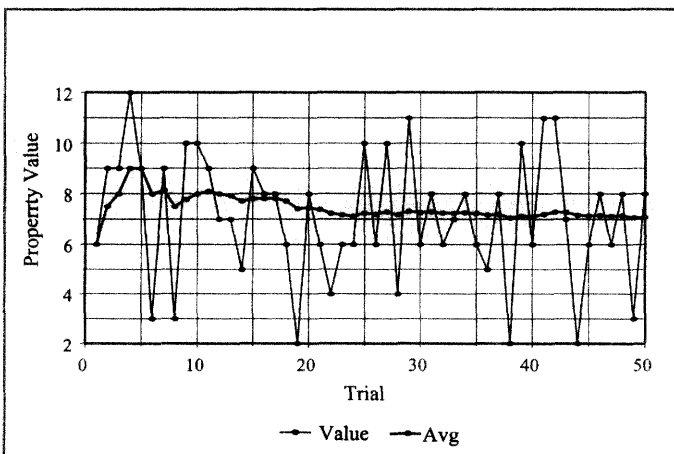


Figure 11-5. Running average.

Figure 11-5 shows a random sampling from a discrete probability distribution. A running average is also plotted. The figure shows that the running average does not stabilize, or approach a constant value, until at least 20 trials have been completed. This is a large number of realizations if history matching is needed for each realization. Indeed, it would be an unacceptably large number of realizations, in most cases, because of the time it takes to perform a history match.

Multiple realizations can also confuse people who are not closely involved with the modeling process because they do not have a single picture of the reservoir. On the other hand, the use of multiple realizations makes it possible to quantify the uncertainty associated with our limited knowledge of properties distributed spatially throughout the field. Table 11-3 summarizes the advantages and concerns associated with geostatistics. There is no established procedure for selecting one or more realizations for history matching from a set of geostatistically derived realizations. One procedure is described by Rossini, et al. [1994]. An application of reservoir geostatistics in the context of a multidisciplinary study is presented by Wang, et al. [1998].

Table 11-3
Geostatistics

Advantages	Concerns
<ul style="list-style-type: none"> ◆ Realism ◆ Quantifies uncertainty 	<ul style="list-style-type: none"> ◆ Cost and confusion of multiple realizations ◆ History matching still necessary to account for model discontinuities such as channeling ◆ History matching complicated by factors such as probabilistically generated heterogeneity

Exercises

Exercise 11.1 (A) Run EXAM1.DAT and record the final time, final pressure and initial oil volume (B) Multiply the volume of the reservoir in EXAM1.DAT by 0.5, 10 and 100. This can be done by altering the gridblock size (see Chapter 24.1.1). Make a table showing the final time, final pressure, and initial oil volume for each case. (C) How does the change in volume affect the pressure

performance of the model as a function of time?

Exercise 11.2 Repeat Exercise 11.1, but make the volume changes by modifying the grid dimensions using the modification option presented in Chapter 24.1.2.

Exercise 11.3 Roll a pair of dice 50 times and record the results. Calculate a running average by calculating a new average after each trial (roll of the dice). Plot the running average for each trial. How many trials are necessary before the average stabilizes, that is, the average approaches a constant value?

Chapter 12

Reservoir Structure

The physical size and shape of the reservoir may be inferred from several methods that serve as sources of information for defining the large-scale structure of the reservoir. These information sources are briefly reviewed below.

12.1 Giga Scale

Seismic measurements discussed in the literature by authors such as Ausburn, et al. [1978], McQuillin, et al. [1984], Sheriff [1989] and Dorn [1998] provide much of the Giga Scale information that can be directly used to characterize a reservoir. Historically, seismic analyses have been of interest primarily as a means of establishing the structural size of the reservoir. People did not believe that seismic data could resolve sufficient detail to provide information beyond overall reservoir structure. But that view has changed with the emergence of 4-D seismic monitoring and reservoir geophysics [for example, see Richardson, 1989; Ruijtenberg, et al., 1990; Anderson, 1995; He, et al., 1996; Johnston, 1997; ; Fanchi, et al. 1999]. It is therefore worthwhile to introduce some basic geophysical concepts within the context of the reservoir management function.

Seismic waves are vibrations that propagate from a source, such as an explosion, through the earth until they encounter a reflecting surface and are reflected into a detector, such as a geophone. Figure 12-1 shows a seismic trace. Each trace represents the signal received by a detector. Changes to the amplitude

of seismic waves occur at reflectors. A seismic reflection occurs at the interface between two regions with different acoustic impedances.

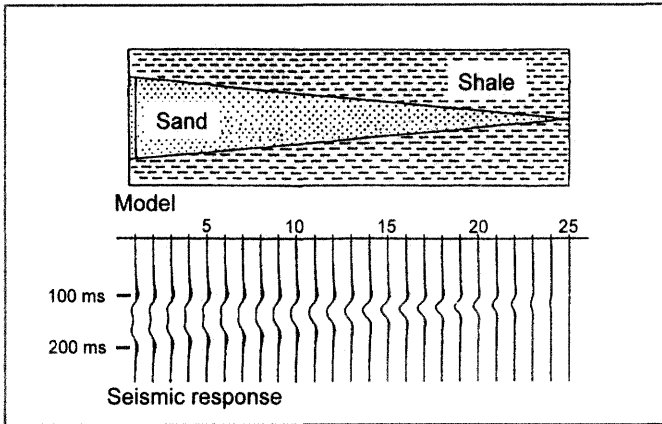


Figure 12-1. Seismic trace for a sand wedge (after Ruijtenberg, 1990; reprinted by permission of the Society of Petroleum Engineers).

Acoustic impedance is a fundamental seismic parameter. Acoustic impedance is defined as $Z = \rho V$ where ρ is the bulk density of the medium and V is the compressional velocity of the wave in the medium. Figure 12-2

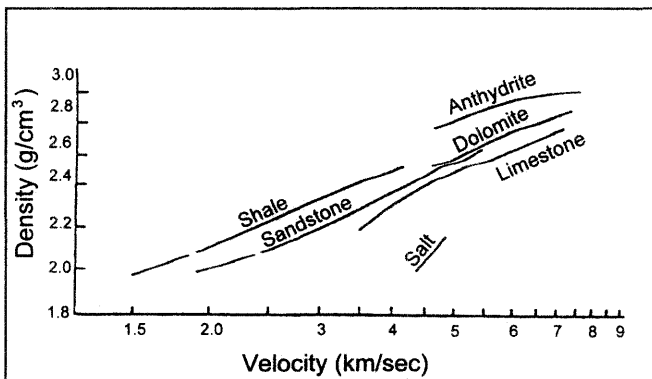


Figure 12-2. Seismic wave velocity and bulk density of rock (after Telford, et al., 1976; reprinted by permission of Cambridge University Press; after Gardner, et al., 1974).

illustrates a correlation between seismic wave velocity and the bulk density of different types of rock. Further discussion of rock properties and their relationship to seismic variables can be found in the literature [for example, Schön 1996].

A change in acoustic impedance will cause a reflection of the sound wave. The ability to reflect a sound wave by a change in acoustic impedance is quantified in terms of the reflection coefficient. The reflection coefficient R at the interface between two contiguous layers is defined in terms of acoustic impedances as

$$R = \frac{Z_2 - Z_1}{Z_2 + Z_1} = \frac{\rho_2 V_2 - \rho_1 V_1}{\rho_2 V_2 + \rho_1 V_1}$$

where subscripts 1 and 2 refer to the contiguous layers.

Reflection coefficient magnitudes for typical subsurface interfaces are illustrated in Table 12-1. Values of reflection coefficients at the sandstone/limestone interface show that reflection coefficient values can be relatively small. In addition to reflection coefficient, a transmission coefficient can be defined. The transmission coefficient is one minus the reflection coefficient.

Table 12-1
Typical Reflection Coefficients

Interface	Reflection Coefficient
Sandstone on limestone	0.040
Limestone on sandstone	- 0.040
Ocean bottom	0.11 (soft) to 0.44 (hard)

Nonzero reflection coefficients occur when a wave encounters a change in acoustic impedance, either because of a change in compressional velocity of the wave as it propagates from one medium to another, or because the bulk densities of the media differ. If the change in acoustic impedance is large enough, the reflection can be measured at the surface. That is why gas tends to show up as bright spots on seismic data – there is a big change in the density of the fluid. By contrast, the presence of an oil/water contact is harder to observe with seismic

measurements because density differences between the oil and water phases are relatively small and result in small changes in acoustic impedance.

The seismic trace plots seismic amplitude versus two-way travel time, or the time it takes the seismic wave to propagate from the source to the receiver. One of the central problems in seismic data processing is to determine the time/depth conversion. The conversion of travel time data to formation depth requires that the velocity associated with each geologic zone be known or can be inferred as the wave evolves with time. When the time/depth conversion is applied to seismic data, it can change the relative depths of seismic amplitudes associated with adjacent traces.

Figure 12-3 shows the amplitude and wavelength of a seismic wave [after de Buyl, et al., 1988]. The sonic log response shown in Figure 12-3 illustrates the relationship between seismic amplitude and the sonic log. Sonic logs are typically used to calibrate seismic data when seismic data is used in reservoir characterization. The sonic log response in Figure 12-3 delineates the top and base of a geologic section.

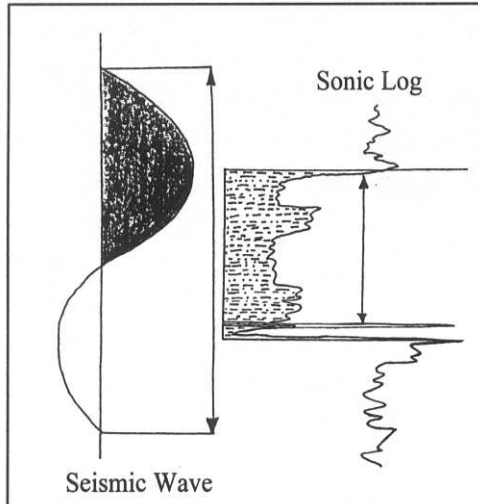


Figure 12-3. Seismic wave and sonic log response.

The wavelength of the seismic wave is the velocity of the wave divided by its frequency. Alternatively, the wavelength is the velocity in a given medium

times the period of the wave. The frequency of the wave is a measure of the energy of the wave and is conserved as the wave propagates from one medium to another. The wavelength, however, can vary from one medium to another.

When waves overlap – or superpose – they create a wavelet, as shown in Figure 12-4. The time duration associated with the wavelet disturbance is denoted Δt . The wavelet has a velocity V in a medium, and the period T is the width of the wavelet when plotted as a trace on a time-map of seismic data. The length of the wave is equal to the velocity V times the period T . Thus, if the wavelet has a 10 millisecond period and the velocity is 5000 feet per second in a particular medium, then the length L of that wavelet is 50 feet.

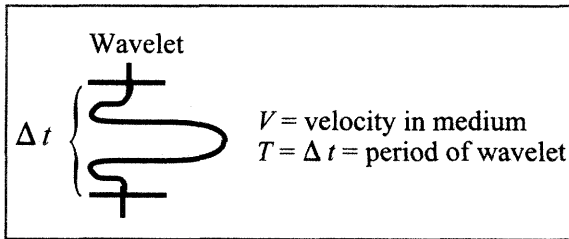


Figure 12-4. Seismic wavelet.

If seismic data has enough resolving power to show the reflecting boundaries of a geologic layer, then the amplitudes of the seismic waves may be useful for further characterizing petrophysical properties of the reservoir. For example, suppose a reservoir region is characterized by a porosity ϕ , permeability K , net thickness h_{net} , and oil saturation S_o . Seismic amplitude may be correlatable with rock quality (for example, Kh_{net} or ϕkh_{net}) or oil productive capacity (for example, $S_o \phi kh_{net}$). When a correlation does exist between seismic amplitude and a grouping of petrophysical parameters, the correlation may be used to help guide the distribution of reservoir properties in areas between wells.

Figures 12-5a and b show two approaches to contouring a set of values at control points. The smooth contour lines shown in Figure 12-5a are preferred by mappers [Tearpock and Bischke, 1991] unless the undulating contour lines in Figure 12-5b are supported by additional data. Seismic correlations can be used to justify the more heterogeneous contouring style shown in Figure 12-5b. A growing body of literature provides additional discussion of this application

in the context of an emerging discipline known as reservoir geophysics. For example, see de Buyl, et al. [1988], Evans [1996], Blackwelder, et al. [1996], Beasley [1996], and Jack [1998].

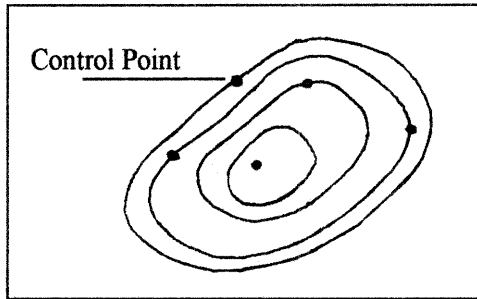


Figure 12-5a. Smooth contour lines.

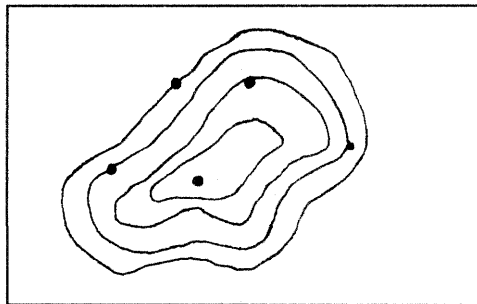


Figure 12-5b. Undulating contour lines.

12.2 Mega Scale

The Giga Scale helps define reservoir architecture, but is too coarse to provide the detail needed to design a reservoir development plan. The Mega Scale is the scale at which we begin to integrate well log and well test data into a working model of the reservoir. Table 12-2 illustrates the type of information that can be obtained at the Mega Scale level from well log data. The most common interpretations of each log response are included in the table. For example, a high gamma ray response implies the presence of shales, while a low gamma ray response implies the presence of clean sands or carbonates. A combination of well logging tools is usually needed to minimize ambiguity in log interpretation, as discussed by Brock [1986].

Table 12-2
Well Log Response

Log	Variable	Response
Gamma ray	Rock type	<p>Detects shale from in situ radioactivity.</p> <ul style="list-style-type: none"> ◆ High GR ⇒ shales ◆ Low GR ⇒ clean sands or carbonates
Resistivity	Fluid type	<p>Measures resistivity of formation water.</p> <ul style="list-style-type: none"> ◆ High resistivity ⇒ hydrocarbons ◆ Low resistivity ⇒ brine
Density	Porosity	<p>Measures electron density by detecting Compton scattered gamma rays. Electron density is related to formation density. Good for detecting hydrocarbon gas with low density compared to rock or liquid.</p> <ul style="list-style-type: none"> ◆ Low response ⇒ low HC gas content ◆ Large response ⇒ high HC gas content
Acoustic (sonic)	Porosity	<p>Measures speed of sound in medium. Speed of sound is faster in rock than in fluid.</p> <ul style="list-style-type: none"> ◆ Long travel time ⇒ slow speed ⇒ large pore space ◆ Short travel time ⇒ high speed ⇒ small pore space
Neutron	Hydrogen content	<p>Fast neutrons are slowed by collisions to thermal energies. Thermal neutrons are captured by nuclei, which then emit detectable gamma rays. Note: Hydrogen has a large capture cross-section for thermal neutrons. Good for detecting gas.</p> <ul style="list-style-type: none"> ◆ Large response ⇒ high H content ◆ Small response ⇒ low H content
Spontaneous potential	Permeable beds	<p>Measures electrical potential (voltage) associated with movement of ions.</p> <ul style="list-style-type: none"> ◆ Low response ⇒ impermeable shales ◆ Large response ⇒ permeable beds

Table 12-3 from Kamal, et al. [1995] illustrates the type of information that can be obtained at the Mega Scale level from well test data. The table also notes the time in the life of the project when the well test is most likely to be run. It is usually necessary to run a variety of well tests as the project matures. These tests help refine the operator's understanding of the field and often motivate changes in the way the well or the field is operated. Additional information about well testing can be found in literature sources such as Matthews and Russell [1967], Earlougher [1977], and Sabet [1991].

Table 12-3
Reservoir Properties Obtainable from Transient Tests

Type of Test	Properties	Development Stage
Drill stem tests	Reservoir behavior Permeability Skin Fracture length Reservoir pressure Reservoir limit Boundaries	Exploration and appraisal wells
Repeat-formation tests / Multiple formation tests	Pressure profile	Exploration and appraisal wells
Drawdown tests	Reservoir behavior Permeability Skin Fracture length Reservoir limit Boundaries	Primary, secondary and enhanced recovery
Buildup tests	Reservoir behavior Permeability Skin Fracture length Reservoir pressure Reservoir limit Boundaries	Primary, secondary, and enhanced recovery

Table 12-3 (cont.)
Reservoir Properties Obtainable from Transient Tests

Step-rate tests	Formation parting pressure Permeability Skin	Secondary and enhanced recovery
Falloff tests	Mobility in various banks Skin Reservoir pressure Fracture length Location of front Boundaries	Secondary and enhanced recovery
Interference and pulse tests	Communication between wells Reservoir type behavior Porosity Interwell permeability Vertical permeability	Primary, secondary, and enhanced recovery
Layered reservoir tests	Properties of individual layers Horizontal permeability Vertical permeability Skin Average layer pressure Outer boundaries	Throughout reservoir life

Tables 12-2 and 12-3 illustrate a few of the methods used to gather Mega Scale information. Advances in technology periodically add to a growing list of transient tests and well log tools [for example, see Kamal, 1995; Felder, 1994]. In many cases, budgetary constraints will be the controlling factor in determining the number and type of tests run. The modeling team must work with whatever information is available. Occasionally, an additional well test or well log will need to be run, but the expense and scheduling make it difficult to justify acquiring new well log or well test information once a simulation study is underway.

12.3 Reservoir Description Using Seismic Data

Reservoir geophysics has the potential to image important reservoir parameters in regions between wells. This potential has limitations, but before discussing these limitations, let us first consider how reservoir geophysics may be used and review an example where the potential of reservoir geophysics was realized.

The reservoir geophysical procedure requires the correlation of seismic data with reservoir properties. Correlations are sought by making crossplots of seismic data with reservoir properties. Some correlation pairs are listed below.

◆ Seismic Amplitude vs Rock Quality

$$\diamond \text{Rock Quality} = kh_{net}, \phi kh_{net}, \text{ etc.}$$

◆ Seismic Amplitude vs Oil Productive Capacity (OPC)

$$\diamond \text{OPC} = S_o \phi kh_{net}$$

◆ Acoustic Impedance vs Porosity

If a statistically significant correlation is found, it can be used to guide the distribution of reservoir properties between wells. Ideally, the property distribution procedure will preserve reservoir properties at wells.

De Buyl, et al. [1988] used reservoir geophysics to predict reservoir properties of two wells. They correlated well-log-derived properties with seismically controlled properties, for example, porosity, then used the correlation to distribute properties. Maps drawn from seismically controlled distributions exhibited more heterogeneity than conventional maps drawn from well-log-derived properties. Unlike geostatistics, where additional heterogeneity is obtained by sampling from a probability distribution, heterogeneity based on seismically controlled distributions represents spatial variations in reservoir properties determined by direct observation, albeit observation based on interpreted seismic data.

An indication of the technical success of the reservoir geophysical technique is given in Table 12-4. Actual values of reservoir parameters at two well locations are compared with values predicted using both well-log-derived properties and seismically controlled properties. This work by De Buyl, et al. [1988] is notable because it scientifically tests the seismic method: it makes

predictions and then uses measurements to assess their validity. In this particular case, a reservoir characterization based on seismically controlled properties yielded more accurate predictions of reservoir properties than predictions made using a reservoir characterization based only on well data.

Table 12-4
Predictions at New Wells from Seismic and Well Data
 [de Buyl, et al., 1988]

Well		Measured Values	Seismic Predicted	Well Data Predicted
I	Top of Reservoir (m)	-178.0	-175.0	-181.0
	Gross Porosity (vol %)	15.0	15.5	15.4
	Net ϕ h (m)	1.78	1.53	1.96
J	Top of Reservoir (m)	-182.0	-179.0	-174.0
	Gross Porosity (vol %)	13.9	10.6	8.0
	Net ϕ h (m)	1.08	1.05	0.15

Although reservoir geophysical techniques are still evolving, it is possible to make some general statements about the relative value of this emerging technology. Table 12-5 summarizes the advantages and concerns associated with reservoir geophysics.

Table 12-5
Reservoir Geophysics

Advantages	Concerns
<ul style="list-style-type: none"> ◆ Able to “see” between wells ◆ Single realizations enhance <ul style="list-style-type: none"> ◇ communication ◇ understanding 	<ul style="list-style-type: none"> ◆ Cost of data acquisition and analysis ◆ Limited applicability ◆ Validity of realization unknown without sensitivity analysis

To demonstrate the limits of applicability of reservoir geophysics, the reservoir geophysical algorithm in WINB4D was used to study a hypothetical reservoir system in which we could expect to see significant changes in seismic properties as a function of field performance over time. In particular, a dipping gas reservoir with aquifer influx was studied. The reservoir grid is shown in Figure 12-6. The reservoir has an initial gas saturation of 70% and an initial

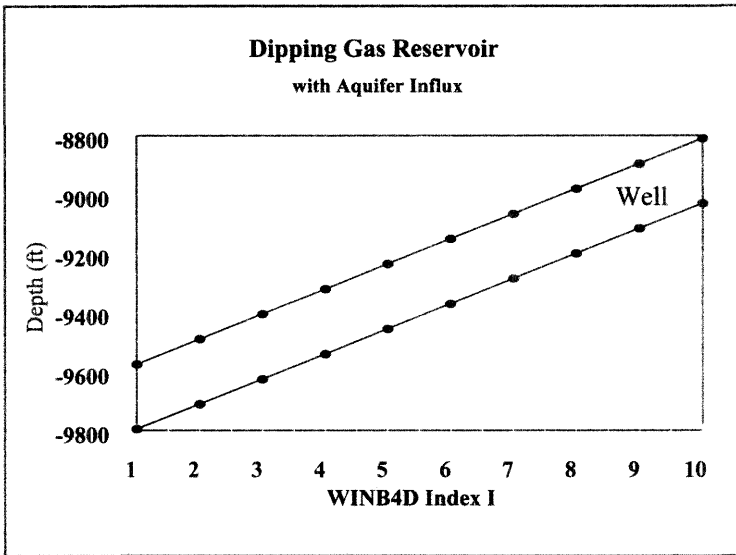


Figure 12-6. Cross-section of dipping gas reservoir.

irreducible water saturation of 30%. The initial ratio of compressional velocity to shear velocity (V_p/V_s) was 1.684. A downdip aquifer provides pressure support and water invasion as the reservoir is produced.

Figure 12-7 shows the results after one year of depletion with aquifer

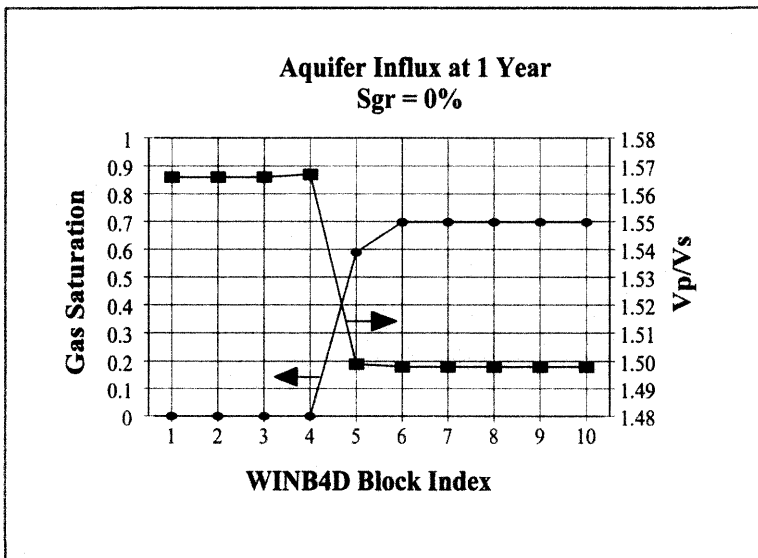


Figure 12-7. Reservoir performance with Sgr = 0%.

influx for a system with an irreducible gas saturation (Sgr) of 0%. The change in gas saturation shows the influx of aquifer water. The change in fluid content changes fluid bulk modulus. As a consequence, the ratio V_p/V_s changes significantly in the waterflooded part of the reservoir.

If we rerun the example with an irreducible gas saturation of three percent, we obtain the results shown in Figure 12-8. The large change in V_p/V_s is no

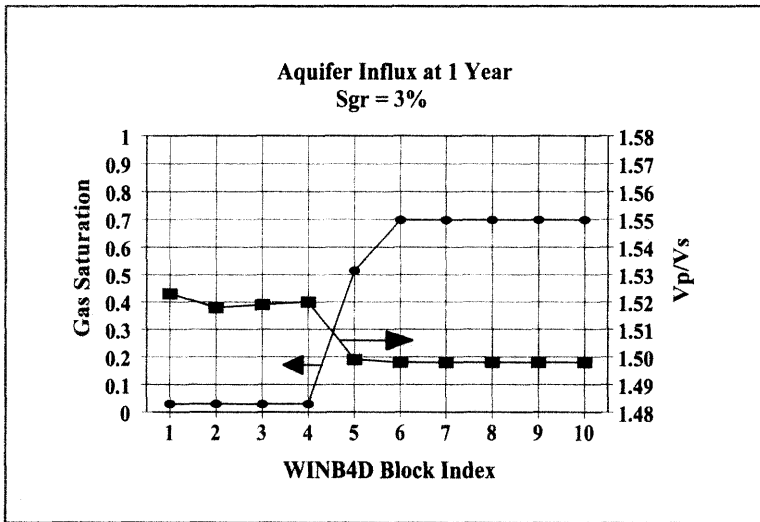


Figure 12-8. Reservoir performance with Sgr = 3%.

longer observed because the presence of a small amount of gas significantly changed the compressibility of the system.

Time-lapse seismic tomography, or 4-D seismic, could be used in our hypothetical example to track the movement of invading aquifer water, but the presence of a small amount of gas in the invaded zone increases the difficulty of detecting the gas-water contact. Calculations of 4-D seismic performance based on algorithms like the one coded in WINB4D can predict 4-D seismic responses [Fanchi, 1999], but such algorithms are not yet widely available in commercial simulators.

Although it is risky to predict technological developments, it is possible to infer trends by extrapolating ongoing research activities in the industry. Thakur [1996], for example, wrote that data management and the integration

of disciplines will play an increasingly important role in the future of reservoir modeling. Many modelers have predicted that the integration of disciplines will manifest itself in reservoir modeling as finer 3-D models with more seismic and geological detail [He, et al., 1996; Kazemi, 1996; Uland, et al., 1997]. This prediction is being borne out with growing interest in shared earth models [Tippee, 1998], model-centric working environments [Tobias, 1998; Fanchi, et al. 1999], and reservoir simulation models with a million or more gridblocks [Dogru, 2000].

Exercises

Exercise 12.1 Seismic Parameters: Data set EXAM11.DAT is a cross-section model of a two-layer gas reservoir undergoing depletion with aquifer influx into the lower layer. (A) Run EXAM11.DAT and find the initial water saturation (S_w), compressional velocity (V_p), reflection coefficient (RC), and ratio of compressional velocity to shear velocity (V_p/V_s) in block I = 1 of layer k = 2. (B) Verify the maps IVPMAP, IRCMAP and IVRMAP are activated using the information given in Chapter 25.1. Record S_w , V_p , RC, and V_p/V_s in block I = 1 of layer K = 2 at the end of the run. Notice how the attributes change as water moves into the layer.

Exercise 12.2 Repeat Exercise 12.1 using a critical gas saturation of 0. This should be achieved by setting the relative permeability of gas to 0.01 at a gas saturation of 0.03.

Exercise 12.3 Repeat Exercise 12.1 using a grain bulk modulus K_G that is equal to the frame bulk modulus K_p . Use Eq (27.13) to explain your results.

Chapter 13

Fluid Properties

Properties of petroleum fluids must be quantified in a reservoir simulator. The range of applicability of a reservoir simulator is defined, in part, by the types of fluids that can be modeled using the mathematical algorithms coded in the simulator. For these reasons, it is worth considering the general types of fluids that may be encountered in a commercial reservoir environment [for example, see Pedersen, et al., 1989; Koederitz, et al., 1989; McCain, 1973; and Amyx, et al., 1960].

13.1 Fluid Types

An estimate of the elemental composition (by mass) of petroleum is given in the following chart:

Carbon	84% - 87%
Hydrogen	11 % - 14%
Sulphur	0.6% - 8 %
Nitrogen	0.02% - 1.7%
Oxygen	0.08% - 1.8%
Metals	0% - 0.14%

It can be seen from the table that petroleum fluids are predominantly hydrocarbons. The most common hydrocarbon molecules are paraffins, naphthenes, and aromatics because of the relative stability of the molecules. A paraffin is

a saturated hydrocarbon, that is, it has a single bond between carbon atoms. Examples include methane and ethane. Paraffins have the general chemical formula C_nH_{2n+2} . Napthenes are saturated hydrocarbons with a ringed structure, as in cyclopentane. They have the general chemical formula C_nH_{2n} . Aromatics are unsaturated hydrocarbons with a ringed structure that have multiple bonds between the carbon atoms as in benzene. The unique ring structure makes aromatics relatively stable and unreactive.

A general PVT diagram of a pure substance displays phase behavior as a function of pressure, volume, and temperature. The types of properties of interest from a reservoir engineering perspective can be conveyed in a pressure-temperature (P-T) diagram of phase behavior like the one shown in Figure 13-1 (after Craft, et al. [1991]). Most reservoir fluids do not exhibit significant temperature effects *in situ*, although condensate reservoirs in thick sands may display a compositional gradient that can influence condensate yield as a function of well perforation depth.

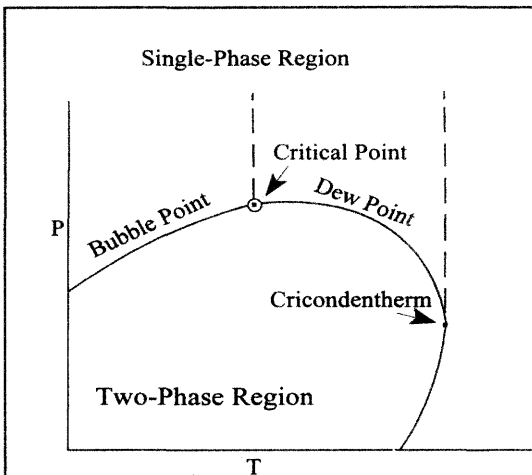


Figure 13-1. P-T diagram.

The P-T diagram includes both single-phase and two-phase regions. The line separating the single-phase region from the two-phase region is called the phase envelope. The black oil region is at low temperature and in the high pressure region above the bubble point curve separating the single-phase and

two-phase regions. If we consider pressures in the single-phase region and move to the right of the diagram by letting temperature increase towards the critical point, we encounter volatile oils. At temperatures above the critical point but less than the cricondentherm, reservoir fluids behave like condensates. The cricondentherm is the maximum temperature at which a fluid can exist in both the gas and liquid phases. When reservoir temperature is greater than the cricondentherm, we encounter gas reservoirs. A summary of these fluid types is given in Table 13-1. Notice that separator gas-oil ratio (GOR) is a useful indicator of fluid type.

Table 13-1
Rules of Thumb for Classifying Fluid Types

Fluid Type	Separator GOR (MSCF/STB)	Pressure Depletion Behavior in Reservoir
Dry gas	No surface liquids	Remains gas
Wet gas	> 100	Remains gas
Condensate	3 - 100	Gas with liquid drop out
Volatile oil	1.5 - 3	Liquid with significant gas
Black oil	0.1 - 1.5	Liquid with some gas
Heavy oil	~ 0	Negligible gas formation

Let us consider a reservoir containing hydrocarbons that are at a pressure and temperature corresponding to the single-phase black oil region. If reservoir pressure declines at constant temperature, the reservoir pressure will eventually cross the bubble point pressure curve and enter the two-phase gas-oil region. Similarly, starting with a single-phase condensate and letting reservoir pressure decline at constant temperature, the reservoir pressure will cross the dew point pressure curve to enter the two-phase region. In this case, a free-phase liquid drops out of the condensate gas. Once liquid drops out, it is very difficult to recover. One recovery method is dry gas cycling, but the recovery efficiency will be substantially less than 100%. If we drop the pressure even further, it is

possible to encounter retrograde condensation for some hydrocarbon compositions.

The P-T diagram also applies to temperature and pressure changes in a wellbore. In the case of wellbore flow, the fluid moves from relatively high reservoir temperature and pressure to relatively low surface temperature and pressure. As a result, it is common to see fluids that are single-phase in the reservoir become two-phase by the time they reach the surface.

Figure 13-2 is a P-T diagram that compares two-phase envelopes for four types of fluids. A reservoir fluid can change from one fluid type to another depending on how the reservoir is produced. A good example is dry gas injection into a black oil reservoir. Dry gas injection increases the relative amount of low molecular weight components in the black oil. The two-phase envelope rotates counter-clockwise in the P-T diagram as the relative amount of lower molecular weight components increases. Similarly, dry gas injection into a condensate can make the phase envelope transform from one fluid type to another. Thus, the way the reservoir is operated has a significant impact on fluid behavior in the reservoir and at the surface.

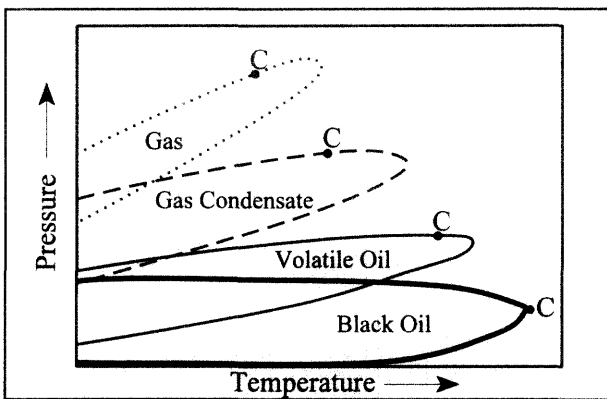


Figure 13-2. Typical two-phase P-T envelopes for different fluid types.

Table 13-2 shows different compositions for typical fluid types. Dry gas usually contains only the lower molecular weight components. Gas condensates start to add higher molecular weight components. Volatile oils continue to add higher molecular weight components. The addition of higher molecular weight components and the reduction of lower molecular weight components eventually

yields a black oil. If we monitor methane content (C_1), we see that it tends to decrease as fluids change from dry gas to black oil.

Table 13-2
Typical Molar Compositions of Petroleum Fluid Types
 [after Pedersen, et al., 1989]

Component	Gas	Gas Condensate	Volatile Oil	Black Oil
N_2	0.3	0.71	1.67	0.67
CO_2	1.1	8.65	2.18	2.11
C_1	90.0	70.86	60.51	34.93
C_2	4.9	8.53	7.52	7.00
C_3	1.9	4.95	4.74	7.82
iC_4+nC_4	1.1	2.00	4.12	5.48
iC_5+nC_5	0.4	0.81	2.97	3.80
iC_6+nC_6	C_{6+} : 0.3	0.46	1.99	3.04
C_7		0.61	2.45	4.39
C_8		0.71	2.41	4.71
C_9		0.39	1.69	3.21
C_{10}		0.28	1.42	1.79
C_{11}		0.20	1.02	1.72
C_{12}		0.15	C_{12+} : 5.31	1.74
C_{13}		0.11		1.74
C_{14}		0.10		1.35
C_{15}		0.07		1.34
C_{16}		0.05		1.06
C_{17}		C_{17+} : 0.37		1.02
C_{18}				1.00
C_{19}				0.90
C_{20}				C_{20+} : 9.18

13.2 Fluid Modeling

In general, fluid behavior is best modeled using an equation of state. Table 13-3 shows some cubic equations of state (EoS) used in commercial compositional simulators. In addition to pressure (P), volume (V), and temperature (T), the EoS contains the gas constant R and a set of adjustable parameters $\{a, b\}$ which may be functions of temperature. The EoS in Table 13-3 are called “cubic” because they yield a cubic equation for the compressibility factor $Z = PV/RT$. In the case of an ideal gas, $Z = 1$.

Table 13-3
Examples of Cubic Equations of State

Redlich-Kwong	$P = \frac{RT}{V-b} - \frac{a/T^{1/2}}{V(V+b)}$
Soave-Redlich-Kwong	$P = \frac{RT}{V-b} - \frac{a(T)}{V(V+b)}$
Peng-Robinson	$P = \frac{RT}{V-b} - \frac{a(T)}{V(V+b) + b(V-b)}$
Zudkevitch-Joffe	$P = \frac{RT}{V-b(T)} - \frac{a(T)/T^{1/2}}{V[V+b(T)]}$

Equations of state are valuable for representing fluid properties in many situations. For example, suppose we want to model a system in which production is commingled from more than one reservoir with more than one fluid type. In this case the most appropriate simulator would be a compositional simulator because a black oil simulator would not provide as accurate a representation of fluid behavior.

The two most common types of reservoir fluid models are black oil models and compositional models. Black oil models are based on the assumption that the saturated phase properties of two hydrocarbon phases (oil and gas) depend on pressure only. Compositional models also assume two hydrocarbon phases, but they allow the definition of many hydrocarbon components. Unlike a black oil simulator, which can be thought of as a compositional simulator with two components, a compositional simulator often has six to ten components. By comparison, process engineering simulators that are used to model surface facilities typically require up to 20 components or more. The cost of running a compositional simulator increases dramatically with increases in the number of components modeled, but the additional components make it possible to more accurately model complex fluid phase behavior. If compositional model results are to be used in a process engineering model, it is often necessary to compromise on the number of components to be used for each application.

Equations of state must be used to calculate equilibrium relations in a compositional model. This entails tuning parameters such as EoS parameters $\{a, b\}$ in Table 13-3. Several regression techniques exist for tuning an EoS. They usually differ in the choice of EoS parameters that are to be varied in an attempt to match lab data with the EoS.

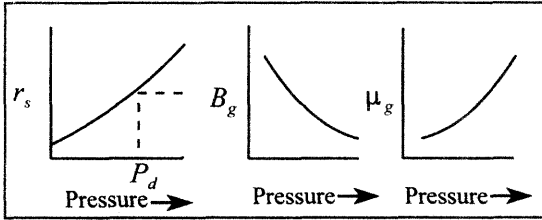


Figure 13-3. Gas phase properties.

Figures 13-3 and 13-4 show typical fluid property behavior of gas and oil properties for a black oil model. Gas phase properties are gas formation volume factor (B_g), gas viscosity (μ_g), and liquid yield (r_s). Oil phase properties are oil formation volume factor (B_o), oil viscosity (μ_o), and solution GOR (R_{so}).

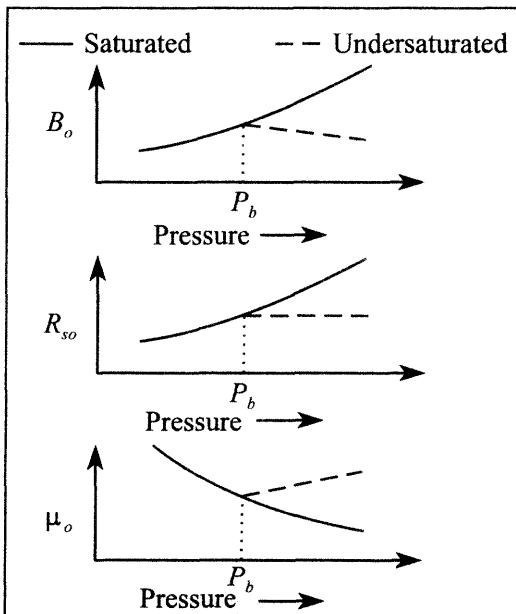


Figure 13-4. Oil phase properties.

Both saturated and undersaturated curves are included as functions of pressure only. Phase changes occur at the saturation pressures. Single-phase oil becomes two-phase gas-oil when pressure drops below the bubble point pressure (P_b), and single-phase gas becomes two-phase gas condensate when pressure drops below the dew point pressure (P_d).

Simulators run most efficiently when fluid property data are smooth curves. Any discontinuity in a curve can cause numerical difficulties. Ordinarily, realistic fluid properties are smooth functions of pressure except at points where phase transitions occur. As a practical matter, it is usually wise to plot input PVT data to verify the smoothness of the data. Most simulators reduce the nonlinearity of the gas formation volume factor B_g by using the inverse $b_g = 1/B_g$ to interpolate gas properties.

Oil properties from a laboratory must usually be corrected for use in a black oil simulator [Moses, 1986]. Flow in the reservoir is a relatively slow process that corresponds to a differential process in the laboratory. A differential process is one in which pressures are allowed to change in relatively small increments. For comparison, a flash process allows pressures in the experiment to change by relatively large increments. The production of oil up the wellbore to surface facilities is considered a flash process. Oil is flashed to the surface through several pressure and temperature regimes. The corrections applied to oil property data are designed to adjust the data to more adequately represent fluids as they flow differentially in the reservoir prior to being flashed to surface conditions. The corrections alter solution gas-oil ratio and oil formation volume factor. The effect of the correction is illustrated by the case study in Chapter 20. The oil property correction is often significant.

Water properties must also be entered in a simulator. Ideally water properties should be measured by performing laboratory analyses on produced water samples. If samples are not available, correlations are often sufficiently accurate for describing the behavior of water.

In the absence of reliable fluid data for one or more of the reservoir fluids, it may be necessary to use correlations. McCain [1991] reviewed the state of the art in the use of correlations to describe fluid properties. New correlations for

estimating bubble point pressure, formation volume factor, and isothermal oil compressibility have been proposed by Levitan and Murtha [1999].

13.3 Fluid Sampling

All laboratory measurements of fluid properties and subsequent analyses are useless if the fluid samples do not adequately represent *in situ* fluids. The goal of fluid sampling is to obtain a sample that is representative of the original fluid in the reservoir. It is often necessary to condition the well before the sample is taken. A well is conditioned by producing any nonrepresentative fluid, such as drilling mud, from within and around the wellbore until it is replaced by original reservoir fluid flowing into the wellbore. Fluid samples may then be taken from either the surface or subsurface.

Subsurface sampling requires lowering a pressurized container to the production interval and subsequently trapping a fluid sample. This is routinely accomplished by drill stem testing, especially when access to surface facilities is limited. It is generally cheaper and easier to take surface samples from separator gas and oil.

If a surface sample is taken, the original *in situ* fluid, that is, the fluid at reservoir conditions, must then be reconstituted by combining separator gas and separator oil samples. The recombination step assumes accurate measurements of flow data at the surface, especially gas-oil ratio. Subsurface sampling from a properly conditioned well avoids the recombination step, but is more difficult and costly than surface sampling, and usually provides a smaller volume of sample fluid. The validity of fluid property data depends on the quality of the fluid sampling procedure.

Exercises

Exercise 13.1 Data set EXAM9.DAT models depletion of a gas reservoir with aquifer support. Initial reservoir pressure is approximately 1947 psia. (A) Run the model at a temperature of 226°F and record time, pressure, gas rate, and water rate at the end of the run. Report the gas viscosity in the gas PVT table

at 2015 psia pressure. (B) Repeat A at a temperature of 150°F. (C) Explain the differences in model performance. For this example, neglect the temperature dependence of water properties. Refer to Chapter 24.6 for a description of WINB4D fluid property input data.

Exercise 13.2 Data file CS-VC4.DAT is a vertical column model with four layers. Layers $K = 1, 3, 4$ are pay zones, and layer $K = 2$ is a shale layer. The data set is a model of primary depletion of an initially undersaturated oil reservoir. (A) Run CS-VC4.DAT for three years and show gas saturation in all 4 layers at the end of the run. You should see gravity segregation and the formation of a gas cap in layer $K = 3$. (B) By referring to Chapter 25 and file WTEMP.WEL, determine which model layers are being depleted through wellbore perforations.

Exercise 13.3 Replace solution gas-oil ratio in CS-VC4.DAT with the following data. Run the modified data set for a period of three years, and then compare the results with the results of Exercise 13.2.

Pressure (psia)	Solution Gas-Oil Ratio (SCF/STB)
14.7	1.0
514.7	54.0
1014.7	105.0
1514.7	209.0
2014.7	292.0
2514.7	357.0
3014.7	421.0
4014.7	486.0
5014.7	522.0
6014.7	550.0

Exercise 13.4 Run the data set prepared in Exercise 13.3 with the assumption that no fluids can flow between model layers (multiply z direction transmissibility by zero).

Exercise 13.5 Run data file CS-VC4.DAT with the bubble point pressure reduced by 500 psia. What effect does this have on solution gas-oil ratio and model performance?

Chapter 14

Rock-Fluid Interaction

The previous two chapters described the data needed to model the solid structure of the reservoir and the behavior of fluids contained within the solid structure. Small-scale laboratory measurements of fluid flow in porous media show that fluid behavior depends on the properties of the solid material. The interaction between rock and fluid is modeled using a variety of physical parameters that include relative permeability and capillary pressure [Collins, 1961; Dake, 1978; Koederitz, et al., 1989]. Laboratory measurements provide information at the core scale (Macro Scale) and, in some cases, at the microscopic scale (Micro Scale). They are the subject of the present chapter.

14.1 Porosity, Permeability, Saturation, and Darcy's Law

Porosity, permeability, and saturation can be obtained from Mega Scale measurements such as well logs and well tests, and by direct measurement in the laboratory. Comparing values of properties obtained using methods at two different scales demonstrates the sensitivity of important physical parameters to the scale at which they were measured. Ideally there will be good agreement between the two scales; that is, well log porosity or well test permeability will agree with corresponding values measured in the laboratory. In many cases, however, there are disagreements. Assuming measurement error is not the source of disagreement, differences in values show that differences in scale can impact the measured value of the physical parameter. A well test permeability, for example, represents an average over an area of investigation that is very large

compared to a laboratory measurement of permeability using a six-inch core sample. The modeling team often has to make judgements about the relative merits of contradictory data. The history matching process recognizes this source of uncertainty, as is discussed in subsequent chapters.

The most common types of reservoir rock are listed in Table 14-1. One of the most fundamental properties of rock that must be included in a reservoir model is porosity. Porosity is the fraction of a porous medium that is void space. If the void space is connected and communicates with a wellbore, it is referred to as effective porosity, otherwise the void space is ineffective porosity. The original porosity resulting from sediment deposition is called primary porosity. Secondary porosity is an incremental increase in primary porosity due to the chemical dissolution of reservoir rocks, especially carbonates. Primary and secondary porosity can be both effective and ineffective. Total porosity is a combination of ineffective porosity and effective (interconnected) porosity.

Table 14-1
Common Reservoir Rocks

Sandstones	Compacted sediment Conglomerate
Shales	Laminated sediment Predominantly clay
Carbonates	Produced by chemical and biochemical sources Limestone

Porosity values depend on rock type, as shown in Table 14-2. There are two basic techniques for directly measuring porosity: core analysis in the laboratory and well logging. Laboratory measurements tend to be more accurate, but sample only a small fraction of the reservoir. Changes in rock properties may also occur when the core is brought from the reservoir to the surface. Well log measurements sample a much larger portion of the reservoir than core analysis, but typically yield less accurate values. Ideally, a correlation can be established between *in situ* measurements such as well logging and surface measurements such as core analysis.

Table 14-2
Dependence of Porosity on Rock Type

Rock Type	Porosity Range (%)	Typical Porosity (%)
Sandstone	15-35	25
Unconsolidated sandstone	20-35	30
Carbonate		
• Intercrystalline limestone	5-20	15
• Oolitic limestone	20-35	25
• Dolomite	10-25	20

Darcy's Law is the basic equation describing fluid flow in a simulator. Darcy's equation for single-phase flow is

$$Q = -0.001127 \frac{KA}{\mu} \frac{\Delta P}{\Delta x}$$

where the physical variables are defined in oil field units as

- Q = flow rate (bbl/day)
- A = cross-sectional area (ft²)
- μ = fluid viscosity (cp)
- K = permeability (md)
- P = pressure (psi)
- x = length (ft)

Darcy's Law says that rate is proportional to cross-sectional area times pressure difference ΔP across a distance Δx , and is inversely proportional to the viscosity of the fluid. The minus sign shows that the direction of flow is opposite to the direction of increasing pressure; fluids flow from high pressure to low pressure in a horizontal (gravity-free) system.

The linearity of Darcy's Law is an approximation that is made by virtually all commercial simulators. Fluid flow in a porous medium can have a nonlinear effect that is represented by the Forcheimer equation [Govier, 1978]. The nonlinear effect becomes more important in high flow rate gas wells.

Permeability is a physical constant describing flow in a given sample for a given fluid and set of experimental conditions. If those conditions are changed, the permeability being measured may not apply. For example, if a waterflood is planned for a reservoir that is undergoing gravity drainage, laboratory measured permeabilities need to represent the injection of water into a core with hydrocarbon and connate water. The permeability distribution and the relative permeability curves put in the model need to reflect the type of processes that occur in the reservoir.

Permeability has meaning as a statistical representation of a large number of pores. A Micro Scale measurement of grain-size distribution shows that different grain sizes and shapes affect permeability. Permeability usually decreases as grain size decreases. It may be viewed as a mathematical convenience for describing the statistical behavior of a given flow experiment. In this context, transient testing gives the best measure of permeability over a large volume. Despite its importance to the calculation of flow, permeability and its distribution will not be known accurately. Seismic data can help define the distribution of permeability between wells if a good correlation exists between seismic amplitude and a rock quality measurement that includes permeability.

It is not unusual to find that permeability has a directional component: that is, permeability is larger in one direction than another [for example, see Fanchi, et al., 1996]. When a model is being designed, the modeling team should account for the direction associated with permeability. In principle, simulators can take all of these effects into account. In practice, however, the tensor permeability discussed in the literature by, for example, Bear [1972] and Lake [1988] is seldom reflected in a simulator. The usual assumption is that permeability is aligned along one of three orthogonal directions known as the principal axes of the tensor. This assumption has implications for model studies that should be considered when assessing model results (see Chapter 15 and Fanchi [1983]).

In many cases vertical permeability is not measured and must be assumed. A rule of thumb is to assume vertical permeability is approximately one tenth of horizontal permeability. These are reasonable assumptions when there is no data to the contrary.

14.2 Relative Permeability and Capillary Pressure

Reservoir models calculate saturation as a function of time. Consider the case of water displacing oil. Initially, oil occupies the interior of pore spaces, and connate water is adjacent to the rock surface of a water-wet reservoir. When the flood begins, water displaces oil through the interconnected pore space. The measure of interconnectedness is permeability. The oil left behind after the waterflood is residual or irreducible oil saturation. Similar behavior is seen for other combinations of multiphase flow, for example, gas-oil, gas-water, and gas-oil-water. Multiphase flow is modeled by including relative permeability curves in the simulator. Saturation end points for the relative permeability curves are used to establish initial fluids-in-place in addition to modeling flow behavior.

A typical set of relative permeability curves is shown in Figure 14-1. Relative permeability curves represent flow mechanisms, such as drainage or imbibition processes, or fluid wettability. Relative permeability data should be obtained by experiments that best model the type of displacement that is thought to dominate reservoir flow performance. For example, water-oil imbibition curves are representative of waterflooding, while water-oil drainage curves describe the movement of oil into a water zone. The modeling team needs to

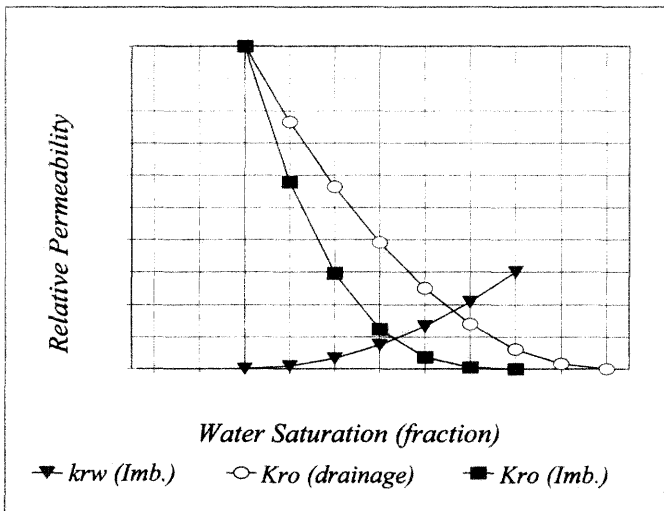


Figure 14-1. Typical water-oil relative permeability curves.

realize that the relative permeability curves used in a flow model are most representative of the type of experiment that was used to measure the curves. Applying these curves to another type of displacement mechanism can introduce significant error.

Several procedures exist for averaging relative permeability data [for example, Schneider, 1987; Mattax and Dalton, 1990; Blunt, 1999]. In practice, relative permeability is one of the most useful physical quantities available for performing a history match. The curves that are initially entered into a reservoir model are often modified during the history matching process. The rationale for changing relative permeability curves is based on the observation that relative permeability curves are usually obtained by flooding core in the laboratory. Laboratory floods correspond to a much smaller scale than flow through the drainage area of a well. Therefore, it is easy to argue that the laboratory curves are not representative of flow on the reservoir scale. In the absence of measured data, correlations such as Honarpour, et al. [1982] give a reasonable starting point for estimating relative permeability. Relative permeability hysteresis effects can also be included in reservoir simulation using a procedure presented by Killough [1976].

Capillary pressure is usually included in reservoir simulators. The relationship between capillary pressure and elevation is used to establish the initial transition zone in the reservoir. The oil-water transition zone, for example, is the zone between water-only flow and oil-only flow. It represents that part of the reservoir where 100% water saturation grades into oil saturation with irreducible water saturation. Similar transition zones may exist at the interface between any pair of immiscible phases.

Capillary pressure data is used primarily for determining initial fluid contacts and transition zones. It is also used in fractured reservoir models for controlling the flow of fluids between the fracture and the rock matrix. If capillary pressure is neglected, transition zones are not included in the model. This is illustrated in Figure 14-2. Figure 14-3 shows the effect of neglecting capillary pressure when a grid is used to represent the reservoir. The fluid content of the block is determined by the location of the block mid-point relative to a contact between two phases. The block mid-point is shown as a dot in the center

of the blocks in Figure 14-3. Thus, if the block mid-point is above the gas-oil contact (GOC), the entire block is treated as a gas cap block (single-phase gas with irreducible water saturation), even if much of the block extends into the oil column. A more accurate representation may be obtained by decreasing the thickness of the gridblocks, but this often results in a substantial increase in the cost of making computer runs. The relative benefits of incremental accuracy versus incremental cost must be considered when modeling transition zones.

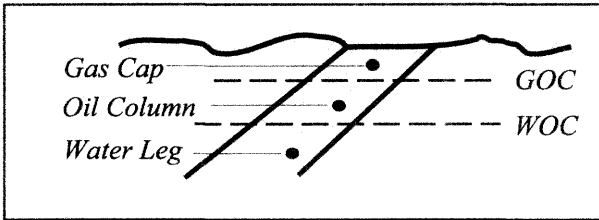


Figure 14-2. Case 1: Neglect transition zones.

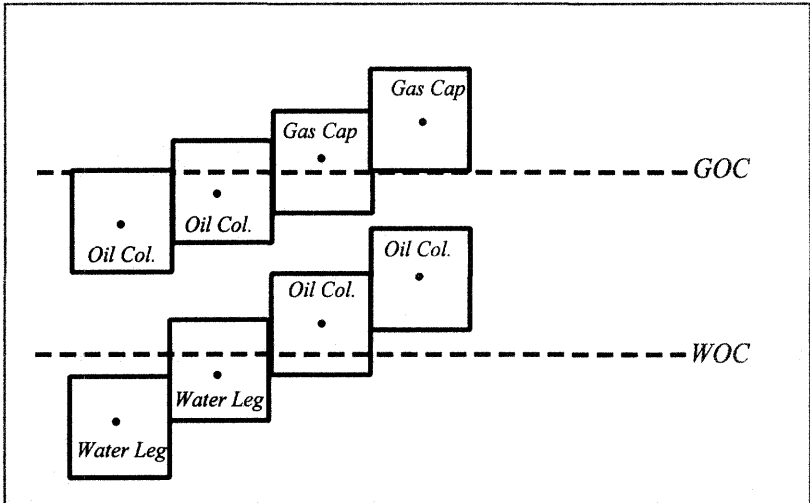


Figure 14-3. Initial fluid distribution in model without transition zone.

The inclusion of a transition zone in the model requires specifying a capillary pressure (P_c) curve as a function of saturation for whatever transition zone is being modeled: oil-water, gas-oil, or gas-water. The height h_{tz} of the transition zone above the free water level (the level corresponding to $P_c = 0$ psia)

is proportional to the capillary pressure and inversely proportional to the density difference between the two fluids (Eq. (3.7)). The height of the transition zone is a function of saturation because capillary pressure depends on saturation. The oil-water transition zone is typically the thickest transition zone because the density difference between oil and water is less than the density difference between gas and an immiscible liquid.

Figures 14-4 and 14-5 illustrate the initialization of a model containing a nonzero capillary pressure curve. First, the height h_{tz} above a specified contact, such as the water-oil contact (WOC), is calculated from P_c and $\Delta\rho$. The saturation of a block with a mid-point at height h_{tz} above the contact is then calculated from the relationship between capillary pressure and saturation.

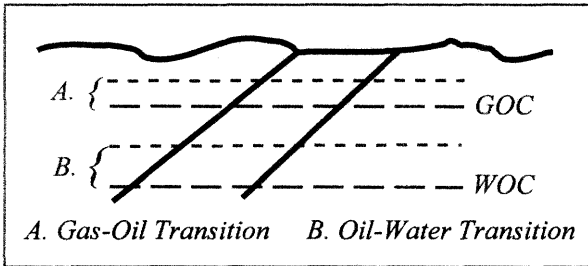


Figure 14-4. Case 2: Include transition zone in model.

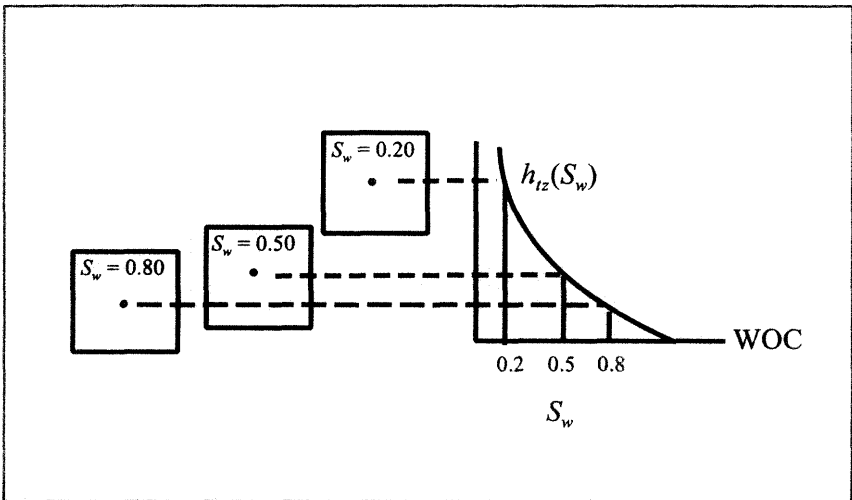


Figure 14-5. Initial gridblock saturations in model with transition zone.

Transition zones complicate the identification of fluid contacts because the definition of fluid contact is not universally accepted. For example, water-oil contact may be defined as the depth at which the capillary pressure is zero (the free water level). The WOC depth can be identified using a Repeat Formation Test by finding the point of intersection between the oil-phase pressure and the water-phase pressure. By contrast, water-oil contact may be defined as the deepest point in the reservoir at which a well can still produce water-free oil. The different definitions of contact result in differences in the transition zone model, so it is important to know which definition is applicable and who has the authority to judge the validity of the model. In some cases, it may be necessary to prepare models with both definitions and treat one definition as the base case while the other definition is viewed as a sensitivity.

The proper way to include capillary pressure in a model study is to correct laboratory measured values to reservoir conditions. This is done by applying the correction:

$$P_{c(res)} = P_{c(lab)} \eta_{corr}, \quad \eta_{corr} \equiv \frac{(\gamma |\cos \theta|)_{res}}{(\gamma |\cos \theta|)_{lab}}$$

where γ is interfacial tension (IFT) is wettability angle [Amyx, et al., 1960]. The problem with the correction is that it requires data that are often poorly known, namely interfacial tension and wettability contact angle at reservoir conditions. Rao and Girard [1997] have described a laboratory technique for measuring wettability using live fluids at reservoir temperature and pressure. Alternative approaches include adjusting capillary pressure curves to be consistent with well log estimates of transition zone thickness, or assuming the contact angle factors out. If laboratory measurements of IFT are not available, IFT can be estimated from the Macleod-Sugden correlation for pure compounds or the Weinaug-Katz correlation for mixtures [Fanchi, 1990].

14.3 Viscous Fingering

Viscous fingering is the unstable displacement of a more viscous fluid by a less viscous fluid. The fingering of an injection fluid into an *in situ* fluid can influence reservoir flow behavior and adversely impact recovery. It is

important to note, however, that fingering occurs even in the absence of a porous medium. If a low viscosity fluid is injected into a cell containing a high viscosity fluid, the low viscosity fluid will begin to form fingers as it moves through the fluid. It will not uniformly displace the higher viscosity fluid. These fingers can have different shapes. Figure 14-6 shows an example of a “skeletal” finger

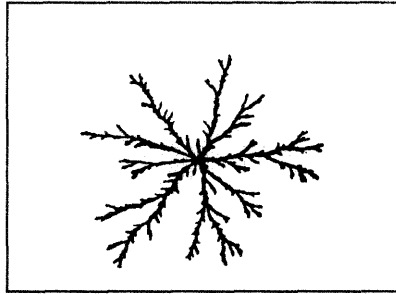


Figure 14-6. “Skeletal” viscous finger (after Daccord, et al. 1986; reprinted by permission of the American Physical Society).

[Daccord, et al., 1986] while Figure 14-7 illustrates “fleshy” fingers [for

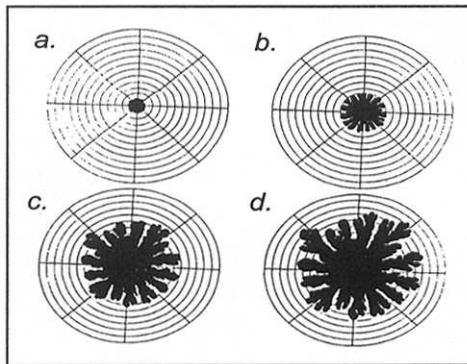


Figure 14-7. Viscous fingering (Fanchi and Christiansen, 1989; reprinted by permission of the Society of Petroleum Engineers).

example, see Paterson, 1985; Fanchi and Christiansen, 1989]. If we watch fingers evolve in a homogeneous medium (Figure 14-7), we see fingering display a

symmetric pattern. The symmetry can be lost if there is some heterogeneity in the system.

Fingering can be a reservoir heterogeneity problem or a fluid displacement problem. Most reservoir simulators do not accurately model fingering effects. It is possible to improve model accuracy by using a very fine grid to cover the area of interest, but the benefits associated with such a fine grid are seldom sufficient to justify the additional cost.

Exercises

Exercise 14.1 Data set EXAM3.DAT is a model of a Buckley-Leverett water-flood. (A) Multiply horizontal permeability by 0.5 and run the model. Plot oil rate as a function of time and WOR as a function of time. (B) Repeat A by multiplying horizontal permeability in the original data set by 10. (C) Explain the difference between parts A and B. Consider breakthrough times (time when water production begins), water-oil ratio, and cumulative oil produced at the end of the run. See Chapters 24.3.1 and 24.3.2 for a description of permeability input data. Cumulative production can be found in WTEMP.PLT.

Exercise 14.2 Repeat Exercise 14.1, but modify horizontal transmissibility instead of horizontal permeability. See Chapter 24.3.3. for details.

Exercise 14.3 Double water relative permeability in EXAM3.DAT and determine the effect on water-oil ratio and breakthrough times.

Chapter 15

Fundamentals of Reservoir Simulation

Previous chapters describe much of the data that is needed by a reservoir simulator. Our goal here is to outline the physical, mathematical and computational basis of reservoir flow simulation. For a more detailed technical presentation, consult one of the many sources available in the literature [for example, see Aziz and Settari, 1979; Bear, 1972; Mattax and Dalton, 1990; Peaceman, 1977; and Thomas, 1982]. The set of equations used in WINB4D is derived in Chapter 32.

15.1 Conservation Laws

The basic conservation laws of reservoir simulation are the conservation of mass, energy, and momentum. Mass balance in a representative elementary volume (REV) or gridblock is achieved by equating the accumulation of mass in the block with the difference between the mass leaving the block and the mass entering the block. The set of equations used in WINB4D are derived from the mass conservation principle in Chapter 4. A material balance is performed for each block. What makes a simulator different from a reservoir engineering material balance program is the ability of the simulator to account for flow between blocks.

A material balance calculation is actually a subset of the simulator capability. This is an important point because it means a reservoir simulator can be used to perform material balance work. The advantage of using a simulator instead of a material balance program is that the simulation model can be

enlarged to include position-dependent effects by modifying the grid representing the reservoir architecture. Thus, a single block material balance calculation in a reservoir simulation model can be expanded with relative ease to include flow in one, two, or three spatial dimensions. This procedure is used in the case study presented in Part III.

Most reservoir simulators assume reservoirs are produced under isothermal conditions. They also assume complete and instantaneous phase equilibration in each cell. Thus, most simulators do not account for either temperature gradients or the time it takes a mixture to reach equilibrium. They assume, instead, that reservoir temperature remains constant throughout the life of the field and that equilibration is established instantaneously. These are often reasonable assumptions.

Momentum conservation is modeled using Darcy's Law. This assumption means that the model does not accurately represent turbulent flow in a reservoir or near the wellbore. Some well models allow the user to model turbulent flow, especially for high flow rate gas wells. Turbulent flow models relate pressure change to a linear flow term, as in Darcy's Law, plus a term that is quadratic in flow rate. This quadratic effect is not usually included in the reservoir model, only in the well model.

15.2 Flow Equations

The general equations for describing fluid flow in a porous medium are shown in Table 15-1 and associated nomenclature is presented in Table 15-2. The molar conservation equation includes a dispersion term, a convection term, a source/sink term representing wells, and the time varying accumulation term. The dispersion term is usually neglected in most workhorse simulators such as black oil and compositional simulators. Neglecting dispersion simplifies program coding and is justified when dispersion is a second-order effect. In some situations, such as miscible gas injection, physical dispersion is an effect that should be considered. Further discussion of dispersion is presented in Chapter 16.

Table 15-1
Molar Conservation Equation for Component k

Physical Source	Term
Dispersion	$\nabla \cdot \left[\sum_{\ell=1}^{n_p} \phi S_{\ell} \underline{D}_{k\ell} \rho_{\ell} \cdot \nabla x_{k\ell} \right]$
Convection	$-\nabla \cdot \left[\sum_{\ell=1}^{n_p} \rho_{\ell} x_{k\ell} \mathbf{V}_{\ell} \right]$
Source/Sink	$+ Q_k$
Accumulation	$= \frac{\partial}{\partial t} \left[\phi \sum_{\ell=1}^{n_p} \rho_{\ell} x_{k\ell} S_{\ell} \right]$
Darcy's Law	$\mathbf{V}_{\ell} = -\underline{K} \frac{k_{r\ell}}{\mu_{\ell}} \cdot (\nabla P_{\ell} - \gamma_{\ell} \nabla z)$

Table 15-2
Terminology of Molar Conservation Equation

Variable	Meaning
$\underline{D}_{k\ell}$	Dispersion tensor of component k in phase ℓ
\underline{K}	Permeability tensor
$k_{r\ell}$	Relative permeability of phase ℓ
n_c	Number of components
n_p	Number of phases
P_{ℓ}	Pressure of phase ℓ
S_{ℓ}	Saturation of phase ℓ
\mathbf{V}_{ℓ}	Darcy's velocity for phase ℓ
$x_{k\ell}$	Mole fraction of component k in phase ℓ
γ_{ℓ}	Pressure gradient of phase ℓ
μ_{ℓ}	Viscosity of phase ℓ
ρ_{ℓ}	Density of phase ℓ
ϕ	Porosity

The molar flow equations were derived using the conservation laws introduced in Chapter 15.1. An energy balance equation can be found in the thermal recovery literature [Prats, 1982]. The energy balance equation is more complex than the flow equations because of the presence of additional nonlinear terms. Energy loss to adjacent non-reservoir rock must also be computed. The resulting complexity requires substantial computation to achieve an energy balance. In many realistic systems, reservoir temperature variation is slight and the energy balance equation can be neglected by imposing the isothermal approximation. The result is a substantial savings in computation expense with a reasonably small loss of accuracy.

Several supplemental – or auxiliary – equations must be specified to complete the definition of the mathematical problem. There must be a flow equation for each modeled phase. Commercial black oil and compositional simulators are formulated to model up to three phases: oil, water, and gas. The inclusion of gas in the water phase can be found in some simulators, though it is neglected in most. The ability to model gas solubility in water is useful for CO₂ floods or for modeling geopressured gas-water reservoirs. Some black oil simulator formulations include a condensate term. It accounts for liquid yield associated with condensate reservoir performance.

In addition to modeling reservoir structure and PVT data, simulators must include rate equations for modeling wells, phase potential calculations, and rock-fluid interaction data such as relative permeability curves and capillary pressure curves. Saturation-dependent rock-fluid interaction data are entered in either tabular or analytical form. More sophisticated simulators let the user represent different types of saturation change processes, such as imbibition, drainage, and hysteresis. Applying such options leads to additional computation and cost.

15.3 Well and Facilities Modeling

Well and surface facility models are simplified representations of real equipment [Williamson and Chappellear, 1981]. The well model, for example, does not account for flow in the wellbore from the reservoir to the surface. This effect can be taken into account by adding a wellbore model. The wellbore model

usually consists of a multivariable table relating surface pressure to such parameters as flow rate and GOR. The tables are often calculated using a separate program that performs a nodal analysis of wellbore flow. Well models typically assume that fluid phases are fully dispersed and that the block containing the well is perforated throughout its thickness. Some commercial simulators will let the user specify a perforation interval under certain conditions.

The different types of well controls include production and injection well controls, and group and field controls for a surface model. The production well model assumes the user specifies one option as the primary control, but may also specify other options as targets for constraining the primary control. For example, if oil rate is the primary control, then the produced GOR may be restricted so that the oil rate is decreased when GOR exceeds the specified value. This provides a more realistic representation of actual field practice.

Injection well controls assume that initial injection well mobility is given by total gridblock mobility. This makes it possible to inject a phase into a block that would otherwise have zero relative permeability to flow.

Allocation of fluids in a well model depends on layer flow capacity and fluid mobility. The fluid allocation procedure in WINB4D is discussed in Chapter 30. Simulators can also describe deviated or horizontal wells depending on how the well completions and parameters are specified.

Well, group and field controls can be specified in commercial simulators with a surface facilities model. The user specifies a hierarchy of controls that most realistically represent how the field is being operated. For example, well production may be constrained by platform separator and storage capacity, which in turn is constrained by pipeline flow capacity. The ability to integrate reservoir and surface flow technology using a single simulator is an area of research that is receiving increasing attention [for example, see Heinemann, et al., 1998].

15.4 Simulator Solution Procedures

Fluid flow equations are a set of nonlinear partial differential equations that must be solved by computer. The partial derivatives are replaced with finite differences, which are in turn derived from Taylor's series [for example, see Aziz

and Settari, 1979; Peaceman, 1977; Rosenberg, 1977; Fanchi, 2000]. This procedure is illustrated in Table 15-3. The spatial finite difference interval Δx along the x -axis is called gridblock length, and the temporal finite difference interval Δt is called the timestep. Indices i, j, k are ordinarily used to label grid locations along the x, y, z coordinate axes, respectively. Index n labels the present time level, so that $n + 1$ represents a future time level. If the finite difference representations of the partial derivatives are substituted into the original flow equations, the result is a set of equations that can be algebraically rearranged to form a set of equations that can be solved numerically. The solution of these equations is the job of the simulator.

Table 15-3
Finite Difference Approximation

- ◆ Formulate fluid flow equations, such as,

$$\frac{\partial}{\partial x} \left[\frac{Kk_r}{\mu B} \left(\frac{\partial P}{\partial x} \right) \right] + q_s \delta(x - x_0) = \frac{\partial}{\partial t} \left(\frac{\phi S}{B} \right)$$

- ◆ Approximate derivatives with finite differences

- ◇ Discretize region into gridblocks Δx :

$$\frac{\partial P}{\partial x} \approx \frac{P_{i+1} - P_i}{x_{i+1} - x_i} \equiv \frac{\Delta P}{\Delta x}$$

- ◇ Discretize time into timesteps Δt :

$$\frac{\partial S}{\partial t} \approx \frac{S^{n+1} - S^n}{t^{n+1} - t^n} \equiv \frac{\Delta S}{\Delta t}$$

- ◆ Numerically solve the resulting set of linear algebraic equations

The two most common solution procedures in use today are IMPES and Newton-Raphson. The terms in the finite difference form of the flow equations are expanded in the Newton-Raphson procedure as the sum of each term at the current iteration level, plus a contribution due to a change of each term with respect to the primary unknown variables over the iteration. To calculate these

changes, it is necessary to calculate derivatives, either numerically or analytically, of the flow equation terms. The derivatives are stored in a matrix called the acceleration matrix or the Jacobian. The Newton-Raphson technique leads to a matrix equation $J \cdot \delta X = R$ that equates the product of the acceleration matrix J and a column vector δX of changes to the primary unknown variables to the column vector of residuals R . It is solved by matrix algebra to yield the changes to the primary unknown variables δX . These changes are added to the value of the primary unknown variables at the beginning of the iteration. If the changes are less than a specified tolerance, the iterative Newton-Raphson technique is considered complete and the simulator proceeds to the next timestep.

The three primary unknown variables for an oil-water-gas system are oil-phase pressure, water saturation, and either gas saturation or solution GOR. The choice of the third variable depends on whether the block contains free gas, which depends, in turn, on whether the block pressure is above or below bubble point pressure. Naturally, the choice of unknowns is different for a gas-water system or a water only-system. The discussion presented here applies to the most general three-phase case.

A simpler procedure is the IMplicit Pressure-EXplicit Saturation (IMPES) procedure. It is much like the Newton-Raphson technique except that flow coefficients are not updated in an iterative process. The Newton-Raphson technique is known as a fully implicit technique because all primary variables are calculated at the same time; that is, primary variables at the new time level are determined simultaneously. By contrast, the IMPES procedure solves for pressure at the new time level using saturations at the old time level, and then uses the pressures at the new time level to explicitly calculate saturations at the new time level. WINB4D, the program provided with this book, is an implementation of a noniterative IMPES formulation [Fanchi, et al., 1982; Fanchi, et al., 1987]. The formulation is outlined in Chapters 27 and 32. A variation of this technique is to iteratively substitute the new time level estimates of primary variables in the calculation of coefficients for the flow equations. The iterative IMPES technique takes longer to run than the non-iterative technique, but generates less material balance error [Ammer and Brummert, 1991].

A flow chart for a typical simulator is shown in Figure 15-1 (see Crichlow, 1977). The simulation program begins by reading input data and initializing the reservoir. This part of the model will not change as a function of time. Information for time-dependent data must then be read. This data includes well and field control data. The coefficients of the flow equations and the primary unknown variables are then calculated. Once the primary variables are determined, the process can be repeated by updating the flow coefficients using the values of the primary variables at the new iteration level. This iterative process can improve material balance. When the solution of the fluid flow equations is complete, flow properties are updated and output files are created before the next timestep calculation begins.

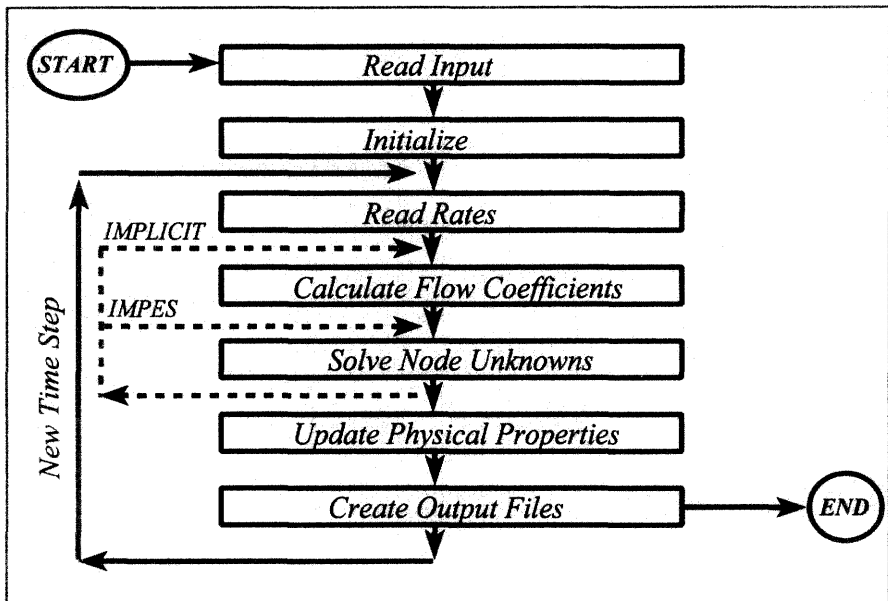


Figure 15-1. Typical simulator flow chart.

Fully implicit techniques do more calculations in a timestep than the IMPES procedure, but are stable over longer timesteps. The unconditional stability of the fully implicit techniques means that a fully implicit simulator can solve problems faster than IMPES techniques by taking significantly longer timesteps.

A problem with large timesteps in the fully implicit technique is the introduction of a numerical effect known as numerical dispersion [Lantz, 1971; Fanchi, 1983]. Numerical dispersion is introduced when the Taylor series approximation is used to replace derivatives with finite differences. The resulting truncation error introduces an error in calculating the movement of saturation fronts that looks like physical dispersion, hence it is called numerical dispersion.

Numerical dispersion arises from time and space discretizations that lead to smeared spatial gradients of saturation or concentration [Lantz, 1971] and grid orientation effects [Fanchi, 1983; and Chapter 16]. The smearing of saturation fronts can impact the modeling of displacement processes. An illustration of front smearing is presented in Figure 15-2 for a linear Buckley-Leverett waterflood model. The numerical front from an IMPES calculation does not exhibit the same piston-like displacement that is shown by the analytical Buckley-Leverett calculation [for example, see Collins, 1961; Wilhite, 1986; Craft, et al., 1991].

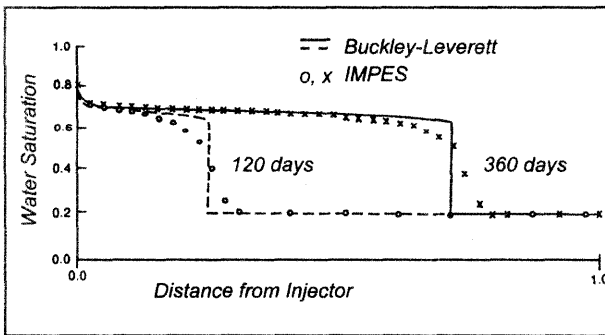


Figure 15-2. Numerical dispersion (after Fanchi, 1986; reprinted by permission of the Society of Petroleum Engineers).

Numerical dispersion D^{num} in one spatial dimension has the form

$$D^{num} = \frac{v}{2} \left(\Delta x \pm \frac{v \Delta t}{\phi} \right)$$

It depends on gridblock size Δx , timestep size Δt , velocity v of frontal advance, porosity ϕ , and numerical formulation. The “+” sign applies to the fully implicit

formulation, and the “-” sign applies to IMPES. Notice that an increase in Δt in the fully implicit formulation increases D^{num} while it decreases D^{num} when the IMPES technique is used. Indeed, it appears that a judicious choice of Δx and Δt could eliminate D^{num} altogether in the IMPES method. Unfortunately, the combination of Δx and Δt that yields $D^{num} = 0$ violates a numerical stability criterion. In general, IMPES numerical dispersion is not as large as that associated with fully implicit techniques.

As a rule of thumb, timestep sizes in fully implicit calculations should not exceed a quarter of a year, otherwise numerical dispersion can dominate front modeling. By contrast, the maximum timestep size in an IMPES simulator can be estimated by applying the rule of thumb that throughput in any block should not exceed 10% of the pore volume of the block. Throughput is the volume of fluid that passes through a block in a single timestep. IMPES timestep sizes are often on the order of a month or less. An example of a throughput calculation is given in Chapter 22.

The IMPES timestep limitation is less of a problem than it might otherwise seem, because it is very common to have production data reported on a monthly basis. The reporting period often controls the frequency with which well control data is read during a history match. Thus, during the history match phase of a study, simulator timestep sizes are dictated by the need to enter historical data. Large timestep sizes reduce the ability of the model to track variations of rate with time because historical data must be averaged over a longer period of time. As a result, the modeler often has to constrain the fully implicit simulator to run at less than optimum numerical efficiency because of the need to more accurately represent the real behavior of the physical system.

Fully implicit techniques represent the most advanced simulation technology, yet IMPES retains vitality as a relatively inexpensive means of modeling some problems. Unless a fully implicit model is readily available, it is not always necessary nor cost-effective to employ the most advanced technology to solve every reservoir simulation problem. The wise modeler will recognize that you do not have to use a sledge hammer to open a peanut!

Simulators also differ in their robustness, that is, their ability to solve a wide range of physically distinct problems. Robustness appears to depend as

much on the coding of the simulator as it does on the formulation technique. The best way to determine simulator robustness is to test the simulator with data sets representing many different types of reservoir management problems. The examples provided with WINB4D are designed to demonstrate the robustness, or range of applicability, of the simulator.

Simulator technology is generally considered proprietary technology, yet it has an economic impact that takes it out of the realm of the research laboratory and makes it a topic of importance in the corporate boardroom. Nevertheless, numerical representations of nature are subject to inaccuracies [for example, see Mattax and Dalton, 1990; Saleri, 1993; and Oreskes, et al., 1994]. This point has been illustrated in several simulator comparison projects sponsored by the Society of Petroleum Engineers beginning with Odeh [1981] and continuing through Killough [1995]. Each comparison project was designed to allow comparisons of proprietary technology by asking participating organizations to solve the same pre-determined problem. Figure 15-3 is taken from the first comparison project [Odeh, 1981]. The first project compared the performance of simulators modeling the injection of gas into a saturated black oil reservoir. Figure 15-3 shows that differences in the formulations of several reservoir simulators lead to differences in predictions of economically important quantities such as oil rate production.

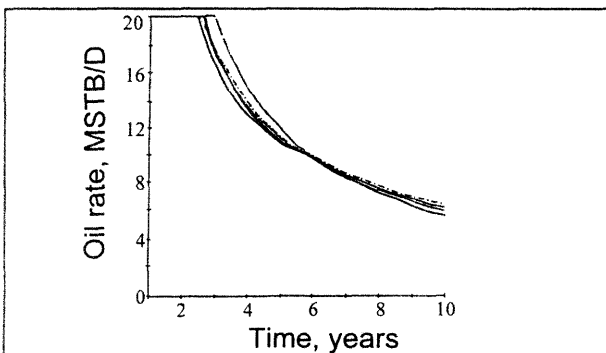


Figure 15-3. Oil rate from first SPE comparative solution project (after Odeh, 1981; reprinted by permission of the Society of Petroleum Engineers).

In summary, a representation of the reservoir is quantified in the reservoir flow simulator. The representation is validated during the history matching process, and forecasts of reservoir performance are then made from the validated reservoir representation.

15.5 Simulator Selection

The selection of a reservoir simulator depends on such factors as the objectives of the study, fluid type, and dimensionality of the system. For purposes of illustration, we focus our attention on a study which uses either a black oil or a compositional simulator. Standard black oil and compositional simulators assume isothermal flow and mass transfer within a block is instantaneous. A compositional simulator represents the fluid as a mixture of hydrocarbon components. Black oil simulators may be viewed as compositional simulators with two components. They can have gas dissolved in the oil phase, as well as oil dissolved in the gas phase. Black oil simulators need both saturated and under-saturated fluid property data, as discussed in Chapter 13.

Black oil and compositional simulators usually assume fluids have a minimal effect on rock properties. Thus, standard versions of the simulators will not model changes in rock properties due to effects like grain dissolution, tar mat formation, or gel formation resulting from a vertical conformance treatment. Special purpose simulators or special options within a standard simulator must be obtained to solve such problems.

Fluid type is needed to decide if the reservoir should be modeled using either a black oil simulator or a compositional simulator. Well logs can distinguish between oil and gas, but are less useful in further classifying fluid type. A pressure-temperature diagram is useful for determining reservoir fluid type, but its preparation requires laboratory work with a fluid sample. A simpler way that is often sufficient for classifying a fluid is to look at solution gas-oil ratio. Table 13-1 shows typical solution GOR ranges for each fluid type. As a rule of thumb, compositional models should be used to model volatile oil and condensate fluids, while black oil and dry gas fluids are most effectively

modeled with a black oil simulator. The applicability of this rule depends on the objectives of the study.

The pressure range associated with fluid property data should cover the entire range of pressures expected to be encountered over the life of the field. The data should be smooth to enhance computational efficiency and to ensure data consistency. A check on data consistency is a calculation of fluid compressibility. If a negative compressibility is encountered, the data need to be corrected. The problem of negative compressibility occurs most often when data is extrapolated beyond measured pressure ranges.

Flow units should be determined by reviewing geological and petrophysical data. It is possible to represent the behavior of a flow unit by defining a set of PVT and Rock property tables for each flow unit. PVT property tables contain data that describe fluid properties, while Rock property tables represent relative permeability and capillary pressure effects. Each set of PVT or Rock property tables applies to a particular region of gridblocks, hence the collection of blocks to which a particular set of PVT or Rock property tables applies is referred to as a PVT or Rock region. The number of flow units, and the corresponding number of PVT and Rock regions, should be kept to the minimum needed to achieve the objectives of the study. This statement is another application of Ockham's Razor (Chapter 17).

Exercises

Exercise 15.1 Data file EXAM8.DAT has a gas well under LIT control. Determine the effect of doubling the turbulence factor on gas rate, cumulative gas production, and reservoir pressure at the end of the run. See Chapters 25.2 and 30 for more discussion.

Exercise 15.2 WINB4D contains a few fieldwide controls (see Chapter 24.8). Data file EXAM4.DAT is a 2D areal model of an undersaturated oil reservoir undergoing primary depletion. Modify data file EXAM4.DAT so that fieldwide pressure is not allowed to drop below the initial bubble point pressure using the

run controls in Chapter 24.8. The initial bubble point pressure is also described in Chapter 24.6. What effect does this have on the duration of the run?

Exercise 15.3 Data set EXAM3.DAT can be used to study the numerical dispersion associated with a Buckley-Leverett type waterflood of an under-saturated oil reservoir. Run EXAM3.DAT with constant timesteps of 5 days, 10 days, and 15 days. Rerun the problem with timestep size beginning at 5 days and allowed to vary from 5 days to 15 days. Make a table showing water breakthrough time (time when the model reaches a water-oil ratio of 0.1) for each case. Timestep controls are discussed in Chapters 24.8 and 25.1.

Exercise 15.4 Data set EXAM7.DAT is one version of the Odeh [1981] SPE comparative solution problem. Run EXAM7.DAT and compare the results to those reported by Odeh. What is the WINB4D material balance error? The material balance error associated with this data set provides a good test of the quality of WINB4D relative to other programs based on the original version of BOAST [for example, Fanchi, et al., 1982; Fanchi, et al., 1987; Louisiana State University, 1997].

Exercise 15.5 Data set EXAM10.DAT illustrates the use of PVT and Rock regions in WINB4D (see Chapter 24.4). Run EXAM10.DAT and determine the number of regions in the data set.

Chapter 16

Modeling Reservoir Architecture

Reservoir architecture is modeled by contouring and digitizing geologic maps. The mapping/contouring process is the point where the geological and geophysical interpretations have their greatest impact on the final representation of the reservoir. This process has been discussed by several authors, including Harpole [1985], Harris [1975], and Tearpock and Bischke [1991]. Methods for numerically representing reservoir architecture are discussed in this chapter.

16.1 Mapping

The different parameters that must be digitized for use in a grid include elevations or structure tops, permeability in three orthogonal directions, porosity, gross thickness, net to gross thickness, and where appropriate, descriptions of faults, fractures, and aquifers. The resulting maps are digitized by overlaying a grid on the maps and reading a value for each gridblock. The digitizing process is sketched in Figures 16-1a through 16-1d.

The resolution of the model depends on the resolution of the grid. A fine grid divides the reservoir into many small gridblocks. It gives the most accurate numerical representation, but has the greatest computational expense. A coarse grid has fewer gridblocks, but the coarse gridblocks must be larger than the fine gridblocks to cover the same model volume. As a result, the coarse grid is less expensive to run than a fine grid, but it is also less accurate numerically. The loss of accuracy is most evident when a coarse grid is used to model the interface between phases such as fluid contacts and displacement fronts. Thus, fine grid

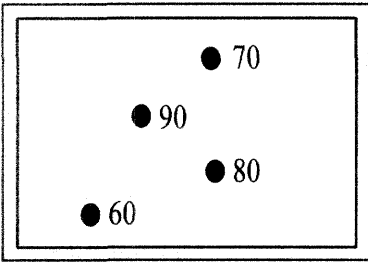


Figure 16-1a. Gather data.

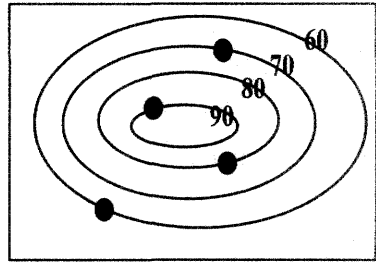


Figure 16-1b. Contour data.

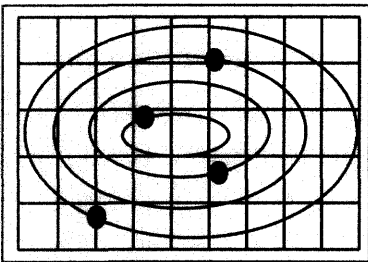


Figure 16-1c. Overlay grid.

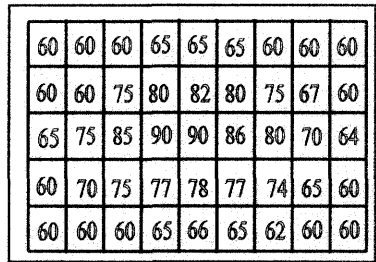


Figure 16-1d. Digitize data.

modeling is often the preferred choice to achieve maximum numerical accuracy. It is important to recognize, however, that a fine grid covering an area defined by sparse data can give the illusion of accuracy. Sensitivity studies can help quantify the uncertainty associated with the model study.

The gridding process is most versatile when used with an integrated 3D reservoir mapping package. Modern mapping techniques include computer generated maps that can be changed relatively quickly once properly set up. Dahlberg [1975] presented one of the first analyses of the relative merits of hand drawn and computer generated maps. Computer generated maps may not include all of the detailed interpretations a geologist might wish to include in the model, particularly with regard to faults, but the maps generated by computer in a 3D mapping program do not have the problems so often associated with the stacking of 2D plan view maps, namely physically unrealistic layer overlaps. Layer overlaps need to be corrected before the history match process begins.

Another problem with computer generated maps is the amount of detail that can be obtained. Computer generated maps can describe a reservoir with

a much finer grid than can be used in a reservoir simulator. For example, a computer mapping program such as that described by Englund and Sparks [1991] or Pannatier [1996] may use a grid with a million or more cells to represent the reservoir, yet reservoir simulation grids are usually 100,000 blocks or less. This means that the reservoir representation in the computer mapping program must be scaled up, or coarsened, for use in a reservoir simulator. Although many attempts have been made to find the most realistic process for scaling up data, there is no widely accepted up-scaling method in use today [for example, see Christie, 1996; Dogru, 2000].

16.2 Grid Preparation

Reservoir grids may be designed in several different ways. For a review of different types of grids, see Aziz [1993]. Definitions of coordinate system orientation vary from one simulator to another and must be clearly defined for effective use in a simulator. Reservoir grids can often be constructed in one-, two-, or three-dimensions, and in Cartesian or cylindrical coordinates. Horizontal 1D models are used to model linear systems that do not include gravity effects. Examples of horizontal 1D models include core floods and linear displacement in a horizontal layer. Core flood modeling has a variety of applications, including the determination of saturation-dependent data such as relative permeability curves. A dipping 1D reservoir is easily defined in a model by specifying structure top as a function of distance from the origin of a grid.

Figure 16-1 is an example of a 2D grid. Grids in 2D may be used to model areal and cross-sectional fluid movement. Grid orientation in 2D is illustrated by comparing Figure 16-1c and Figure 16-2. Although Figure 16-1c has fewer blocks, which is computationally more efficient, Figure 16-2 may be useful in some circumstances. For example, Figure 16-2 is more useful than Figure 16-1c if the boundary of the reservoir is not well known or an aquifer needs to be attached to the flanks of the reservoir to match reservoir behavior.

The use of 2D grids for full field modeling has continued to be popular even as computer power has increased and made large 3D models practical. Figure 16-3 shows a simple 3D grid that is often called a “layer cake” grid.

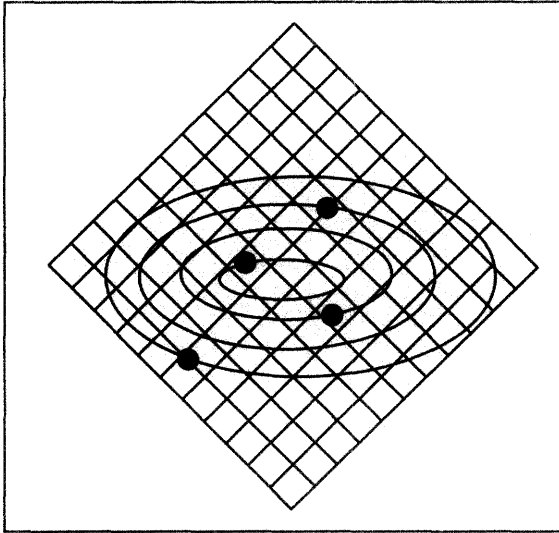


Figure 16-2. Grid orientation.

Techniques are available for approximating the vertical distribution of fluids in 2D cross-sectional and 3D models by modifying relative permeability and capillary pressure curves. The modified curves are called pseudo curves. Taggart, et al. [1995] present a discussion of several pseudoization techniques and their limitations. An example of a pseudoization technique is the vertical equilibrium (VE) approximation. The principal VE assumption is that fluid segregation in the vertical dimension is instantaneous. This assumption is approximated in

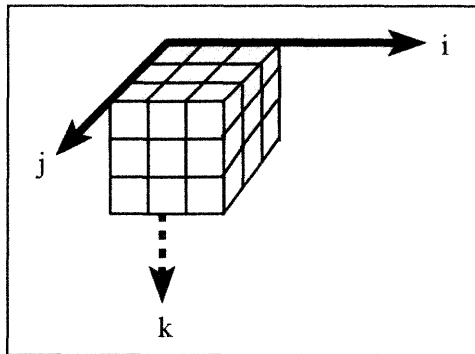


Figure 16-3. Example of a 3D "layer cake" grid.

nature when vertical flow is rapid relative to horizontal flow. This situation occurs when the vertical permeability of the reservoir is comparable in magnitude to its horizontal permeability, and when density differences are significant, such as in gas-oil or gas-water systems. For more discussion of specific pseudoization techniques, see Taggart, et al. [1995] and their references.

One reason for the continuing popularity of 2D grids is that the expectation of what is appropriate grid resolution has changed as simulation technology evolved. Thus, even though 3D models could be used today with the grid resolution that was considered acceptable a decade ago for 2D models, modern expectations often require that even finer grids be used for the same types of problems. This is an example of a task expanding to fit the available resources. It is not obvious that increased grid definition is leading to better reservoir management decisions. Indeed, it can be argued that the technological ability to add complexity is making it more difficult for people to develop a “big picture” understanding of the system being studied because they are too busy focusing on the details of a complex model. Once again, a judicious use of Ockham’s Razor is advisable in selecting a reservoir grid. The grid should be appropriate for achieving study objectives.

Near-wellbore coning models may be either 2D or 3D grids, but are defined in cylindrical rather than Cartesian coordinates. Coning (or radial) models are designed to study rapid pressure and saturation changes. An example of a radial grid is shown in Figure 16-8. High throughput, that is, large flow rate through relatively small, near-wellbore gridblocks is most effectively simulated by a fully implicit formulation. IMPES can be used to model coning, but timesteps must be very small, possibly on the order of minutes or hours. Small timesteps are not a problem if the duration of the modeled history is short, as it would be in the case of a pressure transient test.

Gridblocks may be defined in terms of corner-point geometry or block-centered geometry (Figure 16-4). Block-cen-

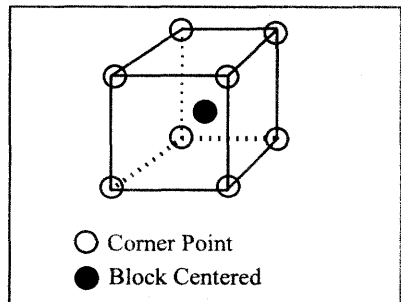


Figure 16-4. Gridblock representation.

tered geometry is the most straight forward technique, but corner-point geometry has gained popularity because it yields more visually realistic representations of reservoir architecture. This is valuable when making presentations to people who are nonspecialists. The different geometric representations are illustrated for a two-layer dipping reservoir in Figure 16-5. Although corner-point geometry is visually more realistic, it is easier to define a grid with block-centered geometry. Block-centered geometry requires the specification of the lengths of each side of the block and the block center or top. Corner-point geometry requires specifying the location of all eight corners of the block. This is most readily accomplished with a computer program.

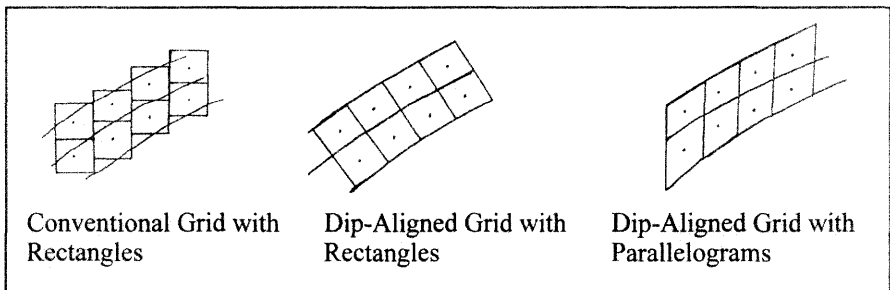


Figure 16-5. Geometric representations of a dipping reservoir.

There is little computational difference between the results of corner-point and block-centered geometry. One caution should be noted with respect to corner-point geometry. It is possible to define very irregularly shaped grids using corner-points. This can lead to the distortion of flood fronts and numerical stability problems. Flood front distortions caused by gridding is an example of the grid orientation effect discussed by many authors, including Aziz and Settari [1979], and Mattax and Dalton [1990].

The grid orientation effect is exhibited by looking at a displacement process in 2D (Figure 16-6). Each producer is equidistant from the single injector in a model that has uniform and isotropic properties. If grid orientation did not matter, the symmetry of the problem would show that both wells would produce injected water at the same time. The figure shows that production is not the same. Injected fluids preferentially follow the most direct grid path to the producer. Thus, even though the producers are symmetrically located relative to the in-

jector and each other, the grid orientation altered the expected flow pattern. Figure 16-6 shows the effect on frontal advance. In this case, the front arrives sooner at the producer in the upper right than the producer in the upper left. If these results are incorporated in a reservoir management plan, they can reduce the overall effectiveness of the plan.

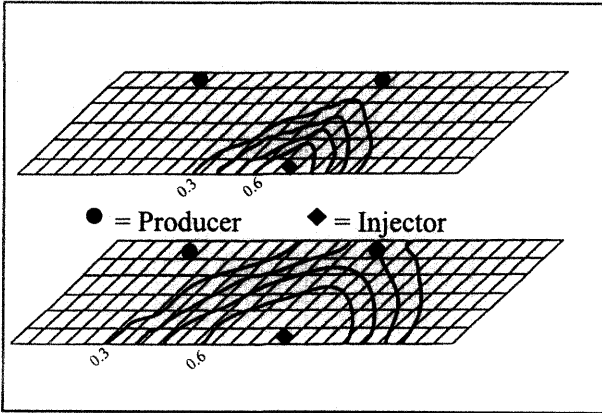
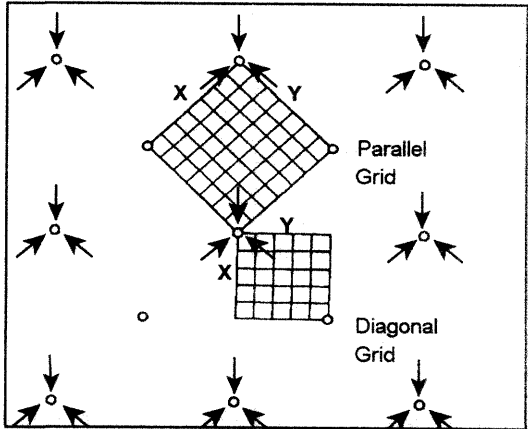


Figure 16-6. Grid orientation effect (after Hegre, et al. 1986; reprinted by permission of the Society of Petroleum Engineers).

Another example of the grid orientation effect arises in connection with the modeling of pattern floods. Figure 16-7 illustrates two grids that can be used to model flow in a five-spot pattern. The parallel grid results in earlier breakthrough of injected fluids than the diagonal grid. This effect can be traced to the finite difference representation of the fluid flow equations.



Most finite difference simulators only account for flow contributions from blocks

Figure 16-7. Parallel and diagonal grids (after Todd, et al. 1972; reprinted by permission of the Society of Petroleum Engineers).

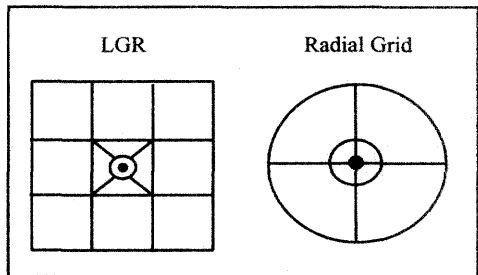
that are nearest neighbors to the central block along orthogonal Cartesian axes. In Table 16-1, the central block is denoted by "C" and the nearest neighbor block contributing to the standard finite difference calculation in 2D are denoted by an asterisk. The five blocks comprise the five-point differencing scheme of the 2D Cartesian grid.

Table 16-1
Finite Difference Stencils

Block	I - 1	I	I + 1
J - 1	9	*	9
J	*	C	*
J + 1	9	*	9

Reservoir simulators are usually formulated with the assumption that diagonal blocks do not contribute because the grid is aligned along the principal axes of the permeability tensor. Diagonal blocks are denoted by "9" in Table 16-1. The nine-point stencil includes all nine blocks in the calculation of flow into and out of the central block. Grid orientation effects can be minimized, at least in principle, if the diagonal blocks are included in the nine-point finite difference formulation [for example, see Young, 1984; Hegre, et al., 1986; Lee, et al., 1997]. This option is available in some commercial simulators. In 3D models, the number of blocks needed to represent all adjacent blocks, including diagonal terms, is 27. By contrast, only seven blocks are used in the conventional formulation of a 3D finite difference model.

Local grid refinement (LGR) is used to provide additional grid definition in a few selected regions of a larger grid. Raleigh [1991] compared local grid refinement with a radial grid (Figure 16-8) and showed that the results are comparable.



When LGR is used, it typically increases computer processor time for a run because of increased throughput in

small blocks. An LGR grid is an example of a flexible or unstructured grid. A flexible grid is made up of polygons in 2D (polyhedra in 3D) whose shape and size vary from one subregion to another in the modeled region.

Although many grid preparation options are available, improving grid preparation capability is an on-going research and development topic. For example, not all flow simulators use a finite difference formulation. Some are based on a control volume finite element formulation that use triangular meshes in 2D (tetrahedral meshes in 3D). Finite difference grids typically display global orthogonality in which the grid axes are aligned along orthogonal coordinate directions. Examples of globally orthogonal coordinate systems include the Cartesian x - y - z system and the cylindrical r - θ - z system. Grids with global orthogonality may be distorted to fit local irregularities such as faults using corner-point geometry. By contrast, finite element grids display orthogonality in which gridblock boundaries are perpendicular to lines joining gridblock nodes on opposite sides of each boundary. An example of a locally orthogonal grid is a perpendicular bisector (PEBI) grid. Aziz [1993], Chin [1993], Heinemann [1994], Verma and Aziz [1997], and Heinemann and Heinemann [1998] provide additional discussion of grid preparation research.

16.3 Model Types

Models may be classified into three different types: full field models, window area models, and conceptual models. Full field models are used to match performance of the entire field. They take into account the interaction between all wells and layers. The results of full field models are already matched to field scale and require no further scaling. The disadvantage of using full field models is that the number of grid blocks may need to be large or the grid size may need to be relatively coarse to include the entire field.

Window area models are designed to look at smaller areas of the field. These models are often constructed from a full field description. Window area models allow finer grid resolution or shorter turnaround time if the model runs faster than a full field model. The window area models are useful for studying recovery mechanisms and for determining reasonable grid preparation criteria

for use in full field models, especially with regard to layering. Full field models require sufficient layering to track fluid contact movement or other depth dependent information that is needed to achieve study objectives. Window area models have the disadvantage of not being able to accurately model flux across window area boundaries. This means that effects of wells outside the window area are not taken into account except through boundary conditions. Some commercial simulators will output time-dependent boundary conditions for use in window area models. Although this information is helpful, the process is cumbersome and does not necessarily yield accurate results. Field history can be used to guide development of the window area model, but has only limited utility as a criterion for validating window model performance. Heinemann [1995] has discussed further concepts and applications of a dynamic windowing technique that is designed to minimize the difficulties of preparing and applying window area models in conjunction with full field models.

One of the most useful types of models is the conceptual model. Conceptual models can be built quickly and require only an approximate description of that part of the reservoir that is relevant to the conceptual study. Computer resource requirements are relatively small when compared with full field or window area models. Results of the conceptual model are qualitative and best used for comparing concepts such as vertical layering. They can also be used to prepare pseudo curves for use in full field or window area models. For example, the saturation of a block in a model with a transition zone depends on the depth of the center-point of the block (see Chapter 6). As a result, a grid that is vertically coarse may have only a rough approximation of the transition zone. More accurate modeling of saturation gradient in a transition zone requires vertical grid refinement or use of pseudo curves. Conceptual models are useful for preparing such pseudo curves. The disadvantage to conceptual models is that their results do not apply directly to the description of a particular field. Since there is no history match, conceptual model results should be viewed as qualitative rather than quantitative estimates of field performance. They do provide useful qualitative information that can be applied to specific fields in window area and full field models.

16.4 Basic Simulator Volumetrics

Reservoir simulators calculate reservoir volume using a procedure similar to the procedure described in this section. Bulk volume V_B of each gridblock defined in a Cartesian coordinate system $\{x, y, z\}$ is calculated from the gross thickness $\Delta z = h$ of each gridblock and the gridblock lengths Δx , Δy along the x and y axes:

$$V_B = h \Delta x \Delta y$$

Porosity ϕ and net-to-gross ratio η are then used to calculate gridblock pore volume

$$V_p = \phi \eta V_B = \phi \eta h \Delta x \Delta y = \phi h_{net} \Delta x \Delta y$$

where net thickness is defined by $h_{net} = \eta h$. The volume of phase ℓ in the gridblock at reservoir conditions is the product of the gridblock pore volume and phase saturation, thus

$$V_\ell = S_\ell V_p = S_\ell \phi h_{net} \Delta x \Delta y$$

where S_ℓ is the saturation of phase ℓ . Total model volumes are calculated by summing over all gridblocks.

Many commercial simulators provide optional variations on the simple procedure outlined above. A comparison of reservoir simulator calculated volumetrics with volumetrics from another source, such as a material balance study or a computer mapping package, provides a means of validating volumetric estimates using independent sources.

Exercises

Exercise 16.1 Sketch the model grids for data sets EXAM1.DAT, EXAM2.DAT, EXAM3.DAT, EXAM5.DAT, and EXAM7.DAT using information from each data set.

Exercise 16.2 Repeat Exercise 16.1 for case study data sets CS-MB.DAT, CS-VC.DAT, and CS-XS.DAT.

Exercise 16.3 Modify the grid in EXAM3.DAT so that it has only five blocks in the x direction, but the model volume is unchanged. Be sure to relocate the wells relative to the grid to keep them in their appropriate physical locations. Use the equations in Chapter 31.2 to correct the PID index. How does the coarser grid affect model performance?

Exercise 16.4 Modify the grid in EXAM2.DAT so that it has $5 \times 5 \times 4$ grid-blocks. The well should be in the center of the reservoir and the reservoir volume should be unchanged by the redefinition of the grid. Use the equations in Chapter 31.2 to correct the PID index. How does the finer grid affect model performance when the model is run for three years?

Chapter 17

Data Preparation for a Typical Study

In a typical study it is necessary to first specify project objectives. The objectives help define the level of detail that will be incorporated in the reservoir model. Once objectives are defined, it is helpful to think of the study proceeding in three phases [Saleri, 1993]: the history match phase; a calibration phase, which provides a smooth transition between the first and third phases; and the prediction phase. The first step toward obtaining a history match is the collection and analysis of data.

17.1 Data Preparation

Data must be acquired and evaluated with a focus on its quality and the identification of relevant drive mechanisms that should be included in the model [for example, see Crichlow, 1977; Saleri, et al., 1992; Raza, 1992]. Given that information, it is possible to select the type of model that will be needed for the study: conceptual, window area, or full field model. In many cases all three of these models may need to be used, as illustrated in Fanchi, et al. [1996]. Data must be acquired for each model.

Some of the data that is required for a model study can be found in existing reports. The modeling team should find as many reports as it can from as many disciplines as possible. Table 17-1 lists the types of data that are needed in a model study. A review of geophysical, geological, petrophysical, and engineering reports provides a background on how the project has been developed and what preconceived interpretations have been established. During

the course of the study, it may be necessary to develop not only a new view of the reservoir, but also to prepare an explanation of why the new view is superior to a previously approved interpretation. If significant gaps exist in the reports, particularly historical performance of the field, it is wise to update them.

Table 17-1
Data Required for a Simulation Study

Property	Sources
Permeability	Pressure transient testing, Core analyses, Correlations, Well performance
Porosity, Rock compressibility	Core analyses, Well logs
Relative permeability and capillary pressure	Laboratory core flow tests
Saturations	Well logs, Core analyses, Pressure cores, Single-well tracer tests
Fluid property (PVT) data	Laboratory analyses of reservoir fluid samples
Faults, boundaries, fluid contacts	Seismic, Pressure transient testing
Aquifers	Seismic, Material balance calculations, Regional exploration studies
Fracture spacing, orientation, connectivity	Core analyses, Well logs, Seismic, Pressure transient tests, Interference testing, Wellbore performance
Rate and pressure data, completion and workover data	Field performance history

A review of rock and fluid property may show that the amount of available data is limited. If so, additional data should be obtained when possible. This may require special laboratory tests, depending on the objectives of the study. If measured data cannot be obtained during the scope of the study, then correlations

or data from analogous fields will have to be used. Values must be entered into the simulator, and it is prudent to select values that can be justified.

Well data should be reviewed. If additional field tests are needed, they should be requested and incorporated into the study schedule. Due to the costs and operating constraints of a project, it may be difficult to justify the expense of acquiring more data or delaying the study while additional data is obtained. The modeling team should take care to avoid underestimating the amount of work that may be needed to prepare an input data set. It can take as long to collect and prepare the data as it does to do the study.

17.2 Pressure Correction

When pressures are matched in a model study, the calculated and observed pressures should be compared at a common datum. In addition, pressures from well tests should be corrected for comparison with model block pressures. A widely used pressure correction is the Peaceman [1978, 1983] correction.

Figure 17-1 illustrates a pressure buildup curve as a function of radial distance from the center of a wellbore with radius r_w . To obtain a well block pressure P_o from a pressure buildup (PBU), Peaceman used a Cartesian grid to model the PBU performance of a well to find an equivalent well block radius r_o . A Horner plot of a PBU test is illustrated in Figure 17-2.

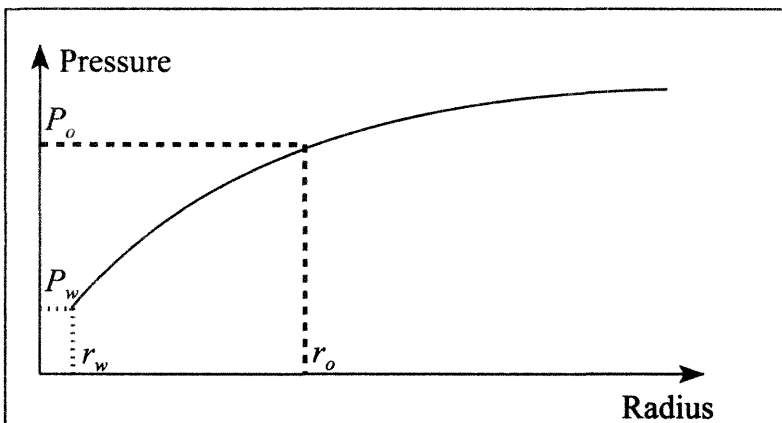


Figure 17-1. Pressure buildup.

Peaceman showed that the shut in pressure P_{ws} of an actual well equals the simulator well block pressure P_o at a shut in time Δt_s given by

$$\Delta t_s = \frac{1688 \phi \mu c_T r_o^2}{K} \tag{17.1}$$

where K is permeability, ϕ is porosity, μ is viscosity, and c_T is total compressibility. Units for all variables are given in Table 17-2 at the end of this section.

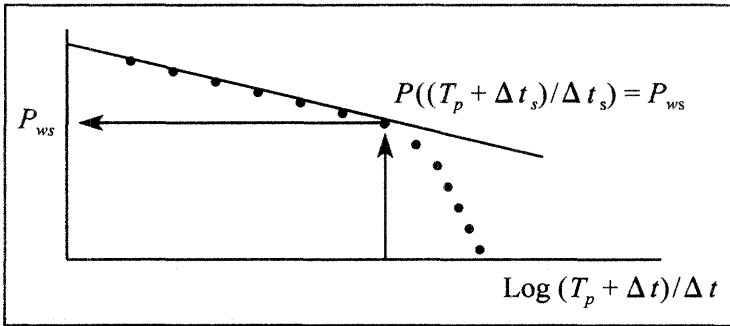


Figure 17-2. Horner plot of PBU.

The relationship between gridblock pressure P_o and flowing pressure P_{wf} at the wellbore is

$$P_{wf} = P_o - 141.2 \frac{QB\mu}{Kh} \left[\ln \frac{r_o}{r_w} + S \right] \tag{17.2}$$

where Q is the flow rate, B is formation volume factor, and S is skin. For an isotropic reservoir, that is, a reservoir in which x -direction permeability equals y direction permeability ($K_x = K_y$), the equivalent well block radius is given in terms of the block lengths $\{\Delta x, \Delta y\}$, thus

$$r_o = 0.14 (\Delta x^2 + \Delta y^2)^{1/2} \tag{17.3}$$

shut in time can be masked by wellbore storage effects. If it is, the shut in pressure P_{ws} may have to be obtained by extrapolation of another part of the curve, such as the radial flow curve. Table 17-2 summarizes the parameters involved in the Peaceman correction for a consistent set of units. An application

of the Peaceman correction is presented in Chapter 22 as part of a case study. Peaceman's work with 2D models was extended to 3D by Odeh [1985].

Table 17-2
Oilfield Units for the Peaceman Correction

Parameter	Units
B	RB/STB
c_T	psi ⁻¹
h	ft
K	md
P_o, P_{wf}, P_{ws}	psia
Q	STB/D
r_o, r_w	ft
S	fraction
Δt_s	hr
$\Delta x, \Delta y$	ft
ϕ	fraction
μ	cp

17.3 Simulator Selection and Ockham's Razor

Several requirements must be considered when selecting a simulator. These requirements can be classified into two general categories: reservoir and non-reservoir. From a reservoir perspective, we are interested in fluid type, reservoir architecture, and the types of recovery processes or drive mechanisms that are anticipated.

Reservoir architecture encompasses a variety of parameters that have a major impact on model design. Study objectives and the geologic model must be considered in establishing the dimensionality of the problem (1D, 2D, or 3D)

and the geometry of the grid. Do we need special grid options, such as radial coning or local grid refinement, or will Cartesian coordinates be satisfactory? If the study is designed to investigate near wellbore flow, it would be wise to select a grid that provides good spatial resolution near the wellbore, for example, radial coordinates. On the other hand, if the study is intended to provide an overview of field performance, a coarse Cartesian grid may be satisfactory.

The level of complexity of the geology will influence grid definition, and in the case of fractured reservoirs, the type of flow equations that must be used [for example, see Reiss, 1980; Aguilera, 1980; Golf-Racht, 1982; and Lough, et al., 1996]. A highly faulted reservoir or a naturally fractured reservoir is more difficult to describe numerically than a homogeneous sand.

Model selection will be influenced by the types of processes and drive mechanisms that dominate flow in the reservoir. Processes range from gas cap drive and water drive under primary depletion, through water or gas injection in pressure maintenance programs, to miscible or thermal flooding in enhanced recovery projects. The choice of model will vary depending on the anticipated process. For example, dry gas injection in a condensate reservoir is typically modeled with a compositional simulator, while steam flooding a heavy oil reservoir should be modeled with a thermal simulator.

A few guidelines are worth noting with regard to simulator selection. Many novice modelers make the mistake of selecting models that are much more complex than they need to be to satisfy the objectives of the study. According to Coats [1969], the modeler should “select the least complicated model and grossest reservoir description that will allow the desired estimation of reservoir performance.” This is a restatement of Ockham’s Razor.

William of Ockham, a fourteenth-century English philosopher, said “plurality must not be posited without necessity” [Jefferys and Berger, 1992]. Today this is interpreted to mean that an explanation of the facts should be no more complicated than necessary. We should favor the simplest hypothesis that is consistent with the data.

Ockham’s Razor should be applied with care, however, because one of the goals of a model study is to establish a consensus about how the reservoir behaves. This consensus is political, to an extent, because the model must satisfy

the people who commissioned the study. Their views may require using a model that has more complexity than required from a technical modeling perspective.

Non-reservoir requirements include personnel, simulator availability, and cost effectiveness. Personnel will be needed to gather and evaluate data, prepare input data, perform the history match, and then make predictions. Data gathering may take a few days or several months depending on the quality and extent of the data base for a particular field. The history matching and prediction phases do not necessarily have to be done by the same modeler. In some companies, history matching is done in a collaborative effort between a specialized technology center and a field office, while most of the prediction work is completed in the field office. This takes advantage of specialized expertise: technology centers, including outside consultants, routinely set up and run models, while day-to-day changes that impact production operations are handled in the field office. The division of labor between history matching and prediction makes sense in some circumstances.

A wide variety of simulators are available for a price. The work horse simulators – black oil and compositional – can often be leased on an as-needed basis or are available through computer networks. More specialized simulators may be obtained from software vendors, or as publicly available research codes developed at university and government laboratories.

As complexity increases, so also does cost. A good economic argument to support Ockham's Razor is to remember that the latest technology is not always the best technology for a project, and its use comes with a cost. Modeling teams are often tempted to apply the latest technology, even if it is not warranted. An example is the use of local grid refinement (LGR) to model horizontal wells. LGR is an innovative grid preparation technique that can improve spatial resolution, but at a substantial increase in computer cost and simulator sophistication. It is very common to find LGR used to model horizontal wells. In some cases, such as feasibility studies, this level of technical detail exceeds the needs of the study objectives and simply adds cost to the project without adding the corresponding value. A wise modeling team will match the level of technology with the objectives of the study. The result will be the selection of the most cost effective method for achieving study objectives.

The cost of a simulation study can be estimated based on previous experience with similar studies. As an example of how to estimate the cost for a black oil simulation study, begin by calculating the product of the number of gridblocks and the number of timesteps denoted by GBTS. Once GBTS is known, it should be related to the computer processing (cpu) time needed to make a run. The amount of cpu time per GBTS is determined by dividing the cpu time needed to make previous model runs by the number of GBTS in those runs. The product of GBTS and cpu time per GBTS gives total cpu time needed for a run. The cost of the study then depends on the number of runs that need to be made. The number of runs can be estimated by assuming that approximately 100 runs will be needed to obtain a history match. A similar approach is applied to estimating the cost of making predictions. Personnel cost is approximately equal to computer cost for the study. This does not include the cost of data collection and evaluation.

Exercises

Exercise 17.1 Data set EXAM10.DAT uses multiple Rock and PVT regions. Review EXAM10.DAT and simplify the data set without altering model results. List the changes you make to the data set. Chapter 24.4 presents a description of Rock and PVT region data records.

Exercise 17.2 A model has $10 \times 10 \times 4$ gridblocks and takes 5 minutes to run 100 timesteps. Calculate cpu time per GBTS. Estimate how long it would take to make 100 runs with 200 timesteps each.

Exercise 17.3 (A) Use Eq. (17.3) to calculate the equivalent well block radius of a block with $\Delta x = \Delta y = 200$ ft. (B) Estimate shut in time for the Peaceman correction using Eq. (17.1). Assume $\phi = 0.15$, $C_T = 1 \times 10^{-5}$ psia⁻¹, $\mu = 2$ cp and $K = 10$ md.

Chapter 18

History Matching

The history matching process begins with clearly defined objectives. Given the objectives, it is necessary to acquire model input data, especially the history of field performance. One of the essential tasks of the data acquisition stage is to determine which data should be matched during the history matching process. For example, if a gas-water reservoir is being modeled, gas rate is usually specified and water production is matched. By contrast, if an oil reservoir is being modeled, oil rate is specified and water and gas production are matched.

Data acquisition is an essential part of model initialization. Model initialization is the stage when the data is prepared in a form that can be used by the simulator. The model is considered initialized when it has all the data it needs to calculate fluids in place. The reservoir must be characterized in a format that can be put in a simulator and that is acceptable to the commissioners of the study. Reservoir characterization includes the selection of a grid and associated data for use in the model. It may also require the study of multiple reservoir realizations in the case of a geostatistical model study [for example, see Pannatier, 1996; Lieber, 1996; Rossini, et al., 1994; Englund and Sparks, 1991; Haldorsen and Damsleth, 1990; and Isaaks and Srivastava, 1989]. All fluid data corrections, such as flash corrections applied to differential PVT data in a black oil simulation, must be completed during the model initialization process.

In many cases, simple conceptual models may be useful in selecting a final grid for the model study, especially when determining the number of layers. As an illustration, suppose we want to track flood front movement in a very large field. In this case, we want as much areal definition as possible (at least 3 to 5

gridblocks between each gridblock containing a well), but this may mean loss of vertical definition. A way to resolve the problem is to set up one or more cross-section models that represent different parts of the field. Vertical conformance effects in these regions are modeled in detail by calculating flow performance with the cross-section models. The flow performance of a detailed cross-section model is then matched by adjusting relative permeability curves in a model with fewer layers. The resulting pseudo-relative permeability curves are considered acceptable for use in an areal model.

Another aspect of model initialization is equilibration. This is the point at which fluid contacts are established and fluid volumes are calculated. Resulting model volumes should be compared with other estimates of fluid in place, notably volumetric and material balance estimates. There should be reasonable agreement between the different methods (for example, within two percent). Finally, the history match can begin.

18.1 Illustrative History Matching Strategies

A universally accepted strategy for performing a history match does not exist. History matching is as much art as science because of the complexity of the problem. Nevertheless, there are some general guidelines that can help move a history match toward successful completion. These guidelines have been presented by such authors as Crichlow [1977], Mattax and Dalton [1990], Thomas [1982], and Saleri, et al. [1992]. One set of guidelines is presented in Table 18-1. The first two steps in the table take precedence over the last two. If the first two steps cannot be achieved, there is a good chance the model is inadequate and revisions will be necessary. An inadequate model may be due to a variety of problems: for example, the wrong model was selected, the reservoir is poorly characterized, or field data is inaccurate or incomplete.

Among the data variables matched in a typical black oil or gas study are pressure, production rate, water-oil ratio (WOR), gas-oil-ratio (GOR), and tracer data if it is available. More specialized studies, such as compositional or thermal studies, should also match data unique to the process, such as well stream composition or the temperature of produced fluids.

Table 18-1
Suggested History Matching Procedure

Step	Remarks
I	Match volumetrics with material balance and identify aquifer support.
II	Match reservoir pressure. Pressure may be matched both globally and locally. The match of average field pressure establishes the global quality of the model as an overall material balance. The pressure distribution obtained by plotting well test results at given points in time shows the spatial variation associated with local variability of field performance.
III	Match saturation dependent variables. These variables include water-oil ratio (WOR) and gas-oil ratio (GOR). WOR and GOR are often the most sensitive production variables in terms of both breakthrough time and the shape of the WOR or GOR curve.
IV	Match well flowing pressures.

The pressure is usually the first dynamical variable to be matched during the history matching process. A comparison of estimated reservoir pressures obtained from well tests of a single well on successive days shows that errors in reported historical pressures can be up to 10 percent of pressure drawdown. This error may be as large or larger than the Peaceman correction discussed in Chapter 17. As a first approximation, it is sufficient to compare uncorrected historical pressures directly with model pressures, particularly if your initial interest is in pressure trends and not in actual pressure values. Pressure corrections should be applied when fine tuning the history match.

Production rates are usually from monthly production records. The modeler specifies one rate or well pressure, and then verifies that the rate is entered properly by comparing observed cumulative production with model cumulative production. After the rate of one phase is specified, the rates of all other phases must be matched by model performance. In many cases, observed rates will be averaged on a monthly or quarterly basis and then compared with

model calculated rates. If the history of reservoir performance is extensive, then it is often wise to place a greater reliance on the validity of the most recent field data when performing a history match.

Phase ratios, such as GOR and WOR, are sensitive indicators of model performance. Matching ratios provides information about pressure depletion and front movements. Tracers are also useful for modeling fluid fronts. Tracers need not be expensive chemicals; they can even be changes in the salinity of produced water. Salinity changes can occur as a result of mixing when injected brine and *in situ* brine have different salinities. Water sample analysis on a periodic basis is useful for tracking salinity variation as a function of time.

Time-Lapse Seismic History Matching

An emerging history matching strategy is to combine time-lapse seismic reservoir monitoring with traditional flow modeling in a process referred to as seismic history matching [Lumley and Behrens, 1997]. Seismic history matching is an iterative process, as illustrated in Figure 18-1. The ovals in the figure represent model preparation, while the rectangles correspond to the history matching process.

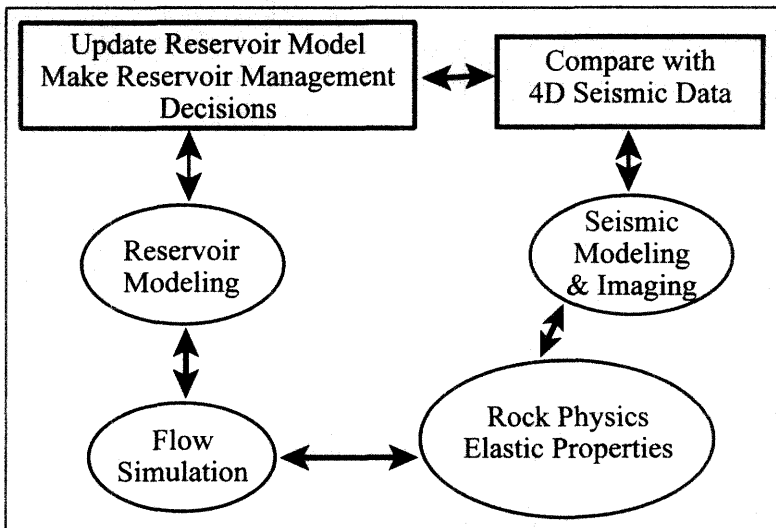


Figure 18-1. Seismic history matching [after Lumley and Behrens, SPE 38696, 1977].

The seismic history matching process includes steps for incorporating time-lapse seismic monitoring information. Time-lapse seismic monitoring is the comparison of two or more 3-D seismic surveys over the same region at different points in time. WINB4D includes algorithms for providing information that can facilitate all of the tasks shown in Figure 18-1. This has been made possible by the inclusion of a petrophysical model in the flow simulator.

18.2 Key History Matching Parameters

A fundamental concept of history matching is the concept of a “hierarchy of uncertainty.” The hierarchy of uncertainty is a ranking of model input data quality that lets the modeler determine which data is most and least reliable. Changes to model input data are then constrained by the principle that the least reliable data should be changed first. The question is: which data are least reliable?

Data reliability is determined when data are collected and evaluated for completeness and validity [Raza, 1992; Saleri, et al., 1992]. This is such an important step in establishing a feel for the data that the modeler should be closely involved with the review of data. Relative permeability data are typically placed at the top of the hierarchy of uncertainty because they are modified more often than other data. Relative permeability curves are often determined from core floods. As a consequence, the applicability of the final set of curves to the rest of the modeled region is always in doubt.

Initial fluid volumes may be modified by changing a variety of input parameters, including relative permeability endpoints and fluid contacts. Model-calculated, original fluid volumes in place are constrained by independent techniques like volumetrics and material balance studies.

Attempts to match well data may require changing the producing interval or the productivity index of a perforation interval. If it is difficult to match well performance in a zone or set of zones, the modeler needs to look at a variety of possibilities, including unexpected completion and wellbore problems. In one study, for example, an unexpectedly high GOR from a perforation interval that was known to be below the gas-oil contact was due to gas flow in the annulus

between the tubing and the casing. This result was confirmed by running a cement bond log and finding a leak in the wellbore interval adjacent to the gas cap. Gas from the gas cap was entering the wellbore and causing the larger than expected production GOR. This effect can be modeled by a variety of options, depending on the degree of accuracy desired: for example, it could be modeled by altering productivity index (PI) in the well model or by designing a near wellbore conceptual model and preparing pseudorelative permeability curves. The choice of method will influence the predictive capability of the model. Thus, a pseudo-relative permeability model will allow for high GOR even if the well is recompleted, whereas the PI could be readily corrected at the time of well recompletion to reflect the improvement in wellbore integrity.

Map adjustments may also be necessary. This used to be considered a last resort change because map changes required substantial effort to redigitize the modified maps and prepare a revised grid. Pre-processing packages and computer-aided geologic modeling are making map changes a more acceptable history match method. In the case of geostatistics, a history matching process may actually involve the use of several different geologic models. Each geologic model is called a stochastic image or realization. Additional discussion of geostatistics is presented in Chapter 11.

Toronyi and Saleri [1988] present a detailed discussion of their approach to history matching. It is noteworthy because they provide guidance on how changes in some history match parameters affect matches of saturation and pressure gradients. A summary is presented in Table 18-2. It shows, for example, that a change in pore volume can effect pressure as it changes with time. As another example, relative permeability changes are useful for matching saturation variations in time and space. Notice that fluid property data are seldom changed to match field history. This is because fluid property data tend to be more accurately measured than other model input data.

History matching must not be achieved by making incorrect parameter modifications. For example, matching pressure may be achieved by adjusting rock compressibility, yet the final match value should be within the set of values typically associated with the type of rock in the formation. In general, modified parameter values must be physically meaningful.

Table 18-2
Influence of Key History Matching Parameters

Parameter	Pressure match	Saturation match
Pore volume	$\Delta P/\Delta t$	*
Permeability thickness	$\Delta P/\Delta x$	$\Delta S/\Delta x$
Relative permeability	Not used	$\Delta S/\Delta x$ and $\Delta S/\Delta t$
Rock compressibility	*	Not used
Bubble-point pressure	$\Delta P/\Delta t$ *	*
*Avoid changing if possible		

18.3 Evaluating the History Match

One way to evaluate the history match is to compare observed and calculated parameters. Typically, observed and calculated parameters are compared by making plots of pressure vs time, cumulative production (or injection) vs time, production (or injection) rates vs time, and GOR, WOR, or water cut vs time. Other comparisons can and should be made if data are available. They include, for example, model saturations versus well log saturations, and tracer concentration (such as salinity) versus time. In the case of compositional simulation, dominant components (typically methane) should be plotted as a function of time.

In many studies, the most sensitive indicators of model performance are plots of GOR, WOR, or water cut vs time. These plots can be used to identify problem areas. For example, suppose we plot all high/low WOR and GOR wells or plot all high/low pressure wells. A review of such plots may reveal a grouping of wells with the same problem. This can identify the presence of a systematic error or flaw in the model that needs to be corrected. If the distribution is random, then local variations in performance due to heterogeneity should be considered.

18.4 Deciding on a Match

There are several ways to decide if a match is satisfactory. In all cases, a clear understanding of the study objectives should be the standard for making the decision. If a coarse study is being performed, the quality of the match between observed and calculated parameters does not need to be as accurate as it would need to be for a more detailed study. For example, pressure may be considered matched if the difference between calculated and observed pressures is within $\pm 10\%$ draw down. The tolerance of $\pm 10\%$ is determined by estimating the uncertainty associated with measured field pressures and the required quality of the study. A study demanding greater reliability in predictions may need to reduce the tolerance to $\pm 5\%$ or even less, but it is unrealistic to seek a tolerance of less than one percent. The uncertainty applies not to individual well gauge pressures, which may be measured to a precision of less than one percent, but to estimates of average field or region pressure from two or more well tests. The latter error is generally much larger than the precision of a single well test. In any event, model-calculated pressure trends should match field or region pressure performance.

Another sensitive indicator of the quality of a history match is the match of WOR, GOR, or water cut. Three factors need to be considered: breakthrough time, the magnitude of the difference between observed and calculated values, and trends. Adjustments in the model should be made to improve the quality of each factor. Saleri [1993] has observed that a match of the field is more easily obtained than a match of individual well performance. Indeed, he notes that matching every well is virtually impossible. As a rule of thumb, the field match may be valid for a year or more without updating, and we can expect the well match to be valid for up to six months without updating. Deviations from this rule will vary widely, and will depend on the type of system modeled and the alignment of the interpreted model with reality. Indeed, gas reservoirs without aquifer influx may be accurately modeled for the life of the field, while a gas reservoir with complex lithology and water influx may never be satisfactorily matched.

Modelers must resist being drawn into the “one more run” syndrome. This occurs when a modeler (or member of the study team) wants to see “just one more run” to try an idea that has not yet been tried. In practice, a final match is often declared when the time or money allotted for the study is depleted.

18.5 History Match Limitations

History matching may be thought of as an inverse problem. An inverse problem exists when the dependent variable is the best known aspect of a system and the independent variable must be determined [Oreskes, et al., 1994]. For example, the “dependent variable” in oil and gas production is the production performance of the field. Production performance depends on input variables such as permeability distribution and fluid properties. The goal of the history match is to find a set of input variables that can reconstruct field performance.

In the context of an inverse problem, the problem is solved by finding a set of reasonable reservoir parameters that minimizes the difference between model performance and historical performance of the field. As usual, we must remember that we are solving a non-unique problem whose solution is often as much art as science. The uniqueness problem arises from many factors. Most notable of these are unreliable or limited field data and numerical effects. Advances in hardware and software technology have made it possible to minimize the effects of numerical problems, or at least estimate their influence on the final history match solution. Data limitations are more difficult to resolve because the system is inherently underdetermined: we do not have enough data to be sure that our final solution is correct.

Test of Reasonableness

A model may be considered reasonable if it does not violate any known physical constraints. In many cases, a model may be acceptable if it is reasonable. In other situations, not only must physical constraints be satisfied, but approved processes for evaluating data must also be followed. Thus a model may be reasonable, but if it is based on an innovative technique that is reasonable but not approved, the model will be unacceptable. The modeler may use a method

that is in the literature, but the commissioner of the study may have a philosophical or empirical objection to the method. Window area modeling is a good example of a method that may be reasonable but not acceptable because failure to adequately describe flux across window area boundaries can yield poor results. If someone in a position of authority or influence has had a bad experience with the modeling method, they may refuse to accept results from the model. Similarly, the modeler needs to be aware that some modeling methods are not universally accepted. At the very least, alternative methods may be needed to corroborate the disputed method as part of a sensitivity analysis or model validation exercise.

Exercises

Exercise 18.1 (A) Run EXAM6.DAT and plot average reservoir pressure as a function of time. (B) Multiply the pore volume of data set EXAM6.DAT by 0.9 and repeat part A. (C) How does the change in pore volume affect pressure as a function of time?

Exercise 18.2 Double the horizontal permeability in layer $K = 1$ of data set EXAM6.DAT. (A) Plot the average reservoir pressure as a function of time. (B) What is the effect on production, by layer, at the end of two years? File WTEMP.WEL provides rate information by layer for all wells.

Exercise 18.3 Set the x direction transmissibility to 0 between $I = 2$ and $I = 3$ for blocks ranging from $J = 1$ to $J = 4$ in layers $K = 1$ and $K = 2$ of data set EXAM6.DAT. This transmissibility barrier represents a flow barrier such as a sealing fault. How does the barrier alter flow patterns and the distribution of reservoir pressure?

Chapter 19

Predictions

The previous chapters have shown how to build a working model of the reservoir and establish a level of confidence in the validity of model results. It is time to recall that modeling was undertaken to prepare a tool that would help us develop recommendations for a reservoir management program. The primary reservoir management objective is to determine the optimum operating conditions needed to maximize the economic recovery of hydrocarbons. This is accomplished, in principle, by marshaling accessible resources to

- ◆ optimize recovery from a reservoir, and
- ◆ minimize capital investments and operating expenses.

The commercial impact of the simulation study is the preparation of a cash flow prediction from projected field performance. Thus, the model study is often completed by making field performance predictions for use in economic analysis of possible operating strategies.

19.1 Prediction Capabilities

Performance predictions are valuable for a variety of purposes. Predictions can be used to better interpret and understand reservoir behavior and they provide a means of determining model sensitivity to changes in input data. This sensitivity analysis can guide the acquisition of additional data for improving reservoir management.

Predictions enable people to estimate project life by predicting recovery vs time. Project life depends not only on the flow behavior of the reservoir, but

also on commercial issues. Models let the user impose a variety of economic constraints on future reservoir performance during the process of estimating project life. These constraints reflect a range of economic criteria that will interest management, shareholders, and prospective investors.

Commercial interests are clearly important to the future of a project, and so are technical issues. It is often necessary to compare different recovery processes as part of a study. Since there is only one field, it is unrealistic to believe that many different recovery processes can be evaluated in the field, even as small-scale pilot projects. Pilot projects tend to be substantially more expensive to run than simulation studies. In some cases, however, it might be worthwhile to confirm a simulation study with a pilot project. This is especially true with expensive processes such as chemical and thermal flooding.

Yet another use for model predictions is the preparation of a reservoir management plan. Reservoir management plans have been discussed in previous sections. Their preparation is often the single most important motivation for performing a simulation study.

19.2 Prediction Process

The prediction process begins with model calibration. It is usually necessary to ensure continuity in well rate when the modeler switches from rate control during the history match to pressure control during the prediction stage of a study. This is illustrated in Figure 19-1 where the solid curve is the predicted rate based on the productivity index (PI) used in the history match. A clear

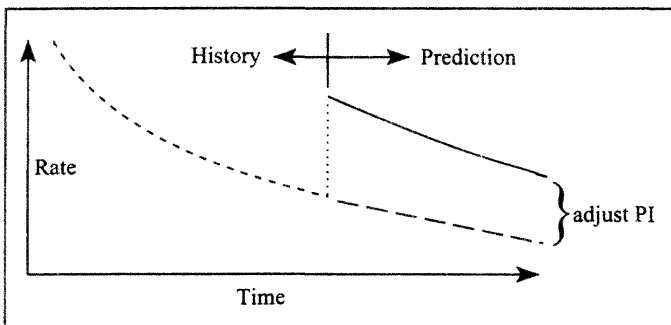


Figure 19-1. Model calibration.

discontinuity in rate is observed between the end of history and the beginning of prediction. The rate difference usually arises because the actual well PI, especially skin effect, is not accurately modeled by the model PI. An adjustment to model PI needs to be made to match final historical rate with initial predicted rate.

The next step is to prepare a base case prediction. The base case prediction is a forecast assuming existing operating conditions apply. For example, the base case for a newly developed field that is undergoing primary depletion should be a primary depletion case that extends to a user-specified economic limit. By contrast, if the field was being waterflooded, the waterflood should be the base case and alternative strategies may include gas injection and WAG (water-alternating-gas).

The base case prediction establishes a basis from which to compare changes in field performance resulting from changes in existing operating conditions. In addition, a sensitivity analysis should be performed to provide insight into the uncertainty associated with model predictions. A procedure for conducting a sensitivity analysis is outlined below.

19.3 Sensitivity Analyses

Sensitivity analyses are often needed in both the history matching and prediction stages [for example, see Crichlow, 1977; Mattax and Dalton, 1990; Saleri, 1993; and Fanchi, et al., 1996]. Any method that quantifies the uncertainty or risk associated with selecting a particular prediction case may be viewed as a sensitivity analysis. An example of a sensitivity analysis technique that is cost-effective in moving a history match forward is conceptual modeling. It can be used to address very specific questions, such as determining the impact of fluid contact movement on hydrocarbon recovery. Similarly, window models that study such issues as the behavior of a horizontal well in a fault block provide useful information on the sensitivity of a model to changes in input parameters.

Another example of a sensitivity analysis technique is risk analysis. Murtha [1997] defines risk analysis as “any form of analysis that studies and hence attempts to quantify risks associated with an investment.” Risk in this

context refers to a potential “change in assets associated with some chance occurrences.” Risk analysis generates probabilities associated with changes of model input parameters. The parameter changes must be contained within ranges that are typically determined by the range of available data, information from analogous fields, and the experience of the modeling team. Each model run using a complete set of model input parameters constitutes a trial. A large number of trials can be used to generate probability distributions. Alternatively, the results of the trials can be used in a multivariable regression analysis to generate analytical expressions, as described below.

One of the most widely used techniques for studying model sensitivity to input parameter changes is to modify model input parameters in the history matched model. The following procedure combines multivariable regression and the results of model trials to generate an analytical expression for quantifying the effect of changing model parameters.

Assume a dependent variable F has the form

$$F = \kappa \prod_{j=1}^n X_j^{e_j}$$

where $\{X_j\}$ are n independent variables and κ is a proportionality constant that depends on the units of the independent variables. Examples of X_j are well separation, saturation end points, and aquifer strength. Taking the logarithm of the defining equation for F linearizes the function F and makes it suitable for multivariable regression analysis, thus

$$\ln F = \ln \kappa + \sum_{j=1}^n e_j \ln X_j$$

A sensitivity model is constructed using the following procedure:

- ◆ Run a model with different values of $\{X_j\}$
- ◆ Obtain values of F for each set of values of $\{X_j\}$

The constants κ , $\{e_j\}$ are obtained by performing a multivariable regression analysis using values of F calculated from the model runs as a function of $\{X_j\}$.

In addition to quantifying behavior, the regression procedure provides an estimate of fractional change of the dependent variable F when we make

fractional changes to the independent variables $\{X_j\}$. The fractional change in F is given by

$$\frac{dF}{F} = \sum_{j=1}^n e_j \frac{dX_j}{X_j}$$

This lets us compare the relative importance of changes to the independent variables. Notice that the proportionality constant κ has been factored out of the expression dF/F for the fractional change in F . Thus, the quantity dF/F does not depend on the system of units used in the sensitivity study.

19.4 Economic Analysis

In addition to providing technical insight into fluid flow performance, model predictions are frequently combined with price forecasts to estimate how much revenue will be generated by a proposed reservoir management plan. The revenue stream is used to pay for capital and operating expenses, and the economic performance of the project depends on the relationship between revenue and expenses [see, for example, Bradley and Wood, 1994; Mian, 1992; Thompson and Wright, 1985]. A discussion of basic economic concepts is given in Chapter 9. It is sufficient to note here the role of economic analysis in the context of a model study.

In a very real sense, the reservoir model determines how much money will be available to pay for wells, compressors, pipelines, platforms, processing facilities, and any other items that are needed to implement the plan represented by the model. For this reason, the modeling team may be expected to generate flow predictions using a combination of reservoir parameters that yield better recoveries than would be expected if a less “optimistic” set of parameters had been used. The sensitivity analysis is a useful process for determining the likelihood that a set of parameters will be realized. Indeed, modern reserves classification systems are designed to present reserves estimates in terms of their probability of occurrence. A probabilistic analysis is discussed in Chapter 9. The probabilistic representation of forecasts gives decision-making bodies such as

corporate managements and financial institutions the information they need to make informed decisions.

19.5 Validity of Model Predictions

The validity of model predictions was studied by Saleri [1993] who compared actual field performance with predicted performance. Figure 19-2

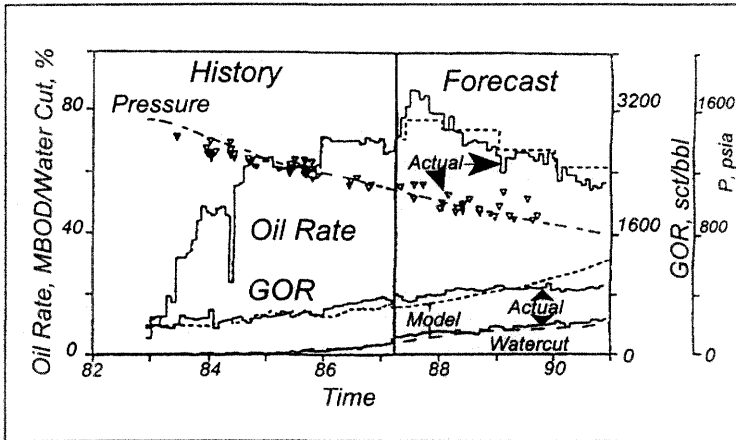


Figure 19-2. Quality of field performance match (after Saleri, 1993; reprinted by permission of the Society of Petroleum Engineers).

illustrates his results. The overall match of field performance, such as total rate and pressure performance, is reasonable. The field match is somewhat deceptive however, because the validity of individual well performance forecasting varies widely. Indeed, the match of water and gas performance for about half of the wells was deemed a “bust” by the author. This is not unusual in a model study. Saleri arrived at the following conclusions:

- ◆ “Barring major geologic and/or reservoir data limitations, fieldwide cumulative production forecast accuracies would tend to range from 10% to 40%.” [Saleri, 1993]
- ◆ “Well performance forecasts are bound to be less successful than fieldwide predictions.” [Saleri, 1993]

These points underscore the need to recognize that the history match process does not yield a unique solution. Forecasts of reservoir behavior depend on the validity of the history match.

Despite the uncertainty associated with simulator-based forecasts, reservoir simulation continues to be the most reliable method for making performance predictions, particularly for reservoirs that do not have an extensive history or for fields that are being considered as candidates for a change in reservoir management strategy. Other methods, such as decline curve analysis and material balance analysis, can generate performance forecasts, but not to the degree of detail provided by a reservoir model study. As Saleri [1993] noted,

◆ “While a 10% to 40% forecast uncertainty may appear alarming in an absolute sense, the majority of reservoir engineering decisions require choices based solely on comparative analyses (for example, peripheral vs. pattern flood). Thus, in selecting optimum management strategies, finite-difference models still offer the most effective tools.”

Saleri’s view is similar to that of Oreskes, et al. [1994]. Even though models are non-unique representations of nature, they still have many uses. In summary, models can be used to

- ◆ corroborate or refute hypotheses about physical systems;
- ◆ identify discrepancies in other models; and
- ◆ perform sensitivity analyses.

Part IV integrates the ideas presented above in the context of a case study.

Exercises

Exercise 19.1 Data set EXAM4.DAT is a 2D areal model of an undersaturated oil reservoir undergoing primary depletion. (A) Run EXAM4.DAT and determine oil recovery at the end of the run. (B) Set the bottomhole pressure (BHP) in well P-1 of EXAM4.DAT to 150 psia and run the model. How much oil is recovered in the modified model?

Exercise 19.2 Beginning at the end of year one, add a water injection well in each of the four corner gridblocks in data set EXAM4.DAT with the BHP

modification described in Exercise 19.1. The maximum allowable BHP for an injection well is 5000 psia. Assume the target rate for the oil production well is 600 STB/D. Maximize oil recovery by varying the amount of water injected. Data set EXAM6.DAT is an example of a data set with the injection wells added.

This page intentionally left blank

Part III

Case Study

This page intentionally left blank

Chapter 20

Study Objectives and Data Gathering

The first step in a study is to identify its objectives. Study objectives provide information about resource requirements. After stating the objectives of the study, the data for characterizing the reservoir is then described.

20.1 Study Objectives

Two objectives of the case study are to increase your understanding of the reservoir simulation process, and to acquire experience working with a simulator. The experience you gained working the exercises in Parts I and II is a transferrable skill. Many of the tasks performed with WINB4D may differ in detail from other simulators, but are conceptually universal. Although the above objectives are important from a pedagogical point of view, they are secondary within the context of the case study.

The reservoir management objective of the case study is to *optimize production from a dipping, undersaturated oil reservoir*. There will be constraints imposed on the case study objective. Before discussing the constraints, however, it is first necessary to gather some background information about the field.

20.2 Reservoir Structure

A seismic line through an east-west cross-section of the field is shown in Figure 20-1. The single well (P-1) has been producing from what appears to

be a fault block bounded upstructure and to the east by an unconformity; downstructure and to the west by a fault or aquifer; and to the north and south by sealing faults.

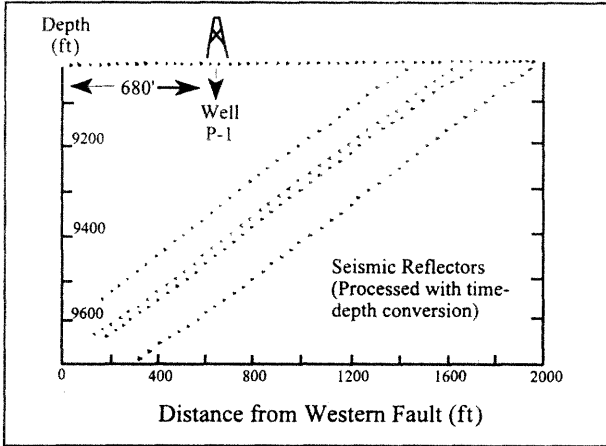


Figure 20-1. East-west seismic line.

A well log trace is shown in Figure 20-2. An analysis of the well log data shows that two major sands are present and are separated by a shale section. Well log results are presented in Table 20-1. The table headings refer to porosity ϕ , water saturation S_w , gross thickness h , and the net-to-gross ratio NTG.

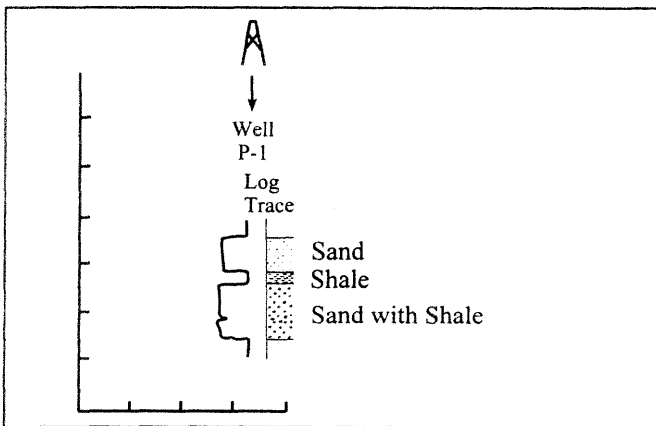


Figure 20-2. Well log trace.

Table 20-1
Well Log Analysis Summary

Lithology (From Cuttings)	Depth (ft) to Top of Formation	ϕ (fr.)	S_w (fr.)	h (ft)	NTG (fr.)
Sandstone	9330	0.20	0.30	80	0.9
Shale	9410	—	—	20	—
Sandstone with Shale Stringer	9430	0.25	0.30	120	0.8

A conceptual sketch of the reservoir cross-section is shown in Figure 20-3. Notice that we have adopted an unconformity as our geologic model.

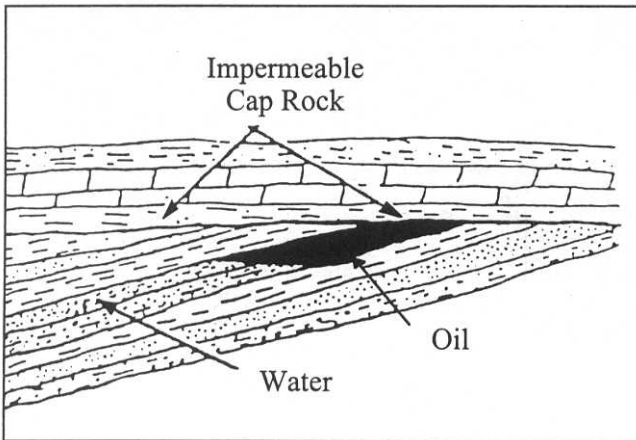


Figure 20-3. Conceptual sketch of reservoir cross-section (after Clark, 1969; reprinted by permission of the Society of Petroleum Engineers).

20.3 Production History

Well P-1 has produced for a year. Its production history is shown in Tables 20-2a and 20-2b.

**Table 20-2a
Production History**

	RATES				
TIME	OIL	GAS	WATER	GOR	WOR
DAYS	STB/D	MSCF/D	STB/D	SCF/STB	
5	500	228	0	457	0
13	500	228	0	457	0
24	500	228	0	457	0
41	500	228	0	457	0
66	500	228	0	457	0
91	500	228	1	457	0
122	500	228	1	457	0
153	500	228	1	457	0
183	500	228	2	457	0
214	500	228	2	457	0
245	500	228	2	457	0
274	500	228	3	457	0
305	500	228	3	457	0
336	500	228	4	457	0
365	500	228	5	457	0

A review of Tables 20-2a and 20-2b shows that oil rate has remained constant. Real data would show some variability, of course, but we are using an idealized data set to simplify the problem. Gas production has also remained constant, and there has been no change in the gas-oil ratio. This suggests that the reservoir is undersaturated; that is, reservoir pressure is above bubble point pressure. Only one hydrocarbon phase – the liquid phase – is produced at reservoir conditions from an undersaturated reservoir. The fact that GOR does not change over the life of the field is interpreted to mean that the reservoir was undersaturated at initial conditions.

Table 20-2b
Production History

TIME DAYS	AVG RES PRESSURE PSIA	CUM PROD		
		OIL MSTB	GAS MMSCF	WATER MSTB
5	3929	3	1	0
13	3915	6	3	0
24	3906	12	5	0
41	3901	20	9	0
66	3899	33	15	0
91	3898	46	21	0
122	3897	61	28	0
153	3897	77	35	0
183	3897	91	42	0
214	3896	107	49	0
245	3895	122	56	0
274	3895	137	63	0
305	3894	152	70	0
336	3893	168	77	1
365	3892	183	83	1

20.4 Drill Stem Test

Well P-1 logs and cores showed the presence of two major sands. A drill stem test (DST) was subsequently run in each major sand. Basic facts from the DST are summarized in Table 20-3.

Table 20-3
Summary of Well P-1 DST Results

Wellbore Radius	0.25 ft
Wellbore Skin	-0.5
Initial Pressure	3936 psia at 9360 ft
No-Flow Boundary	Within 700 ft

Permeability was estimated from the DST data for each sand. The results, together with average water saturation (S_w) values and calculated oil saturation (S_o) values, are presented in Table 20-4 for both major sands.

Table 20-4
Saturation and Permeability Values for Each Major Sand

Sand	S_w	$S_o = 1 - S_w$	Permeability (md)
1	0.3	0.7	75
2	0.3	0.7	250

20.4.1 DST Radius of Investigation

The radius of investigation for a DST can be estimated at various shut-in times by using the formula

$$r_i = 0.029 \sqrt{\frac{K \Delta t}{\phi \mu c_T}}$$

where K is permeability in md, ϕ is fractional porosity, μ is viscosity in cp, c_T is total compressibility in 1/psia, and Δt is shut-in time in hours. The following physical properties apply to the case study DST:

K	permeability	250 md
ϕ	porosity	0.228
μ	viscosity	0.71 cp
c_T	total compressibility	13×10^{-6} psia ⁻¹

Substituting values for the physical parameters gives

$$\begin{aligned} r_i &= 0.029 \sqrt{\frac{K \Delta t}{\phi \mu c_T}} \\ &= 0.029 \sqrt{\frac{250 \times \Delta t}{.228 \times 0.71 \times 13 \times 10^{-6}}} \\ &= 316 \sqrt{\Delta t} \end{aligned}$$

Table 20-5 shows values of r_i for shut-in times of 0.25 day, 0.5 day, and 1 day.

Table 20-5
Estimating the Radius of Investigation

Shut-in time		Radius of Investigation [ft]
days	hrs	
0.25	6	770
0.50	12	1100
1.00	24	1550

The DST showed that a no-flow boundary exists within approximately 700 ft of production well P-1.

20.5 Fluid Properties

In addition to pressure, flow capacity, and boundary information, the DST was used to acquire a fluid sample. Table 20-6 presents fluid properties from a laboratory analysis of the DST fluid sample.

Table 20-6
Fluid Properties

Pressure	Oil		Rso	Gas		Water	
	Vis	FVF		Vis	FVF	Vis	FVF
psia	cp	RB/ STB	SCF/ STB	cp	RCF/ SCF	cp	RB/ STB
14.7	1.04	1.06	1	0	0.9358	0.5	1.019
514.7	0.910	1.207	150	0.0112	0.0352	0.5005	1.0175
1014.7	0.830	1.295	280	0.0140	0.0180	0.5010	1.0160
1514.7	0.765	1.365	390	0.0165	0.0120	0.5015	1.0145
2014.7	0.695	1.435	480	0.0189	0.0091	0.5020	1.0130
2514.7	0.641	1.500	550	0.0208	0.0074	0.5025	1.0115
3014.7	0.594	1.550	620	0.0228	0.0063	0.5030	1.0100
4014.7	0.510	1.600	690	0.0260	0.0049	0.5040	1.0070
5014.7	0.450	1.620	730	0.0285	0.0040	0.5050	1.0040
6014.7	0.410	1.630	760	0.0300	0.0034	0.5060	1.0010

Initial reservoir pressure was estimated from the DST to be 3936 psia at a depth of 9360 ft below sea level. This pressure is over 1400 psia greater than the laboratory measured bubble point pressure of 2514 psia. Table 20-6 presents fluid properties for undersaturated oil that must be corrected for use in a reservoir simulator.

20.5.1 Black Oil PVT Correction

Fluid properties for the oil phase are shown in Table 20-7a.

Table 20-7a
Corrected Oil Phase Properties

Pressure (psia)	Oil Vis (cp)	Oil FVF (RB/STB)	Oil R _{so} (SCF/STB)	Gas Vis (cp)	Gas FVF (RCF/SCF)	Water Vis (cp)	Water FVF (RB/STB)
14.7	1.040	1.062	1	0.0080	0.9358	0.5000	1.0190
514.7	0.910	1.207	150	0.0112	0.0352	0.5005	1.0175
1014.7	0.830	1.295	280	0.0140	0.0180	0.5010	1.0160
1514.7	0.765	1.365	390	0.0165	0.0120	0.5015	1.0145
2014.7	0.695	1.435	480	0.0189	0.0091	0.5020	1.0130
2514.7	0.641	1.500	550	0.0208	0.0074	0.5025	1.0115
3014.7	0.594	1.550	620	0.0228	0.0063	0.5030	1.0100
4014.7	0.510	1.600	690	0.0260	0.0049	0.5040	1.0070
5014.7	0.450	1.620	730	0.0285	0.0040	0.5050	1.0040
6014.7	0.410	1.630	760	0.0300	0.0034	0.5060	1.0010

The corrections for adjusting laboratory-measured differential liberation and separator data to a form suitable for use in a black oil simulator are given by the conversion equations [Moses, 1986]:

$$B_o(p) = B_{od}(p) \frac{B_{ofbp}}{B_{odbp}}$$

$$R_{so}(p) = R_{sofbp} - [R_{sodbp} - R_{sod}(p)] \frac{B_{ofbp}}{B_{odbp}}$$

where B_o is the oil formation volume factor and R_{so} is the solution gas-oil ratio. The subscripts are defined as d = differential liberation data; f = flash data; and bp = bubble point. For the case study, laboratory measurements include a flash

from 6000 psig to 0 psig. The separator test conditions and results are presented in Table 20-7b.

Table 20-7b
Separator Test (Flash)

Sep. P (psig)	GOR (SCF/STB)	FVF (RB/STB)
100	572	
↓		
0	78	
Total GOR = 650		1.5

The values needed to perform the differential to flash conversion are the following:

B_{ofbp}	1.50 RB/STB	R_{sodbp}	760 SCF/STB
B_{odbp}	1.63 RB/STB	R_{sofbp}	650 SCF/STB

The corresponding correction factors are

$$B_o(p) = B_{od}(p) \times \frac{1.50}{1.63} = B_{od}(p) \times 0.92$$

$$R_{so}(p) = 650 - [760 - R_{sod}(p)] \times 0.92$$

Applying these corrections to the differential data yields the corrected results shown in Table 20-7c.

Table 20-7c
Corrected Oil-Phase Properties

Pressure (psia)	Oil FVF (RB/STB)	Oil Rso (SCF/STB)
14.7	1.062	1
514.7	1.110	89
1014.7	1.191	208
1514.7	1.256	310
2014.7	1.320	392
2514.7	1.380	457

Table 20-7c
Corrected Oil-Phase Properties

Pressure (psia)	Oil FVF (RB/STB)	Oil R _{so} (SCF/STB)
3014.7	1.426	521
4014.7	1.472	586
5014.7	1.490	622
6014.7	1.500	650

20.5.2 Undersaturated Oil Properties

Slopes for undersaturated oil properties are calculated from Table 20-8. The slopes are discussed in Chapter 24.6.

Table 20-8
Undersaturated Oil Properties

Pressure (psia)	Corrected B_{opb} (RB/STB)	μ_o (cp)	Remarks
2515	1.3800	0.641	Bubble Point
3935	1.3473	0.706	Undersaturated Values

The rate of change of oil FVF with respect to pressure for the undersaturated oil is approximated by the difference

$$\frac{\Delta B_o}{\Delta P} = \frac{1.3473 - 1.3800}{3935 - 2515} \approx -0.000023 \frac{RB/STB}{psia}$$

This linear approximation is reasonable in many cases. Nonlinear, undersaturated slopes can be modeled by some simulators.

Similarly, the rate of change of oil viscosity with respect to pressure for the undersaturated oil is

$$\frac{\Delta \mu_o}{\Delta P} = \frac{0.706 - 0.641}{3935 - 2515} \approx 0.000046 \frac{RB/STB}{psia}$$

The rate of change of solution GOR (R_{so}) is zero in the pressure regime above the bubble point pressure.

20.6 Reservoir Management Constraints

Reservoir management constraints are presented in Table 20-9. They include limits on capital expenditures, such as the number of wells that can be drilled, and operating constraints. In this case, for example, it is considered important to keep water-oil ratio (WOR) less than five STB water/STB oil. These constraints are typically imposed by considerations ranging from technical to commercial. The constraints are especially important in the prediction phase of the study.

Table 20-9
Reservoir Management Constraints

- | |
|--|
| <ul style="list-style-type: none">◆ One additional well may be drilled.◆ Completion interval in existing well may be changed.<ul style="list-style-type: none">◇ The well is presently completed in entire pay interval.◆ Target oil rate \approx 1000 STB/D◆ Water is available for injection if desired.◆ Limit WOR < 5◆ Minimum allowed BHP = 2600 psia◆ Maximum allowed injection pressure = 5000 psia◆ Minimum economic oil rate = 100 STB/D |
|--|

Exercises

Exercise 20.1 Plot FVF, viscosity, and solution GOR versus pressure for saturated and undersaturated oil.

Exercise 20.2 Verify that the PVT values are properly entered in data set CS-MB.DAT. What is the bubble point pressure in the model?

Chapter 21

Model Initialization

The initial reservoir fluid saturation and pressure distributions are based on data presented in this chapter. These distributions provide a volumetric estimate of initial fluids in place that can be compared with basic reservoir analysis of field performance. The basic reservoir analysis described below includes a geologic estimate of volumetrics and a material balance determination of initial fluids in place.

21.1 Volumetrics

A volumetric estimate of oil volume is a useful number for checking the accuracy of the numerical representation of the reservoir in a reservoir model. The volume of oil in the reservoir may be estimated as the product of bulk volume V_B , porosity ϕ , and oil saturation S_o .

The bulk volume of the reservoir is estimated by writing bulk volume V_B as the product $\Delta x \Delta y \Delta z$ where Δx , Δy , and Δz approximate the length, width, and net thickness of the pay interval, respectively.

- ◆ From maps: $\Delta x = 2000'$ and $\Delta y = 1200'$ for an area ≈ 55 acres
- ◆ From well logs: $\Delta z = 72' + 96' = 168'$

The resulting estimate of bulk volume V_B is $4.03 \times 10^8 \text{ ft}^3$.

Pore Volume V_p is the product ϕV_B . Porosity ϕ is estimated as the thickness weighted average porosity from well logs:

$$\phi \approx \frac{72 \times 0.20 + 96 \times 0.25}{168} \approx 0.228$$

Taking the product of porosity and bulk volume gives the following estimate of pore volume:

$$V_P = \phi V_B \approx 9.18 \times 10^7 \text{ft}^3 \approx 16.4 \times 10^6 \text{RB}$$

The product of oil saturation and pore volume gives an estimate of oil volume in reservoir barrels. Dividing this volume by an average oil formation volume factor B_o for the reservoir gives an estimate of oil volume in stock tank barrels. The value of oil FVF at an initial average reservoir pressure of 3935 psia is 1.3473 RB/STB. This value is obtained from laboratory data that has been corrected for use in a reservoir simulator (Chapter 20.5). The resulting oil volume is

$$V_o = \frac{S_o V_P}{B_o} \approx \frac{0.7 V_P}{B_o} \sim \frac{11.5 \times 10^6 \text{RB}}{1.3473 \text{RB/STB}} \sim 8.5 \times 10^6 \text{STB}$$

21.2 Material Balance

Volumetrics provides one measure of the quality of a reservoir model, but it is based on information that does not change with time. Another estimate of original oil volume can be obtained from a material balance study if a reasonable amount of production data is available, such as the historical data presented in Chapter 20. At this point we have surmised that the reservoir was initially undersaturated, but it may not have aquifer support.

The presence of a few barrels of water during the latter months of the first year of production indicates that mobile water is present, but its source is unknown. The volume of produced water is small enough to be water mobilized by swelling as reservoir pressure declines, or it could be the first indication of water production from aquifer influx. Both of these scenarios can be assessed if we consider the possibilities of depletion with and without aquifer influx.

We begin by deriving the material balance equation for the more general case: depletion of an undersaturated oil reservoir with water influx. The derivation is simplified by assuming formation compressibility is negligible and then setting the decrease in oil volume at reservoir conditions equal to the

increase in water volume at reservoir conditions as oil is produced and reservoir pressure decreases.

1. Calculate the decrease in oil volume ΔV_o (RB):

Let

- N = original oil in place = OOIP (STB)
- B_{oi} = oil FVF (RB/STB) at initial pressure P_i
- N_p = oil produced (STB) at pressure P and time t
- B_o = oil FVF (RB/STB) at pressure P and time t

Then

- NB_{oi} = OOIP (RB) at initial reservoir pressure P_i
- $(N - N_p) B_o$ = OIP (RB) at pressure P and time t

Therefore the change in oil volume is given by

$$\Delta V_o = NB_{oi} - (N - N_p) B_o$$

2. Calculate the increase in water volume ΔV_w (RB):

Let

- W = original water in place = OWIP (RB) at initial pressure P_i
- B_w = water FVF (RB/STB) at pressure P and time t
- W_p = water produced (STB) at pressure P and time t
- W_e = water influx (RB)

Then

- $W_p B_w$ = cumulative water produced (RB) at pressure P and time t

Therefore the change in water volume is given by

$$\Delta V_w = (W + W_e - W_p B_w) - W = W_e - W_p B_w$$

3. The assumption that the volume of the reservoir remains constant implies $\Delta V_o = \Delta V_w$. Combining results from steps 1 and 2 above gives the material balance equation for depletion of an incompressible, undersaturated oil reservoir with aquifer influx:

$$NB_{oi} - (N - N_p)B_o = W_e - W_p B_w$$

The two unknowns in the equation are N and W_e .

The simplest production scenario is to assume that water influx is negligible, that is, $W_e = 0$. If we further observe that water production W_p is insignificant, we have

$$N = \frac{N_p B_o}{B_o - B_{oi}}$$

where $B_{oi} = 1.3473$ RB/STB at $P_i = 3935$ psia. Oil FVF has been corrected for use in this calculation (see Chapter 20 for details). The corresponding estimate for OOIP is $N \approx 1500 N_p$ with $B_o - B_{oi} \approx 0.0009$ RB/STB. The results of the calculation are presented in Table 21-1.

Table 21-1
Results Assuming No Water Influx

Time (days)	Pressure (psia)	B_o (RB/STB)	N_p (MSTB)	N (MMSTB)
91	3898	1.3482	46	69
183	3897	1.3482	91	136
274	3895	1.3482	137	205
365	3892	1.3483	183	274

The value of N increases at each time. This implies that the material balance model does not account for all of the pressure support and suggests that an aquifer influx model should be considered.

If we use a volumetric estimate of N , namely $N_{vol} = 8.5$ MMSTB from Chapter 21.1, we can calculate W_e . Again recognizing that $W_p \approx 0$, the material balance equation becomes

$$W_e = N(B_{oi} - B_o) + N_p B_o$$

Results of the calculation are shown in Table 21-2.

Table 21-2
Results Assuming Water Influx with Volumetric OOIP

Time (days)	Pressure (psia)	B_o (RB/STB)	N_p (MSTB)	W_e (MMSTB)
90	3898	1.3482	46	54 (52)
180	3897	1.3482	91	115 (113)
270	3895	1.3482	137	177 (174)
365	3892	1.3483	183	239 (234)

Notice that W_e increases as a function of time. The values in parentheses are WINB4D values when the correct aquifer model is used.

21.3 Relative Permeability

As we continue our preparation of a three-dimensional simulation model, we observe that not all of the data needed by the simulator is available. Since we cannot ignore data and still perform a credible model study, we must complete the data set. Several options are available, such as ordering additional measurements or finding reasonable correlations or analogies for the missing data. In this case, our commercial interests are best served by moving the project forward without additional expense or delays.

We do not have laboratory-measured relative permeability data. We could attempt to construct relative permeability data from production data, but our production history is essentially single-phase oil. Since we must specify relative permeability to run the model, we can turn to analogous reservoirs or correlations for guidance. Let us choose the Honarpour, et al. [1982] correlation for a water-wet sandstone as a starting point for determining relative permeability curves. Well logs provide some information about saturation end points such as initial and irreducible water saturation. Core floods and capillary pressure measurements could provide information about residual hydrocarbon saturations, but they are not available. For that reason, end points like residual oil saturation must be estimated. Results of the calculation are shown in WINB4D format (Chapter 24.5) in Table 21-3 and Figure 21-1. The acronyms in Table 21-3 are defined as follows:

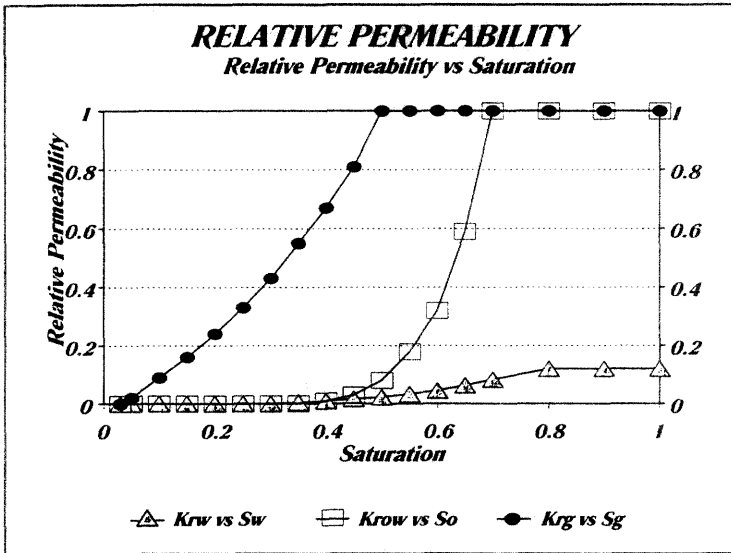


Figure 21-1. Correlation based on Honarpour, et al. [1982].

- ◆ SAT is the saturation associated with each phase
- ◆ KROW is the relative permeability of oil in the presence of water expressed as a function of oil saturation
- ◆ KRW is the relative permeability of water in a water-oil system expressed as a function of water saturation
- ◆ KRG is the relative permeability of gas in a gas-oil system expressed as a function of gas saturation
- ◆ KROG is the relative permeability of oil in the presence of gas expressed as a function of liquid saturation

Table 21-3
Relative Permeability

SAT	KROW	KRW	KRG	KROG
0.000	0.000	0.000	0.000	0.000
0.030	0.000	0.000	0.000	0.000
0.050	0.000	0.000	0.020	0.000
0.100	0.000	0.000	0.090	0.000
0.150	0.000	0.000	0.160	0.000
0.200	0.000	0.000	0.240	0.000

Table 21-3 (cont.)
Relative Permeability

SAT	KROW	KRW	KRG	KROG
0.250	0.000	0.000	0.330	0.000
0.300	0.000	0.000	0.430	0.000
0.350	0.001	0.005	0.550	0.000
0.400	0.010	0.010	0.670	0.000
0.450	0.030	0.017	0.810	0.000
0.500	0.080	0.023	1.000	0.000
0.550	0.180	0.034	1.000	0.000
0.600	0.320	0.045	1.000	0.000
0.650	0.590	0.064	1.000	0.000
0.700	1.000	0.083	1.000	0.000
0.800	1.000	0.120	1.000	0.000
0.900	1.000	0.120	1.000	0.000
1.000	1.000	0.120	1.000	0.000

If our choice of relative permeability correlations does not match field performance, we will have to change the relative permeability curves. In any event, we recognize that in this case study relative permeability is poorly known and should be considered uncertain.

21.4 Fluid Contacts

A water-oil contact (WOC) was not seen on either well logs or seismic data. The production of a small amount of water suggests that there may be a WOC in the vicinity of the reservoir. The data are not compelling, however. We could assume the oil zone extends well below the bottom depth of our well, but this would be an optimistic assumption that could prove to be economically disastrous. In the interest of protecting our investment, let us make the more conservative assumption that a WOC does exist and is just beyond the range of our observations, namely well log and seismic data. We assume WOC \approx 9600 ft, which is near the bottom of the seismically observed reservoir structure. The pressure at this WOC depth is estimated to be about 4000 psia.

21.5 Grid Preparation

Figure 21-2 is a sketch of the well location relative to the interpreted reservoir boundaries. Based on seismic data shown in Chapter 20.2, the reservoir is thought to be bounded to the east by a facies change.

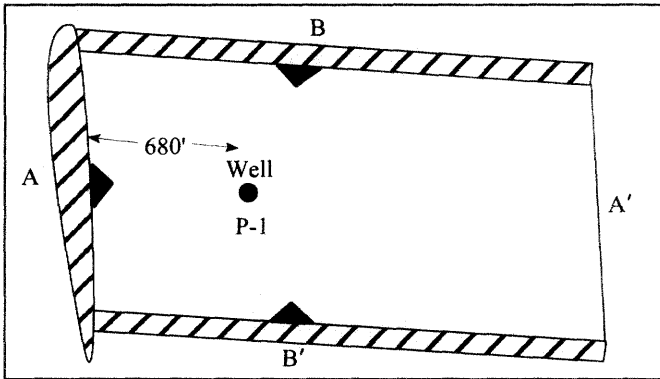


Figure 21-2. Plan view.

A cross-section through points B and B' is shown in Figure 21-3. The sides of the reservoir appear to be bounded by faults. Without evidence to the contrary, we assume that the faults are sealing. This assumption is subject to verification during the history match phase of the study.

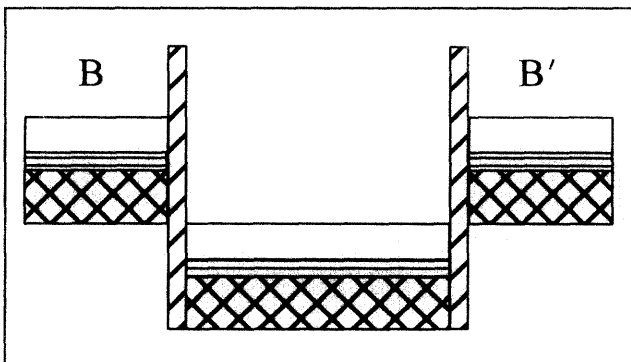


Figure 21-3. BB' cross-section.

A cross-section through points A and A' is sketched in Figure 21-4. It illustrates the dip of the reservoir and the layering. The structure of the reservoir

is based on well log and seismic interpretation. The downdip fault is speculative. It is based on the assumption that the fault shown on the western side of Figure 21-2 extends down through the formation. This is not obvious from seismic data. Indeed, if the reservoir is receiving aquifer support, the aquifer influx will come from downdip as the reservoir is depleted. Bear in mind, however, that both the fault and the aquifer may be present. This could happen, for example, if the fault is not sealing. The fault could be providing a flow path for water influx from another horizon.

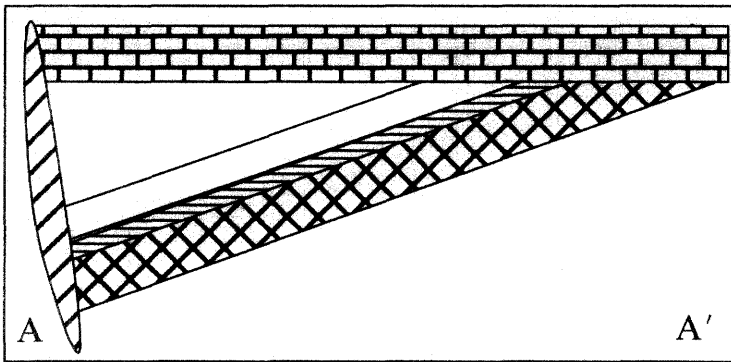


Figure 21-4. AA' cross-section.

Exercises

Exercise 21.1 Verify the calculations reported in Tables 21-1 and 21-2.

Exercise 21.2 Data file CS-MB.DAT is an input file for a material balance analysis of the case study. It represents the reservoir as a single gridblock, or "tank" model. The tank model is equivalent to a material balance calculation. Run WINB4D with the file CS-MB.DAT. Verify that the original volume of oil in the model agrees with the volumetric estimate presented in Chapter 21.1.

Exercise 21.3 Use data file CS-MB.DAT to study the effect of aquifer influx on material balance performance. This is done by modifying the input data set to include an aquifer model, then adjusting aquifer parameters until model pore

volume weighted average reservoir pressures match the pressures reported in Chapter 20. Note: the pore volume weighted average reservoir pressure P_{av} is given by

$$P_{av} = \frac{\sum_{j=i}^N P_j V_{pj}}{\sum_{j=i}^N V_{pj}}$$

where N is the total number of gridblocks in the model grid, P_j is the oil phase pressure in gridblock j , and V_{pj} is the pore volume of gridblock j . Chapter 24.10 contains details on how to set up an analytic aquifer. For an example of a data set with an analytic aquifer model, see data file EXAM9.DAT.

Exercise 21.4 Data set CS-VC.DAT is a vertical column model of the case study. Sketch the grid to scale, locate the contacts on the sketch, and match reservoir pressure.

Exercise 21.5 Repeat Exercise 21.4 beginning with the cross-section model data set CS-XS.DAT.

Chapter 22

History Matching and Predictions

The history match is now well under way. The models discussed in the exercises of Chapter 21 are conceptual models designed to provide you with a sense of how fluids move in the reservoir. This is the art of modeling. As you work with various models of the reservoir, you should begin to develop a knowledge base for determining how changes to model parameters will help achieve a match for a particular observable. This knowledge base is valuable as you develop your feel for the study.

The previous chapters set the stage for preparing a 3D model of the case study reservoir. A 3D model should provide enough reservoir definition to let us make meaningful performance predictions. Before matching the 3D model, we discuss how to incorporate well information into the model. Once the well model has been prepared, we proceed to history matching and performance predictions.

22.1 Well Model Preparation

Well model calculations require estimates of productivity index and flowing bottomhole pressure. These calculations are illustrated here.

Productivity Index Estimate

Well model calculations in WINB4D need to have the quasi-stationary productivity index factor (PID) specified by the user. PID is estimated from the expression (Chapter 30)

$$PID = \frac{0.00708 K_{abs} h_{net}}{\ln(r_e/r_w) + S}$$

where

- r_e = drainage radius (ft)
- r_w = wellbore radius (ft)
- S = skin
- $K_e = k_{ro} K_{abs}$ = effective permeability (md)
- h_{net} = net thickness (ft)

Given $S = -0.5$, $r_w = 0.25$ ft and

$$r_o \approx 0.14(\Delta x^2 + \Delta y^2)^{1/2} \approx 40 \text{ ft}$$

with $\Delta x = \Delta y = 200$ ft., we find

$$PID = 1.55 \times 10^{-3} K_{abs} h_{net}$$

where $r_e \approx r_o$. Table 22-1 presents the calculation of *PID* for each layer identified by well log analysis.

Table 22-1
Estimate of PID by Layer

Layer	K_{abs} [md]	h_{net} [ft]	PID
1	75	72	8.4
2	0	20	0
3	250	64	24.8
4	250	32	12.4

Oil Well FBHP Estimate

The production well model needs a flowing bottomhole pressure (FBHP). Assuming an oil column in the wellbore, we can prepare a quick estimate of FBHP for a single-phase oil well that is completed at a 9500 ft depth by assuming $FBHP \approx$ oil head. Consequently, oil head is approximated by

$$\gamma_o \Delta z \approx FBHP$$

where γ_o is the oil pressure gradient and Δz is the height of the oil column. An estimate of average oil pressure gradient for the oil column is found by averaging the pressure gradient at surface and reservoir conditions:

- ◆ Approximate pressure gradient at surface conditions:

$$\rho_s = 46.244 \frac{\text{lb}}{\text{ft}^3} \approx 0.321 \frac{\text{psia}}{\text{ft}}$$

where oil density at surface conditions (ρ_s) is 46.244 lbm/SCF.

- ◆ Approximate pressure gradient at reservoir conditions:

$$\rho_R = \frac{\rho_s}{B_o} \approx 34.3 \frac{\text{lb}}{\text{ft}^3} \approx 0.238 \frac{\text{psia}}{\text{ft}}$$

where oil FVF (B_o) at bottomhole conditions is 1.3482 RB/STB.

The resulting FBHP for use in WINB4D is

$$\text{FBHP} = \frac{1}{2} \left[0.321 \frac{\text{psia}}{\text{ft}} + 0.238 \frac{\text{psia}}{\text{ft}} \right] \times 9500 \text{ ft} \approx 2660 \text{ psia}$$

A more accurate estimate can be obtained from wellbore correlations or nodal analysis as discussed by such authors as Brown and Lea [1985].

Well Block Pressure from PBU

In Chapter 17 we saw that a pressure correction was needed to properly relate the pressure buildup (PBU) curve to simulator well block pressures. To illustrate this correction, suppose a well is in a block with grid dimensions $\Delta x = 200$ ft and $\Delta y = 200$ ft. We want to compare the simulator well block pressure with a pressure from a PBU. Peaceman [1978, 1983] showed that shut-in pressure P_{ws} of the actual well should equal the simulator well block pressure P_o at a shut-in time Δt_s given by

$$\Delta t_s = \frac{1688 \phi \mu c_T r_o^2}{K}$$

For an isotropic reservoir in which horizontal permeability does not depend on direction, that is, $K_x = K_y$, we estimate the equivalent radius of a well in the center of a gridblock as

$$r_o \approx 0.14(\Delta x^2 + \Delta y^2)^{1/2}$$

The shut in time Δt_s at which the PBU pressure should be obtained is calculated from the following physical parameters:

c_r	$3 \times 10^{-6} \text{ psia}^{-1}$
c_o	$13 \times 10^{-6} \text{ psia}^{-1}$
c_w	$3 \times 10^{-6} \text{ psia}^{-1}$
S_o	0.7
S_w	0.3
μ_o	0.71 cp
ϕ	0.20
K	75 md

The equivalent radius of the well block is estimated to be $r_o \approx 0.14(200^2 + 200^2)^{1/2} = 39.6$ ft, while the total compressibility is given by $c_T = c_r + S_o c_o + S_w c_w = 3 \times 10^{-6} + 0.7(13 \times 10^{-6}) + 0.3(3 \times 10^{-6}) \approx 13 \times 10^{-6} \text{ psia}^{-1}$. The PBU shut in time corresponding to these values is

$$\begin{aligned} \Delta t_s &= 1688 \frac{(0.20)(0.71)(13 \times 10^{-6})(39.6)^2}{75} \\ &= 0.065 \text{ hr.} \approx 4 \text{ minutes} \end{aligned}$$

This early time part of the PBU curve could be masked by wellbore storage effects. Since the shut in pressure P_{ws} of the actual well equals the simulator well block pressure P_o at a shut in time Δt_s , the shut in pressure P_{ws} may have to be obtained by extrapolation of the radial flow curve.

Throughput Estimate

Model timestep size is estimated by calculating pore volume throughput from well flow rates. In our case, pore volume throughput is given by

$$V_{PT} = \frac{Q\Delta t}{V_P} \quad (5.6146)$$

where

V_P = $\phi \Delta x \Delta y \Delta z$ = pore volume (ft³)

Q = volumetric flow rate at reservoir conditions (RB/day)

Δt = timestep size (day)

Timesteps for an IMPES simulator should correspond to about 10% throughput or less. The maximum timestep is estimated as follows.

Suppose $\phi = 22.5\%$, $\Delta x = \Delta y = 200'$, $\Delta z = h_{net}$, and $Q = 400$ RB/day. Then Δt is found by setting $V_{PT} = 0.10$ and rearranging the pore volume throughput equation to give

$$\begin{aligned} \Delta t &= \frac{(0.1)V_P}{5.6146Q} = (0.1) \frac{\phi \Delta x \Delta y \Delta z}{5.6146Q} \\ &= 0.4h_{net} \quad (\text{days}) \end{aligned}$$

If $h_{net} = 100$ ft, then $\Delta t \approx 40$ days is an estimate of the maximum IMPES timestep size.

22.2 Full Field (3D) Model History Match

Data file CS-HM.DAT is the three-dimensional model used to prepare the production history presented in Chapter 20. The grid in Figure 22-1 was used

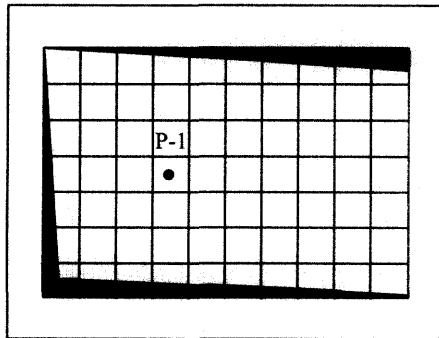


Figure 22-1. Plan view of grid.

to model the reservoir shown in Figure 21-2. Each gridblock is a square with lengths $\Delta x = \Delta y = 200$ ft. The dark areas of the grid are outside the reservoir area. The pore volume in the dark area is made inactive in data file CS-HM.DAT by using porosity multipliers.

The depth and thickness of each gridblock depend on reservoir architecture. The model grid should approximate the structure depicted in Figure 21-4, which is based on Figures 20-1 and 20-2. The dip of the reservoir is included by specifying the tops of each gridblock. The gridblock length modifications are designed to cut off those parts of the block that continue the grid beyond the surface of the unconformity sketched in Figure 21-4.

Transmissibility multipliers in the vertical direction are set to 0 to simulate impermeable shale barriers. This includes the shale streak that divides the second major sand into two thinner sands with a shale break. The interpretation of seismic data was unable to resolve this feature, but the well log shown in Figure 22-2 does indicate the presence of a shale streak.

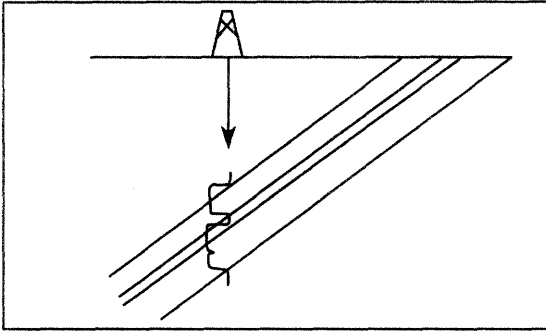


Figure 22-2. Overlay of seismic and well log data.

The water-oil contact is at 9600 ft. A steady-state aquifer is in communication with all three oil layers at this depth. It is the source of water production shown in Table 20-2.

22.3 Predictions

Now that we have a history match model, we are ready to make predictions. The first step is to establish a base case prediction which assumes there

will be no changes in operating strategy. Given a base case prediction, several runs should be made to optimize reservoir performance within the constraints imposed by the commissioners of the study. If the model is run with well P-1 switched from oil rate to bottom hole pressure control, the PI for well P-1 needs to be calibrated to assure continuity in the oil rate. The following exercises are designed to guide you through the prediction process.

Exercises

Exercise 22.1 Repeat the shut in time calculation using $\Delta x = 1000$ ft and $\Delta y = 1000$ ft. The new shut in time Δt_s should be less than one hour.

Exercise 22.2 Run data set CS-XS.DAT with maximum timestep sizes ranging from 15 days to 60 days. Select a maximum timestep size by monitoring the material balance error and the stability of the solution. A solution is unstable if it oscillates, that is, variables like GOR or WOR vary between a high and low value from one timestep to the next.

Exercise 22.3 What is the effect of doubling the PID in data set CS-XS.DAT?

Exercise 22.4 How does model performance change if skin $S = 0$?

Exercise 22.5 What is the effect of reducing the well FBHP by 1000 psia? The reduction in FBHP is one way to simulate gas lift or pumping.

Exercise 22.6 Data set CS-HM.DAT was used as the basis of the case study. Run data set CS-HM.DAT and verify that it matches the data shown in Table 20-2.

Exercise 22.7 Several sensitivity runs may be made by varying model parameters and noting reservoir performance. As an example of a sensitivity study, vary the WOC by ± 100 ft. How does this variation affect water breakthrough and oil recovery during the history match period?

Exercise 22.8 Run data set CS-HM.DAT for five years (four years into the future) with Well P-1 under oil rate control. This run establishes a base case prediction.

Exercise 22.9 Data set CS-PD.DAT is the base case prediction. Beginning with this data set, maximize oil recovery given the constraints listed in Table 20-9. Two ideas to consider are downdip water injection after drilling an updip producer; and downdip production after drilling an updip gas injector.

This page intentionally left blank

Part IV
WINB4D User's Manual

This page intentionally left blank

Chapter 23

Introduction to WINB4D

WINB4D simulates isothermal, Darcy flow in up to three dimensions. It assumes reservoir fluids can be described by up to three fluid phases (oil, gas, and water) with physical properties that depend on pressure only. Gas is allowed to dissolve in both the oil and water phases. A feature unique to WINB4D is the inclusion of compressional velocity and acoustic impedance calculations. These reservoir geophysical calculations make it possible to track changes in seismic variables as a function of time, which is the basis for 4D seismic analysis.

WINB4D was designed to run on Windows-based personal computers with 486 or better math co-processors. This size simulator is well-suited for learning how to use a reservoir simulator, developing an understanding of reservoir management concepts, and for solving many types of reservoir engineering problems. It is an inexpensive tool for performing studies that call for more sophistication than is provided by analytical solutions, yet do not require the use of full-featured commercial simulators.

WINB4D is a modified version of the black oil simulator BOAST II that was published by the U.S. Department of Energy in 1987 [Fanchi, et al., 1987]. BOAST II was an improved version of BOAST, an implicit pressure-explicit saturation (IMPES) simulator published by the U.S. Department of Energy in 1982 [Fanchi, et al., 1982]. There have been several modifications of BOAST II published by the Bartlesville Project Office of the U.S. Department of Energy. WINB4D is based on BOAST II.

A comparison of differences between BOAST II and WINB4D is given in Tables 23-1 and 23-2. The first table shows that a variety of useful geophysical

and reservoir engineering features have been added to WINB4D, including the ability to perform material balance studies with a tank model, the representation of horizontal or deviated wells, and the calculation of important reservoir geophysical information.

Table 23-1
Comparison of Reservoir Modeling Differences

FEATURE	BOAST II	WINB4D
Material balance tank model (1 gridblock)	Not available	New
Well completions	Vertically contiguous	Flexible - may skip layers
Horizontal well	Not available	New
Slanted well	Not available	New
Compressional velocity	Not available	New
Shear velocity	Not available	New
Acoustic impedance	Not available	New
Reflection coefficient	Not available	New
Modify ϕ , K	Input ϕ , K	Added multiply by factor
Modify transmissibility	Input transmissibility	Multiply trans. by factor
Saturation initialization	User specified	Added gravity segregated option

Table 23-3 presents WINB4D enhancements designed to improve computational performance. For example, a more accurate algorithm for interpolating gas formation volume factor B_g .

BOAST II has been tested under a wide range of conditions. Detailed comparisons with other simulators were made for four types of problems: oil and gas depletion, waterflooding, gas injection with constant bubble point pressure, and gas injection with variable bubble point pressure. Favorable comparisons were observed with respect to oil rates, GORs, gas saturations, and pressures. The one exception is the reservoir pressure comparison for the variable

bubble point pressure case. In this case, BOAST II reservoir pressures were consistently lower than other simulator values. A mass conserving expansion of accumulation terms can improve the accuracy for variable bubble point pressure problems [Fanchi, 1986], but the mass conserving expansion option requires additional run time and is not included in WINB4D.

Table 23-2
Comparison of Computational Differences

FEATURE	BOAST II	WINB4D
Interpolation	B_g	$b_g = 1/B_g$ Improves material balance
Saturation table end points	Set to -0.1 and 1.1	Set to 0.0 and 1.0
Timestepping and reports	Counter and user specified	Simplify to user specified only
Debug codes	Optional	Deleted
Restart	Available	Deleted - restart by specifying arrays
Stabilized IMPES	Available	Deleted - not robust

WINB4D retains the robustness of BOAST II while substantially increasing program accuracy. WINB4D has an improved interpolation algorithm that reduces material balance error for some problems by as much as a factor of ten relative to the DOE versions BOAST and BOAST II. This feature increases the range of applicability of WINB4D and is especially valuable for gas and gas-oil systems. The algorithm does not degrade program speed.

23.1 Program Configuration

The user needs to have at least 1 Megabyte RAM to run WINB4D. The version of WINB4D accompanying this book allows the user to define grids with up to 1000 gridblocks. Parameters that may be dimensioned by the user at the time of the run are listed below.

Table 23-3
Standard Configuration of WINB4D

Dimensioning Parameters	
Maximum number of blocks in model	1000
Maximum number of Rock regions	3
Maximum number of entries in a Rock region table	30
Maximum number of PVT regions	3
Maximum number of entries in a PVT region table	30
Maximum number of wells	25
Maximum number of connections per well	5

WINB4D must be copied to a folder on your hard drive before running. The following procedure is recommended for a CD drive D and hard drive C running Windows 95/98/NT:

- ◆ Open **Windows Explorer** and select your CD drive.
- ◆ Use a **Windows-based Unzip** program to extract all of the files from the **WINB4D** file on the CD to a folder on your hard drive.
- ◆ Respond to questions.

23.2 Input Data File - WTEMP.DAT

WINB4D reads a file called WTEMP.DAT and outputs to files WTEMP.TSS, WTEMP.PLT, WTEMP.WEL, WTEMP.ROF, and WTEMP.-ARR. The output files are described in Chapter 26. You should rename any runs you wish to save because WINB4D overwrites the WTEMP.* files when it is executed.

The easiest way to prepare a new data file is to edit an old one. This will give you an example of the formats needed for most options. If you start with an old data set, make sure that you check all applicable data entries and make changes where appropriate.

23.3 Data Input Requirements

WINB4D input data is divided into two parts: initialization data, and recurrent data. Initialization data is described in Chapter 24. It includes data that is set at the beginning of the study and is not expected to change during a model run. Such data includes the reservoir description and fluid properties. Recurrent data is described in Chapter 25 and refers to data that is expected to change during the course of a simulation. It includes well schedules and timestep control information. Additional discussion of WINB4D is presented in Part V: Technical Supplement.

Title or heading records are read before each major and many minor sections. These records are designed to make the input data file easier to read and edit.

All input data, with the exception of well names, is entered as free format data. Two free format data entries must be separated by a comma or a space if they are entered on the same line.

In many cases, codes are read that will specify the type of input to follow and the number of values that will be read. These codes increase the efficiency and flexibility of entering input data.

Input tabular data should cover the entire range of values expected to occur in a simulation. Examples of tabular data include fluid property data entered as functions of pressure and relative permeability data entered as functions of saturation. The linear table interpolation algorithms in WINB4D will return tabulated endpoint values if the independent variable goes outside the range of the input tabular values. No message will be printed if this occurs.

If an array of input values must be read, the following input order must be followed. Layer 1 ($K = 1$) is read first. The data in each layer are read by rows, starting with row 1 ($J = 1$). Values of the array element are read for the first row starting with column 1 ($I = 1$) and proceeding to the end of the row (column $I = II$). After II values are read, the next row ($J = 2$) of values are entered. These values must begin on a new line. This data entry procedure is repeated for all rows and, subsequently, for all layers until the complete set of array elements has been entered.

23.4 Example Input Data Sets

Several example input data sets are included with the book. A few are listed below.

FILE	GRID $II \times JJ \times KK$	MODEL TYPE	REMARKS
EXAM1.DAT	$1 \times 1 \times 1$	Material Balance	Primary depletion of an under-saturated oil reservoir (high GOR)
EXAM2.DAT	$1 \times 1 \times 4$	1D Vertical	Primary depletion of an under-saturated oil reservoir (moderate GOR)
EXAM3.DAT	$10 \times 1 \times 1$	1D Horizontal	Buckley-Leverett waterflood
EXAM4.DAT	$9 \times 9 \times 1$	2D Areal	Primary depletion of an undersaturated oil reservoir (high GOR)
EXAM5.DAT	$10 \times 1 \times 4$	2D Cross- section	Multi-layer waterflood of an undersaturated oil reservoir (high GOR)
EXAM6.DAT	$9 \times 9 \times 2$	3D	5-spot waterflood of an under-saturated oil reservoir (high GOR)
EXAM7.DAT	$10 \times 10 \times 3$	3D	Gas injection into undersaturated oil reservoir (high GOR) - Odeh example
EXAM8.DAT	$9 \times 9 \times 2$	3D	Depletion of gas reservoir
EXAM9.DAT	$9 \times 9 \times 2$	3D	Depletion of gas reservoir with aquifer support
EXAM10.DAT	$10 \times 8 \times 4$	3D	Depletion of a faulted oil reservoir with multiple PVT and ROCK regions
EXAM11.DAT	$10 \times 1 \times 2$	2D Cross- section	Depletion of gas reservoir with aquifer support

Example Input Data Set

The following data set is presented to illustrate the WINB4D input file format. Additional spacing has been provided between some lines to improve data set readability. The actual WINB4D data set should contain no blank lines between records.

----- BEGINNING OF DATA SET -----
PRIMARY DEPLETION OF AN OIL RESERVOIR - VERTICAL COLUMN MODEL
GRID DIMENSIONS
1, 1, 4, 3, 3, 30, 10, 10
Gridblock LENGTHS
-1 -1 0 0
2000.0
1200.0
2*50.0 2*60.0
2*36.0 2*38.0
Gridblock LENGTH MODIFICATIONS
0, 0, 0, 0, 0
DEPTH TO TOP OF UPPER SAND
2
9330
9380
9430
9490
MODULI AND ROCK DENSITY
-1 -1 -1 -1
3E6
3E6
3E6
168
MODULI AND ROCK DENSITY MODIFICATIONS
0 0 0 0
POROSITY AND PERMEABILITY DISTRIBUTIONS
0 0 0 0
2*0.20 2*0.25
2*75 2*250
2*75 2*250
2*7.5 2*25
POROSITY AND PERMEABILITY MODIFICATION CARDS
0, 0, 0, 0, 0
TRANSMISSIBILITY MOD. - NO FLOW BETWEEN LAYERS 2 AND 3
0, 0, 1, 0
1 1 1 1 3 3 0.0
ROCK AND PVT REGIONS
1, 1

SAT	KRO	KRW	KRG	KROG	PCOW	PCGO
0.00	0.00	0.00	0.00	0.0	0.0	0.0
0.03	0.00	0.00	0.00	0.0	0.0	0.0
0.05	0.00	0.00	0.02	0.0	0.0	0.0
0.10	0.00	0.00	0.09	0.0	0.0	0.0
0.15	0.00	0.00	0.16	0.0	0.0	0.0
0.20	0.00	0.00	0.24	0.0	0.0	0.0
0.25	0.00	0.00	0.33	0.0	0.0	0.0
0.30	0.0001	0.00	0.43	0.0	0.0	0.0
0.35	0.001	0.005	0.55	0.0	0.0	0.0
0.40	0.01	0.010	0.67	0.0	0.0	0.0
0.45	0.03	0.017	0.81	0.0	0.0	0.0
0.50	0.08	0.023	1.00	0.0	0.0	0.0
0.55	0.18	0.034	1.00	0.0	0.0	0.0
0.60	0.32	0.045	1.00	0.0	0.0	0.0
0.65	0.59	0.064	1.00	0.0	0.0	0.0
0.70	1.00	0.083	1.00	0.0	0.0	0.0
0.80	1.00	0.12	1.00	0.0	0.0	0.0
0.90	1.00	0.12	1.00	0.0	0.0	0.0
1.00	1.00	0.12	1.00	0.0	0.0	0.0

ITHREE SW(IRR.)

0, 0.30

PBO PBODAT PBGRAD

2514.7, 9200.0, 0.0

VSLOPE BSLOPE RSLOPE PMAX REPRS

0.000046, -0.000023, 0.0, 6014.7, 0

OIL: P MUO BO RSO

14.7 1.0400 1.0620 1.0

514.7, 0.9100, 1.1110, 89.0

1014.7, 0.8300, 1.1920, 208.0

1514.7, 0.7650, 1.2560, 309.0

2014.7, 0.6950, 1.3200, 392.0

2514.7, 0.6410, 1.3800, 457.0

3014.7, 0.5940, 1.4260, 521.0

4014.7, 0.5100, 1.4720, 586.0

5014.7, 0.4500, 1.4900, 622.0

6014.7, 0.4100, 1.5000, 650.0

WATER: P	MUW	BW	RSW
14.7,	0.5000,	1.0190,	0.0
514.7,	0.5005,	1.0175	0.0
1014.7,	0.5010,	1.0160,	0.0
1514.7,	0.5015,	1.0145,	0.0
2014.7,	0.5020,	1.0130,	0.0
2514.7,	0.5025,	1.0115,	0.0
3014.7,	0.5030,	1.0100,	0.0
4014.7,	0.5040,	1.0070,	0.0
5014.7,	0.5050,	1.0040,	0.0
6014.7,	0.5060,	1.0010,	0.0

GAS AND ROCK PROPERTIES

P	MUG	BG	PSI	CR
14.7,	0.008000,	0.935800,	0.0,	0.000003
514.7,	0.011200,	0.035200,	0.0,	0.000003
1014.7,	0.014000,	0.018000,	0.0,	0.000003
1514.7,	0.016500,	0.012000,	0.0,	0.000003
2014.7,	0.018900,	0.009100,	0.0,	0.000003
2514.7,	0.020800,	0.007400,	0.0,	0.000003
3014.7,	0.022800,	0.006300,	0.0,	0.000003
4014.7,	0.026000,	0.004900,	0.0,	0.000003
5014.7,	0.028500,	0.004000,	0.0,	0.000003
6014.7,	0.030000,	0.003400,	0.0,	0.000003

RHOSCO RHOSCW RHOSCG

46.244, 62.238, 0.0647

EQUILIBRIUM PRESSURE INIT. / CONSTANT SATURATION INIT.

1, 1, 0, 0

4000, 9600, 0, 8000

0.70, 0, 0.25

NMAX	FACT1	FACT2	TMAX	WORMAX	GORMAX	PAMIN	PAMAX
1000,	1.50,	0.50,	365,	5.0,	500000,	1500,	6000
KSOL	MITR	OMEGA	TOL	TOL1	DSMAX	DPMAX	NUMDIS
1,	100,	1.50,	0.1,	0.001,	0.05,	100.0,	1

AQUIFER MODEL

0

RECURRENT DATA

*** DATA SET 1 - HISTORY ***

1, 4

91.25 182.5 273.75 365.0

1, 1, 1, 0, 0, 1

0, 0, 0, 0, 0

5.0, 1.0, 10.0

WELL INFORMATION

1 0

238 *Principles of Applied Reservoir Simulation*

WELL P-1

P-1

1 4

1, 1, 1, 2.7 2600

1, 1, 2, 2.7 2600

1, 1, 3, 9.4 2600

1, 1, 4, 9.4 2600

1, 500.0, 0.0, 0.0, 0.0

-----END OF DATA SET -----

Chapter 24

Initialization Data

Initialization data records are read once at the beginning of the simulation. They must be read in the order presented below.

1. **Title** Up to 80 characters; this record will appear as run title.

24.1 Grid Dimensions and Geometry

24.1.1 Grid Dimensions

1. **Heading** Up to 80 characters.
2. **II, JJ, KK, IOROK, IOPVT, IOTBL, IONWL, IOCON**

Code	Meaning
II	number of gridblocks in the x direction
JJ	number of gridblocks in the y direction
KK	number of gridblocks in the z direction
IOROK	maximum number of Rock regions (such as 3)
IOPVT	maximum number of PVT regions (such as 3)

Code	Meaning
IOTBL	maximum number of entries in PVT and Saturation tables (such as 30)
IONWL	maximum number of wells (such as 10)
IOCON	maximum number of connections per well (such as 10)

3. **Heading** Up to 80 characters.

4. **KDX, KDY, KDZ, KDZNET**

KDX Control code for input of x direction grid size.

KDY Control code for input of y direction grid size.

KDZ Control code for input of z direction gross gridblock thicknesses.

KDZNET Control code for input of z direction net gridblock thicknesses.

Code	Value	Meaning
KDX	-1	The x direction grid dimensions are the same for all blocks in the grid. Read only one value.
	0	The x direction dimensions are read for each block in the first row ($J = 1$) of layer one ($K = 1$). These same values are assigned to all other rows and all other layers in the model grid. Read II values.
	1	The x direction dimensions are read for each block in layer one ($K = 1$). These same values are assigned to all other layers in the grid. Read $II \times JJ$ values.
KDY	-1	The y direction grid dimensions are the same for all blocks in the grid. Read only one value.
	0	The y direction dimensions are read for each block in the first column ($I = 1$) of layer one ($K = 1$). These values are assigned to all other columns and all other layers in the model grid. Read JJ values.

Code	Value	Meaning
	1	The y direction dimensions are read for each block in layer one ($K = 1$). These same values are assigned to all other layers in the grid. Read $II \times JJ$ values.
KDZ	-1	The z direction gross thickness is the same for all blocks in the grid. Read only one value.
	0	A constant value of gross thickness is read for each layer in the grid; each layer may have a different, but constant value. Read KK values.
	1	The z direction gross thickness is read for each block in the grid. Read $II \times JJ \times KK$ values.
KDZNET	-1	The z direction net thickness is the same for all blocks in the grid. Read only one value.
	0	A constant value of net thickness is read for each layer in the grid; each layer may have a different, but constant value. Read KK values.
	1	The z direction net thickness is read for each block in the grid. Read $II \times JJ \times KK$ values.

5. **DX**
 DX Gridblock size in x direction (ft).
 If KDX = -1, read one constant value.
 If KDX = 0, read II values (one for each row).
 If KDX = +1, read $II \times JJ$ values (one for each $K = 1$ block).

6. **DY**
 DY Gridblock size in y direction (ft).
 If KDY = -1, read one constant value.
 If KDY = 0, read JJ values (one for each column).
 If KDY = +1, read $II \times JJ$ values (one for each $K = 1$ block).

7. **DZ**
 DZ Gross gridblock thickness in z direction (ft).
 If KDZ = -1, read one constant value.
 If KDZ = 0, read KK values (one for each layer).

If KDZ = +1, read $II \times JJ \times KK$ values (one for each block).

8. **DZNET**

DZNET Net gridblock thickness in z direction (ft).

If KDZ = -1, read one constant value.

If KDZ = 0, read KK values (one for each layer).

If KDZ = +1, read $II \times JJ \times KK$ values (one for each block).

24.1.2 Modifications to Grid Dimensions

1. **Heading** Up to 80 characters.

2. **NUMDX, NUMDY, NUMDZ, NUMDZN, IDCODE**

NUMDX Number of regions where x direction grid size (DX) is changed.

NUMDY Number of regions where y direction grid size (DY) is changed.

NUMDZ Number of regions where z direction gross thickness (DZ) is changed.

NUMDZN Number of regions where z direction net thickness (DZN) is changed.

IDCODE = 0 means do not print the modified distributions;
= 1 means print the modified distributions.

3. **I1, I2, J1, J2, K1, K2, DX**

Omit this record if NUMDX = 0.

I1 Coordinate of first region block in I direction.

I2 Coordinate of last region block in I direction.

J1 Coordinate of first region block in J direction.

J2 Coordinate of last region block in J direction.

K1 Coordinate of first region block in K direction.

K2 Coordinate of last region block in K direction.

DX New value of x direction grid size for region (ft).

NOTE: NUMDX records must be read.

4. **I1, I2, J1, J2, K1, K2, DY**

Omit this record if NUMDY = 0.

- I1 Coordinate of first region block in I direction.
- I2 Coordinate of last region block in I direction.
- J1 Coordinate of first region block in J direction.
- J2 Coordinate of last region block in J direction.
- K1 Coordinate of first region block in K direction.
- K2 Coordinate of last region block in K direction.
- DY New value of y direction grid size for region (ft).

NOTE: NUMDY records must be read.

5. **I1, I2, J1, J2, K1, K2, DZ**

Omit this record if NUMDZ = 0.

- I1 Coordinate of first region block in I direction.
- I2 Coordinate of last region block in I direction.
- J1 Coordinate of first region block in J direction.
- J2 Coordinate of last region block in J direction.
- K1 Coordinate of first region block in K direction.
- K2 Coordinate of last region block in K direction.
- DZ New value of z direction gross thickness for region (ft).

NOTE: NUMDZ records must be read.

6. **I1, I2, J1, J2, K1, K2, DZNET**

Omit this record if NUMDZN = 0.

- I1 Coordinate of first region block in I direction.
- I2 Coordinate of last region block in I direction.
- J1 Coordinate of first region block in J direction.
- J2 Coordinate of last region block in J direction.
- K1 Coordinate of first region block in K direction.
- K2 Coordinate of last region block in K direction.
- DZNET New value of z direction net thickness for region (ft).

NOTE: NUMDZN records must be read.

24.1.3 Depths to Top of Gridblocks

The coordinate system used in WINB4D is defined so that values in the z (vertical) direction increase as the layer gets deeper. Thus, depths must be read as depths below the user-selected reference datum. Negative values will be read as heights above the datum.

1. **Heading** Up to 80 characters.
2. **KEL**
 KEL Control code for input of depth values.

KEL	Meaning
0	A single constant value is read for the depth to the top of all gridblocks in layer 1 (horizontal plane). Each layer is contiguous in this option. Depths to the top of gridblocks in layers below layer 1 are calculated by adding the layer thickness to the preceding layer top; thus $Top(I, J, K + 1) = Top(I, J, K) + DZ(I, J, K)$
1	A separate depth value must be read for each gridblock in layer 1. Read $II \times JJ$ values. Each layer is contiguous in this option. Depths to the top of gridblocks in layers below layer 1 are calculated by adding the layer thickness to the preceding layer top; thus $Top(I, J, K + 1) = Top(I, J, K) + DZ(I, J, K)$
2	A separate depth value is read for each layer. Read KK values. Each layer is horizontal (layer cake) in this option.
3	A separate depth value is read for each gridblock. Read $II \times JJ \times KK$ values.

3. **ELEV**
 ELEV Depth to top of gridblock (ft).
 If $KEL = 0$, read one constant value.
 If $KEL = 1$, read $II \times JJ$ values (one for each block in layer 1).
 If $KEL = 2$, read KK values (one for each layer).
 If $KEL = 3$, read $II \times JJ \times KK$ values (one for each block).

24.2 Seismic Velocity Parameters

24.2.1 Moduli and Grain Densities

1. **Heading** Up to 80 characters.
2. **KKB, KKG, KMU, KRHO**
 - KKB** Control code for input of the frame bulk modulus (evacuated porous rock).
 - KKG** Control code for input of the grain bulk modulus (solid matrix material).
 - KMU** Control code for input of the shear modulus (evacuated porous rock).
 - KRHO** Control code for input of the grain density (solid matrix material).

Code	Value	Meaning
KKB	-1	Frame bulk moduli are the same for all blocks in the grid. Read only one value.
	0	A constant value of frame bulk modulus is read for each layer in the grid; each layer may have a different, but constant value. Read KK values.
	1	Frame bulk moduli are read for each block in the grid. Read $II \times JJ \times KK$ values.
KKG	-1	Grain bulk moduli are the same for all blocks in the grid. Read only one value.
	0	A constant value of grain bulk modulus is read for each layer in the grid; each layer may have a different, but constant value. Read KK values.
	1	Grain bulk moduli are read for each block in the grid. Read $II \times JJ \times KK$ values.

Code	Value	Meaning
KMU	-1	Shear moduli are the same for all blocks in the grid. Read only one value.
	0	A constant value of shear modulus is read for each layer in the grid; each layer may have a different, but constant value. Read KK values.
	1	Shear moduli are read for each block in the grid. Read $II \times JJ \times KK$ values.
KRHO	-1	Grain densities are the same for all blocks in the grid. Read only one value.
	0	A constant value of grain density is read for each layer in the grid; each layer may have a different, but constant value. Read KK values.
	1	Grain densities are read for each block in the grid. Read $II \times JJ \times KK$ values.

3. **KB**
 KB Frame bulk modulus (psia).
 If KKB = -1, read one constant value.
 If KKB = 0, read KK values (one for each layer).
 If KKB = +1, read $II \times JJ \times KK$ values (one for each block).
NOTE: In the absence of relevant data, a value of 3×10^6 psia is a reasonable estimate.

4. **KG**
 KG Grain bulk modulus (psia).
 If KKG = -1, read one constant value.
 If KKG = 0, read JJ values (one for each layer).
 If KKG = +1, read $II \times JJ$ values (one for each block).
NOTE: In the absence of relevant data, a value of 3×10^6 psia is a reasonable estimate.

5. **MU**
 MU Shear modulus (psia).

If KMU = -1, read one constant value.

If KMU = 0, read KK values (one for each layer).

If KMU = +1, read $II \times JJ \times KK$ values (one for each block).

NOTE: In the absence of relevant data, a value of 3×10^6 psia is a reasonable estimate.

6. **RHOMA**

RHOMA Grain density (lbf/ft³).

If KRHO = -1, read one constant value.

If KRHO = 0, read KK values (one for each layer).

If KRHO = +1, read $II \times JJ \times KK$ values (one for each block).

NOTE: In the absence of relevant data, a value of 168 lbf/ft³ (corresponding to 2.7 g/cm³) is a reasonable estimate.

24.2.2 Modifications to Moduli and Grain Densities

1. **Heading** Up to 80 characters.

2. **NUMKB, NUMKG, NUMMU, NUMRHO, IDCODE**

NUMKB Number of regions where frame bulk modulus (KB) is changed.

NUMKG Number of regions where grain bulk modulus (KG) is changed.

NUMMU Number of regions where shear modulus (MU) is changed.

NUMRHO Number of regions where grain density (RHO) is changed.

IDCODE = 0 means do not print the modified distributions;
= 1 means print the modified distributions.

3. **I1, I2, J1, J2, K1, K2, KB**

Omit this record if NUMKB = 0.

- I1 Coordinate of first region block in I direction.
 - I2 Coordinate of last region block in I direction.
 - J1 Coordinate of first region block in J direction.
 - J2 Coordinate of last region block in J direction.
 - K1 Coordinate of first region block in K direction.
 - K2 Coordinate of last region block in K direction.
 - KB New value of frame bulk modulus (psia).
- NOTE:** NUMKB records must be read.

4. **I1, I2, J1, J2, K1, K2, KG**

Omit this record if NUMKG = 0.

- I1 Coordinate of first region block in I direction.
 - I2 Coordinate of last region block in I direction.
 - J1 Coordinate of first region block in J direction.
 - J2 Coordinate of last region block in J direction.
 - K1 Coordinate of first region block in K direction.
 - K2 Coordinate of last region block in K direction.
 - KG New value of grain bulk modulus (psia).
- NOTE:** NUMKG records must be read.

5. **I1, I2, J1, J2, K1, K2, MU**

Omit this record if NUMMU = 0.

- I1 Coordinate of first region block in I direction.
 - I2 Coordinate of last region block in I direction.
 - J1 Coordinate of first region block in J direction.
 - J2 Coordinate of last region block in J direction.
 - K1 Coordinate of first region block in K direction.
 - K2 Coordinate of last region block in K direction.
 - MU New value of shear modulus.
- NOTE:** NUMMU records must be read.

6. **I1, I2, J1, J2, K1, K2, RHO**

Omit this record if NUMRHO = 0.

- I1 Coordinate of first region block in I direction.
- I2 Coordinate of last region block in I direction.
- J1 Coordinate of first region block in J direction.
- J2 Coordinate of last region block in J direction.
- K1 Coordinate of first region block in K direction.
- K2 Coordinate of last region block in K direction.
- RHO New value of grain density (lb/ft³).

NOTE: NUMRHO records must be read.

24.3 Porosity, Permeability, and Transmissibility Distributions

24.3.1 Porosity and Permeability

1. **Heading** Up to 80 characters.

2. **KPH, KXX, KKY, KKZ**
 - KPH Control code for input of porosity.
 - KXX Control code for input of *x* direction permeability.
 - KKY Control code for input of *y* direction permeability.
 - KKZ Control code for input of *z* direction permeability.

Code	Value	Meaning
KPH	-1	The porosity is constant for all gridblocks. Read only one value.
	0	A constant value is read for each layer in the grid. Read KK values.
	1	A value is read for each block in the grid. Read II × JJ × KK values.
KXX	-1	The <i>x</i> direction permeability is constant for all gridblocks. Read only one value.
	0	A constant value is read for each layer in the grid. Read KK values.
	1	A value is read for each block in the grid. Read II × JJ × KK values.

Code	Value	Meaning
KKY	-1	The y direction permeability is constant for all gridblocks. Read only one value.
	0	A constant value is read for each layer in the grid. Read KK values.
	1	A value is read for each block in the grid. Read $II \times JJ \times KK$ values.
KKZ	-1	The z direction permeability is constant for all gridblocks. Read only one value.
	0	A constant value is read for each layer in the grid. Read KK values.
	1	A value is read for each block in the grid. Read $II \times JJ \times KK$ values.

3. **PHI**

- PHI Porosity (fraction).
 If KPH = -1, read one constant value.
 If KPH = 0, read KK values (one for each layer).
 If KPH = +1, read $II \times JJ \times KK$ values (one for each block).

4. **PERMX**

- PERMX Permeability in x direction (md).
 If KPX = -1, read one constant value.
 If KPX = 0, read KK values (one for each layer).
 If KPX = +1, read $II \times JJ \times KK$ values (one for each block).

5. **PERMY**

- PERMY Permeability in y direction (md).
 If KKY = -1, read one constant value.
 If KKY = 0, read KK values (one for each layer).
 If KKY = +1, read $II \times JJ \times KK$ values (one for each block).

6. **PERMZ**
 PERMZ Permeability in z direction (md).
 If KKZ = -1, read one constant value.
 If KKZ = 0, read KK values (one for each layer).
 If KKZ = +1, read $II \times JJ \times KK$ values (one for each block).

24.3.2 Modifications to Porosities and Permeabilities

1. **Heading** Up to 80 characters.
2. **NUMP, NUMKX, NUMKY, NUMKZ, IPCODE**
 NUMP Number of regions where porosity (PHI) is changed.
 NUMKX Number of regions where x direction permeability (PERMX) is changed.
 NUMKY Number of regions where y direction permeability (PERMY) is changed.
 NUMKZ Number of regions where z direction permeability (PERMZ) is changed.
 IPCODE = 0 means do not print the modified distributions;
 = 1 means print the modified distributions.
3. **I1, I2, J1, J2, K1, K2, VALPHI**
Omit this record if NUMP = 0.
 I1 Coordinate of first region block in I direction.
 I2 Coordinate of last region block in I direction.
 J1 Coordinate of first region block in J direction.
 J2 Coordinate of last region block in J direction.
 K1 Coordinate of first region block in K direction.
 K2 Coordinate of last region block in K direction.

Code	Value	Meaning
NUMP	< 0	New value of porosity for region (fr).
	> 0	Multiply value of porosity by VALPHI.

NOTE: |NUMP| records must be read where |...| denotes the absolute value.

4. **I1, I2, J1, J2, K1, K2, VALKX**

Omit this record if NUMKX = 0.

- I1 Coordinate of first region block in I direction.
- I2 Coordinate of last region block in I direction.
- J1 Coordinate of first region block in J direction.
- J2 Coordinate of last region block in J direction.
- K1 Coordinate of first region block in K direction.
- K2 Coordinate of last region block in K direction.

Code	Value	Meaning
NUMKX	< 0	New value of x direction permeability for region (md).
	> 0	Multiply value of x direction permeability by VALKX.

NOTE: |NUMKX| records must be read.

5. **I1, I2, J1, J2, K1, K2, VALKY**

Omit this record if NUMKY = 0.

- I1 Coordinate of first region block in I direction.
- I2 Coordinate of last region block in I direction.
- J1 Coordinate of first region block in J direction.
- J2 Coordinate of last region block in J direction.
- K1 Coordinate of first region block in K direction.
- K2 Coordinate of last region block in K direction.

Code	Value	Meaning
NUMKY	< 0	New value of y direction permeability for region (md).

Code	Value	Meaning
	> 0	Multiply value of y direction permeability by VALKY.

NOTE: |NUMKY| records must be read.

6. I1, I2, J1, J2, K1, K2, VALKZ

Omit this record if NUMKZ = 0.

- I1 Coordinate of first region block in I direction.
- I2 Coordinate of last region block in I direction.
- J1 Coordinate of first region block in J direction.
- J2 Coordinate of last region block in J direction.
- K1 Coordinate of first region block in K direction.
- K2 Coordinate of last region block in K direction.

Code	Value	Meaning
NUMKZ	< 0	New value of z direction permeability for region (md).
	> 0	Multiply value of z direction permeability by VALKZ.

NOTE: |NUMKZ| records must be read.

24.3.3 Modifications to Transmissibilities

It is important to keep in mind the directional convention used in specifying transmissibility modifications. For example, in gridblock (I, J, K):

TX(I, J, K) refers to flow across the boundary between blocks I-1 and I,

TY(I, J, K) refers to flow across the boundary between blocks J-1 and J, and

TZ(I, J, K) refers to flow across the boundary between blocks K-1 and K.

1. **Heading** Up to 80 characters.

2. **NUMTX, NUMTY, NUMTZ, ITCODE**

- NUMTX Number of regions where x direction transmissibility (TX) is changed.
- NUMTY Number of regions where y direction transmissibility (TY) is changed.
- NUMTZ Number of regions where z direction transmissibility (TZ) is changed.
- ITCODE = 0 means do not print the modified distributions;
 = 1 means print the modified distributions.

3. **I1, I2, J1, J2, K1, K2, VALTX**

Omit this record if NUMTX = 0.

- I1 Coordinate of first region block in I direction.
- I2 Coordinate of last region block in I direction.
- J1 Coordinate of first region block in J direction.
- J2 Coordinate of last region block in J direction.
- K1 Coordinate of first region block in K direction.
- K2 Coordinate of last region block in K direction.
- VALTX Multiplier of x direction transmissibility for region.
- NOTE:** NUMTX records must be read.

4. **I1, I2, J1, J2, K1, K2, VALTY**

Omit this record if NUMTY = 0.

- I1 Coordinate of first region block in I direction.
- I2 Coordinate of last region block in I direction.
- J1 Coordinate of first region block in J direction.
- J2 Coordinate of last region block in J direction.
- K1 Coordinate of first region block in K direction.
- K2 Coordinate of last region block in K direction.
- VALTY Multiplier of y direction transmissibility for region.
- NOTE:** NUMTY records must be read.

5. **I1, I2, J1, J2, K1, K2, VALTZ**
Omit this record if NUMTZ = 0.
- I1 Coordinate of first region block in I direction.
 I2 Coordinate of last region block in I direction.
 J1 Coordinate of first region block in J direction.
 J2 Coordinate of last region block in J direction.
 K1 Coordinate of first region block in K direction.
 K2 Coordinate of last region block in K direction.
 VALTZ Multiplier of z direction transmissibility for region.
- NOTE:** NUMTZ records must be read.

24.4 Rock and PVT Regions

1. **Heading** Up to 80 characters.
2. **NROCK, NPVT**
 NROCK Number of distinct Rock regions. A separate set of saturation-dependent data must be entered for each Rock region.
 NPVT Number of distinct PVT regions. A separate set of pressure-dependent data must be entered for each PVT region.
3. **Heading** Up to 80 characters.
Omit this record if NROCK = 1.
4. **NUMROK**
Omit this record if NROCK = 1.
 NUMROK = 0 Enter Rock region value for each block.
 NUMROK > 0 Number of regions where the Rock region default value of 1 is changed.
5. **IVAL**
Omit this record if NROCK = 1 or NUMROK > 0.
 IVAL Array of Rock region values. Read II × JJ × KK values.

6. **I1, I2, J1, J2, K1, K2, IVAL**

Omit this record if NROCK = 1 or NUMROK = 0.

I1 Coordinate of first region block in I direction.

I2 Coordinate of last region block in I direction.

J1 Coordinate of first region block in J direction.

J2 Coordinate of last region block in J direction.

K1 Coordinate of first region block in K direction.

K2 Coordinate of last region block in K direction.

IVAL Number of the saturation-dependent data set to be assigned to this Rock region and $IVAL \leq NROCK$.

NOTE: NUMROK records must be read.

7. **Heading** Up to 80 characters.

Omit this record if NPVT = 1.

8. **NUMPVT**

Omit this record if NPVT = 1.

NUMPVT = 0 Enter PVT region value for each block.

NUMPVT > 0 Number of regions where the PVT region default value of 1 is changed.

9. **IVAL**

Omit this record if NPVT = 1 or NUMPVT > 0.

IVAL Array of PVT region values. Read $II \times JJ \times KK$ values.

10. **I1, I2, J1, J2, K1, K2, IVAL**

Omit this record if NPVT = 1 or NUMPVT = 0.

I1 Coordinate of first region block in I direction.

I2 Coordinate of last region block in I direction.

J1 Coordinate of first region block in J direction.

J2 Coordinate of last region block in J direction.

K1 Coordinate of first region block in K direction.

K2 Coordinate of last region block in K direction.

IVAL Number of the pressure-dependent data set to be assigned to this PVT region and $IVAL \leq NPVT$.
NOTE: NUMPVT records must be read.

24.5 Relative Permeability and Capillary Pressure Tables

The following saturation-dependent data should be entered a total of NROCK times – one set of records for each Rock region defined in Section 24.4.

1. **Heading** Up to 80 characters.

2. **SAT1 KROW1 KRW1 KRG1 KROG1 PCOW1 PCGO1**

 :

SATn KROWn KRWn KRGn KROGn PCOWn PCGOn

SAT Phase saturation (fr). Set SAT1 = 0.0 and SATn = 1.0.

KROW Oil relative permeability for oil-water system (fr).

KRW Water relative permeability for oil-water system (fr).

KRG Gas relative permeability for gas-oil system (fr).

KROG Oil relative permeability for gas-oil system (fr).

PCOW Oil/water capillary pressure (psi).

PCGO Gas/oil capillary pressure (psi).

NOTE: SAT refers to the saturation of each particular phase. For example, in a data line following SAT = 0.2 we have

KROW Oil relative permeability at 20% oil saturation.

KRW Water relative permeability at 20% water saturation.

KRG Gas relative permeability at 20% gas saturation.

KROG Oil relative permeability at 20% liquid (water plus oil) saturation.

PCOW Oil/water capillary pressure at 20% water saturation.

PCGO Gas/oil capillary pressure at 20% gas saturation.

NOTE: KROG is used only when a three-phase oil relative permeability is calculated (ITHREE = 1 in Record 4 below).

Capillary pressures are defined as $PCOW = P_o - P_w$ and $PCGO = P_g - P_o$ where P_o , P_w , and P_g are the oil-, water-, and gas-phase pressures, respectively.

- 3. **Heading** Up to 80 characters.
- 4. **ITHREE, SWR**
 ITHREE Code specifying desired relative permeability option.
 SWR Irreducible water saturation (fraction).

Code	Value	Meaning
ITHREE	0	Oil relative permeability read from the relative permeability data for the two-phase water/oil system.
	1	Oil relative permeability calculated from Stone's three-phase relative permeability model

Repeat records 1 to 4 a total of NROCK times.

24.6 Fluid PVT Tables

The following pressure-dependent data should be entered a total of NPVT times – one set of records for each PVT region defined in Section 24.4.

- 1. **Heading** Up to 80 characters.
- 2. **PBO, PBODAT, PBGRAD**
 PBO Initial bubble point pressure (psia).
 PBODAT Depth at which PBO applies (ft).
 PBGRAD Constant bubble point pressure gradient (psia/ft).
- 3. **Heading** Up to 80 characters.

4. **VSLOPE, BSLOPE, RSLOPE, PMAX, IREPRS**
- VSLOPE** Slope of the oil viscosity versus pressure curve for undersaturated oil, i.e. for pressures above PBO. The slope ($\Delta\mu_o/\Delta P_o$) should be in cp/psia.
- BSLOPE** Slope of the oil formation volume factor versus pressure curve for undersaturated oil. The slope ($\Delta B_o/\Delta P_o$) should be in RB/STB/psia and should be negative or zero. BSLOPE is not the same as the undersaturated oil compressibility.
- RSLOPE** Slope of the solution gas-oil ratio versus pressure curve. The slope ($\Delta R_{so}/\Delta P_o$) should be in SCF/STB/psia and is normally zero.
- PMAX** Maximum pressure entry for all PVT tables (psia).
- IREPRS** = 0; constant bubble point pressure.
= 1; estimate variable bubble point pressure.

5. **Heading** Up to 80 characters; oil table follows.

6. **P1 MUO1 BO1 RSO1**
:
PMAX MUO(PMAX) BO(PMAX) RSO(PMAX)
P Pressure (psia). Pressures must be in ascending order from P1 (normally 14.7 psia) to PMAX. The last table entry must be PMAX.
- MUO** Saturated oil viscosity (cp).
- BO** Saturated oil formation volume factor (RB/STB).
- RSO** Saturated oil solution gas-oil ratio (SCF/STB).
- NOTE:** Oil properties must be entered as saturated oil over the entire pressure range.

7. **Heading** Up to 80 characters; water table follows.

8. **P1 MUW1 BW1 RSW1**
:

- P** **PMAX** **MUW(PMAX)** **BW(PMAX)** **RSW(PMAX)**
 Pressure (psia). Pressures must be in ascending order from P1 (normally 14.7 psia) to PMAX. The last table entry must be PMAX.
- MUW** Water viscosity (cp).
- BW** Water formation volume factor (RB/STB).
- RSW** Water solution gas-water ratio (SCF/STB).

NOTE: It is usually assumed in black oil simulations that the solubility of gas in water can be neglected. In this case, set RSW = 0.0 for all pressures.

9. **Heading** Up to 80 characters.

10. **KGCOR**

Code	Value	Meaning
KGCOR	0	Read gas and rock properties table
	1	Activate gas correlation option and read rock compressibility vs pressure table

11. **Heading** Up to 80 characters; gas table follows.

12. **P1** **MUG1** **BG1** **PSI1** **CR1**

PMAX **MUG(PMAX)** **BG(PMAX)** **PSI(PMAX)** **CR(PMAX)**

Omit this record if KGCOR = 1

- P** Pressure (psia). Pressures must be in ascending order from P1 (normally 14.7 psia) to PMAX. The last table entry must be PMAX.
- MUG** Gas viscosity (cp).
- BG** Gas formation volume factor (RCF/SCF).
- PSI** Gas pseudo-pressure (psia²/cp).
- CR** Rock compressibility (1/psia).

13. **KODEA, MPGT, TEM, SPG**

Omit this record if KGCOR = 0.

- KODEA Gas composition option (see Chapter 28.3).
- MPGT Number of gas PVT table entries ($1 < \text{MPGT} \leq 25$).
- TEM Reservoir temperature ($^{\circ}\text{F}$).
- SPG Gas specific gravity (air = 1.0).

14. **FRCI**

Omit this record if KGCOR = 0.

FRCI Component mole fraction of gas. Read 12 entries in the following order.

FRCI(I)	Component I	FRCI(I)	Component I
1	H ₂ S	7	iC ₄
2	CO ₂	8	nC ₄
3	N ₂	9	iC ₅
4	C ₁	10	nC ₅
5	C ₂	11	C ₆
6	C ₃	12	C ₇₊

15. **PRSCI, TEMCI, RMWTI**

Omit this record if KGCOR = 0 or if KODEA \neq 4.

- PRSCI Critical pressure (psia).
- TEMCI Critical temperature ($^{\circ}\text{R}$).
- RMWTI Molecular weight.

16. **Heading** Up to 80 characters; rock compressibility table follows.

Omit this record if KGCOR = 0.

17. **P1 CR1**

:

PMAX CR(PMAX)

Omit this record if KGCOR = 0.

Option	Code	Meaning
Constant rock compressibility	PMAX	Maximum table pressure (psia) from record 4.
NOTE: Enter 1 record.	CR	Rock compressibility (1/psia)
Pressure-dependent rock compressibility	P	Pressure (psia). Pressures must be in ascending order from P1 (normally 14.7 psia) to PMAX. The last table entry must be PMAX.
NOTE: Enter MPGT records.	CR	Rock compressibility (1/psia)

18. **Heading** Up to 80 characters.

19. **RHOSCO, RHOSCW, RHOSCG**

RHOSCO Stock tank oil density (lb/cu ft).

RHOSCW Stock tank water density (lb/cu ft).

RHOSCG Gas density at standard conditions (lb/cu ft).

NOTE: At standard conditions (14.7 psia and 60 degrees F for oilfield units) pure water has a density of 62.4 lb/cu ft and air has a density of 0.0765 lb/cu ft.

Repeat records 1 through 19 a total of NPVT times.

24.7 Pressure and Saturation Initialization

1. **Heading** Up to 80 characters.

2. **KPI, KSI, PDATUM, GRAD**

KPI Pressure initialization code.

KSI Saturation initialization code.

PDATUM Depth to pressure datum (ft).

GRAD Estimated pressure gradient (psia/ft) for pressure corrections to PDATUM. If GRAD = 0, a map of pressures corrected to PDATUM will not be printed. If GRAD ≠ 0, a map of

pressures corrected to PDATUM will be printed using pressure gradient GRAD.

Code	Value	Meaning
KPI	0	Read II × JJ × KK pressures (one for each block).
	1	Equilibrium pressure initialization. Requires pressures and depths at the OWC and GOC.
KSI	0	Read II × JJ × KK oil saturations (one for each block) and II × JJ × KK water saturations. Gas saturations will be calculated by the program.
	1	Gravity segregated oil, water and gas saturation initialization.

NOTE: Options KPI and KSI may be used to prepare a restart data file.

3. **PO**

Omit this record if KPI = 1.

PO Oil-phase pressure (psia). Read II × JJ × KK values.

4. **PWOC, WOC, PGOC, GOC**

Omit this record if KPI = 0.

PWOC Pressure at the water-oil contact (psia).

WOC Depth to the water-oil contact (ft below datum).

PGOC Pressure at the gas-oil contact (psia).

GOC Depth to the gas-oil contact (ft below datum).

NOTE: Repeat this record a total of NROCK times – one record for each Rock region.

5. **SO**

Omit this record if KSI = 1.

SO Oil saturation array (fraction). Read II × JJ × KK values.

6. **SW**

Omit this record if KSI = 1.

SW Water saturation array (fraction). Read II × JJ × KK values.

7. **SOI, SGI, SOR**

Omit this record if KSI = 0.

SOI Initial oil saturation for the oil-water zone to be assigned to all blocks in the rock region (fraction). Initial water saturation in the oil-water zone is $1 - \text{SOI}$.

SGI Initial gas saturation for the gas-water zone to be assigned to all blocks in the rock region (fraction). Initial water saturation in the gas-water zone is $1 - \text{SGI}$.

SOR Irreducible oil saturation to be assigned to all blocks in the rock region (fraction). If $\text{SOR} > 0$, calculated S_o will be set to 0 when $S_o < \text{SOR}$. Water and gas saturations are then renormalized.

NOTE: Repeat this record a total of **NROCK** times – one record for each Rock region.

24.8 Run Control Parameters

1. **Heading** Up to 80 characters.

2. **NMAX, FACT1, FACT2, TMAX, WORMAX, GORMAX, PAMIN, PAMAX**
 - NMAX** Maximum number of timesteps allowed.
 - FACT1** Factor for increasing timestep size using automatic timestep control. $\text{FACT1} = 1.0$ for fixed timestep size. A common value for **FACT1** is 1.25.
 - FACT2** Factor for decreasing timestep size using automatic timestep control. $\text{FACT2} = 1.0$ for fixed timestep size. A common value for **FACT2** is 0.5.
 - TMAX** Maximum elapsed time to be simulated (days); the run will be terminated when the time exceeds **TMAX**.
 - WORMAX** Maximum allowed water-oil ratio for a producing oil well (STB/STB); $\text{WORMAX} \geq 0$.

GORMAX Maximum allowed gas-oil ratio for a producing oil well (SCF/STB); $GORMAX \geq 0$.

PAMIN Minimum field average pressure (psia); the run will be terminated when the pore volume weighted average reservoir pressure $<$ PAMIN.

PAMAX Maximum field average pressure (psia); the run will be terminated when the pore volume weighted average reservoir pressure $>$ PAMAX.

NOTE: PAMIN and PAMAX should be within the range of pressures covered by the fluid PVT tables discussed in Chapter 24.6.

3. **WOROCK**

Omit this record if $WORMAX \neq 0$.

WOROCK Maximum WOR allowed in the corresponding Rock region.

NOTE: If a well is completed in more than one Rock region, the largest maximum WOR which applies to the Rock regions penetrated by the well will be used as the WOR control for that well. Enter NROCK records – one for each Rock region.

4. **GOROCK**

Omit this record if $GORMAX \neq 0$.

GOROCK Maximum GOR allowed in the corresponding Rock region.

NOTE: If a well is completed in more than one Rock region, the largest maximum GOR which applies to the Rock regions penetrated by the well will be used as the GOR control for that well. Enter NROCK records – one for each Rock region.

24.9 Solution Method Specification

1. **Heading** Up to 80 characters.

2. **KSOL, MITR, OMEGA, TOL, TOL1, DSMAX, DPMAX, NUMDIS**
- KSOL** Solution method code.
- MITR** Maximum number of LSOR iterations per timestep. A typical value is 100.
- OMEGA** Initial LSOR acceleration parameter. Values of OMEGA should be between 1.0 and 2.0. A typical initial value is 1.5.
- TOL** Maximum acceptable pressure change for convergence of LSOR iterations (psia). A typical value is 0.1.
- TOL1** Parameter for determining when to change OMEGA. A typical value is 0.001. If TOL1 = 0.0, the initial value of OMEGA will be used for the entire run.
- DSMAX** Maximum saturation change allowed per timestep (fraction). The timestep size will be reduced by FACT2 if the saturation change of a phase in any gridblock exceeds DSMAX during a timestep. A typical value for DSMAX is 0.05.
- DPMAX** Maximum pressure change allowed per timestep (psia). The timestep size will be reduced by FACT2 if the pressure change in any gridblock exceeds DPMAX during a timestep. A typical value of DPMAX is 100 psia.
- NUMDIS** Code for controlling numerical dispersion

Code	Value	Meaning
KSOL	1	1D Tridiagonal Algorithm. Use with 1D problems and 0D (tank) problems, i.e. when II = JJ = KK = 1.
	2	Direct solution band algorithm. Use with 2D and 3D problems.
	3	LSORX - Iterative matrix solver with direct solver in x direction.
	4	LSORY - Iterative matrix solver with direct solver in y direction.
	5	LSORZ - Iterative matrix solver with direct solver in z direction.

Code	Value	Meaning
NUMDIS	1	Single-point upstream weighting.
	2	Two-point upstream weighting.

24.10 Analytic Aquifer Models

1. **Heading** Up to 80 characters.
2. **IAQOPT**
IAQOPT Analytic aquifer model code.

Code	Value	Meaning
IAQOPT	0	No analytic aquifer model
	1	Pot aquifer model (small and bounded aquifer)
	2	Steady-state aquifer model (constant aquifer pressure)
	3	Carter-Tracy aquifer model: $Re/Rw = 1.5$
	4	Carter-Tracy aquifer model: $Re/Rw = 2.0$
	5	Carter-Tracy aquifer model: $Re/Rw = 3.0$
	6	Carter-Tracy aquifer model: $Re/Rw = 4.0$
	7	Carter-Tracy aquifer model: $Re/Rw = 5.0$
	8	Carter-Tracy aquifer model: $Re/Rw = 6.0$
	9	Carter-Tracy aquifer model: $Re/Rw = 8.0$
	10	Carter-Tracy aquifer model: $Re/Rw = 10.0$
11	Carter-Tracy aquifer model: $Re/Rw = \infty$	

NOTE: Only one aquifer model option (IAQOPT) may be selected for a given run. Different aquifer influx strengths may be specified for a given aquifer.

3. **NAQEN**
Omit this record if IAQOPT \neq 1.

NAQEN Number of regions containing a pot aquifer.

4. **I1, I2, J1, J2, K1, K2, POT**

Omit this record if IAQOPT ≠ 1.

I1 Coordinate of first region block in I direction.

I2 Coordinate of last region block in I direction.

J1 Coordinate of first region block in J direction.

J2 Coordinate of last region block in J direction.

K1 Coordinate of first region block in K direction.

K2 Coordinate of last region block in K direction.

POT Pot aquifer strength (SCF/psia).

NOTE: NAQEN records must be read.

5. **NAQEN**

Omit this record if IAQOPT ≠ 2.

NAQEN Number of regions containing a steady-state aquifer.

6. **I1, I2, J1, J2, K1, K2, SSAQ**

Omit this record if IAQOPT ≠ 2.

I1 Coordinate of first region block in I direction.

I2 Coordinate of last region block in I direction.

J1 Coordinate of first region block in J direction.

J2 Coordinate of last region block in J direction.

K1 Coordinate of first region block in K direction.

K2 Coordinate of last region block in K direction.

SSAQ Steady-state aquifer strength (SCF/day/psia).

NOTE: NAQEN records must be read.

7. **NAQREG**

Omit this record if IAQOPT < 3.

NAQREG Number of Carter-Tracy aquifer parameter regions.

8. **AQCR, AQCW, AQMUW, AQK, AQPFI, AQH, AQS, AQRE**

Omit this record if IAQOPT < 3.

AQCR	Aquifer rock compressibility (1/psia).
AQCW	Aquifer water compressibility (1/psia).
AQMUW	Aquifer water viscosity (cp).
AQK	Aquifer permeability (md).
AQPFI	Aquifer porosity (fraction).
AQH	Aquifer net thickness (ft).
AQS	Aquifer to reservoir boundary interface (fraction). A value of 0 implies there is no boundary (hence no influx); a value of 1 implies that the aquifer surrounds the gridblock.
AQRE	External aquifer radius (ft).

9. **NAQEN**

Omit this record if IAQOPT < 3.

NAQEN	Number of regions containing a Carter-Tracy aquifer.
-------	--

10. **I1, I2, J1, J2, K1, K2**

Omit this record if IAQOPT < 3.

I1	Coordinate of first region block in I direction.
I2	Coordinate of last region block in I direction.
J1	Coordinate of first region block in J direction.
J2	Coordinate of last region block in J direction.
K1	Coordinate of first region block in K direction.
K2	Coordinate of last region block in K direction.

NOTE: NAQEN lines must be read. Repeat records 8 through 10 a total of NAQREG times.

Chapter 25

Recurrent Data

Recurrent data records are read periodically during the course of the simulation run. These data include the location and specification of wells in the model, changes in well completions and field operations over time, a schedule of well rate and/or pressure performance over time, timestep control information for advancing the simulation through time, and controls on the type and frequency of printout information provided by the simulator.

1. **Major Heading** Up to 80 characters.

NOTE: This record signifies the start of the recurrent data section.

25.1 Timestep and Output Control

Timestep and output control records must be read to start the simulation.

1. **Heading** Up to 80 characters.
2. **IWLCNG, IOMETH**
IWLCNG Controls reading of well information.
IOMETH Controls program output and well scheduling.

Code	Value	Meaning
IWLCNG	0	Do not read well information
	1	Read well information
IOMETH	≥ 1	Number of elapsed time values to be read on record 3. The program will print results to output files at these elapsed times and allow you to change well characteristics after the last elapsed time entered during this recurrent data period.

3. **FTIO**

FTIO Array containing total elapsed times at which output will occur (days). Up to 50 monotonically increasing values may be entered. The first entry must be greater than 0 and greater than the last entry of any previously completed recurrent data periods.

NOTE: When the elapsed time of a run equals an FTIO value, the well and basic summary reports will be printed. Maps will also be printed according to the instructions given in record 4.

4. **IPMAP, ISOMAP, ISWMAP, ISGMAP, IPBMAP, IAQMAP**

- IPMAP Control code for printing pressure array.
- ISOMAP Control code for printing oil saturation array.
- ISWMAP Control code for printing water saturation array.
- ISGMAP Control code for printing gas saturation array.
- IPBMAP Control code for printing bubble point pressure array.
- IAQMAP Control code for printing aquifer influx array.

Code Value	Meaning
0	Do not print the array
1	Print the array
2	Print the array and a digital contour plot

5. **IVPMAP, IZMAP, IRCMAP, IVSMAP, IVRMAP**

- IVPMAP Control code for printing seismic compressional velocity (Vp) array.
- IZMAP Control code for printing seismic acoustic impedance array.
- IRCMAP Control code for printing seismic reflection coefficient array.
- IVSMAP Control code for printing seismic shear velocity (Vs) array.
- IVRMAP Control code for printing seismic velocity ratio Vp/Vs array.

Code Value	Meaning
0	Do not print the array
1	Print the array
2	Print the array and a digital contour plot

NOTE: If IVRMAP > 0, time-dependent arrays will be appended to file WTEMP.ARR.

6. **DT, DTMIN, DTMAX**

- DT Starting timestep size (days). DT may vary between DTMIN and DTMAX when automatic timestep control is invoked.
- DTMIN Minimum timestep size allowed (days). A typical value is 1 day.
- DTMAX Maximum timestep size allowed (days). A typical value is 30 days.

25.2 Well Information

Omit this section if IWLCNG = 0.

1. **Heading** Up to 80 characters.
2. **NWELLN, NWELLO**
 - NWELLN Number of new wells for which complete well information is entered.
 - NWELLO Number of previously defined wells for which new rates and/or rate controls are entered.

3. **Heading** Up to 80 characters.
Omit this record if $NWELLN = 0$.

4. **WELLID**
Omit this record if $NWELLN = 0$.

WELLID Well name with up to five characters.

5. **IDWELL, KONECT**
Omit this record if $NWELLN = 0$.

IDWELL Well identification number. Each well should have a unique IDWELL number. If two or more wells have the same IDWELL number, the characteristics of the last well entered will be used.

KONECT Total number of gridblocks connected to well IDWELL.

6. **I, J, K, PID, PWF**
Omit this record if $NWELLN = 0$.

I x coordinate of gridblock containing well.

J y coordinate of gridblock containing well.

K z coordinate of gridblock containing well.

PID Layer flow index for gridblock.

PWF Flowing bottomhole pressure for block (psia). This value is used only if KIP is negative for this well.

NOTE: KONECT records must be read. PID for a vertical well can be estimated as

$$PID = 0.00708 \frac{Kh}{\ln\left(\frac{r_o}{r_w}\right) + S}$$

where

$$r_o \approx 0.14(DX^2 + DY^2)^{1/2}$$

and

- K = layer absolute permeability (md)
- h = layer thickness (ft)
- DX = x direction gridblock length (ft)
- DY = y direction gridblock length (ft)
- r_w = wellbore radius (ft)
- r_o = equivalent well block radius (ft)
- S = layer skin factor

Deviated (slanted) and horizontal wells may be represented by calculating an appropriate PID and specifying gridblock locations that model the expected well trajectory. For example, a horizontal well that is aligned in the x direction will have constant J and K indices, and index I will vary if there is more than one connection.

To shut in a connection, set that connection PID to 0. To shut in a well, set all of its connection PID values to zero.

7. **KIP, QO, QW, QG, QT**

Omit this record if $NWELLN = 0$.

KIP Code for specifying well operating characteristics.

Rate Controlled Well ($KIP > 0$):

- QO** Oil rate (STB/D).
- QW** Water rate (STB/D).
- QG** Gas rate (MSCF/D).
- QT** Total fluid voidage rate (RB/D).

NOTE: The total fluid rate given by QT is the oil plus water plus gas production for the well or the total reservoir voidage rate at reservoir conditions. For multi-layer systems, QT is a target rate.

BHP Controlled Production Well with Optional Rate Constraints ($KIP = -1$):

- QO** Minimum oil production rate required (STB/D).
- QW** Maximum oil production rate allowed (STB/D).
- QG** 0.0
- QT** Maximum liquid withdrawal rate allowed (STB/D).

NOTE: Rate constraints are not activated if the corresponding rate equals zero.

BHP Controlled Water Injection Well with Optional Rate Constraints

(KIP = -2):

QO 0.0

QW Maximum water injection rate allowed (STB/D).

QG 0.0

QT 0.0

NOTE: QW should be a negative number or zero. The rate constraint is not activated if QW = 0.

BHP Controlled Gas Injection Well with Optional Rate Constraints (KIP

= -3):

QO 0.0

QW 0.0

QG Maximum gas injection rate allowed (MSCF/D).

QT 0.0

NOTE: QG should be a negative number or zero. The rate constraint is not activated if QG = 0.

Gas Production Well (KIP = -4):

QO 0.0

QW 0.0

QG 0.0

QT 0.0

NOTE: Sign conventions for rates:

Negative rates indicate fluid injection.

Positive rates indicate fluid production.

Summary of KIP Values	
Code	Meaning
3	Gas well – injection rate specified
2	Water well – injection rate specified

Summary of KIP Values	
Code	Meaning
1	Production well – rate specified ♦ Oil rate specified: $QO > 0, QW = QG = QT = 0$ ♦ Water rate specified: $QW > 0, QO = QG = QT = 0$ ♦ Gas rate specified: $QG > 0, QO = QW = QT = 0$ ♦ Total rate specified: $QT > 0, QO = QW = QG = 0$
-1	Oil and/or water production well – PI and FBHP control
-2	Water well – PI and FBHP control
-3	Gas injection well – PI and FBHP control
-4	Gas production well – LIT representation

8. **ALIT, BLIT**

Omit this record if $NWELLN = 0$ or $KIP \neq -4$.

ALIT “a” coefficient of LIT gas well analysis.

BLIT “b” coefficient of LIT gas well analysis.

NOTE: Records 4 through 8 should be repeated $NWELLN$ times.

9. **Heading** Up to 80 characters.

Omit this record if $NWELLO = 0$.

10. **WELLID**

Omit this record if $NWELLO = 0$.

WELLID Well name with up to five characters.

11. **IDWELL, KONECT**

Omit this record if $NWELLO = 0$.

IDWELL Well identification number. Each well should have a unique IDWELL number. If two or more wells have the same

IDWELL number, the characteristics of the last well entered will be used.

KONECT Total number of gridblocks connected to well IDWELL.

12. **I, J, K, PID, PWF**

Omit this record if NWELLO = 0.

I x coordinate of gridblock containing well.

J y coordinate of gridblock containing well.

K z coordinate of gridblock containing well.

PID Layer flow index for gridblock.

PWF Flowing bottomhole pressure for block (psia). This value is used only if KIP is negative for this well.

NOTE: KONECT records must be read.

13. **KIP, QO, QW, QG, QT**

Omit this record if NWELLO = 0.

KIP Code for specifying well operating characteristics. See record 6 for a description of the KIP options.

14. **ALIT, BLIT**

Omit this record if NWELLO = 0 or KIP ≠ -4.

ALIT "a" coefficient of LIT gas well analysis.

BLIT "b" coefficient of LIT gas well analysis.

NOTE: Records 10 through 14 should be repeated NWELLO times.

Chapter 26

Program Output Evaluation

You are given the option at the start of a WINB4D run to direct output to either the screen or to a set of files. It is often worthwhile to send output to the screen when first building and debugging a data set. WINB4D will abort at the point in the data set where it encounters improperly entered data. For evaluating run results, it is preferable to send output to files. In this case, a one line timestep summary is sent to the screen each timestep so that you can monitor the progress of a run. All output files are in text format.

A run may be aborted by typing <Cntrl> C. You may then choose to terminate the job.

26.1 Initialization Data

The reservoir flow simulator WINB4D outputs the following initialization data in text file WTEMP.ARR:

- ◆ Gridblock sizes
- ◆ Node midpoint elevations
- ◆ Porosity distributions
- ◆ Permeability distributions
- ◆ Rock and PVT region distributions
- ◆ Relative permeability and capillary pressure tables
- ◆ PVT tables
- ◆ Slopes calculated from PVT data
- ◆ Timestep control parameters

- ◆ Analytic aquifer model selection
- ◆ Initial fluid volumes-in-place
- ◆ Initial pressure and saturation arrays
- ◆ Initial seismic velocities array
- ◆ Initial acoustic impedance array
- ◆ Initial well information

Other output can be obtained at your request. For example, if a modification option is invoked, you may print out the altered array. It is worthwhile to do this as a check on the input changes.

26.2 Recurrent Data

All output files are text files so that they may be read by a variety of commercially available spreadsheets. WINB4D output may then be manipulated using spreadsheet options. This is especially useful for making plots or displaying array data. Different output files are defined so that simulator output file sizes are more manageable. The output files are designed to contain information that is logically connected, e.g. well data in one file, reservoir property distributions in another file. The different output files are described below.

26.2.1 Timestep Summary File – WTEMP.TSS

A one line timestep summary is automatically printed out as a record of the progress of the run. This summary provides you with necessary information for evaluating the stability of the solution as a function of time. Significant oscillations in GOR or WOR, or large material balance errors are indicative of simulation problems and should be corrected. A smaller timestep through the difficult period is often sufficient to correct IMPES instabilities.

26.2.2 Run Summary And Plot File – WTEMP.PLT

The run summary file contains a concise summary of total field production and injection and fieldwide aquifer influx. The WOR and GOR are ratios of total

producing fluid rates. Consequently these ratios are comparable to observed fieldwide ratios.

The output quantities include: cumulative production of oil, water and gas; cumulative injection of water and gas; pore volume weighted average pressure; aquifer influx rate and cumulative aquifer influx; and fieldwide WOR and GOR values. These quantities are output as functions of time and timestep number.

26.2.3 Well Report File – WTEMP.WEL

Rates and cumulative production/injection data for each layer of each well are summarized in the well report at times you specify. Field totals are also included.

26.2.4 Distribution Arrays File – WTEMP.ROF

You may output the following arrays whenever desired: pressure, saturations, bubble point pressure, cumulative aquifer influx, compressional velocity, acoustic impedance, and seismic reflection coefficient. Output arrays may be used as input pressure and saturation distributions for restarting a run.

It is usually unnecessary to print all of the arrays. To avoid excessive output and correspondingly large output files, you should be judicious in deciding which arrays are printed. In addition to arrays, you may wish to output digital contour plots.

Digital contour plots provide a simplified picture of the physical parameter distribution. The plot subroutine finds the minimum (AMIN) and maximum (AMAX) values of the array APLOT. A new array AOUT is constructed using the normalized parameter values given by

$$AV = (APLOT(I, J, K) - AMIN)/ADIF$$

where $ADIF = AMAX - AMIN > 0.001$. The values of AOUT are defined as follows:

AOUT	Meaning (± 0.05)
–	AV < 0.05
1	AV = 0.10
2	AV = 0.20

AOUT	Meaning (± 0.05)
3	AV = 0.30
4	AV = 0.40
5	AV = 0.50
6	AV = 0.60
7	AV = 0.70
8	AV = 0.80
9	AV = 0.90
T	AV > 0.95

Digital contour plots highlight changes in parameter values and let you visually monitor such items as saturation fronts, movements of pressure pulses, and changes in acoustic impedance. The output array AOUT is printed so that it can be used for drawing a rough contour plot.

This page intentionally left blank

Part V
Technical Supplements

This page intentionally left blank

Chapter 27

Simulator Formulation

WINB4D is an implicit pressure-explicit saturation finite difference simulator. It can simulate isothermal Darcy flow in up to three dimensions. Reservoir fluids are described by up to three fluid phases (oil, gas, and water), whose physical properties are functions of pressure only. Solution gas may be present in both the oil and water phases.

27.1 Equations

The black oil simulator mass conservation equations for the oil-, water- and gas-phases are derived in Chapter 4. They can be succinctly written in vector notation as follows:

Oil

$$-\nabla \cdot \frac{\vec{v}_o}{B_o} - \frac{q_o}{\rho_{osc}} = \frac{\partial}{\partial t} \left(\phi \frac{S_o}{B_o} \right) \quad (27.1)$$

Water

$$-\nabla \cdot \frac{\vec{v}_w}{B_w} - \frac{q_w}{\rho_{wsc}} = \frac{\partial}{\partial t} \left(\phi \frac{S_w}{B_w} \right) \quad (27.2)$$

Gas

$$\begin{aligned}
 & -\nabla \cdot \left[\frac{\bar{v}_g}{B_g} + \frac{R_{so}}{B_o} \bar{v}_o + \frac{R_{sw}}{B_w} \bar{v}_w \right] - \frac{q_g}{\rho_{gsc}} \\
 & = \frac{\partial}{\partial t} \left\{ \Phi \left[\frac{S_g}{B_g} + \frac{R_{so}}{B_o} S_o + \frac{R_{sw}}{B_w} S_w \right] \right\}
 \end{aligned}
 \tag{27.3}$$

Letting the subscript i denote o (oil), w (water), and g (gas), the symbols in Eqs. (27.1) to (27.3) have the following definitions:

- B_i = formation volume factor of phase i
- q_i = mass flow rate per unit reservoir volume of phase i
- R_{so} = solubility of gas in oil
- R_{sw} = solubility of gas in water
- S_i = saturation of phase i
- v_i = Darcy's velocity of phase i
- ρ_{isc} = density of phase i at standard conditions
- Φ = porosity

Three additional equations – called auxiliary equations – are employed when solving the preceding fluid flow equations. They are the saturation constraint

$$S_o + S_w + S_g = 1 \tag{27.4}$$

and the capillary pressure relationships

$$P_{cow}(S_w) = P_o - P_w \tag{27.5}$$

$$P_{cgo}(S_g) = P_g - P_o \tag{27.6}$$

where P_i is the pressure of phase i , P_{cow} is the oil-water capillary pressure, and P_{cgo} is the gas-oil capillary pressure.

Darcy's velocity for phase i is

$$\bar{v}_i = -K \frac{k_{ri}}{\mu_i} \nabla \Phi_i \tag{27.7}$$

where K is a permeability tensor that is usually assumed to be diagonalized along its principal axes, k_{ri} is relative permeability and μ_i is viscosity of phase i . The phase potentials Φ_i are given as functions of depth z by

$$\Phi_o = P_o - \frac{\rho_o z}{144}, \quad \Phi_w = P_o - P_{cow} - \frac{\rho_w z}{144}, \quad \Phi_g = P_o + P_{cgo} - \frac{\rho_g z}{144} \quad (27.8)$$

Phase densities are calculated from input PVT data as

$$\rho_o = \frac{1}{B_o} [\rho_{osc} + R_{so} \rho_{gsc}], \quad \rho_w = \frac{1}{B_w} [\rho_{osc} + R_{sw} \rho_{gsc}], \quad \rho_g = \frac{\rho_{gsc}}{B_g} \quad (27.9)$$

Expressions for rock and phase compressibilities are

$$c_r = \frac{1}{\phi} \frac{\partial \phi}{\partial P_o}, \quad c_g = -\frac{1}{B_g} \frac{\partial B_g}{\partial P_o},$$

$$c_o = -\left[\frac{1}{B_o} \frac{\partial B_o}{\partial P_o} - \frac{B_g}{B_o} \frac{\partial R_{so}}{\partial P_o} \right], \quad c_w = -\left[\frac{1}{B_w} \frac{\partial B_w}{\partial P_o} - \frac{B_g}{B_w} \frac{\partial R_{sw}}{\partial P_o} \right] \quad (27.10)$$

These equations are discretized and solved numerically in WINB4D. The procedure for solving these equations is outlined in Chapter 32.

27.2 Coordinate Orientation

The WINB4D reservoir model assumes a block-centered grid with the axes aligned using the right-handed coordinate system illustrated in Figure 27-1.

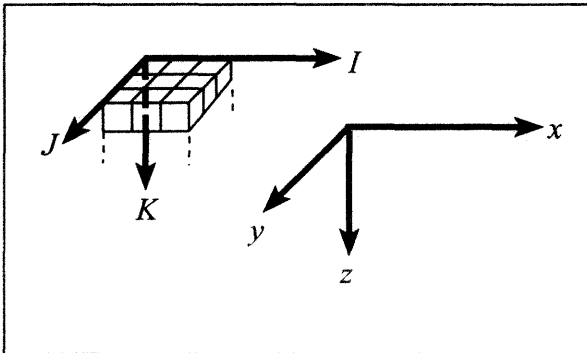


Figure 27-1. Coordinate system.

The top layer ($K = 1$) is shown. The second layer ($K = 2$) is below the $K = 1$ layer, and so on. The top of each gridblock may vary from one block to another. This allows the model to perform calculations using grid representations of reservoirs ranging from flat layer cake models to dipping structures such as anticlines and domes. An anticlinal structure is shown in Figure 27-2.

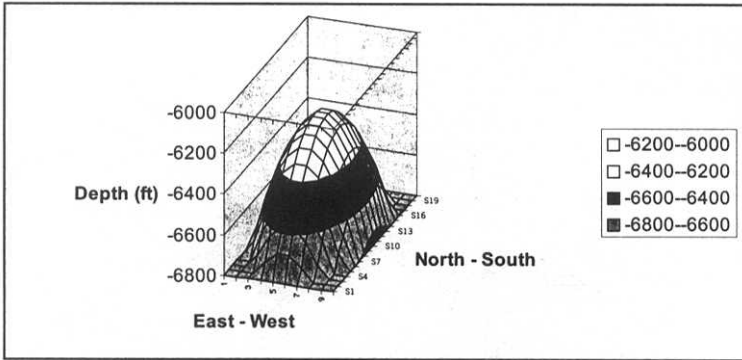


Figure 27-2. Depth to top of anticlinal structure.

27.3 Petrophysical Model

Monitoring changes in the seismic characteristics of a reservoir as the reservoir is produced is the basis of time-lapse (4D) seismic monitoring [Anderson, et al., 1995; He, et al., 1996; Fanchi, et al. 1999]. Changes in seismic characteristics are determined in WINB4D by calculating seismic attributes as a function of time. The seismic attributes calculated in WINB4D are defined below.

Compressional and Shear Velocities

Seismic compressional velocity and shear velocity are calculated from the expressions [Schön, 1996; McQuillin, et al., 1984]:

$$V_P = \sqrt{\frac{K^* + \frac{4\mu^*}{3}}{\rho_B}} \tag{27.11}$$

and

$$V_S = \sqrt{\frac{\mu^*}{\rho_B}} \quad (27.12)$$

where

- V_P = compressional velocity
- V_S = shear velocity
- K^* = effective bulk modulus
- μ^* = effective shear modulus
- ρ_B = effective bulk density = $(1-\phi)\rho_{ma} + \phi\rho_f$
- ρ_{ma} = density of grains (solid matrix material)
- ρ_f = fluid density = $\rho_o S_o + \rho_w S_w + \rho_g S_g$
- ϕ = porosity

Gassman [1951] derived an expression for K^* from the theory of elasticity of porous media [Schön, 1996; McQuillin, et al., 1984]:

$$K^* = K_B + \frac{\left[1 - \frac{K_B}{K_G}\right]^2}{\frac{\phi}{K_F} + \frac{1-\phi}{K_G} - \frac{K_B}{K_G^2}} \quad (27.13)$$

where

- K_B = bulk modulus of empty reservoir, that is, dry rock or porous matrix material
- K_G = bulk modulus of grains (solid matrix material)
- K_F = bulk modulus of fluid = $1/c_f$
- c_f = fluid compressibility = $c_o S_o + c_w S_w + c_g S_g$

The grain modulus K_G equals the bulk modulus K_B when porosity equals zero. Figure 27-3 shows that bulk modulus and shear modulus are linear functions of porosity for quartz sandstone [Murphy, et al., 1993] for porosity less than 35%.

The WINB4D user must enter data that cannot be calculated from traditional black oil simulator input data. In particular, the user must enter K_B , K_G , μ^* , and ρ_{ma} . The references give values that may be used if the data are not

available from well logs such as shear wave logging tools or laboratory measurements of parameters such as acoustic velocities or the dry frame Poisson's ratio.

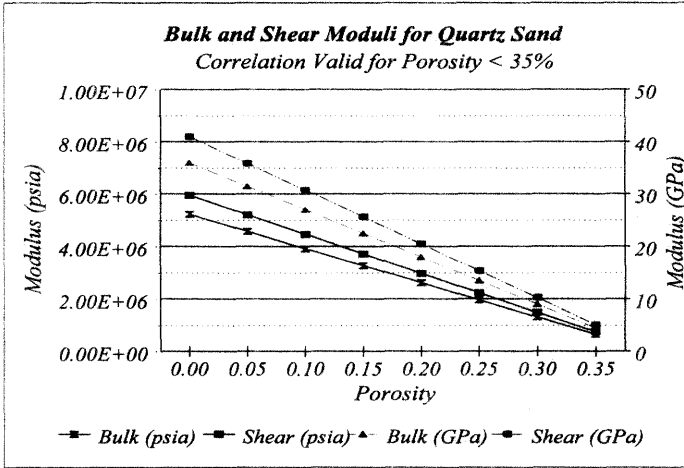


Figure 27-3. Correlation for bulk and shear moduli.

Acoustic Impedance and Reflection Coefficients

Acoustic impedance Z is defined as

$$Z = \rho_B V_P \tag{27.14}$$

The reflection coefficient RC at the interface between two layers with acoustic impedances Z_1 and Z_2 is given by

$$RC = \frac{Z_2 - Z_1}{Z_2 + Z_1} \tag{27.15}$$

The transmission coefficient TC is

$$TC = \frac{2Z_1}{Z_2 + Z_1} \tag{27.16}$$

or $TC = 1 - RC$.

27.4 Material Balance

Material balance is one measure of the numerical stability and accuracy of a simulator. The WINB4D material balance calculation at time t is given by

$$\text{Material Balance} = \frac{\text{FIP}}{\text{OFIP} - \text{Prod} + \text{Inj}} \quad (27.17)$$

where

- FIP = fluid in place at time t
- OFIP = original fluid in place
- Prod = cumulative fluid produced at time t
- Inj = cumulative fluid injected at time t

Based on this definition, material balance should equal one in an idealized calculation. Actual simulator material balance may not equal one.

Material balance error reported by WINB4D is calculated using the formula

$$\% \text{ Error} = \left\{ \frac{\text{FIP}}{\text{OFIP} - \text{Prod} + \text{Inj}} - 1 \right\} \times 100\% \quad (27.18)$$

Material balance can be a sensitive indicator of error. Material balance error is greatest in WINB4D when a gridblock undergoes a phase transition, for example, when a gridblock passes from single phase oil to two-phase oil and gas during a timestep.

Material balance errors can be corrected by adding or subtracting enough fluid to reestablish an exact material balance [Nolen and Berry, 1973; Spillette, et al., 1986]. This material balance correction technique is equivalent to adding a source/sink term to the mass conservation equations for every gridblock. These terms are not included in the WINB4D formulation. The exercises in Parts I and II show that the uncorrected formulation can be used with good accuracy in many practical situations.

Chapter 28

Rock and Fluid Models

The interaction between reservoir rock and *in situ* fluids is modeled with relative permeability and capillary pressure data. This chapter defines the three-phase oil relative permeability model used in WINB4D and its use in transmissibility calculations. It then presents additional details of the fluid property model after reviewing a few commonly used thermodynamic terms.

28.1 Three-Phase Relative Permeability

Relative permeability curves are some of the most critical data in the simulator because relative permeability curves can have a significant impact on simulator performance. Relative permeability curves are an important part of the algorithm that is used to model the interaction between reservoir rock and fluids. Unfortunately, relative permeability curves are often among the missing or poorer quality data.

Relative permeability data are affected significantly by alterations in wettability conditions in the core. Ideally, the relative permeability data should be measured in the laboratory under the same conditions of wettability that exist in the reservoir. One method of approaching this ideal is to use preserved, “native state” core samples.

“Native state” core samples are cores that are drilled using crude oil or a special coring fluid designed to minimize wettability alterations. The cores are sealed at the well site to minimize exposure to oxygen or drying and then preserved until ready to undergo flow testing in the laboratory. However, this

process is expensive and most relative permeability data are obtained on restored state cores in the laboratory.

In principle, three-phase relative permeability should be used when oil, water, and gas are flowing simultaneously. As a practical matter, the difficulty of accurately measuring three-phase relative permeabilities often makes their use meaningless. It is often sufficient to work with the two-phase relative permeability curves only.

Despite their shortcomings, it may be of interest to perform a simulation using a set of three-phase relative permeability curves. For this case, WINB4D contains an option for computing a three-phase oil relative permeability curve using water-oil and gas-oil relative permeability curves. As with most calculations of this type, we assume:

- a. The water relative permeability curve (k_{rw}) obtained for a water-oil system depends only on water saturation, and
- b. The gas relative permeability curve (k_{rg}) obtained for a gas-oil system depends only on gas saturation.

The validity of these assumptions depends on such factors as wettability and degree of consolidation. Given the above assumptions, k_{rw} and k_{rg} for water-oil and gas-oil systems, respectively, are also valid for a water-gas-oil system. The three-phase oil relative permeability k_{ro3} is calculated as

$$k_{ro3} = \frac{(k_{row} + k_{rw})(k_{rog} + k_{rg})}{k_{row}^*} - (k_{rw} + k_{rg}) \quad (28.1)$$

where

- k_{row} = oil relative permeability for water-oil system
- k_{rog} = oil relative permeability for gas-oil system
- k_{row}^* = oil relative permeability for water-oil system evaluated at the oil saturation corresponding to irreducible water saturation

Equation (28.1) is based on the work by Stone [1973], and it corresponds to Model II of Dietrich and Bondor [1976]. For a discussion of alternative models of three-phase oil relative permeability, see Blunt [1999].

When the three-phase calculation is activated, the user must be sure the input water-oil and gas-oil relative permeability curves are realistic. For example,

if we write irreducible water saturation as S_{wr} , the relative permeability constraint $k_{row} (1 - S_{wr}) = k_{rog} (S_o + S_w = 1.0)$ must be satisfied since $S_g = 0$ in both cases.

28.2 Transmissibility

The simulator offers no-flow boundary conditions, which lets you stop flow between specified gridblocks in chosen directions. The no-flow conditions are implemented by setting transmissibilities at boundary interfaces to zero. The Transmissibility Modifications section in Chapter 24.3.3 describes the directional conventions for transmissibility in the model.

Flow between neighboring blocks is treated as a series application of Darcy's law. A transmissibility term at the interface between two blocks is defined using the product of average values of relative permeability $k_{r\ell}$ of phase ℓ , absolute permeability K of each block at the interface, and cross-sectional area A_c of each block at the interface, divided by the product of viscosity μ_ℓ and formation volume factor B_ℓ of the phase in each block. The transmissibility to each phase is determined using a harmonic average calculation of the product of absolute permeability and cross-sectional area at the interface between neighboring blocks. An arithmetic average of phase viscosities and formation volume factors is used. The average relative permeability is determined using an upstream weighted averaging technique. The resulting Darcy transmissibility is

$$A'_{\ell,i-1/2} \equiv \frac{4k_{r\ell(\text{upstream})}}{(\mu_{\ell,i-1} + \mu_{\ell,i})(B_{\ell,i-1} + B_{\ell,i})} \left[\frac{2(KA_c)_{i-1}(KA_c)_i}{\Delta x_{i-1}(KA_c)_i + \Delta x_i(KA_c)_{i-1}} \right]$$

and the finite difference transmissibility $A_{\ell,i-1/2}$ for phase ℓ between block $i-1$ and block i used in the simulator is

$$A_{\ell,i-1/2} = A'_{\ell,i-1/2} \frac{\Delta x_i}{\left(\frac{\Delta x' + \Delta x''}{2} \right)}$$

where the j, k indices are suppressed and the spatial differences are

$$\Delta x' = x_i - x_{i-1}, \quad \Delta x'' = x_{i+1} - x_i$$

Similar definitions of transmissibility apply in all three coordinate directions.

28.3 Terminology and General Comments

Some of the fluid property terms that are most frequently used in black oil simulation are defined here.

Density

Density is defined as the mass of a substance divided by the volume it occupies. The density of a fluid depends on the pressure, temperature, and composition of the fluid.

Composition

The composition of a fluid depends on whether the fluid consists of a pure component, such as water or methane, or is a mixture. For example, petroleum and *in situ* water are mixtures. Petroleum is a mixture of hydrocarbon compounds, and *in situ* water usually contains dissolved solids, such as salt, and may contain dissolved gases such as methane and carbon dioxide. The composition of a fluid is a list of the components contained in the fluid.

The relative amount of each component in a mixture is defined as the concentration of the component. Concentration may be expressed in a variety of units, such as volume fraction, weight fraction, or molar fraction. It is important to know the units associated with the composition. If the concentration units are not clearly expressed in a fluid report, they should be determined before use in calculations. It is common to find composition expressed in mole fractions. The symbols $\{x_i, y_i, z_i\}$ are often used to denote the mole fraction of component i in the oil phase, gas phase, and wellstream respectively.

The equilibrium K value is a measure of the amount of component i in the gas phase relative to the oil phase. It is defined as the ratio

$$K_i = y_i/x_i$$

If component i exists entirely in the oil phase, then y_i is 0 and K_i is 0. Conversely, if component i exists entirely in the gas phase, then x_i is 0 and K_i approaches infinity. Thus, the equilibrium K value for component i may range from 0 to

infinity. It should be noted that these concepts apply to both hydrocarbon components and any other distinct molecular species, such as carbon dioxide and nitrogen.

Pressure

The average pressure on a surface is the total normal force applied to the surface divided by the area of the surface. The normal force is the component of the force that is acting perpendicularly to the surface.

Consider a fluid in the pore space of a rock. The pressure at any point in the fluid is equal in all directions. If the fluid is at rest in the pore space, the pressure is equal at all points in the fluid at the same depth. Pascal's law says that pressure applied to an enclosed fluid will be transmitted without a change in magnitude to every point of the fluid and to the walls of the container.

Temperature

Temperature is a measure of the average kinetic energy of a system. Several temperature scales are in use. The most commonly used temperature scales are the Fahrenheit and Celsius scales. The relationship between these scales is

$$T_C = \frac{5}{9}(T_F - 32)$$

where T_C and T_F are temperatures in degrees Celsius and degrees Fahrenheit respectively.

Applications of equations of state require the use of absolute temperature scales. Absolute temperature may be expressed in terms of degrees Kelvin or degrees Rankine. The Kelvin scale is related to the Celsius scale by

$$T_K = T_C + 273$$

where T_K is temperature in degrees Kelvin. The Rankine scale is related to the Fahrenheit scale by

$$T_R = T_F + 460$$

where T_R is temperature in degrees Rankine.

Intensive and Extensive Properties

Pressure, temperature, and density are examples of intensive properties. An intensive property is a fluid property which is independent of the amount of material. For example, if a cubic cell of gas in an equilibrium state is divided into two halves by a vertical partition, the gas in each half of the cell should have the same pressure and temperature. By contrast, the mass and volume in each half will be one half of the original mass and volume. Mass and volume are examples of extensive properties. An extensive property is a property that depends on the amount of material.

Compressibility

If the surface of an object is subjected to an external force, the resulting pressure applied to the object can change the volume of the object. Compressibility is a measure of the volume change resulting from the applied pressure. The fractional volume change $\Delta V/V$ of an object may be estimated from

$$\frac{\Delta V}{V} \approx -c \Delta P$$

where c is the compressibility of the object, ΔP is the pressure applied, and the minus sign implies that an increase (decrease) in applied pressure results in a decrease (increase) in the volume of the object.

Formation Volume Factor

Formation volume factor is defined as the volume occupied by a fluid phase at reservoir conditions divided by the volume occupied by the fluid phase at standard conditions. The fluid phase volume may change substantially as pressure and temperature change.

Ordinarily the volume of a fluid with constant composition will increase as the applied pressure and temperature decrease. The behavior of petroleum is made more complex because it is a mixture and can experience a change in composition as temperature and pressure change. For example, a barrel of oil at reservoir conditions (relatively high pressure and temperature) will shrink as the barrel is brought to the surface (relatively low pressure and temperature). The shrinkage is associated with the release of solution gas as the pressure and

temperature of the oil decline from reservoir to surface conditions. Consequently, measurements of the change in volume as a function of pressure are desirable, especially for the oil phase.

The determination of gas formation volume factor provides an interesting contrast to the determination of oil formation volume factor. Gas formation volume factor is often determined with reasonable accuracy using the real gas equation of state $PV = ZnRT$ where n is the number of moles of gas in volume V at pressure P and temperature T . The gas compressibility factor Z equals one if the gas is an ideal gas. For real gases, $Z \neq 1$ for most pressures and temperatures.

Specific Gravity

Specific gravity is defined as the density of a fluid divided by a reference density. Gas specific gravity is calculated at standard conditions using air density as the reference density. The specific gravity of gas is defined by

$$\gamma_g = \frac{M_a(\text{gas})}{M_a(\text{air})} \approx \frac{M_a(\text{gas})}{29}$$

where M_a is apparent molecular weight. Apparent molecular weight is calculated as the mole fraction weighted average

$$M_a = \sum_{i=1}^{N_c} y_i M_i$$

where N_c is the number of components, y_i is the mole fraction of component i , and M_i is the molecular weight of component i .

Oil specific gravity is calculated at standard conditions using fresh water density as the reference density. Oils are often characterized by specifying their API gravity, which is related to oil specific gravity γ_o at standard temperature and pressure by the equation

$$API = \frac{141.5}{\gamma_o} - 131.5$$

Heavy oils are oils with a relatively large γ_o and a relatively low API gravity. Heavy oils typically do not contain much gas in solution. By contrast, light oils

have a relatively small γ_g and a correspondingly large API gravity. Light oils typically contain a large amount of gas in solution.

Gas-Liquid Ratio

The gas-liquid ratio is defined as the volume of gas divided by the volume of liquid, usually oil or water. The gas volume and liquid volume should be expressed at the same temperature and pressure.

Viscosity

The coefficient of viscosity is a measure of resistance to flow of the fluid. In general, gases have a lower viscosity than liquids. The inverse of viscosity is called fluidity [McCain, 1990]. Thus, a fluid with a large viscosity has a low fluidity.

The relationship between viscosity and shear rate defines the rheology of the fluid. If fluid viscosity is independent of flow rate, the fluid is referred to as a Newtonian fluid. If fluid viscosity depends on flow rate, the fluid is considered a non-Newtonian fluid.

Two types of viscosity may be specified: dynamic viscosity μ and kinematic viscosity ν . They are related by the expression $\mu = \rho\nu$ where ρ is the density of the fluid. Dynamic viscosity μ is used in Darcy's law to calculate the rate of fluid movement fluid flow in porous media. Typically, the unit of dynamic viscosity μ is centipoise. If fluid density ρ has the unit of g/cc, then kinematic viscosity ν has the unit of centistoke. Thus, 1 centistoke equals 1 centipoise divided by 1 g/cc.

Reservoir fluid properties (PVT data) include fluid viscosities, densities, formation volume factors, gas solubilities, etc. These data are usually obtained by laboratory analyses applied to fluid samples taken from the reservoir. They are sketched in Chapter 13.

Differential to Flash Conversion

Laboratory reservoir fluid analyses generally provide data from both a differential liberation experiment and a flash experiment approximating field separator conditions. The differential and flash liberation data can be signifi-

cantly different for some oils. The actual behavior of the production process is some combination of the differential and flash processes. The assumption normally made in preparing PVT data for use in a black oil simulator is that the differential liberation data represent the process occurring in the reservoir and the flash data represent production to stock tank conditions. Thus, for use in the simulator, the differential liberation data should be corrected to flash values at field separation conditions. This procedure is described in the literature [Amyx, et al., 1960; Moses, 1986] and is summarized below.

Physical property data obtained from a testing laboratory for a black oil system will generally be a differential liberation study coupled with a separator study. Most reservoir simulators require that these data be converted to flash form so that the effects of the surface separation facility are included. Conversion of the data is restricted to oil formation volume factor and solution gas-oil ratio data. If the separator B_o and R_{s_o} are known, the conversion equations are:

$$B_o(p) = B_{od}(p) \frac{B_{ofbp}}{B_{odbp}}$$

and

$$R_{s_o}(p) = R_{sofbp} - (R_{sodbp} - R_{sod}(p)) \frac{B_{ofbp}}{B_{odbp}}$$

where subscripts are defined as:

- d = differential liberation data
- f = flash data
- bp = bubble point

28.4 Extrapolating Saturated Curves

Guidelines for extrapolating PVT data to pressures above the measured saturation pressure are presented below.

1. The B_g versus pressure curve is strongly non-linear and an extrapolation of this curve to small B_g values at high pressures can result in errors. For

most natural gases, the relationship $1/B_g$ versus pressure will be very nearly linear, especially at moderate to high pressures. Plotting $1/B_g$ versus pressure and extrapolating to PMAX should provide more realistic values of B_g at higher pressures. Interpolating B_g using $1/B_g$ versus pressure substantially improves material balance.

2. Once the B_g versus P curve is fixed, R_{so} versus P and B_o versus P curves must be extrapolated so as to avoid a negative oil compressibility being calculated over any pressure increment. To ensure that negative oil compressibilities will not be calculated by the program, the following test should be used. For any pressure increment P_1 to P_2 , where $P_2 > P_1$, the following relationship should hold:

$$0 \leq - (B_{o2} - B_{o1}) + \frac{B_{g2}(R_{so2} - R_{so1})}{5.615} \quad (28.1)$$

where the units of B_o , B_g , and R_{so} are RB/STB, RCF/SCF, and SCF/STB, respectively. Note that this test applies only to the saturated oil PVT data.

3. The above concepts also apply to the water PVT data. However, for most simulations, it can be assumed that $R_{sw} = 0.0$, thus $-\Delta B_w/B_w \Delta P$ approximates water compressibility.

28.5 Gas PVT Correlation Option

Basic Gas Properties

Following Govier [1975], real gas Z -factors are computed using the Dranchuk, et al. [1974] representation of the Standing-Katz Z -factor charts [1942]. This representation employs the Benedict-Webb-Rubin [1940] eight-parameter equation of state to express the Z -factor as a function of pseudo-critical temperature T_r and pseudo-critical pressure P_r , thus

$$Z = Z(P_r, T_r) \quad (28.2)$$

Once Z is known, the gas formation volume factor is easily determined for a given temperature and pressure using the real gas law.

The isothermal gas compressibility c_g is obtained from Eq. (28.2) as

$$c_g = \frac{1}{P_c} \left[\frac{1}{P_r} - \frac{1}{Z} \left(\frac{\partial Z}{\partial P_r} \right)_{T_r} \right] \tag{28.3}$$

where P_c is the critical pressure (psia).

Real gas viscosities are computed using the method described in Govier [1975]. This method is a computerized version of the Carr, Kobayashi, and Burrows [1954] hydrocarbon gas viscosity determination procedure.

Pseudo-Pressure Calculations

Pseudo-pressures are defined by

$$\psi(P) = 2 \int_{P_o}^P \frac{P'}{\mu_g Z} dP' \tag{28.4}$$

where

- P' = dummy integration variable with pressure units (psia)
- P_o = reference pressure = 14.7 psia
- P = specified pressure (psia)
- μ_g = gas viscosity (cp)
- Z = gas compressibility factor

The pseudo-pressure $\psi(P)$ is often written as $m(P)$. Since μ_g and Z depend on P' , evaluation of Eq. (28.4) is accomplished by numerical integration using the trapezoidal rule and a user-specified pressure increment $\Delta P' \approx dP'$.

Gas Property Description

Four different gas property descriptions may be specified. Their descriptions and control parameter (KODEA) values follow:

KODEA	GAS DESCRIPTION
1	Sweet gas: input 12 component mole fractions as 0. 0. 0. 1. 0. 0. 0. 0. 0. 0. 0. 0.

KODEA	GAS DESCRIPTION
2	Sour gas: input 12 component mole fractions in the order y_1 y_2 y_3 y_4 0. 0. 0. 0. 0. 0. 0. 0. 0. 0. 0. 0. where y_1 = mole fraction of H ₂ S, y_2 = mole fraction of CO ₂ y_3 = mole fraction of N ₂ , and $y_4 = 1 - (y_1 + y_2 + y_3)$.
3	Sweet or sour gas with the following 12 component mole fractions read in the following order: H ₂ S, CO ₂ , N ₂ , C ₁ , C ₂ , C ₃ , iC ₄ , nC ₄ , iC ₅ , nC ₅ , C ₆ , C ₇₊ . The sum of the mole fractions should equal one.
4	Same as KODEA = 3 but also read critical pressure, critical temperature, and molecular weight of C ₇₊ .

Correlation Range Limits

The following range limits apply to correlations used in calculating gas Z-factors, compressibilities and viscosities:

$$1.05 < \frac{T}{T_c} < 3.0$$

$$0.01 < \frac{P}{P_c} < 15.0$$

$$0.55 < SPG < 1.5$$

$$40 < T < 400$$

where

T_c = pseudo-critical temperature (°R)

P_c = pseudo-critical pressure (psia)

T = temperature (°R)

P = pressure (psia)

SPG = gas specific gravity

No values of T , P , or SPG should be used that exceed the above correlation ranges. If the range limit is exceeded, a fatal error will occur.

Chapter 29

Initialization

It is important when making cross-section or 3D runs that the pressures in the model are correctly initialized. If not, phase potential differences due to gravity terms could cause fluid migration even though no wells are active. Consequently, a simple pressure initialization algorithm is used in WINB4D. It is reviewed below along with an option to correct pressures to a user-specified datum and an option to initialize saturations using gravity segregation.

29.1 Pressure Initialization

Consider a gridblock that may have a gas-oil contact and a water-oil contact as in Figure 29-1.

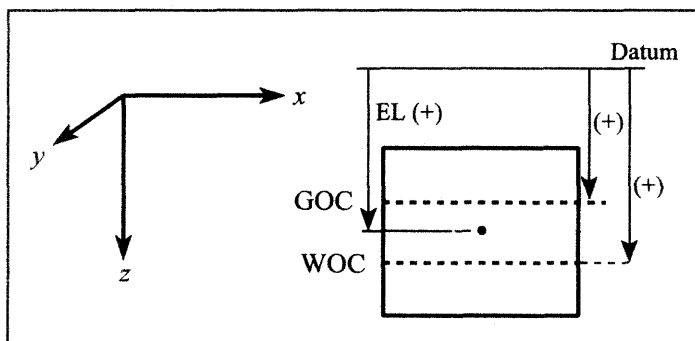


Figure 29-1. Depths for pressure initialization algorithm.

We assume the pressure in the gridblock at model location (i, j, k) is dominated by the density of the phase at the block midpoint and that there are

no transition zones between different phases initially. The pressure and depth at the gas-oil contact are PGOC and GOC, respectively. Similarly, for the water-oil contact we have PWOC and WOC.

The initial pressure assigned to the gridblock in Figure 29-1 is determined by the depth of the node (midpoint) relative to the respective contact elevations.

Let us define the depth of the block midpoint from datum as EL_{ijk} . With this definition, the pressure in the block is given by the following algorithm:

- a. If $EL_{ijk} < GOC$ then

$$\rho_g = \rho_{gsc}/B_g \text{ and } P_{ijk} = PGOC + \rho_g (EL_{ijk} - GOC)/144$$

- b. If $EL_{ijk} > WOC$ then

$$\rho_w = (\rho_{wsc} + R_{sw} \cdot \rho_{gsc})/B_w \text{ and}$$

$$P_{ijk} = PWOC + \rho_w (EL_{ijk} - GOC)/144$$

- c. If $GOC \leq EL_{ijk} \leq WOC$ then

$$\rho_o = (\rho_{osc} + R_{so} \cdot \rho_{gsc})/B_o \text{ and}$$

$$P_{ijk} = PWOC + \rho_o (EL_{ijk} - GOC)/144$$

The above algorithm should be reasonable for systems with initial transition zones that are small relative to the total thickness of the formation.

Pressure Corrected to Datum

Pressure $P(I, J, K)$ of gridblock I, J, K with mid-point elevation $EL(I, J, K)$ may be corrected to a datum depth $PDATUM$ by specifying a pressure gradient $GRAD$. The pressure at datum is given by $PDAT(I, J, K) = P(I, J, K) + (PDATUM - EL(I, J, K)) * GRAD$.

29.2 Gravity-Segregated Saturation Initialization

A simple model of a gravity-segregated saturation distribution is calculated when $KSI = 1$. For depths increasing downward, we calculate elevations and thicknesses using the geometry shown in Figure 29-1 as follows:

$$\begin{aligned} \text{Block BOT} &= EL + 0.5 * DZ \\ \text{Block THICK} &= DZ \end{aligned}$$

Block TOP = BOT - THICK

Water zone thickness

WTHICK = BOT - WOC

Gas zone thickness

GTHICK = GOC - TOP

The user must specify the initial oil saturation (SOI) for an oil-water system and the initial gas saturation (SGI) for a water-gas system. Given the initial saturations SOI and SGI, the following algorithm is applied [Fanchi, 1986].

Case 1	GOC _____ TOP _____ BOT _____ WOC _____	$S_g = 0$ $S_o = SOI$ $S_w = 1 - SOI$	
Case 2	TOP _____ } f_g GOC _____ } WOC _____ } f_w BOT _____ }	$f_g = \frac{GTHICK}{THICK}$ $f_w = \frac{WTHICK}{THICK}$ $S_g = f_g * SGI$ $S_o = (1 - f_g - f_w) * SOI$ $S_w = 1 - S_o - S_g$	If $S_o < S_{or}$, then $S_o = 0$ $S_g = \frac{f_g * SGI}{(f_g + f_w)}$ $S_w = 1 - S_g$
Case 3	TOP _____ GOC _____ } f BOT _____ } WOC _____ }	$f = 1 - \frac{GTHICK}{THICK}$ $S_o = 1 - SOI * f$ $S_g = (1 - f) * SGI$ $S_w = 1 - S_o - S_g$	If $S_o < S_{or}$, then $S_o = 0$ $S_w = 1 - SGI$ $S_g = SGI$
Case 4	GOC _____ TOP _____ } f WOC _____ } BOT _____ }	$f = 1 - \frac{WTHICK}{THICK}$ $S_g = 0$ $S_w = 1 - SOI * f$ $S_o = SOI * f$	If $S_o < S_{or}$, then $S_o = 0$ $S_w = 1$

Case 5	TOP _____ BOT _____ GOC _____ WOC _____	$S_o = 0$ $S_w = 1 - SGI$ $S_g = SGI$	
Case 6	GOC _____ WOC _____ TOP _____ BOT _____	$S_o = S_g = 0$ $S_w = 1$	

Water saturation is calculated as $S_w = 1 - S_o - S_g$ in all cases. Cases 2 through 4 require the user to enter residual oil saturation S_{or} .

29.3 Aquifer Models

A reservoir-aquifer system can be modeled using small gridblocks to define the reservoir and increasingly larger gridblocks to define the aquifer. This approach has the advantage of providing a numerically uniform analysis of the reservoir-aquifer system, but it has the disadvantage of requiring more computer storage and computing time because additional gridblocks are used to model the aquifer. A more time- and cost-effective means of representing an aquifer is to represent aquifer influx with an analytic model. Three models are available as options in WINB4D.

Pot Aquifer

Aquifer influx is calculated assuming the aquifer is both small and bounded. The pot aquifer influx rate q_{wp} is dependent on the pressure change over a timestep for a specified gridblock:

$$q_{wp} = - \left[\text{POT} \frac{(P^n - P^{n+1})}{\Delta t} \right]; \text{POT} \geq 0 \quad (29.1)$$

where $P^n, \Delta t^n$ are gridblock pressure and timestep at the present time level n ; $P^{n+1}, \Delta t^{n+1}$ are gridblock pressure and timestep at the future time level $n + 1$;

and POT is the pot aquifer coefficient. The minus sign preceding the bracketed term indicates water is entering the block when $P^n > P^{n+1}$.

Steady-State Aquifer

The steady-state aquifer model is based on Schilthuis’s assumption that the water influx rate q_{wss} is proportional to the pressure difference between the aquifer and the hydrocarbon reservoir. It is further assumed that the aquifer is sufficiently large that it experiences no net pressure change throughout the producing life of the reservoir. With these assumptions, WINB4D computes steady-state aquifer influx into a specified gridblock as

$$q_{wss} = -[SSAQ (P^0 - P^{n+1})]; SSAQ \geq 0 \tag{29.2}$$

where P^{n+1} is the gridblock pressure at the future time level $n + 1$; P^0 is the initial gridblock pressure; and SSAQ is the proportionality constant. The minus sign preceding the bracketed term indicates water is entering the block when we have the inequality $P^0 > P^{n+1}$.

Carter-Tracy Aquifer

The Carter-Tracy [1960] modification of the Hurst-van Everdingen [1949] unsteady-state aquifer influx calculation is available in WINB4D. The Carter-Tracy aquifer influx rate q_{wct} for a specified gridblock is

$$q_{wct} = -[A - B(P^{n+1} - P^n)] \tag{29.3}$$

where P^n, P^{n+1} are gridblock pressures at time levels n and $n + 1$, respectively. The coefficients A and B are given by

$$A = K_t \left[\frac{\beta(P^0 - P^n) - W_e^n P_{td}'^{n+1}}{DENOM} \right] \tag{29.4}$$

with

$$B = K_t \frac{\beta}{DENOM} \tag{29.5}$$

$$DENOM = P_{iD}^{n+1} - t_D^n P_{iD}'^{n+1} \tag{29.6}$$

$$P'_{tD}{}^{n+1} = \left[\frac{dP_{tD}}{dt_D} \right]^{n+1} \quad (29.7)$$

$$K_t = 0.00633 \frac{k}{(\phi \mu c r_e^2)} = \text{AQPAR 1} \quad (29.8)$$

$$\beta = 2\pi \phi h c r_e^2 s = \text{AQPAR 2} \quad (29.9)$$

and

$$c = c_r + c_w \quad (29.10)$$

The quantities t_D and P_{tD} are dimensionless time and pressure, respectively, with

$$t_D = K_t t$$

and P_{tD} is the Carter-Tracy influence function for the constant terminal rate case. The functions P_{tD} and P'_{tD} are numerically represented by regression equations [Fanchi, 1985]. All remaining parameters are defined as follows:

- c_r = rock compressibility (psi⁻¹)
- c_w = water compressibility (psi⁻¹)
- h = aquifer net thickness (ft)
- k = aquifer permeability (md)
- r_e = external aquifer radius (ft)
- r_w = external reservoir radius (ft)
- s = $\theta/360^\circ$ where θ is the angle of aquifer/reservoir interface
- W_e^n = cumulative water influx at time level n , SCF
- μ = aquifer water viscosity (cp)
- ϕ = aquifer porosity

Chapter 30

Well Models

The well models contained in WINB4D are described in this chapter. User-specified parameters for controlling these well models are defined in Chapter 25.

30.1 Rate Constraint Representation

Case 1: Oil Production Rate Q_o Specified

In this representation, rates may be specified for injectors or producers. We assume the well may be completed in a total of K connections, and the production rates for each connection k for a specified oil rate are:

Oil

$$Q_{ok} = Q_o \frac{\left[(\text{PID}) \frac{\lambda_o}{B_o} \right]_k}{\sum_{k=1}^K \left[(\text{PID}) \frac{\lambda_o}{B_o} \right]_k} \quad (30.1)$$

Water

$$Q_{wk} = Q_{ok} \left(\frac{\lambda_w/B_w}{\lambda_o/B_o} \right)_k \quad (30.2)$$

Gas

$$Q_{gk} = \left(\frac{\lambda_g/B_g}{\lambda_o/B_o} \right)_k Q_{ok} + (R_{so})_k Q_{ok} + (R_{sw})_k Q_{wk} \quad (30.3)$$

where λ_ℓ is the fluid mobility of phase ℓ and PID is the well productivity index. For a more detailed discussion of PID, see Chapter 31. Notice that a PID may be specified for each connection. This capability lets the WINB4D user take into account permeability contrast.

Case 2: Water Production Rate Q_w Specified

Assuming the well may be completed in K connections, the production rates of connection k for a specified water rate are:

Water

$$Q_{wk} = Q_w \frac{[(PID)\lambda_w/B_w]_k}{\sum_{k=1}^K [(PID)\lambda_w/B_w]_k} \quad (30.4)$$

Oil

$$Q_{ok} = Q_{wk} \left(\frac{\lambda_o/B_o}{\lambda_w/B_w} \right)_k \quad (30.5)$$

Gas

$$Q_{gk} = \left(\frac{\lambda_g/B_g}{\lambda_w/B_w} \right)_k Q_{wk} + (R_{sw})_k Q_{wk} + (R_{so})_k Q_{ok} \quad (30.6)$$

Case 3: Gas Production Rate Q_g Specified

Assuming the well may be completed in K connections, the production rates of connection k for a specified gas rate are:

Gas

$$Q_{gk} = Q_g \frac{[(PID)\lambda_g/B_g]_k}{\sum_{k=1}^K [(PID)\lambda_g/B_g]_k} \quad (30.7)$$

Oil

$$Q_{ok} = Q_{gk} \left(\frac{\lambda_o/B_o}{\lambda_g/B_g} \right)_k \quad (30.8)$$

Water

$$Q_{wk} = Q_{gk} \left(\frac{\lambda_w/B_w}{\lambda_g/B_g} \right)_k \quad (30.9)$$

Solution gas in both oil and water is neglected when a gas production rate is specified. This is a reasonable assumption for wells producing primarily free gas.

Case 4: Total Production Rate Specified

When the total reservoir voidage rate Q_T is specified, we first compute the phase mobility ratio for all connections:

Oil Mobility Ratio

$$\alpha_{oT} = \sum_{k=1}^K \left(\frac{\lambda_o}{\lambda_o + \lambda_w + \lambda_g} \right)_k \quad (30.10)$$

Water Mobility Ratio

$$\alpha_{wT} = \sum_{k=1}^K \left(\frac{\lambda_w}{\lambda_o + \lambda_w + \lambda_g} \right)_k \quad (30.11)$$

Gas Mobility Ratio

$$\alpha_{gT} = \sum_{k=1}^K \left(\frac{\lambda_g}{\lambda_o + \lambda_w + \lambda_g} \right)_k \quad (30.12)$$

We now compute the total oil rate

$$Q_o = \left(\frac{\alpha_{oT}}{\alpha_{oT} + \alpha_{wT} + \alpha_{gT}} \right) \frac{Q_T}{B_o} \quad (30.13)$$

where

$$\bar{B}_o = \frac{1}{K} \sum_{k=1}^K (B_o)_k \quad (30.14)$$

is the average oil formation volume factor for all connections in which the well is completed. Given Eq. (30.13), we simply proceed as in Eqs. (30.1) through (30.3) above.

Case 5: Injection Rate Specified

If the well is a water or gas injector, the user must specify the total water or gas injection rates Q_w or Q_g , respectively, and a well injectivity index (WI) for each connection. The injection rate for each connection is then allocated as follows:

Water Injection Rate

$$Q_{wk} = Q_w \frac{[\text{WI}(\lambda_o + \lambda_w + \lambda_g)]_k}{\sum_{k=1}^K [\text{WI}(\lambda_o + \lambda_w + \lambda_g)]_k} \quad (30.15)$$

Gas Injection Rate

$$Q_{gk} = Q_g \frac{[\text{WI}(\lambda_o + \lambda_w + \lambda_g)]_k}{\sum_{k=1}^K [\text{WI}(\lambda_o + \lambda_w + \lambda_g)]_k} \quad (30.16)$$

It is important to note that allocation of injection fluids is based on total mobilities, and not just injected fluid mobility. This is necessary for the following reason: If an injector is placed in a block where the relative permeability to the injection fluid is zero, then the simulator using injection fluid mobility only would prohibit fluid injection even though a real well would allow fluid injection. A common example would be water injection into a block containing oil and irreducible water. To avoid the unrealistic result of no fluid injection, we assume the total mobility of the block should be used. For most cases, the error of this method will only persist for a few timesteps because, in time, the mobile fluid saturation in the block will be dominated by the injected fluid.

30.2 Explicit Pressure Constraint Representation

Case 1: Oil and/or Water Production Wells

We assume that flowing bottomhole pressures (PWF) and well PIDs are specified for a pressure-constrained well. The oil and water rates in STB/D for connection k are given by

$$Q_{ok} = \left[\text{PID} \frac{\lambda_o}{B_o} \right]_k^n (P^n - \text{PWF})_k \tag{30.17}$$

and

$$Q_{wk} = \left[\text{PID} \frac{\lambda_w}{B_w} \right]_k^n (P^n - \text{PWF})_k \tag{30.18}$$

where the explicit pressure P^n is used. If $P^n < \text{PWF}$, the well is shut in. When $P^n > \text{PWF}$, Q_{ok} and Q_{wk} are calculated and then substituted into Eq. (30.3) to find Q_{gk} .

Case 2: Gas Production Well

The laminar-inertial-turbulent (LIT) method may be used to represent a gas production well. The LIT method entails fitting gas well test data to the equation

$$\Delta \psi = aQ_g + bQ_g^2 = \psi_R - \psi_{wf} \tag{30.19}$$

where

ψ_R = pseudo-pressure corresponding to shut-in pressure P_R (psia²/cp)

ψ_{wf} = pseudo-pressure corresponding to a specified well flowing pressure P_{wf} (psia²/cp)

aQ_g = laminar flow

bQ_g^2 = inertial and turbulent flow

WINB4D employs user specified values of a , b , P_{wf} , and a table of pseudo-pressure versus pressure values to compute total gas well production rate as

$$Q_g = \frac{-a + \sqrt{a^2 + 4b\Delta\Psi}}{2b} \quad (30.20)$$

where Ψ_R is the pseudo-pressure corresponding to the nodal pressure P^n . Rates for each phase in connection k are computed by mobility allocation as shown in Eqs. (30.7) through (30.9).

Case 3: Injection Wells

The injection rate for a water or gas injection well is computed from

$$Q_{pk} = \left[\text{PID} \left(\frac{\lambda_o + \lambda_w + \lambda_g}{B_p} \right) \right]_k^n (P^n - \text{PWF})_k \quad (30.21)$$

where the subscript p denotes water or gas, and $\text{PID} = \text{WI}$. Fluid injection occurs when $P^n < \text{PWF}$. If $P^n > \text{PWF}$, the injection well is shut in. Also note that total mobility is used for the injection well rate calculation. The reason for this was discussed in the first section of this chapter.

30.3 GOR/WOR Constraints

Maximum gas-oil and water-oil ratios (GORMAX, WORMAX respectively) are input by the user and apply to every oil production well. GOR for a well is defined as total gas production divided by total oil production for all active well completion intervals. If GOR for the well exceeds GORMAX, then the completion interval (connection) with the highest GOR will be shut in. If more than one connection has the same maximum GOR, the shallowest connection will be shut in first. The procedure is repeated until GOR is less than GORMAX or until the well is shut in.

The ratio WOR is defined as total water production divided by total oil production for all active well completion intervals. If WOR for the well exceeds WORMAX, then the completion interval (connection) with the highest WOR will be shut in. If more than one connection has the same maximum WOR, the deepest connection will be shut in first. The procedure is repeated until WOR is less than WORMAX or until the well is shut in.

30.4 Fluid Withdrawal Constraints

Fluid withdrawal from explicit pressure controlled production wells can be constrained as follows:

- a. A minimum oil production rate can be specified;
- b. A maximum oil production rate can be specified; and
- c. A maximum liquid (water plus oil) withdrawal rate can be specified.

A positive value of QO for a pressure controlled production well is used as the minimum allowed oil production rate. If the calculated oil production rate drops below the minimum allowed value, the well is shut in.

A positive value of QW for a pressure controlled production well is used as the maximum allowed oil production rate. If the calculated oil production rate exceeds the maximum allowed value, calculated production will be reduced to the allowed value. Production from each connection is proportionally reduced by the ratio of allowed to calculated oil production rates.

A positive value of QT for a pressure controlled production well is used as the maximum allowed liquid withdrawal rate. If the sum of oil and water production exceeds the maximum allowed value, calculated production is reduced to the allowed value. The reduction is made by multiplying production from each connection by the ratio of allowed-to-calculated liquid withdrawal rates. **IMPORTANT:** When used to control total liquid withdrawal, the units of QT are STB/Day.

30.5 Fluid Injection Constraints

Fluid injection into explicit pressure controlled injection wells can be constrained as follows:

- a. A maximum water injection rate can be specified; and
- b. A maximum gas injection rate can be specified.

A negative value of QW for a pressure controlled water injection well is used as the maximum allowed water injection rate. If the calculated water injection rate exceeds the allowed value, calculated water injection will be

reduced to the allowed value. Water injection into each connection is proportionally reduced by the ratio of allowed to calculated water injection rates.

A negative value of QG for a pressure controlled gas injection well is used as the maximum allowed gas injection rate in direct analogy to the water injection rate constraint described previously.

Chapter 31

Well Flow Index (PID)

31.1 Productivity Index

Productivity index (PI) is defined as the ratio of rate Q to pressure drop ΔP , or $PI = Q/\Delta P$, where $\Delta P = P_e - P_w$, P_e = average reservoir pressure, and P_w = wellbore bottomhole pressure BHP. From Darcy's Law for radial oil flow we can write PI as

$$PI = \frac{Q_o}{\Delta P} = \frac{0.00708 K_e h_{net}}{\mu_o B_o [\ln(r_e/r_w) + S]} \quad (31.1)$$

The meaning and units of all terms are given as follows:

- μ_o = oil viscosity (cp)
- B_o = oil FVF (RB/STB)
- r_e = drainage radius (ft)
- r_w = wellbore radius (ft)
- S = skin
- K_e = effective permeability (md) = $k_{ro} K_{abs}$
- k_{ro} = relative permeability to oil
- K_{abs} = absolute permeability (md)
- h_{net} = net thickness (ft)
- Q_o = oil rate (STB/D)

Some of the terms in Eq. (31.1) depend on time-varying pressure and saturation, while other factors change relatively slowly or are constant with respect to time. We separate these terms to obtain

$$PI = \frac{k_{ro}}{\mu_o B_o} PID$$

where the quasi-stationary factors are collected in the PID term, that is,

$$PID = \frac{0.00708 K_{abs} h_{net}}{\ell n(r_e/r_w) + S}$$

The WINB4D user is expected to provide a PID for each well connection. A connection is a gridblock with a well perforation.

31.2 Vertical Wells

A value of the connection flow index PID for a vertical well can be estimated from a formula derived by Peaceman [1978]:

$$PID_k = \left[\frac{0.00708 Kh}{\ell n\left(\frac{r_e}{r_w}\right) + S} \right]_k \quad (31.2)$$

where

$$r_e \approx r_o = 0.14(\Delta x^2 + \Delta y^2)^{1/2}$$

for an isotropic system. With respect to permeability, an isotropic system is a system in which x direction and y direction permeabilities are equal, ($K_x = K_y$). For a square well block in an isotropic system, $\Delta x = \Delta y$ and $r_o \approx 0.2 \Delta x$. The subscript k in Eq. (31.2) denotes the k th connection. For a well in a rectangular gridblock and an anisotropic system (that is, $K_x \neq K_y$), well PID is estimated using an effective permeability

$$K = \sqrt{K_x K_y}$$

and an equivalent well block radius

$$r_o = 0.28 \frac{[(K_y/K_x)^{1/2} \Delta x^2 + (K_x/K_y)^{1/2} \Delta]}{(K_y/K_x)^{1/4} + (K_x/K_y)^{1/4}}$$

The remaining parameters are defined as:

- K = horizontal permeability of connection k (md)
- h = thickness of connection k (ft)
- r_w = wellbore radius (ft)
- S = dimensionless skin factor

In principle, the well flow index can be related to measured values. In practice, however, the terms r_e , S , and $k_{ro}/\mu_o B_o$ are seldom well known, especially for a multiphase flowing well. As a matter of expediency, therefore, Eq. (31.2) is often used to compute an initial estimate of PID. This value can then be improved by adjusting it until the well rates computed by the simulator match the initial observed well rates.

31.3 Horizontal Wells

There are many ways to estimate connection flow index PID for a horizontal well [Joshi, 1991]. A PID value can be estimated for horizontal wells in a manner similar to that for vertical wells by using the Joshi formula

$$PID_k = \left[\frac{0.00708Kh}{\ln \left(\frac{a + \sqrt{a^2 - \left(\frac{L}{2}\right)^2}}{L/2} \right) + \frac{h}{L} \ln \left(\frac{h}{2r_w} \right) + S} \right]_k \tag{31.3}$$

where

$$a = \frac{L}{2} \left[0.5 + \sqrt{0.25 + \left(\frac{2r_{eh}}{L}\right)^4} \right]^{1/2}$$

The subscript k in Eq. (31.3) denotes the k^{th} connection. The remaining parameters are defined as follows:

- K = horizontal permeability of connection k (md)
- h = thickness of connection k (ft)
- L = horizontal well length (ft)
- r_w = wellbore radius (ft)
- r_{eh} = drainage radius of horizontal well (ft)
- S = dimensionless skin factor

The drainage radius r_{eh} of the horizontal well needs to account for elliptical flow into the wellbore. Babu and Odeh [1989] present a procedure for estimating r_{eh} .

Chapter 32

The IMPES Formulation

The following section from Fanchi, et al. [1982] shows how the flow equations for a black oil simulator can be recast in a form that is suitable for solution by a numerical technique. The numerical technique is based on the formulation originally presented by Sawyer and Mercer [1978].

32.1 Flow Equations and Phase Potentials

The form of the Darcy velocities (Eqs. (4.10) through (4.12)) may be simplified by defining the potential Φ_p of phase p as

$$\Phi_p = P_p - \frac{\rho_p z}{144} \quad (32.1)$$

and we have used the assumption that $g = g_c$. In this notation, including x, y , and z directional permeabilities and unit vectors $\hat{i}, \hat{j}, \hat{k}$, the Darcy velocities may be written as

$$\vec{v}_o = -\vec{K} \cdot \lambda_o \nabla \Phi_o = -\lambda_o \left[\hat{i} K_x \frac{\partial \Phi_o}{\partial x} + \hat{j} K_y \frac{\partial \Phi_o}{\partial y} + \hat{k} K_z \frac{\partial \Phi_o}{\partial z} \right] \quad (32.2)$$

$$\vec{v}_w = -\vec{K} \cdot \lambda_w \nabla \Phi_w = -\lambda_w \left[\hat{i} K_x \frac{\partial \Phi_w}{\partial x} + \hat{j} K_y \frac{\partial \Phi_w}{\partial y} + \hat{k} K_z \frac{\partial \Phi_w}{\partial z} \right] \quad (32.3)$$

$$\vec{v}_g = -\vec{K} \cdot \lambda_g \nabla \Phi_g = -\lambda_g \left[\hat{i}K_x \frac{\partial \Phi_g}{\partial x} + \hat{j}K_y \frac{\partial \Phi_g}{\partial y} + \hat{k}K_z \frac{\partial \Phi_g}{\partial z} \right] \quad (32.4)$$

have used the dyadic notation \vec{K} to signify that permeability is a tensor of rank two. The expanded form of Eqs. (32.2) through (32.4) employs the common assumption that the coordinate axes of our reference system are aligned along the principal axes of \vec{K} . As discussed in Chapters 7 and 8, and associated references, this assumption impacts the ability of the simulator to accurately model fluid flow.

Combining Eqs. (4.27) through (4.29) with Eqs. (32.2) through (32.4) gives

$$\nabla \cdot \frac{\vec{K} \lambda_o \cdot \nabla \Phi_o}{B_o} - \frac{q_o}{\rho_{osc}} = \frac{\partial}{\partial t} \left(\frac{\Phi S_o}{B_o} \right) \quad (32.5)$$

$$\nabla \cdot \frac{\vec{K} \lambda_w \cdot \nabla \Phi_w}{B_w} - \frac{q_w}{\rho_{wsc}} = \frac{\partial}{\partial t} \left(\frac{\Phi S_w}{B_w} \right) \quad (32.6)$$

and

$$\begin{aligned} \nabla \cdot \vec{K} \cdot \left[\frac{\lambda_g \nabla \Phi_g}{B_g} + \frac{R_{so} \lambda_o \nabla \Phi_o}{B_o} + \frac{\lambda_w R_{sw} \nabla \Phi_w}{B_w} \right] - \frac{q_g}{\rho_{gsc}} \\ = \frac{\partial}{\partial t} \left[\Phi \left(\frac{S_g}{B_g} + R_{so} \frac{S_o}{B_o} + R_{sw} \frac{S_w}{B_w} \right) \right] \end{aligned} \quad (32.7)$$

Equations (32.5) through (32.7) are equivalent to Peaceman's [1977] Eqs. (1-105) through (1-107) for a three-dimensional system, except we have also allowed gas to dissolve in the water phase. Our rate and coordinate system sign conventions also differ. If these differences are taken into consideration, the formulations are seen to be equivalent.

32.2 Introduction of the Capillary Pressure Concept

The presence of oil-, water-, and gas-phase pressures in Eqs. (32.5) through (32.7) complicates the problem. We simplify the handling of the phase

pressures and potentials in the flow equations by using the capillary pressure concept. Let us define the difference in phase pressures as

$$P_{cow} = P_o - P_w \tag{32.8}$$

and

$$P_{cgo} = P_g - P_o. \tag{32.9}$$

The differences P_{cow} and P_{cgo} are the capillary pressures for oil-water and gas-water systems, respectively. Experimentally P_{cow} and P_{cgo} have been observed to be principally functions of water and gas saturations, respectively. Using Eqs. (32.8) and (32.9) lets us write the water and gas phase potentials as

$$\Phi_w = P_o - P_{cow} - \frac{\rho_w z}{144} \tag{32.10}$$

and

$$\Phi_g = P_o + P_{cgo} - \frac{\rho_g z}{144} \tag{32.11}$$

Combining Eqs. (32.5) through (32.7) with Eqs. (32.10) and (32.11) and rearranging yields

Oil

$$\nabla \cdot \vec{K} \cdot \left(\frac{\lambda_o}{B_o} \right) \nabla P_o + CG_o - \frac{q_o}{\rho_{osc}} = \frac{\partial}{\partial t} \left(\phi \frac{S_o}{B_o} \right) \tag{32.12}$$

Water

$$\nabla \cdot \vec{K} \cdot \left(\frac{\lambda_w}{B_w} \right) \nabla P_o + CG_w - \frac{q_w}{\rho_{wsc}} = \frac{\partial}{\partial t} \left(\phi \frac{S_w}{B_w} \right) \tag{32.13}$$

Gas

$$\begin{aligned} \nabla \cdot \left[\vec{K} \cdot \left(\frac{\lambda_g}{B_g} + \frac{R_{so}\lambda_o}{B_o} + \frac{R_{sw}\lambda_w}{B_w} \right) \right] \nabla P_o + CG_g - \frac{q_g}{\rho_{gsw}} \\ = \frac{\partial}{\partial t} \left[\Phi \left(\frac{S_g}{B_g} + \frac{R_{so}S_o}{B_o} + \frac{R_{sw}S_w}{B_w} \right) \right] \end{aligned} \quad (32.14)$$

The gravity and capillary contributions to the phase pressures have been collected in the terms CG_o , CG_w , and CG_g :

$$CG_o = -\nabla \cdot \vec{K} \cdot \left(\frac{\lambda_o}{B_o} \right) \nabla \left(\frac{\rho_o z}{144} \right) \quad (32.15)$$

$$CG_w = -\nabla \cdot \vec{K} \cdot \left(\frac{\lambda_w}{B_w} \right) \nabla \left(\frac{\rho_w z}{144} + P_{cow} \right) \quad (32.16)$$

and

$$\begin{aligned} CG_g = \nabla \cdot \vec{K} \cdot \frac{\lambda_g}{B_g} \nabla \left(P_{cgo} - \frac{\rho_g z}{144} \right) \\ - \nabla \cdot \vec{K} \cdot \left[\frac{R_{so}\lambda_o}{B_o} \nabla \left(\frac{\rho_o z}{144} \right) + \frac{R_{sw}\lambda_w}{B_w} \nabla \left(P_{cow} + \frac{\rho_w z}{144} \right) \right] \end{aligned} \quad (32.17)$$

Essentially our task is to solve Eqs. (32.12) through (32.14) and saturation constraint Eq. (4.20) for the four unknowns P_o , S_o , S_w , and S_g . All other physical properties in the equations are known, in principle, as functions of the four unknowns, or from field and laboratory data.

32.3 The Pressure Equation

The procedure used in WINB4D to solve the flow equations requires that we first combine Eqs. (4.20) and (32.12) through (32.14) such that we have only

one equation remaining for the unknown pressure P_o . We proceed by using the following shorthand for Eqs. (32.12) through (32.14):

Oil

$$L_o = \frac{\partial}{\partial t} \left(\phi \frac{S_o}{B_o} \right) \quad (32.18)$$

Water

$$L_w = \frac{\partial}{\partial t} \left(\phi \frac{S_w}{B_w} \right) \quad (32.19)$$

Gas

$$L_g = \frac{\partial}{\partial t} \left[\phi \left(\frac{S_g}{B_g} + \frac{R_{so}S_o}{B_o} + \frac{R_{sw}S_w}{B_w} \right) \right] \quad (32.20)$$

where

$$L_o = \nabla \cdot \vec{K} \cdot \frac{\lambda_o}{B_o} \nabla P_o + CG_o - \frac{q_o}{\rho_{osc}}, \quad (32.21)$$

$$L_w = \nabla \cdot \vec{K} \cdot \frac{\lambda_w}{B_w} \nabla P_o + CG_w - \frac{q_w}{\rho_{wsc}}, \quad (32.22)$$

and

$$L_g = \nabla \cdot \left[\vec{K} \cdot \left(\frac{\lambda_g}{B_g} + \frac{R_{so}\lambda_o}{B_o} + \frac{R_{sw}\lambda_w}{B_w} \right) \right] \nabla P_o + CG_g - \frac{q_g}{\rho_{gsc}} \quad (32.23)$$

Recognizing that formation volume factors, gas solubilities, and porosity are functions of pressure, we use the chain rule to expand the accumulation terms (time derivatives) of Eqs. (32.18) through (32.20):

Oil

$$L_o = \frac{\phi}{B_o} \frac{\partial S_o}{\partial t} + \left[\frac{S_o}{B_o} \frac{\partial \phi}{\partial P_o} - \frac{S_o \phi}{B_o^2} \frac{\partial B_o}{\partial P_o} \right] \frac{\partial P_o}{\partial t}, \quad (32.24)$$

Water

$$L_w = \frac{\phi}{B_w} \frac{\partial S_w}{\partial t} + \left[\frac{S_w}{B_w} \frac{\partial \phi}{\partial P_o} - \frac{S_w \phi}{B_w^2} \frac{\partial B_w}{\partial P_o} \right] \frac{\partial P_o}{\partial t}, \quad (32.25)$$

Gas

$$\begin{aligned} L_g = & \frac{\phi}{B_g} \frac{\partial S_g}{\partial t} + \left[\frac{S_g}{B_g} \frac{\partial \phi}{\partial P_o} - \frac{S_g \phi}{B_g^2} \frac{\partial B_g}{\partial P_o} \right] \frac{\partial P_o}{\partial t} \\ & + \frac{\phi R_{s_o}}{B_o^2} \frac{\partial S_o}{\partial t} \\ & + \left[\frac{S_o R_{s_o}}{B_o} \frac{\partial \phi}{\partial P_o} + \frac{\phi S_o}{B_o} \frac{\partial R_{s_o}}{\partial P_o} - \frac{\phi S_o R_{s_o}}{B_o^2} \frac{\partial B_o}{\partial P_o} \right] \frac{\partial P_o}{\partial t} \\ & + \frac{\phi R_{s_w}}{B_w} \frac{\partial S_w}{\partial t} \\ & + \left[\frac{S_w R_{s_w}}{B_w} \frac{\partial \phi}{\partial P_o} + \frac{\phi S_w}{B_w} \frac{\partial R_{s_w}}{\partial P_o} - \frac{\phi S_w R_{s_w}}{B_w^2} \frac{\partial B_w}{\partial P_o} \right] \frac{\partial P_o}{\partial t} \end{aligned} \quad (32.26)$$

The saturation constraint

$$S_o + S_w + S_g = 1 \quad (32.27)$$

is now used to remove $\partial S_g / \partial t$ from Eq. (32.26). Differentiation of Eq. (32.27) by t and rearranging gives

$$\frac{\partial S_g}{\partial t} = - \frac{\partial S_o}{\partial t} - \frac{\partial S_w}{\partial t}. \quad (32.28)$$

Substituting Eq. (32.28) into Eq. (32.26) and simplifying yields

$$\begin{aligned}
 L_g = & \left(\frac{\phi R_{s_o}}{B_o} - \frac{\phi}{B_g} \right) \frac{\partial S_o}{\partial t} + \left(\frac{\phi R_{s_w}}{B_w} - \frac{\phi}{B_g} \right) \frac{\partial S_w}{\partial t} \\
 & + \left\{ \frac{S_g}{B_g} \frac{\partial \phi}{\partial P_o} - \frac{S_g \phi}{\partial B_g^2} \frac{\partial B_g}{\partial P_o} + \frac{S_o R_{s_o}}{B_o} \frac{\partial \phi}{\partial P_o} \right\} \frac{\partial P_o}{\partial t} \\
 & + \left\{ \frac{\phi S_o}{B_o} \frac{\partial R_{s_o}}{\partial P_o} - \frac{\phi S_o}{B_o^2} \frac{\partial B_o}{\partial P_o} \right\} \frac{\partial P_o}{\partial t} \\
 & + \left\{ \frac{S_w R_{s_w}}{B_w} \frac{\partial \phi}{\partial P_o} + \frac{\phi S_w}{B_w} \frac{\partial R_{s_w}}{\partial P_o} - \frac{\phi S_w R_{s_w}}{B_w^2} \frac{\partial B_w}{\partial P_o} \right\} \frac{\partial P_o}{\partial t}.
 \end{aligned} \tag{32.29}$$

Equations (32.24), (32.25), and (32.29) are three equations for the three unknowns P_o , S_o , S_w . Multiplying Eq. (32.24) by $(B_o - R_{s_o} B_g)$, Eq. (32.25) by $(B_w - R_{s_w} B_g)$, Eq. (32.29) by B_g , and adding the results gives

$$\begin{aligned}
 & (B_o - R_{so}B_g)L_o + (B_w - R_{sw}B_g)L_w + B_g L_g \\
 &= (B_o - R_{so}B_g) \frac{\phi}{B_o} \frac{\partial S_o}{\partial t} + (B_w - R_{sw}B_g) \frac{\phi}{B_w} \frac{\partial S_w}{\partial t} \\
 &+ B_g \left(\frac{\phi R_{so}}{B_o} - \frac{\phi}{B_g} \right) \frac{\partial S_o}{\partial t} + B_g \left(\frac{\phi R_{sw}}{B_w} - \frac{\phi}{B_g} \right) \frac{\partial S_w}{\partial t} \\
 &+ [B_o - R_{so}B_g] \left[\frac{S_o}{B_o} \frac{\partial \phi}{\partial P_o} - \frac{S_o \phi}{B_o^2} \frac{\partial B_o}{\partial P_o} \right] \frac{\partial P_o}{\partial t} \\
 &+ [B_w - R_{sw}B_g] \left[\frac{S_w}{B_w} \frac{\partial \phi}{\partial P_o} - \frac{S_w \phi}{B_w^2} \frac{\partial B_w}{\partial P_o} \right] \frac{\partial P_o}{\partial t} \tag{32.30} \\
 &+ \left\{ S_g \frac{\partial \phi}{\partial P_o} - \frac{S_g \phi}{B_g} \frac{\partial B_g}{\partial P_o} + \frac{B_g S_o R_{so}}{B_o} \frac{\partial \phi}{\partial P_o} \right\} \frac{\partial P_o}{\partial t} \\
 &+ \left\{ \frac{B_g \phi S_o}{B_o} \frac{\partial R_{so}}{\partial P_o} - \frac{\phi B_g S_o R_{so}}{B_o^2} \frac{\partial B_o}{\partial P_o} \right\} \frac{\partial P_o}{\partial t} \\
 &+ \left\{ \frac{B_g S_w R_{sw}}{B_w} \frac{\partial \phi}{\partial P_o} + \frac{B_g \phi S_w}{B_w} \frac{\partial R_{sw}}{\partial P_o} - \frac{\phi B_g S_w R_{sw}}{B_w^2} \frac{\partial B_w}{\partial P_o} \right\} \frac{\partial P_o}{\partial t}
 \end{aligned}$$

where some simplification has been performed. This mess can be greatly simplified by multiplying the bracketed terms and then combining with appropriate terms in the curly brackets. We also notice the terms involving time derivatives of S_o and S_w vanish identically. The result is

$$\begin{aligned}
 & (B_o - R_{so}B_g)L_o + (B_w - R_{sw}B_g)L_w + B_g L_g \\
 &= \left[(S_g + S_w + S_o) \frac{\partial \phi}{\partial P_o} - \frac{\phi S_g}{B_g} \frac{\partial B_g}{\partial P_o} \right] \frac{\partial P_o}{\partial t} \tag{32.31} \\
 &+ \left[\phi S_o \left(\frac{B_g}{B_o} \frac{\partial R_{so}}{\partial P_o} - \frac{1}{B_o} \frac{\partial B_o}{\partial P_o} \right) + \phi S_w \left(\frac{B_g}{B_w} \frac{\partial R_{sw}}{\partial P_o} - \frac{1}{B_w} \frac{\partial B_w}{\partial P_o} \right) \right] \frac{\partial P_o}{\partial t}
 \end{aligned}$$

Oil and water compressibilities include the effect of gas:

$$c_o = -\frac{1}{B_o} \frac{\partial B_o}{\partial P_o} + \frac{B_g}{B_o} \frac{\partial R_{so}}{\partial P_o}, \tag{32.32}$$

$$c_w = -\frac{1}{B_w} \frac{\partial B_w}{\partial P_o} + \frac{B_g}{B_w} \frac{\partial R_{sw}}{\partial P_o}, \tag{32.33}$$

Gas compressibility is

$$c_g = -\frac{1}{B_g} \frac{\partial B_g}{\partial P_o}, \tag{32.34}$$

while rock compressibility has the form

$$c_r = \frac{1}{\phi} \frac{\partial \phi}{\partial P_o}, \tag{32.35}$$

Total compressibility for the system is the sum

$$c_t = c_r + c_o S_o + c_w S_w + c_g S_g \tag{32.36}$$

Employing these definitions, Eqs. (32.21) through (32.23) and (32.27) in Eq. (32.31) gives

$$\begin{aligned} & (B_o - R_{so} B_g) \left[\nabla \cdot \vec{K} \cdot \frac{\lambda_o}{B_o} \nabla P_o + CG_o - \frac{q_o}{\rho_{osc}} \right] \\ & + (B_w - R_{sw} B_g) \left[\nabla \cdot \vec{K} \cdot \frac{\lambda_w}{B_w} \nabla P_o + CG_w - \frac{q_w}{\rho_{wsc}} \right] \\ & + B_g \left[\nabla \cdot \vec{K} \cdot \left(\frac{\lambda_g}{B_g} + \frac{R_{so} \lambda_o}{B_o} + \frac{R_{sw} \lambda_w}{B_w} \right) \nabla P_o + CG_g - \frac{q_g}{\rho_{gsc}} \right] \\ & = \phi c_t \frac{\partial P_o}{\partial t}. \end{aligned} \tag{32.37}$$

Equation (32.37) is called the pressure equation. The pressure equation does not contain any time derivatives of saturations. WINB4D is coded to solve the three-

dimensional, three-phase flow equations by first numerically solving the pressure equation for P_o , then using the results in Eqs. (32.18), (32.19) and (32.27) to find the phase saturations. This procedure is an example of a numerical method known as the IMplicit Pressure/Explicit Saturation (IMPES) procedure.

This page intentionally left blank

References

- Abramowitz, M.A. and I.A. Stegun (1972): **Handbook of Mathematical Functions**, ninth printing, New York: Dover.
- Aguilera, R. (1980): **Naturally Fractured Reservoirs**, Tulsa, OK: PennWell Publishing.
- Al-Hussainy, R. and N. Humphreys (1996): "Reservoir Management: Principles and Practices," *Journal of Petroleum Technology*, pp. 1129-1135.
- Ammer, J.R. and A.C. Brummert (1991): "Miscible Applied Simulation Techniques for Energy Recovery – Version 2.0," U.S. Department of Energy Report DOE/BC-91/2/SP, Morgantown Energy Technology Center, WV.
- Amyx, J.W., D.H. Bass, and R.L. Whiting (1960): **Petroleum Reservoir Engineering**, New York: McGraw-Hill.
- Anderson, R.N. (1995): "Method Described for Using 4D Seismic to Track Reservoir Fluid Movement," *Oil & Gas Journal*, pp. 70-74, April 3.
- Arps, J.J. (1945): "Analysis of Decline Curves," *Transaction of AIME*, Volume 160, pp. 228-247.
- Ausburn, B.E., A.K. Nath and T.R. Wittick (Nov. 1978): "Modern Seismic Methods – An Aid for the Petroleum Engineer," *Journal of Petroleum Technology*, pp. 1519-1530.
- Aziz, K. (1993): "Reservoir Simulation Grids: Opportunities and Problems," *Journal of Petroleum Technology*, pp. 658-663.
- Aziz, K. and A. Settari (1979): **Petroleum Reservoir Simulation**, New York: Elsevier.
- Babu, D.K. and A. S. Odeh (1989): "Productivity of a Horizontal Well," *Society of Petroleum Engineers Journal*, pp. 417-421.
- Bear, J. (1972): **Dynamics of Fluids in Porous Media**, New York: Elsevier.
- Beasley, C.J. (1996): "Seismic Advances Aid Reservoir Description," *Journal of Petroleum Technology*, pp. 29-30.
- Benedict, M., G.B. Webb, and L.C. Rubin (1940): *Journal of Chemical Physics*, Volume 8, p. 334.

- Blackwelder, B., L. Canales, and J. Dubose (1996): "New Technologies in Reservoir Characterization," *Journal of Petroleum Technology*, pp. 26-27.
- Blunt, M.J. (1999): "An Empirical Model for Three-Phase Relative Permeability," Paper SPE 56474, *Proceedings of the 1999 Annual Technical Conference And Exhibition of Society of Petroleum Engineers*, Houston, TX, Oct. 3-6.
- Bradley, M.E. and A.R.O. Wood (Nov. 1994): "Forecasting Oil Field Economic Performances," *Journal of Petroleum Technology*, pp. 965-971 and references therein.
- Brown, K.E. and J.F. Lea (Oct. 1985): "Nodal Systems Analysis of Oil and Gas Wells," *Journal of Petroleum Technology*, pp. 1751-1763.
- Brock, J. (1986): **Applied Open-Hole Log Analysis**, Houston: Gulf Publishing.
- de Buyl, M., T. Guidish, and F. Bell (1988): "Reservoir Description from Seismic Lithologic Parameter Estimation," *Journal of Petroleum Technology*, pp. 475-482.
- Carr, N.L., R. Kobayashi, and D.B. Burrows (1954): "Viscosity of Hydrocarbon Gases Under Pressure," *Transactions of AIME*, Volume 201, pp. 264-272.
- Carter, R.D. and G.W. Tracy (1960) "An Improved Method for Calculating Water Influx," *Transactions of AIME*, Volume 219, pp. 415-417.
- Chin, W.C. (1993): **Modern Reservoir Flow and Well Transient Analysis**, Houston: Gulf Publishing.
- Christie, M.A. (Nov. 1996): "Upscaling for Reservoir Simulation," *Journal of Petroleum Technology*, pp. 1004-1010.
- Clark, N.J. (1969): **Elements of Petroleum Reservoirs**, Richardson, TX: Society of Petroleum Engineers.
- Coats, K.H. (1969): "Use and Misuse of Reservoir Simulation Models," *Journal of Petroleum Technology*, pp. 183-190.
- Collins, R.E. (1961): **Flow of Fluids Through Porous Materials**, Tulsa, OK: Petroleum Publishing-Reinhold.
- Craft, B.C., M.F. Hawkins, and R.E. Terry (1991): **Applied Petroleum Reservoir Engineering, Second Edition**, Englewood Cliffs, NJ: Prentice-Hall.
- Craig, F.F. (1971): **The Reservoir Engineering Aspects of Waterflooding**, SPE Monograph Series, Richardson, TX: Society of Petroleum Engineers.
- Crichlow, H.B. (1977): **Modern Reservoir Engineering – A Simulation Approach**, Englewood Cliffs, NJ: Prentice Hall.

- Daccord, G., J. Nittmann and H.E. Stanley (1986): "Radial Viscous Fingers and Diffusion-Limited Aggregation: Fractal Dimension and Growth Sites," *Physical Review Letters*, Volume 56, 336-339.
- Dahlberg, E.C. (1975): "Relative Effectiveness of Geologists and Computers in Mapping Potential Hydrocarbon Exploration Targets," *Mathematical Geology*, Volume 7, pp. 373-394.
- Dake, L.P. (1978): **Fundamentals of Reservoir Engineering**, Amsterdam: Elsevier.
- Dietrich, J.K. and P.L. Bondor (1976): "Three-Phase Oil Relative Permeability Models," SPE Paper 6044, *Proceedings of 51st Fall Technical Conference and Exhibition of Society of Petroleum Engineers and AIME*, New Orleans, LA, Oct. 3-6.
- Dietrich, F.L., F.G. Brown, Z.H. Zhou, M.A. Maure (1996): "Microbial EOR Technology Advancement: Case Studies of Successful Projects," paper SPE 36746 presented at the 1996 SPE Annual Technical Conference and Exhibition, Denver, Colorado, October 6-9.
- Dogru, A.H. (May, 2000): "Megacell Reservoir Simulation," *Journal of Petroleum Technology*, pp. 54-60.
- Dorn, G.A. (September, 1998): "Modern 3-D Seismic Interpretation," *The Leading Edge*, pp. 1262-1283.
- Dranchuk, P.M., R.A. Purvis, and D.B. Robinson (1974): "Computer Calculation of Natural Gas Compressibility Factors Using the Standing and Katz Correlations," *Institute of Petroleum Technology*, IP-74-008.
- van Dyke, K. (1997): **Fundamentals of Petroleum**, 4th Edition, The University of Texas at Austin: Petroleum Extension Service.
- Earlougher, R.C., Jr. (1977): **Advances in Well Test Analysis**, SPE Monograph Series, Richardson, TX: Society of Petroleum Engineers.
- Ebanks, W.J., Jr. (1987): "Flow Unit Concept – Integrated Approach to Reservoir Description for Engineering Projects," paper presented at the AAPG Annual Meeting, Los Angeles.
- Englund, E. and A. Sparks (1991): "Geo-EAS 1.2.1 User's Guide," *EPA Report #600/8-91/008 Environmental Protection Agency-EMSL*, Las Vegas, NV.
- Evans, W.S. (1996): "Technologies for Multidisciplinary Reservoir Characterization," *Journal of Petroleum Technology*, pp. 24-25.
- van Everdingen, A.F. and W. Hurst (1949): "The Application of the Laplace Transformation to Flow Problems in Reservoirs," *Transactions of AIME*, Volume 186, pp. 305-324.
- Fanchi, J.R. (1983): "Multidimensional Numerical Dispersion," *Society of Petroleum Engineering Journal*, pp. 143-151.

- Fanchi, J.R. (June 1985): "Analytical Representation of the van Everdingen-Hurst Aquifer Influence Functions for Reservoir Simulation," *Society of Petroleum Engineering Journal*, pp. 405-406.
- Fanchi, J.R. (1986): "BOAST-DRC: Black Oil and Condensate Reservoir Simulation on an IBM-PC," Paper SPE 15297, *Proceedings from Symposium on Petroleum Industry Applications of Microcomputers of SPE*, Silver Creek, CO, June 18-20.
- Fanchi, J.R. (1990): "Calculation of Parachors for Compositional Simulation: An Update," *Society of Petroleum Engineers Reservoir Engineering*, pp. 433-436.
- Fanchi, J.R. (1999): "Flow Models Time 4-D Seismic Surveys," *Oil & Gas Journal*, pp. 46-51.
- Fanchi, J.R. (2000): **Math Refresher for Scientists and Engineers, Second Edition**, New York: J. Wiley and Sons.
- Fanchi, J.R. and R.L. Christiansen (1989): "Applicability of Fractals to the Description of Viscous Fingering," Paper SPE 19782, *Proceedings of 64th Annual Technical Conference And Exhibition of Society of Petroleum Engineers*, San Antonio, TX, Oct. 8-11.
- Fanchi, J.R., K.J. Harpole, and S.W. Bujnowski (1982): "BOAST: A Three-Dimensional, Three-Phase Black Oil Applied Simulation Tool," 2 Volumes, U.S. Department of Energy, Bartlesville Energy Technology Center, OK.
- Fanchi, J.R., J.E. Kennedy, and D.L. Dauben (1987): "BOAST II: A Three-Dimensional, Three-Phase Black Oil Applied Simulation Tool," U.S. Department of Energy, Bartlesville Energy Technology Center, OK.
- Fanchi, J.R., H.Z. Meng, R.P. Stoltz, and M.W. Owen (1996): "Nash Reservoir Management Study with Stochastic Images: A Case Study," *Society of Petroleum Engineers Formation Evaluation*, pp. 155-161.
- Fanchi, J.R., T.A. Pagano and T.L. Davis (1999): "State of the Art of 4D Seismic Monitoring: The Technique, The Record, and The Future," *Oil & Gas Journal*, pp. 38-43.
- Fayers, F.J. and T.A. Hewett (1992): "A Review of Current Trends in Petroleum Reservoir Description and Assessing the Impacts on Oil Recovery," *Proceedings of Ninth International Conference On Computational Methods in Water Resources*, June 9-11.
- Felder, R.D. (1994): "Advances in Openhole Well Logging," *Journal of Petroleum Technology*, pp. 693-701.
- Fredrich, J.T., G.L. Deitrick, J.G. Arguello and E.P. DeRouffignac (1998): "Reservoir Compaction, Surface Subsidence, and Casing Damage: A Geomechanics Approach to Mitigation and Reservoir Management," *Journal of Petroleum Technology*, pp. 68-70.

- Gaddy, D.E. (Apr. 26, 1999): "Coalbed Methane Production Shows Wide Range of Variability," *Oil & Gas Journal*, pp. 41-42.
- Gardner, H.F., L.W. Gardner, and A.H. Gregory (1974): "Formation Velocity and Density – the Diagnostic Basis for Stratigraphic Traps," *Geophysics* Volume 39, pp. 770-780.
- Gassman, F. (1951): "Elastic Waves Through a Packing of Spheres," *Geophysics*, Volume 16, pp. 673-685.
- Golf-Racht, T.D. van (1982): **Fundamentals of Fractured Reservoir Engineering**, New York: Elsevier.
- Govier, G.W., Editor (1978): **Theory and Practice of the Testing of Gas Wells**, Calgary: Energy Resources Conservation Board.
- Grace, J.D., R.H. Caldwell, and D.I. Heather (Sept. 1993): "Comparative Reserves Definitions: USA, Europe, and the Former Soviet Union," *Journal of Petroleum Technology*, pp. 866-872.
- Green, D.W. and G.P. Willhite (1998): **Enhanced Oil Recovery**, Richardson, TX: Society of Petroleum Engineers.
- Guerrero, E.T. (1966): "Material Balance Principles," Reservoir Engineering Refresher Course, Tulsa: Mid-Continent Section of AIME.
- Gunter, G.W., J.M. Finneran, D.J. Hartmann, and J.D. Miller (1997): "Early Determination of Reservoir Flow Units Using an Integrated Petrophysical Method," Paper SPE 38679, *Proceedings of the 1997 SPE Annual Technical Conference And Exhibition*, Richardson, TX: Society of Petroleum Engineers.
- Haldorsen, H.H. and E. Damselth (1993): "Challenges in Reservoir Characterization," *American Association of Petroleum Geologists Bulletin*, Volume 77, No. 4, pp. 541-551.
- Haldorsen, H.H. and E. Damsleth (April 1990): "Stochastic Modeling," *Journal of Petroleum Technology*, pp. 404-412.
- Haldorsen, H.H. and L.W. Lake (1989): "A New Approach to Shale Management in Field-Scale Models," **Reservoir Characterization-2**, SPE Reprint Series #27, Richardson, TX: Society of Petroleum Engineers.
- Harpole, K.J. (1985): **Reservoir Environments and Their Characterization**, Boston: International Human Resources Development Corporation.
- Harris, D.G. (May 1975): "The Role of Geology in Reservoir Simulation Studies," *Journal of Petroleum Technology*, pp. 625-632.
- He, W., R.N. Anderson, L. Xu, A. Boulanger, B. Meadow, and R. Neal (May 20, 1996): "4D Seismic Monitoring Grows as Production Tool," *Oil & Gas Journal*, pp. 41-46.

- Hebert, H., A.T. Bourgoyne, Jr., and J. Tyler (May 1993): "BOAST II for the IBM 3090 and RISC 6000", U.S. Department of Energy Report DOE/ID/12842-2, Bartlesville Energy Technology Center, OK.
- Hegre, T.M., V. Dalen, and A. Henriquez (1986): "Generalized Transmissibilities for Distorted Grids in Reservoir Simulation," Paper SPE 15622, *Proceedings of 61st Annual Technical Conference And Exhibition*, Richardson, TX: Society of Petroleum Engineers.
- Heinemann, R.F., S.L. Lyons, S. Vasantharajan, and W.-P. Tai (Jan. 1998): "Next Generation Reservoir Optimization," *World Oil*, pp. 47-54.
- Heinemann, Z.E. (1994): "Interactive Generation of Irregular Simulation Grids and its Practical Applications," Paper SPE 27998, Richardson, TX: Society of Petroleum Engineers.
- Heinemann, Z.E. and G.F. Heinemann (1998): "Modeling Heavily Faulted Reservoirs," Paper SPE 48998, *Proceedings of the 1998 Society of Petroleum Engineers Annual Technical Conference and Exhibition*, Richardson, TX: Society of Petroleum Engineers.
- Honarpour, M., L.F. Koederitz, and A.H. Harvey (1982): "Empirical Equations for Estimating Two-Phase Relative Permeability in Consolidated Rock," *Journal of Petroleum Technology*, pp. 2905-2908.
- Isaaks, E.H. and R.M. Srivastava (1989): **Applied Geostatistics**, New York: Oxford University Press.
- Jack, I. (1998): **Time-Lapse Seismic in Reservoir Management**, 1998 Distinguished Instructor Short Course, Tulsa: Society of Exploration Geophysicists.
- Jefferys, W.H. and J.O. Berger (1992): "Ockham's Razor and Bayesian Analysis," *American Scientist*, Volume 80, pp. 64-72.
- Johnston, D.H. (1997): "A Tutorial on Time-Lapse Seismic Reservoir Monitoring," *Journal of Petroleum Technology*, pp. 473-475.
- Joshi, S.D. (1991): **Horizontal Well Technology**, Tulsa, OK: PennWell Publishing Company.
- Kamal, M.M., D.G. Freyder, and M.A. Murray (1995): "Use of Transient Testing in Reservoir Management," *Journal of Petroleum Technology*, pp. 992-999.
- Kanter, R.M. (1988): "When a Thousand Flowers Bloom: Structural, Collective and Social Conditions for Innovation in Organization," *Research in Organizational Behavior*, Volume 10, pp. 169-211.
- Kasap, E. and L.W. Lake (June 1990): "Calculating the Effective Permeability Tensor of a Gridblock," *Society of Petroleum Engineers Formation Evaluation*, pp. 192-200.

- Katz, D.L. and R.L. Lee (1990): **Natural Gas Engineering**, New York: McGraw-Hill.
- Kazemi, H. (Oct. 1996): "Future of Reservoir Simulation", *Society of Petroleum Engineers Computer Applications*, pp. 120-121.
- Killough, J.E. (1976): "Reservoir Simulation with History-Dependent Saturation Functions," *Society of Petroleum Engineers Journal*, pp. 37-48.
- Killough, J.E. (1995): "Ninth SPE Comparative Solution Project: A Reexamination of Black-Oil Simulation," Paper SPE 29110, *Proceedings of 13th Society of Petroleum Engineers Symposium on Reservoir Simulation*, Feb. 12-15.
- Koederitz, L.F., A.H. Harvey, and M. Honarpour (1989): **Introduction to Petroleum Reservoir Analysis**, Houston: Gulf Publishing.
- Kreyszig, E. (1999): **Advanced Engineering Mathematics, Eighth Edition**, New York: J. Wiley and Sons.
- Kuuskræa, V.A. and C.F. Brandenburg (Oct. 9, 1989): "Coalbed Methane Sparks a New Energy Industry," *Oil & Gas Journal*, pp. 49.
- Lake, L.W. (April 1988): "The Origins of Anisotropy," *Journal of Petroleum Technology*, pp. 395-396.
- Lake, L.W. (1989): **Enhanced Oil Recovery**, Englewood Cliffs, NJ: Prentice Hall.
- Lantz, R.B. (1971): "Quantitative Evaluation of Numerical Diffusion," *Society of Petroleum Engineering Journal*, pp. 315-320.
- Lee, S.H., L.J. Durlofsky, M.F. Lough, and W.H. Chen (1997): "Finite Difference Simulation of Geologically Complex Reservoirs with Tensor Permeabilities," Paper SPE 38002, *Proceedings of 1997 SPE Reservoir Simulation Symposium*, Richardson, TX: Society of Petroleum Engineers.
- Levitán, L.L. and M. Murtha (1999): "New Correlations estimate P_b , FVF," *Oil & Gas Journal*, pp. 70-76.
- Lieber, Bob (Mar/Apr 1996): "Geostatistics: The Next Step in Reservoir Modeling," *Petro Systems World*, pp. 28-29.
- Lough, M.F., S.H. Lee, and J. Kamath (Nov. 1996): "Gridblock Effective-Permeability Calculation for Simulation of Naturally Fractured Reservoirs," *Journal of Petroleum Technology*, pp. 1033-1034.
- Louisiana State University (1997): "'BOAST 3' A Modified Version of BOAST II with Post Processors B3PLOT2 and COLORGRID," Version 1.50, U.S. Department of Energy Report DOE/BC/14831-18, Bartlesville Energy Technology Center, OK.
- Lumley, D. and R. Behrens (1997): "Practical Issues for 4D Reservoir Modeling," *Journal of Petroleum Technology*, pp. 998-999.

- Lynch, M.C. (1996): "The Mirage of Higher Petroleum Prices," *Journal of Petroleum Technology*, pp. 169-170.
- Maddox, R.B. (1988): **Team Building: An Exercise in Leadership**, Crisp Publications, Inc.
- Makogon, Y.F., W.A. Dunlap and S.A. Holditch (1997): "Recent Research on Properties of Gas Hydrates," Paper OTC 8299, *Proceedings of the 1997 Offshore Technology Conference*, Richardson, TX: Society of Petroleum Engineers.
- Martin, F.D. (1992): "Enhanced Oil Recovery for Independent Producers," Paper SPE/DOE 24142, *Proceedings of the SPE/DOE Eighth Symposium*, Richardson, TX: Society of Petroleum Engineers.
- Mattax, C.C. and R.L. Dalton (1990): **Reservoir Simulation**, SPE Monograph #13, Richardson, TX: Society of Petroleum Engineers.
- Matthews, C.S. and D.G. Russell (1967): **The Reservoir Engineering Aspects of Waterflooding**, SPE Monograph Series, Richardson, TX: Society of Petroleum Engineers.
- Mavor, M., T. Pratt and R. DeBruyn (Apr. 26, 1999): "Study Quantifies Powder River Coal Seam Properties," *Oil & Gas Journal*, pp. 35-40.
- McCain, W.D., Jr. (1973): **The Properties of Petroleum Fluids**, Tulsa, OK: Petroleum Publishing.
- McCain, W.D., Jr. (1991): "Reservoir-Fluid Property Correlations – State of the Art," *Society of Petroleum Engineers Reservoir Engineering*, pp. 266-272.
- McIntosh, I., H. Salzew, and C. Christensen (1991): "The Challenge of Teamwork," Paper CIM/AOSTRA 91-19, *Proceedings of CIM/AOSTRA 1991 Technical Conference*, Banff, Canada.
- McQuillin, R., M. Bacon, and W. Barclay (1984): **An Introduction to Seismic Interpretation**, Houston: Gulf Publishing.
- Mian, M.A. (1992): **Petroleum Engineering Handbook for the Practicing Engineer**, Volumes I and II, Tulsa, OK: PennWell Publishing.
- Millheim, K.M. (1997): "Fields of Vision," *Journal of Petroleum Technology*, p. 684.
- Moses, P.L. (July 1986): "Engineering Applications of Phase Behavior of Crude Oil and Condensate Systems," *Journal of Petroleum Technology*, pp. 715-723; and F.H. Poettmann and R.S. Thompson (1986): "Discussion of Engineering Applications of Phase Behavior of Crude Oil and Condensate Systems," *Journal of Petroleum Technology*, pp. 1263-1264.
- Murphy, W., A. Reisher, and K. Hsu (1993): "Modulus Decomposition of Compressional and Shear Velocities in Sand Bodies," *Geophysics*, Volume 58, pp. 227-239.

- Murtha, J.A. (1997): "Monte Carlo Simulation: Its Status and Future," *Journal of Petroleum Technology*, pp. 361-373.
- Nemchenko, N.N., M. Ya. Zykin, A.A. Arbatov, V.I. Poroskun, and I.S. Gutman (1995): "Distinctions in the Oil and Gas Reserves and Resources Classifications Assumed in Russia and USA – Source of Distinctions," *Energy Exploration and Exploitation*, Volume 13, #6, Essex, United Kingdom: Multi-Science Publishing Company.
- Nolen, J.S. and D.W. Berry (1973): "Test of the Stability and Time-Step Sensitivity of Semi-Implicit Reservoir Simulation Techniques," **Numerical Simulation**, SPE Reprint Series #11, Richardson, TX: Society of Petroleum Engineers.
- Norton, R. (Nov. 1994): "Economics for Managers," *Fortune*, p. 3.
- Novakovic, D. (1999): "Gravity Assisted Tertiary Gas Injection in Water-flooded Reservoirs – Mathematical Modeling of Drive Parameters," Louisiana State University preprint, presented at the June 1999 Reservoir Management Summer School, Dubrovnik, Croatia.
- Odeh, A.S. (1981): "Comparison of Solutions to a Three-Dimensional Black-Oil Reservoir Simulation Problem," *Journal of Petroleum Technology*, pp. 13-25.
- Odeh, A.S. (Feb. 1985): "The Proper Interpretation of Field-Determined Buildup Pressure and Skin Values for Simulator Use," *Society of Petroleum Engineering Journal*, pp. 125-131.
- Offshore staff [Sep. 1998]: 'Refurbishment/Abandonment,' *Offshore Magazine*, pp. 148 and 186.
- Oreskes, N., K. Shrader-Frechette, and K. Belitz (1994): "Verification, Validation, and Confirmation of Numerical Models in the Earth Sciences", *Science*, pp. 641-646, Feb. 4.
- Pannatier, Y. (1996): **VARIOWIN: Software for Spatial Data Analysis in 2D**, New York: Springer-Verlag.
- Paterson, L. (January 1985): "Fingering with Miscible Fluids in a Hele- Shaw Cell," *Physics of Fluids*, Volume 28 (1), 26-30.
- Peaceman, D.W. (1977): **Fundamentals of Numerical Reservoir Simulation**, New York: Elsevier.
- Peaceman, D.W. (June 1978): "Interpretation of Well-Block Pressures in Numerical Reservoir Simulation," *Society of Petroleum Engineering Journal*, pp. 183-194.

Peaceman, D.W. (June 1983): "Interpretation of Well-Block Pressures in Numerical Reservoir Simulation with Nonsquare Grid Blocks and Anisotropic Permeability," *Society of Petroleum Engineering Journal*, pp. 531-543.

Pedersen, K.S., A. Fredenslund, and P. Thomassen (1989): **Properties of Oil and Natural Gases**, Houston: Gulf Publishing.

Prats, M. (1982): **Thermal Recovery**, SPE Monograph Series, Richardson TX: Society of Petroleum Engineers.

Raleigh, M. (Sept. 1991): *ECLIPSE Newsletter*, Houston: Schlumberger GeoQuest.

Rao, N.D. and M.G. Girard (Jan. 1997): "A New Technique for Reservoir Wettability Characterization," *Journal of Canadian Petroleum Technology*, Volume 35, pp. 31-39.

Raza, S.H. (1992): "Data Acquisition and Analysis for Efficient Reservoir Management," *Journal of Petroleum Technology*, pp. 466-468.

Reiss, L.H. (1980): **The Reservoir Engineering Aspects of Fractured Reservoirs**, Houston: Gulf Publishing.

Richardson, J.G., J.B. Sangree, and R.M. Sneider (1987a): "Applications of Geophysics to Geologic Models and to Reservoir Descriptions," *Journal of Petroleum Technology*, pp. 753-755.

Richardson, J.G., J.B. Sangree and R.M. Sneider (1987b): "Introduction to Geologic Models," *Journal of Petroleum Technology* (first of series), pp. 401-403.

Richardson, J.G. (Feb. 1989): "Appraisal and Development of Reservoirs," *Geophysics: The Leading Edge of Exploration*, pp. 42 ff.

Rogers, R.E. (1994): **Coalbed Methane: Principles and Practice**, Englewood Cliffs, New Jersey: Prentice-Hall.

Rosenberg, D. U. von (1977): **Methods for the Numerical Solution of Partial Differential Equations**, Tulsa, OK: Farrar and Associates.

Rossini, C., F. Brega, L. Piro, M. Rovellini, and G. Spotti (Nov. 1994): "Combined Geostatistical and Dynamic Simulations for Developing a Reservoir Management Strategy: A Case History," *Journal of Petroleum Technology*, pp. 979-985.

Ruijtenberg, P.A., R. Buchanan, and P. Marke (1990): "Three-Dimensional Data Improve Reservoir Mapping," *Journal of Petroleum Technology*, pp. 22-25, 59-61.

Sabet, M.A. (1991): **Well Test Analysis**, Houston: Gulf Publishing.

Saleri, N.G. (1993): "Reservoir Performance Forecasting: Acceleration by Parallel Planning," *Journal of Petroleum Technology*, pp. 652-657.

- Salari, N.G., R.M. Toronyi, and D.E. Snyder (1992): "Data and Data Hierarchy," *Journal of Petroleum Technology*, pp. 1286-1293.
- Satter, A. and G. Thakur (1994): **Integrated Petroleum Reservoir Management**, Tulsa: PennWell Publishing.
- Satter, A., J.E. Varnon, and M.T. Hoang (1994): "Integrated Reservoir Management," *Journal of Petroleum Technology*, pp. 1057-1064.
- Sawyer, W.K. and J.C. Mercer (August 1978): "Applied Simulation Techniques for Energy Recovery," Department of Energy Report METC/RI-78/9, Morgantown, WV.
- Schneider, F.N. (May 1987): "Three Procedures Enhance Relative Permeability Data," *Oil & Gas Journal*, pp. 45-51.
- Schilthuis, R.D. (1936): "Active Oil and Reservoir Energy," *Transactions of the AIME*, Volume 118, pg. 33 ff.
- Schön, J.H. (1996): **Physical Properties of Rocks: Fundamentals and Principles of Petrophysics**, Volume 18, New York: Elsevier.
- Sears, M. (June 1994): organizational development specialist at Bell Atlantic, quoted in *Journal of Petroleum Technology*, pp. 505.
- Selley, R.C. (1998): **Elements of Petroleum Geology**, 2nd Edition, San Diego: Academic Press
- Settari, A. and D.A. Walters (1999): "Advances in Coupled Geomechanical and Reservoir Modeling with Applications to Reservoir Compaction," Paper SPE 51927, *Proceedings of the 1999 SPE Reservoir Simulation Symposium*, Richardson, TX: Society of Petroleum Engineers.
- Sheriff, R.E. (1989): **Geophysical Methods**, Englewood Cliffs, NJ: Prentice-Hall.
- Slatt, R.M. and G.L. Hopkins (1990): "Scaling Geologic Reservoir Description to Engineering Needs," *Journal of Petroleum Technology*, pp. 202-210.
- Smith, R.V. (1990): **Practical Natural Gas Engineering**, Tulsa: PennWell Publishing.
- Spillette, A.G, J.G. Hillestad, and H.L. Stone (1986): "A High-Stability Sequential Solution Approach to Reservoir Simulation," **Numerical Simulation II**, SPE Reprint Series #20, Richardson, TX: Society of Petroleum Engineers.
- Staff-JPT (Aug. 1994): "New Management Structures: Flat and Lean, Not Mean," *Journal of Petroleum Technology*, pp. 647-648.
- Staff-JPT (May 1997): "SPE/WPC Reserves Definitions Approved," *Journal of Petroleum Technology*, pp. 527-528.
- Standing, M.B. and D.L. Katz (1942): "Density of Natural Gases," *Transactions of AIME*, Volume 146, 140.
- Stone, H.L. (Oct.-Dec. 1973); "Estimation of Three-Phase Relative Permeability and Residual Oil Data," *Journal of Canadian Petroleum Technology*, pp. 53ff.

- Taber, J.J. and F.D. Martin (1983): "Technical Screening Guides for the Enhanced Recovery of Oil," Paper SPE 12069, *Proceedings of the 58th Annual Technical Conference and Exhibition*, Richardson, TX: Society of Petroleum Engineers.
- Taber, J.J., F.D. Martin and R.S. Seright (1996): "EOR Screening Criteria Revisited," Paper SPE 35385, *Proceedings of the 1996 SPE Improved Oil Recovery Symposium*, Richardson, TX: Society of Petroleum Engineers.
- Taggart, I.J., E. Soedarmo, and L. Paterson (1995): "Limitations in the Use of Pseudofunctions for Up-Scaling Reservoir Simulation Models," Paper SPE 29126, *Proceedings 13th Society of Petroleum Engineers Symposium on Reservoir Simulation*, San Antonio, TX, Feb. 12-15.
- Tearpock, D.J. and R.E. Bischke (1991): **Applied Subsurface Geological Mapping**, Englewood Cliffs, NJ: Prentice Hall.
- Teeuw, D. (Sept. 1971): "Prediction of Formation Compaction from Laboratory Compressibility Data," *Society of Petroleum Engineering Journal*, pp. 263-271.
- Tek, M.R. (1996): **Natural Gas Storage Underground: Inventory and Deliverability**, Tulsa: PennWell Publishing.
- Telford, W.M., L.P. Geldart, R.E. Sheriff, and D.A. Keys (1976): **Applied Geophysics**, Cambridge: Cambridge University Press.
- Thakur, G.C. (1996): "What Is Reservoir Management?" *Journal of Petroleum Technology*, pp. 520-525.
- Thomas, G.W. (1982): **Principles of Hydrocarbon Reservoir Simulation**, Boston: International Human Resources Development Corporation.
- Thompson, R.S. and J.D. Wright (1985): **Oil Property Evaluation**, Second Edition, Golden, Colorado: Thompson-Wright Associates.
- Tippee, Bob (1998): "Collaborative Effort Seeks Computing Platform for Shared Earth Modeling," *Oil & Gas Journal*, pp. 58-62 (30 November).
- Tobias, S. (1998): "From G&G to S&S: Watershed Changes in Exploration-Development Work Flow," *Oil and Gas Journal*, pp. 38-47 (30 November).
- Todd, M.R., P.M. Odell, and G.J. Hiraski (Dec. 1972): "Methods for Increased Accuracy in Numerical Reservoir Simulators," *Society of Petroleum Engineering Journal*, pp. 515-530.
- Toronyi, R.M. and N.G. Saleri (1988): "Engineering Control in Reservoir Simulation," SPE 17937, *Proceedings of 1988 Society of Petroleum Engineers Fall Conference*, Oct. 2-5.

- Uland, M.J., S.W. Tinker, and D.H. Caldwell (1997): "3-D Reservoir Characterization for Improved Reservoir Management," paper presented at the 1997 Society of Petroleum Engineers' 10th Middle East Oil Show and Conference, Bahrain (March 15-18).
- Verma, S. and K. Aziz (1997): "A Control Volume Scheme for Flexible Grids in Reservoir Simulation," Paper SPE 37999, *Proceedings of the 1997 Society of Petroleum Engineers Reservoir Simulation Symposium*, Richardson, TX: Society of Petroleum Engineers.
- Wang, F.P., J. Dai, and C. Kerans (1998): "Modeling Dolomitized Carbonate-Ramp Reservoirs: A Case Study of the Seminole San Andres Unit – Part II, Seismic Modeling, Reservoir Geostatistics, and Reservoir Simulation," *Geophysics*, Volume 63, pp. 1876-1884.
- Westlake, D.W.S. (1999): "Bioremediation, Regulatory Agencies, and Public Acceptance of this Technology," *Journal of Canadian Petroleum Technology*, Volume 38, pp. 48-50.
- Whittaker, M. (1999): "Emerging 'triple bottom line' model for industry weighs environmental, economic, and social considerations," *Oil & Gas Journal*, pp. 23-28 (20 December).
- Wiggins, M.L. and R.A. Startzman (1990): "An Approach to Reservoir Management," Paper SPE 20747, *Proceedings of 65th Annual Technical Conference And Exhibition*, New Orleans, LA.
- Wilhite, G.P. (1986): **Waterflooding**, SPE Textbook Series Volume 3, Richardson, Texas: Society of Petroleum Engineers.
- Williamson, A.E. and J.E. Chappellear (June 1981): "Representing Wells in Numerical Reservoir Simulation: Part I – Theory," *Society of Petroleum Engineers Journal*, pp. 323-338; and "Part II – Implementation," *Society of Petroleum Engineers Journal*, pp. 339-344.
- Young, L.C. (1984): "A Study of Spatial Approximations for Simulating Fluid Displacements in Petroleum Reservoirs," **Computer Methods in Applied Mechanics and Engineering**, New York: Elsevier, pp. 3-46.

This page intentionally left blank

INDEX

A

absolute permeability 25, 26, 28, 46, 274, 294, 318
accumulation 32, 142-144, 231, 326
acoustic 107-109, 112, 115, 229, 230, 272, 279-281, 290
acoustic impedance 107-109, 115, 229, 230, 272, 279-281, 290
algorithm 45, 90, 116, 230, 231, 266, 292, 304-306
allocation 1, 6, 146, 313, 315
analytic aquifer 217, 267, 279
aquifer 14, 60, 70, 102, 116-119, 128, 158, 178, 183, 189, 198, 209-212, 216, 217, 223, 234, 237, 267-269, 271, 279, 280, 307-309
aquifer model 212, 216, 217, 237, 267, 279, 308
areal model 154, 177, 192
average 43, 46, 62, 76, 85, 99, 103, 104, 107, 108, 114, 131, 178, 183, 185, 202, 208, 209, 217, 220, 265, 280, 294, 296, 298, 313, 318

B

barrier 185
base case 92, 139, 188, 223-225
baseline 85, 92
bioremediation 82
black oil 36, 37, 71, 121-127, 143, 145, 152-154, 174, 175, 176, 177, 204, 229, 260, 285, 289, 295, 300, 322
black oil
model 126
simulator 36, 37, 71, 125, 127,

145, 153, 154, 204, 229, 285, 289, 300, 322

block

centered 160, 161
pressure 148, 170, 171, 220, 221
bottomhole pressure 192, 218, 219, 273, 318
boundaries 64, 113, 114, 164, 165, 169, 185, 215
boundary conditions 45, 49, 50, 52, 165, 294
bubble point 57, 121, 122, 127, 128, 130, 148, 154, 155, 200, 204, 206, 207, 230, 231, 258, 259, 271, 280, 300
Buckley-Leverett 39, 41, 44, 49, 90, 141, 150, 155, 234
buildup 113, 170, 220
bulk
density 107, 108, 289
modulus 118, 119, 245-248, 289
volume 166, 208, 209

C

C-D equation 44, 45
calibration 168, 187
capillary pressure 198, 22-24, 26-30, 39, 44, 49, 52, 131, 135-139, 145, 154, 159, 169, 212, 257, 278, 286, 292, 323, 324
Carter-Tracy 308, 309
Cartesian 158, 160, 163, 164, 166, 170, 173
cash flow 1, 2, 77, 78, 81, 186
chemical 21, 68, 69, 72, 73, 121, 132, 187
coalbed methane 71

completion 7, 169, 177, 180, 207, 315
compositional
 model 125, 126
 simulator 125, 153, 173
compressibility 15, 17, 18, 82, 83, 85, 98, 118, 124, 128, 154, 169, 171, 181, 182, 202, 209, 221, 259-262, 269, 289, 297, 298, 301, 302, 309, 330
compressional velocity 107, 108, 117, 119, 229, 230, 272, 280, 288, 289
computer
 mapping 158, 166
 program 7, 161
concentration 32, 44, 45, 150, 182, 295
conceptual model 165, 181
condensate 121, 121, 124, 127, 145, 153, 173
configuration 231, 232
conformance 153
coning 160, 173
consensus modeling 2
conservation
 laws 91, 142, 145
 of mass 12, 31, 40, 91, 142
constraint 35, 275, 286, 294, 310, 314, 317, 325, 327
contact angle 19, 21-23, 139
continuity equation 33, 48
contour 42, 110, 111, 157, 271, 272, 280, 281
convection 39, 44, 45, 143, 144
core 12, 21, 63, 96, 97, 102, 131, 132, 134, 136, 158, 169, 180, 212, 292
core
 analysis 12, 97, 132
 permeability 102
corner-point 160, 161

corporate 2, 81, 152, 191
correction 83, 127, 139, 170-172, 175, 178, 204, 205, 220, 291
correlation 20, 90, 102, 108, 110, 115, 132, 134, 139, 212, 213, 260, 290, 301, 303
cricondentherm 122
cross-section 112, 117, 119, 177, 197, 199, 215-217, 304
cross-section model 119, 177, 217
cubic 73, 124, 125, 297
cylindrical 158, 160, 164

D

Darcy's law 48, 131, 133, 142, 144, 294, 299, 318
data
 acquisition 116, 176
 preparation 168
 quality 180
datum 99, 170, 244, 262, 263, 304, 305
decision making 6, 81
decline curve 11, 16, 17, 80, 90, 192
density 20, 22-24, 28, 33, 37, 61, 68, 72, 107-109, 112, 138, 144, 160, 220, 235, 245-247, 249, 262, 286, 289, 295, 297-299, 304
density gradient 22, 23
depletion 17, 65, 67, 72, 73, 82, 83, 85, 94, 117, 119, 122, 128, 129, 154, 173, 179, 188, 192, 209, 210, 230, 234, 235
depth 32, 56, 98, 99, 109, 121, 139, 165, 199, 204, 214, 219, 223, 235, 244, 258, 262, 263, 287, 288, 296, 305
deterministic 101, 102
dew point 122, 127
diagonal grid 162

differential 41, 45, 52, 53, 127,
146, 176, 204, 205, 299, 300
differential
 equations 52, 146
 liberation 204, 299, 300
digitize 156
dimensionality 153, 172
dipping 28, 51, 52, 65, 116, 117,
158, 161, 197, 288
direct solution 266
directory 7
disciplines 2-4, 11, 93, 100, 119,
168
discount rate 77-79, 81
discretize 147
dispersion 39, 44, 143, 144, 150,
151, 155, 266
drawdown 113, 178, 183
drill stem test 201
drive 7, 13, 15, 17, 59-61, 65-67,
70, 73, 89, 168, 172, 173, 232
dry gas 122-124, 153, 173
dyadic 323
Dykstra-Parsons 62, 63
dynamic viscosity 299

E
economic
 forecast 2, 77
 recovery 1, 2, 186
economics 61, 75, 84
elevation 136, 305
endpoint 233
energy balance 145
Enhanced Oil Recovery 57, 64, 68,
69
environment 75, 81, 82, 95, 120
EOR 69-71, 74
equation of state 124, 298, 301
equilibration 143, 159, 177
equilibrium 14, 22, 126, 143, 159,
237, 263, 295, 297

equivalent radius 221
expenses 1, 78, 186, 190
explicit pressure 314, 316

F
facilities 91, 125, 127, 128, 145,
146, 190
falloff 114
fault 185, 188, 198, 216
files 7, 8, 149, 232, 271, 278-280
financial 82, 191
fine grid 141, 156, 157
fingering 139-141
finite
 difference 147, 162-164, 285,
294
 element 164
five-point 163
five-spot 59, 60, 62, 162
flash 127, 176, 204, 205, 299, 300
flow
 chart 149
 equations 31, 33, 36, 37, 45, 91,
99, 143, 145-149, 162, 173,
286, 322, 324, 325, 331
 unit 97-99, 154
fluid
 contacts 136, 139, 156, 169,
177, 180, 214
 modeling 124
 movement 158, 299
 properties 120, 125, 127, 128,
154, 184, 203, 204, 233, 299
 sampling 128
 type 56, 60, 112, 122, 123, 125,
153, 172
fluidity 299
flux 31-33, 37, 165, 185
forecasting 92, 191
format 101, 176, 212, 232, 234,
278
formation volume factor 12, 18,

57, 126-128, 171, 204, 209,
230, 259, 260, 286, 294,
297, 298, 300, 302, 313
fractional flow 19, 26-29, 39-42,
44, 46, 49
fracture 71, 113, 114, 136, 169
frontal advance 40-42, 48, 51-53,
150, 162
full field model 101, 164, 168
fully implicit 148-151, 160

G

gamma ray 111, 112
gas
cap 8, 14, 17, 18, 65, 66, 129,
137, 173, 181
hydrate 72, 73
gas-oil 12, 18, 20, 24, 29, 60, 70,
122, 127-130, 135, 137, 153,
160, 177, 178, 180, 200, 204,
213, 231, 263, 265, 286, 293,
300, 304, 305, 315
gas-oil
contact 24, 60, 137, 180, 263,
304, 305
ratio 12, 18, 122, 127-130, 153,
178, 200, 204, 265, 300
gas-water 18, 72, 73, 118, 135,
137, 145, 148, 160, 176, 264,
324
geologic model 172, 181, 199
geology 173
geometry 40, 51, 60, 160, 161,
164, 173, 239, 305
geophysics 101, 106, 111, 115,
116
geostatistics 101, 102, 104, 115,
181
giga scale 96, 106, 111
gradient 22, 23, 65, 71, 72, 121,
144, 165, 220, 258, 262, 263,
305

grain density 245-247, 249
gravity
drainage 65, 70, 134
segregated 263
segregation 15, 65, 129, 304
grid 143, 147, 150, 156, 157-165,
167, 170, 173, 174, 176, 215,
217, 220, 223, 235, 239, 240,
242, 287, 288
grid
orientation 150, 158, 159, 161-
163
preparation 158, 164, 174, 215
size 164, 240, 242, 243
gross thickness 100, 102, 156, 166,
198, 241-243

H

hand-drawn 102, 103
hard drive 7, 232
heavy oil 122, 173
heterogeneity 62, 63, 103, 104,
115, 141, 182
hierarchy of uncertainty 180
historical data 92, 151, 209
history
match limitations 184
matching 92, 100, 104, 132,
136, 153, 174, 176-182,
184, 188, 218
Honarpour 136, 212, 213
horizontal
permeability 114, 134, 141,
160, 185, 221, 320, 321
well 188, 230, 274, 320, 321
hysteresis 136, 145

I

immiscible 19, 20, 22-24, 29, 39,
40, 44, 49, 68-70, 136, 138
IMPES 147-151, 160, 222, 229,
231, 279, 322, 331

- implicit 148-151, 160, 229, 285, 331
 Improved Oil Recovery 68
 incompressible 39, 40, 49, 61, 210
 infill 61, 68
 inflation rate 79
 influx 14, 18, 65, 70, 116, 118, 119, 183, 209-212, 216, 267, 269, 271, 279, 280, 307-309
 initialization 138, 176, 177, 208, 230, 233, 239, 262, 263, 278, 304, 305
 integration 18, 54, 95, 97, 118, 119, 302
 interfacial tension 19, 20, 22, 44, 68, 69, 139
 interference testing 169
 inverse problem 92, 184
 investment 77-79, 81, 85, 188, 214
 irreducible 42, 117, 118, 135-137, 212, 258, 264, 293, 294, 313
 isothermal 14, 91, 128, 143, 145, 153, 229, 285, 302
 isotropic 161, 171, 221, 319
 iterations 266
- J**
 Jacobian 148
 Joshi formula 320
- K**
 k value 295
 kinematic viscosity 299
- L**
 laboratory 21, 22, 71, 93, 127, 128, 131, 132, 134, 136, 139, 152, 153, 169, 203, 204, 209, 212, 290, 292, 293, 299, 300, 325
 laboratory measurements 21, 128, 131, 132, 139, 204
 layer cake 158, 159, 244, 288
 linear 27, 29, 39, 43, 45, 48, 52, 53, 58, 143, 147, 150, 158, 206, 233, 289, 300, 301
 LIT gas well analysis 276, 277
 LIT method 314
 local grid refinement (LGR) 163, 174
 logging 97, 111, 132, 290
- M**
 Macleod-Sugden 20, 139
 macro scale 97, 131
 mapping 103, 156-158, 166
 mass
 balance 142
 conservation 32, 33, 35, 142, 285, 291
 material
 balance equation 13-15, 17, 66, 209-211
 balance error 148, 155, 224, 231, 291
 matrix 4, 71, 72, 136, 148, 245, 266, 289
 matrix material 245, 289
 mega scale 96, 111, 113, 114, 131
 micro scale 97, 131, 134
 microbial 69-71
 miscible 39, 44, 45, 57, 69, 143, 173
 miscibility 69, 70
 mobility 19, 24-26, 34, 46, 49, 50, 55, 61-63, 67, 69, 70, 114, 146, 311-313, 315
 mobility ratio 25, 26, 46, 50, 55, 61-63, 69, 70, 312
 model initialization 176, 177, 208
 molar conservation 142, 144
 mole fraction 20, 144, 261, 295, 298, 303
 molecular weight 20, 123, 261, 298, 303

momentum 91, 142, 143
multidisciplinary 104

N

naturally fractured 173
near wellbore 173, 181
net present value 77-81
neutron 112
Newton-Raphson 147, 148
nine-point 163
nonlinear 41, 53, 133, 145, 146,
206
normal distribution 63, 76, 77, 85
numerical
dispersion 150, 151, 155, 266

O

objectives 5, 85, 90, 153, 154, 160,
165, 168, 169, 172-174, 176,
183, 197
Ockham's Razor 3, 154, 160, 172-
174
oil productive capacity 110, 115
oil-water 21, 24, 26, 28, 46, 49, 60,
70, 135-138, 148, 264, 286,
306, 324
oscillations 279
output 6, 8, 17, 47, 63, 149, 165,
232, 270, 271, 278-281

P

P-T diagram 121, 123
parallel grid 162
parachor 20
partial differential equations 146
pattern 56, 58-62, 69, 141, 162,
192
payout 78, 81
PEBI 164
performance
data 3
predictions 89, 186, 192, 218

petrophysical model 288
phase
behavior 121, 125
envelope 121, 123
plot file 279
Poisson's ratio 83, 86, 290
pore
radius 23, 30
volume 14, 40, 44, 56, 151,
166, 181, 182, 185, 208,
209, 217, 221-223, 265, 280
porous 6, 34, 39, 48, 49, 89, 131-
133, 140, 143, 245, 289, 299
pot aquifer 267, 268, 307, 308
prediction 2, 77, 92, 93, 119, 168,
174, 186-188, 207, 223-225
prediction process 187, 224
pressure
correction 170, 220
equation 325, 331
initialization 262, 263, 304
maintenance 67, 68, 83, 173
price forecast 1, 92, 93
primary production 64
pseudoization 159, 160
pulse 114
PVT 121, 127, 128, 145, 154, 155,
169, 175, 176, 204, 207, 232,
234, 235, 239, 240, 255-259,
261, 265, 278, 299-301
PVT region 175, 232, 255-258,
278, 287

R

radial
coordinates 173
flow 171, 221
radius 22, 23, 30, 61, 95, 170, 171,
175, 201-203, 219, 221, 269,
274, 309, 318-321
rate
constraint 275, 310, 317

of return 77, 80, 81
 realizations 3, 104, 116, 176
 reasonableness 3, 184
 recovery efficiency 13, 56-58, 61,
 63, 65, 68, 122
 recurrent data 233, 237, 270, 271,
 279
 reflection coefficient 108, 119,
 230, 272, 280, 290
 regression 20, 126, 189, 309
 reliability 96, 180, 183
 repeat formation test 139
 representation 3, 97, 125, 134,
 137, 146, 153, 156, 158, 190,
 208, 230, 276, 301, 310, 314
 representative elementary volume
 142
 reserves 73, 75-77, 80, 81, 85, 190
 reservoir
 architecture 96, 111, 143, 156,
 161, 172, 223
 characterization 82, 89, 96,
 101, 109, 116, 176
 description 92, 115, 173, 233
 engineering 6, 80, 89, 121, 142,
 192, 229, 230
 geophysics 101, 106, 111, 115,
 116
 management 1, 2, 65, 68, 75,
 82, 83, 90-93, 101, 106,
 152, 160, 162, 186, 187,
 190, 192, 197, 207, 229
 simulation 6, 11, 80, 89, 92, 93,
 119, 136, 142, 143, 151,
 158, 192, 197
 structure 7, 8, 60, 106, 145,
 197, 214
 resistivity 112
 restart 231, 263
 restored state 293
 revenue 78, 79, 190
 risk 93, 95, 103, 188, 189

robustness 151, 152, 231
 rock
 compressibility 181, 182, 260-
 262, 269, 309, 330
 quality 110, 115, 134
 region 154, 232, 255-257, 263-
 265
 rock-fluid interaction 131, 145
 run summary 279

S
 saturated 121, 125, 127, 152, 153,
 234, 259, 300, 301
 saturation constraint 286, 325, 327
 scale 21, 95-97, 99, 103, 106, 111,
 113, 114, 131, 134, 136, 164,
 187, 217, 296
 secondary production 67
 seismic
 history matching 179, 180
 line 197, 198
 trace 106, 107, 109
 velocity 245, 272
 waves 106, 107, 110
 semi-variance 102
 sensitivity 2, 76, 80, 82, 116, 131,
 139, 157, 185, 186, 188-190,
 192, 224
 sensitivity
 analyses 188, 192
 study 190, 224
 separator 91, 122, 128, 146, 204,
 205, 299, 300
 shear
 modulus 245-248, 289
 velocity 117, 119, 230, 272,
 288, 289
 simulator selection 153, 172, 173
 slanted well 230
 slope 16, 17, 42-44, 99, 259
 solubilities 33, 34, 48, 49, 53, 54,
 299, 326

solution method 265, 266
sonic 109, 112
source/sink 32, 143, 144, 291
spacing 58, 60, 61, 68, 169, 234
SPE/WPC 75, 76
specific gravity 29, 30, 261, 298, 303
spontaneous potential 112
stability 86, 120, 149, 151, 161, 224, 279, 291
standard deviation 76, 85
Standing-Katz 301
steady-state aquifer 223, 308
stochastic image 102, 181
subsidence 82, 83, 85, 86
surface model 90, 91, 146
sweep 39, 57, 58, 62
sweep efficiency 39, 58, 62
symmetry 141, 161

T

tank model 216, 230
Taylor 150
team 4-6, 76, 89, 90, 93, 114, 132, 134, 135, 168, 170, 174, 184, 189, 190
temperature 65, 91, 92, 121-124, 127-129, 139, 143, 145, 153, 177, 261, 295-299, 301-303
tensor 134, 144, 163, 287, 323
terminal 309
tertiary production 68
thermal 68-70, 91, 112, 145, 173, 177, 187
thickness 12, 58, 61, 82, 83, 85, 100-102, 110, 137, 139, 146, 156, 166, 182, 198, 208, 219, 223, 241-244, 269, 274, 305, 306, 309, 318, 320, 321
three-dimensional model 222
three-phase
 flow 33, 331

 relative permeability 258, 292, 293
throughput 151, 160, 163, 221, 222
time-lapse (4D) seismic 106, 227, 288
timestep 38, 147-151, 155, 221, 222, 224, 233, 264, 266 270, 272, 278-280, 291, 307
timestep
 summary 38, 278, 279
tomography 118
tracer 103, 169, 177, 182
transient tests 113, 114, 169
transition zone 23, 24, 30, 49, 136-139, 165
transmissibility 103, 130, 141, 185, 223, 230, 235, 249, 253-255, 292, 294, 295
transmission coefficient 108, 290
two-point upstream 267

U

uncertainty 93, 104, 132, 157, 180, 183, 188, 192
unconformity 198, 199, 223
undersaturated 94, 127, 129, 154, 155, 192, 197, 200, 204, 206, 207, 209, 210, 234, 259
uniqueness problem 184

V

validity 92, 116, 128, 139, 179, 180, 186, 191, 192, 293
vector 36, 37, 102, 148, 285
velocity 33, 37, 42, 44, 49, 50, 52, 53, 107-110, 117, 119, 144, 150, 229, 230, 245, 272, 280, 286, 288, 289
vertical
 conformance 153
 equilibrium (VE) 159

well 273, 319
 viscosity 25, 28-30, 34, 46, 61, 63,
 69, 70, 126, 128, 133, 140, 144,
 171, 202, 206, 207, 259, 260,
 269, 287, 294, 299, 302, 309,
 318
 viscous fingering 139
 voidage 274, 312
 volatile oil 122, 124, 153
 volume element 40, 99
 volumetric 12, 18, 26, 29, 40, 56-
 58, 62, 89, 103, 166, 177, 208,
 211, 212, 216, 222

W

water
 drive 65, 67, 173
 saturation 24, 26, 40-44, 46, 47,
 50, 117, 119, 136, 137, 148,
 198, 202, 212, 213, 257,
 258, 263, 264, 271, 293,
 294, 307
 water-oil
 contact 138, 139, 214, 223,
 263, 304, 305
 ratio 141, 155, 177, 178, 207,
 264
 waterflood 26, 42, 43, 57, 63, 68,
 70, 73, 90, 134, 135, 141, 150,
 155, 188, 234
 wave 86, 107-110, 290
 Weinaug-Katz 20, 139
 Welge 42

well

density 61, 68
 log 12, 95, 96, 111, 112, 114,
 131, 132, 139, 182, 198,
 199, 214, 216, 219, 223
 model 90, 91, 143, 145, 146,
 181, 218, 219
 pattern 56, 60
 productivity 311
 report 280
 spacing 60, 61, 68
 testing 113
 wellbore 61, 86, 90, 91, 95, 123,
 127-129, 132, 143, 145, 146,
 160, 169-171, 173, 180, 181,
 201, 219-221, 274, 318, 320,
 321
 wellbore
 model 90, 91, 145
 storage 171, 221
 wet gas 122
 wettability 19-22, 68, 135, 139,
 292, 293
 window 164, 165, 168, 185, 188
 workover 169

Y

yield 11, 69, 76, 90, 121, 124, 126,
 132, 145, 148, 165, 185, 190,
 192

Z

Z-factor 301